The role of meprin β for the pathogenesis of Alzheimer's disease

Dissertation

zur Erlangung des Doktorgrades

der

Mathematisch-Naturwissenschaftlichen Fakultät

der

Christian-Albrechts-Universität zu Kiel

vorgelegt von

Fred Armbrust

Kiel, 2021

Erster Gutachter:	Prof. Dr. Christoph Becker-Pauly
Zweiter Gutachter:	Prof. Dr. Thomas Roeder

Tag der mündlichen Prüfung:	29.04.2021
Zum Druck genehmigt:	29.04.2021

Preface

This dissertation was partly created cumulative. The data obtained during preparing this thesis were described in detail in six manuscripts. The most relevant results from these manuscripts are briefly summarized within the thesis. Unpublished data are described in detail. The respective manuscripts are attached as appendix 1-6:

1. **Armbrust, F.**, Bickenbach, K., Kodelka, T., Tholey, A., Pietrzik, C.U., and Becker-Pauly, C. (2021). Phosphorylation of meprin β at the C-terminus controls its enzymatic activity at the cell surface. submitted

2. Marengo, L., **Armbrust, F.**, Schoenherr, C., Storck, S.E., Schmitt, U., Zampar, S., Wirths, O., Altmeppen, H., Glatzel, M., Weggen, S., Becker-Pauly, C., and Pietrzik, C.U. (2021). Meprin β knockout reduces brain Aβ levels and rescues learning and memory impairments in the APP/lon mouse model for Alzheimer's disease. submitted

3. Berner, D.K.*, Wessolowski, L.*, **Armbrust, F.**, Schneppenheim, J., Schlepckow, K., Koudelka, T., Scharfenberg, F., Lucius, R., Tholey, A., Kleinberger, G., Haass, C., Arnold, P., and Becker-Pauly, C. (2020). Meprin β cleaves TREM2 and controls its phagocytic activity on macrophages. Federation of American Societies for Experimental Biology 34, 6675-6687. doi: 10.1096/fj.201902183R
   *These Authors contributed equally to this work.

4. **Armbrust, F.**, Colmorgen, C., Pietrzik, C.U., and Becker-Pauly, C. (2019). The Alzheimer's disease associated bacterial protease RgpB from P. gingivalis activates the alternative β-secretase meprin β thereby increasing Aβ generation. Pre-print-server: www.biorxiv.com. doi: 10.1101/748814

5. Scharfenberg, F., **Armbrust, F.**, Marengo, L., Pietrzik, C., and Becker-Pauly, C. (2019). Regulation of the alternative β-secretase meprin β by ADAM-mediated shedding. Cellular and molecular life sciences 76, 3193-3206. doi: 10.1007/s00018-019-03179-1

6. Peters, F., Scharfenberg, F., Colmorgen, C., **Armbrust, F.**, Wichert, R., Arnold, P., Potempa, B., Potempa, J., Pietrzik, C.U., Häsler, R., Rosenstiel, P., and Becker-Pauly, C. (2019). Tethering soluble meprin α in an enzyme complex to the cell surface affects IBD-associated genes. Federation of American Societies for Experimental Biology 33, 7490-7504. doi: 10.1096/fj.201802391R

Table of Contents

List of Figures

List of Tables

Abstract

Alzheimer's disease (AD) is the most common type of dementia, however, incurable thus far. The release of neurotoxic amyloid-β (Aβ) peptides, which are generated from the amyloid precursor protein (APP) upon cleavage at the β- and γ-secretase sites, play a central role for neurodegeneration in AD. Since the β-site of APP cleaving enzyme (BACE1) was identified as the major β-secretase, it was considered as one of the most promising therapeutic targets for AD treatment. However, so far every BACE1 inhibitor failed in clinical trials. Interestingly, besides the conventional Aβ peptides, also N-terminally truncated Aβ species such as Aβ2-42 were identified to be elevated in AD patient brains. Taking into account that BACE1 is not involved in the generation of these truncated Aβ species, the characterization of alternative β-secretases is of interest for AD research. The metalloprotease meprin β is upregulated in AD patient brains, capable of cleaving APP and thereby releasing N-terminally truncated Aβ. This thesis aimed to provide deeper insight into the mechanistic regulation of APP processing by meprin β and to evaluate the *in vivo* role of meprin β in AD using different mouse models. Analyzing the regulation of meprin β, C-terminal phosphorylation of meprin β was found to diminish its surface activity and leads to decreased APP processing. Moreover, a bacterial protease arginine-gingipain B (RgpB) was characterized as meprin β activator promoting amyloidogenic APP processing. Furthermore, meprin β was observed to diminish the phagocytic potential of myeloid cells by shedding the cells surface receptor triggering receptor expressed on myeloid cells 2 (TREM2). This might reduce the capability of Aβ uptake by microglia. In order to evaluate the *in vivo* relevance of meprin β for AD, mice expressing the London APP (APPlon) variant were crossed with meprin β knock-out mice and characterized with regard to AD-like pathology. Of note, the amyloid phenotype of the APPlon mice was markedly reduced and cognitive impairments were completely recovered, when meprin β was abolished. Therefore, a crucial *in vivo* role of meprin β in AD was hypothesized. As meprin β is upregulated in AD patient brains, another approach was the overexpression of meprin β in wild-type mouse brains. Since astrocytes were previously identified to produce Aβ2-42 rather than other brain cell types, meprin β was conditionally overexpressed in astrocytes. Intriguingly, amyloidogenic APP processing and Aβ release were elevated in these mice. Therefore, meprin β emerges as a promising target for inhibitor application to prevent from the generation of Aβ, which may serve as therapeutic approach for AD treatment. Beyond APP as a substrate, N-terminomic analyses of mice overexpressing meprin β in astrocytes revealed several new candidate substrates of meprin β.

In summary, this thesis further enlightens the mechanistic regulation of APP cleavage by meprin β and provides evidence for an *in vivo* role of meprin β for the pathogenesis of AD.

Zusammenfassung

Die Alzheimer-Erkrankung (AD) ist die häufigste Form der Demenz und bisher nicht therapierbar. Die Freisetzung von neurotoxischen Amyloid-β (Aβ)-Peptiden durch die Spaltung des Amyloiden-Vorläufer-Proteins (APP) an der β- und γ-Sekretase-Spaltstelle spielt eine zentrale Rolle für die Entwicklung der Neurodegeneration bei der AD. Da die Aspartat-Protease *β-site of APP cleaving enzyme* (BACE1) in der Lage ist, APP an der β-Sekretase-Spaltstelle zu prozessieren und dabei Aβ-Peptide freigesetzt werden, stellt dies ein vielversprechendes Zielprotein für AD-Therapieansätze dar. Jedoch scheiterten bisher alle BACE1-Inhibitoren in klinischen Studien. Interessanterweise wurden neben den konventionellen Aβ-Peptiden vermehrt N-terminal verkürzte Aβ-Formen, wie z.B. Aβ2-42, in Hirnen von AD-Patienten identifiziert. Da BACE1 nicht an der Generierung dieser verkürzten Aβ-Formen beteiligt ist, ist die Charakterisierung von alternativen β-Sekretasen für die AD-Forschung von Bedeutung. Interessanterweise ist die Expression der Metalloprotease Meprin β in Hirnen von AD-Patienten erhöht und als APP spaltendes Enzym ist es an der Generierung von verkürzten Aβ-Peptiden beteiligt. Daher wurde in dieser Thesis die Regulation der APP-Spaltung durch Meprin β näher charakterisiert sowie die *in vivo*-Rolle von Meprin β bei der AD mit Hilfe verschiedener Mausmodelle beurteilt. Bei der Analyse der Regulierung von Meprin β wurde die Phosphorylierung des C-Terminus als Mechanismus identifiziert, welcher zu einer Reduktion der Meprin β-Aktivität an der Zelloberfläche führt und die APP-Prozessierung vermindert. Des Weiteren wurde die bakterielle Protease *arginine-gingipain B* (RgpB) als Meprin β-Aktivator charakterisiert, durch den die amyloidogene APP-Prozessierung gesteigert wird. Außerdem wurde herausgefunden, dass durch die Spaltung des *triggering receptor expressed on myeloid cells 2* (TREM2) durch Meprin β das Phagozytose-Potential von myeloiden Zellen herabgesetzt wird. Dies könnte eine reduzierte Aufnahme von Aβ durch Mikroglia bedingen. Um die *in vivo*-Relevanz von Meprin β bei der AD zu evaluieren, wurden Meprin β-defiziente AD-Modell-Mäuse, die APP mit der London-Mutation (APPlon) exprimieren, charakterisiert. Hierbei zeigte sich, dass die Abwesenheit von Meprin β mit einem verringerten Aβ-Vorkommen in den Hirnen der APPlon-Mäuse und einer Steigerung ihrer kognitiven Funktionen assoziiert war. Da die Meprin β-Expression in Hirnen von AD-Patienten erhöht ist, wurde in einem weiteren Versuch Meprin β in Astrozyten von Wild-Typ-Mäusen überexprimiert. In diesen Mäusen konnte verstärkte amyloidogene APP-Prozessierung und Aβ-Freisetzung detektiert werden. Daher könnte die Inhibition von Meprin β einen therapeutischen Ansatz für die Behandlung von AD-Patienten darstellen. Außerdem wurden mittels N-Terminomic-Analysen von Maushirnen, die Meprin β in Astrozyten überexprimieren, neue potentielle Meprin β-Substrate identifiziert.

Zusammenfassend wurden in dieser Arbeit neue Mechanismen der Regulation von APP-Prozessierung durch Meprin β beschrieben und es konnte gezeigt werden, dass Meprin β eine wichtige Rolle für die Pathogenese der AD spielen könnte.

1. Introduction

Alzheimer disease (AD) is the most common type of dementia (reviewed in Fymat, 2018). In 2017, more than 100,000 people died from AD in the United States. Thus, it was ranked as the sixth-leading cause of death (Heron, 2019). AD was first described in 1907 by the clinical psychiatrist and neuroanatomist Alois Alzheimer examining a 51-year old female patient, who suffered from harsh cognitive impairments. *Post mortem*, Alois Alzheimer observed extracellular and intracellular located fibril-like deposits in the brain, nowadays known as amyloid-β (Aβ) plaques and neurofibrilar tangles (NFTs), respectively. Both became pathophysiological hallmarks of AD (Alzheimer, 1907; reviewed in Hippius and Neundörfer, 2003). In the past decades, the pathobiochemistry of AD has been continuously investigated. It is known, that NFTs consist of hyperphosphorylated tau protein aggregates (reviewed in Iqbal et al., 2010; reviewed in Chong et al., 2018). Tau is a microtubule-binding protein predominantly expressed in neurons (Kempf et al., 1996). Under healthy conditions, it was shown to promote microtubule stabilization *in vitro* (Gustke et al., 1994; Choi et al., 2009) and *in vivo* (Goedert and Jakes, 1990). In AD patient brains though, tau was observed to be hyperphosphorylated (Grundke-Iqbal et al., 1986; Bancher et al., 1989). Upon hyperphosporylation, it undergoes a conformational change (Mondragón-Rodríguez et al., 2008) and loses its ability to bind and stabilize microtubules, which might contribute to neuronal dysfunction (Lindwall and Cole, 1984; Barbier et al., 2019). Apart from that, hyperphosphorylated tau proteins oligomerize to pairwise helical filaments, which then form the NFTs (Kosik et al., 1986; reviewed in Chong et al., 2018). However, it was reported that NFTs themselves might not be involved in neurotoxicity, but rather intermediary tau oligomers are assigned most toxic properties due to synaptic impairment (Fá et al., 2016).

Besides NFTs, Aβ plaques have been considered as a pathophysiological hallmark of AD. Aβ peptides are composed of approximately 40 amino acids. They are released from the amyloid precursor protein (APP) upon proteolytic processing by so-called β- and γ-secretases. Aβ is prone to form oligomers resulting in large aggregates referred to as amyloid plaques (reviewed in Nunan and Small, 2000; reviewed in Murphy and LeVine, 2010; reviewed in Prasansuklab and Tencomnao, 2013). Even though, it has been assumed for a long time that Aβ plaques exhibit neurotoxic properties, several studies showed harmful effects of oligomeric Aβ independent of Aβ deposits (Lesné et al., 2008; Tomiyama et al., 2010). Aβ oligomers were shown to disturb cell membrane integrity, impair neuronal transmission, and promote neurodegeneration (Pike et al., 1993; Stéphan et al., 2001; Porat et al., 2003).

1.1 APP processing

APP is a ubiquitously expressed type I transmembrane protein. The three main isoforms APP695, APP751 and APP770 are generated by alternative splicing and differ in their ectodomain (reviewed in Nalivaeva and Turner, 2013). In the brain, APP695 is the most abundant isoform and predominantly expressed in neurons (Tanaka et al., 1989; Guo et al., 2012). APP plays a role in cell and synaptic adhesion. On the one hand, it has been found to interact with extracellular matrix components such as heparin (Clarris et al., 1997), collagen type I (Beher et al., 1996) as well as laminin (Kibbey et al., 1993). On the other hand, APP molecules on neighboring cells can interact with each other promoting synaptogenesis (Wang et al., 2009). In line with this observations, deletion or reduction of APP in mice leads to reduced synaptic activity and reactive gliosis as well as decreased locomotor activity (Zheng et al., 1995; Hérard et al., 2006). During the pathogenesis of AD, APP plays a role as the precursor protein of Aβ peptides (Fig. 1). Of note, cell culture experiments, in which different APP isoforms were overexpressed, revealed that Aβ is predominantly generated from APP695 (Belyaev et al., 2010). Upon cleavage at the β-secretase site, a soluble APP fragment referred to as sAPPβ is released. The remaining membrane-bound C-terminal fragment CTF-β can be further processed by the γ-secretase complex, which leads to the generation of the Aβ peptide. This is referred to as the amyloidogenic pathway (reviewed in Castro et al., 2019). Within an antagonistic pathway, α-secretases can cleave within the Aβ sequence, thus preventing from Aβ formation. Instead, the soluble APP fragment sAPPα is released, whereas the C-terminal fragment CTF-α remains in the membrane. This AD protective processing is termed as non-amyloidogenic pathway (reviewed in Kojro and Fahrenholz, 2005).

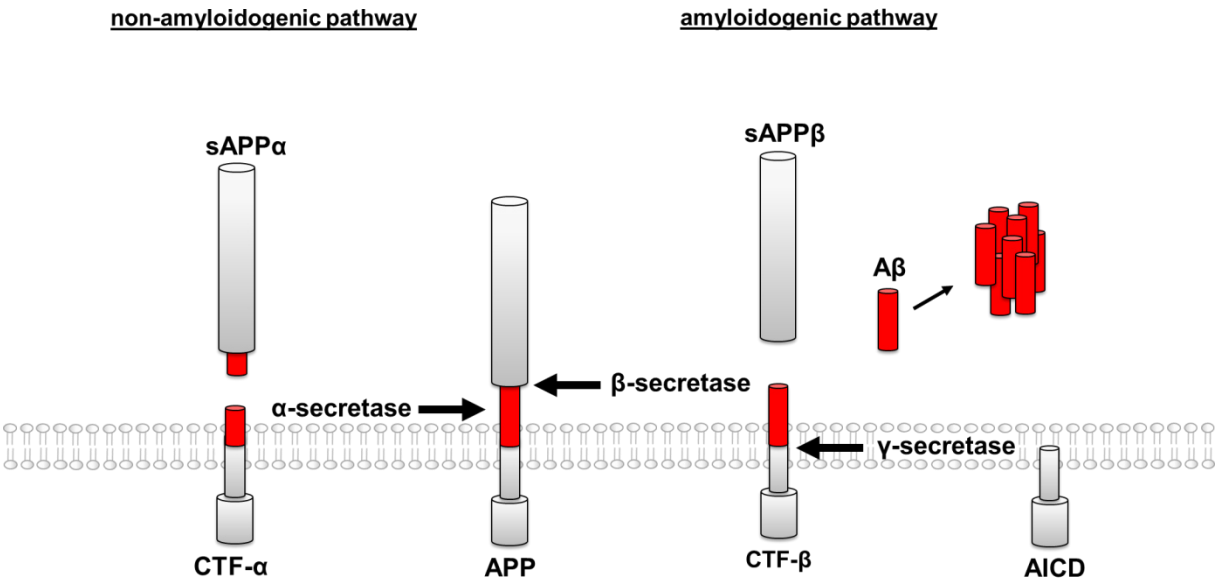

Fig. 1: APP cleavage by different secretases.

In the non-amyloidogenic pathway, APP is processed by an α-secretase resulting in a membrane-bound C-terminal fragment-α (CTF-α) and the soluble APP fragment sAPPα. In the amyloidogenic pathway, a β-secretase cleaves APP, thereby releasing the soluble APP fragment sAPPβ and the membrane-bound C-terminal fragment-β (CTF-β), which can be further processed by the γ-secretase. As a result, the APP intracellular domain (AICD) is generated and Aβ is released, which is prone to form aggregates.

1.1.1 BACE1 – the prevalent β-secretase

β-site APP cleaving enzyme (BACE1) is a transmembrane aspartyl protease and considered as the prevalent β-secretase (reviewed in Cole and Vassar, 2008). Since its enzymatic optimum is at pH 4.5 (Vassar et al., 1999), BACE1 is active in acidic cellular compartments. It is sorted either directly from the trans-Golgi network (TGN) or via the plasma membrane to endosomes (Huse et al., 2000; Pastorino et al., 2002). Moreover, it is constantly recycled from endosomes to the TGN (Walter et al., 2001). Beyond its pathophysiological role as a β-secretase, the physiological relevance of BACE1 has scarcely been addressed. BACE1 deficiency only leads to mild abnormalities in mouse models. Altered neurological behavior such as elevated pain sensitivity and reduced grip strength was observed. Furthermore, BACE1-deficient mice show diminished myelination, however, axonal development proceeds normally (Hu et al., 2006). β-secretase cleavage of APP by BACE1 occurs between M671 und D672 (using the numbering of APP770 isoform annotated in UniProt (The UniProt Consortium, 2021, https://www.uniprot.org/uniprot/P05067)) (Fig. 2). Thus, D672 is referred to as position 1 of Aβ. Due to the enzymatic optimum at low pH (Vassar et al., 1999), a huge reduction of Aβ level upon blocking surface endocytosis (Koo and Squazzo, 1994) and the endosomal interaction of BACE1 and APP (Kinoshita et al., 2003), Aβ generation by BACE1 is hypothesized to occur mainly in endosomes (reviewed in O'Brien and Wong, 2011). In an AD mouse model, in which Aβ formation and deposition is reinforced, a BACE1 knock-out leads

to decreased Aβ1-x levels, diminished plaque deposition and a cognitive benefit (Hu et al., 2018). Moreover, the association of BACE1 and AD is supported by increased BACE1 activity during aging and in AD patient brains (Fukumoto et al., 2004).

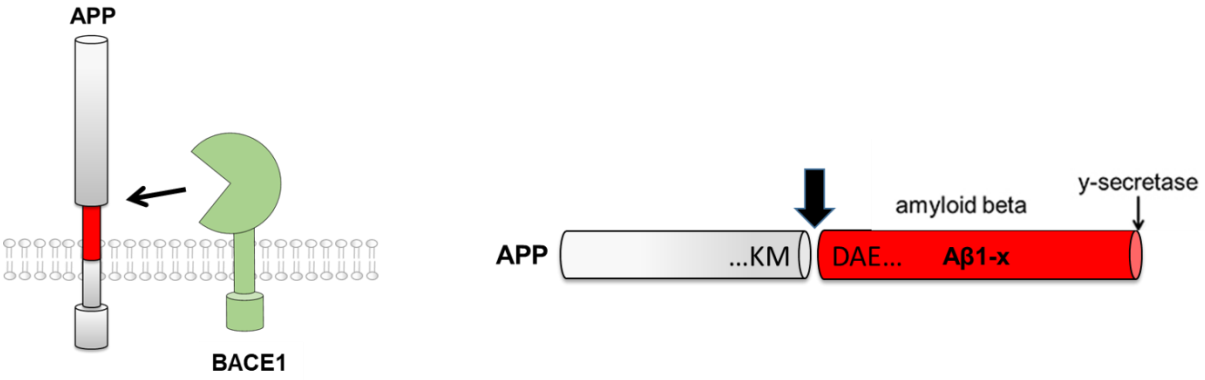

Fig. 2: The main APP cleavage site of BACE1.

BACE1 predominantly cleaves APP between M671 and D672 (using the numbering of APP770 annotated in UniProt (The UniProt Consortium, 2021, https://www.uniprot.org/uniprot/P05067)). As a result, Aβ1-x is released upon γ-secretase cleavage. The figure was created based on Vassar et al., 1999.

Of note, a characterization of Aβ species in AD brains revealed that not only Aβ forms starting at D672 are elevated, but also the N-terminal truncated species Aβ2-42 starting at position A673 is highly increased (Fig. 3) (Wiltfang et al., 2001). These truncated Aβ peptides cannot be linked to BACE1 activity (Wiltfang et al., 2001; Schieb et al., 2010) and show an increased potential to form aggregates (Schönherr et al., 2016). Therefore, alternative β-secretases may play a so far underestimated role in AD.

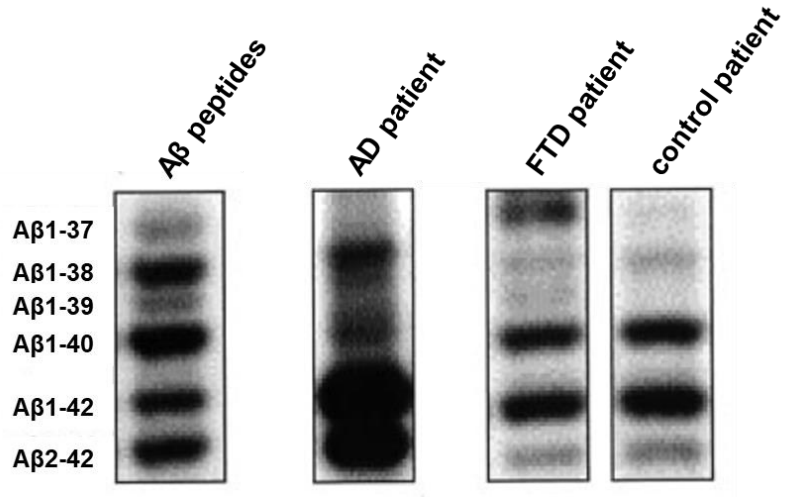

Fig. 3: Characteristic band pattern of Aβ peptides in Western blot analysis of AD brain tissue

Frontal lobe samples were analyzed by Western Blot. Synthetic Aβ peptides served as control for individual Aβ species (Aβ peptides). The representative Alzheimer´s disease (AD) patient frontal lobe shows elevated Aβ2-42 levels, which is not the case for frontal temporal disease (FTD) patients or healthy control patients. The AD patient sample was 20-fold diluted prior analysis. The figure was adapted from Wiltfang et al., 2001.

1.1.2 γ- and α-secretases

In addition to β-secretase processing, the formation of Aβ peptides requires a subsequent cleavage event accomplished by the γ-secretase complex (reviewed in Steiner et al., 2018). The γ-secretase complex is a protein complex consisting of presenilin (PS) 1 and -2, presenilin enhancer 2 (PEN-2), anterior pharynx-defective 1 (APH-1) and nicastrin. Presenilins represent the catalytic subunits of the γ-secretase complex (Wolfe et al., 1999). During maturation, they are processed in an N-terminal fragment (NTF) and C-terminal fragment (CTF) (Thinakaran et al., 1996). PEN-2 is involved in the modulation of this proteolytic maturation (Takasugi et al., 2003). However, the underlying regulatory mechanism is completely unknown. Nicastrin and APH-1 are required for stabilization of the whole protein complex (Edbauer et al., 2002; Takasugi et al., 2003). The γ-secretase belongs to the family of intramembrane cleaving proteases. It cleaves its substrates within the plane of the lipid bilayer in a process referred to as regulated intramembrane proteolysis (reviewed in Steiner et al., 2008). One of the most investigated substrates of the γ-secretase complex is Notch1. Upon γ-secretase cleavage the Notch intracellular domain (NICD) is released and mediates cell fate during development via regulating gene transcription (reviewed in Kopan, 2012). Deficiency of γ-secretase components PS1 (Donoviel et al., 1999), nicastrin (Li et al., 2003), or APH-1 (Ma et al., 2005) leads to embryonic lethality due to ablation of Notch signaling.

In terms of γ-secretase mediated Aβ-generation, the remaining CTF-β of APP after β-processing, is initially cleaved by the γ-secretase complex at position 48 or 49 (Gu et al., 2001; Sastre et al., 2001; Weidemann et al., 2002). These peptides are immediately shortened by carboxy-terminal trimming by the same complex, which leads to the release of Aβ species ending between position 37 and 45 including the major form Aβx-40 and the highly pathogenic variants Aβx-42 and Aβx-43 (Yu et al., 2001; Qi-Takahara et al., 2005; Zhao et al., 2005).

As mentioned above, APP can also be processed in a protective anti-amyloidogenic pathway by α-secretases cleaving within the Aβ sequence (Esch et al., 1990). A disintegrin and metalloprotease (ADAM) 10 was considered as primarily responsible for α-cleavage (Jorissen et al., 2010; Kuhn et al., 2010), however, also ADAM17 and ADAM9 are capable of cleaving APP at the α-secretase site (Koike et al., 1999; Slack et al., 2001). Since α- and β-secretases compete for APP as a substrate, elevated activity of α-secretases leads to diminished Aβ production (Skovronsky et al., 2000). Moreover, sAPPα itself is a neuroprotective factor as it promotes neuronal survival (Goodman and Mattson, 1994; Barger et al., 1995) and elevated levels in the cerebrospinal fluid (CSF) correlate with cognitive performance (Anderson et al., 1999; Fellgiebel et al., 2009). The CTF-α remaining after α-processing can also be cleaved by the γ-secretase complex. However, the function of the released peptide, referred to as p3, is

controversely discussed in the literature. Whereas p3 is often mentioned as non-amyloidogenic product (Näslund et al., 1994; Coronel et al., 2018), several studies observed the ability of p3 to form amyloidogenic aggregates (Vandersteen et al., 2012; Kuhn et al., 2020). Thus, the role of p3 remains unclear so far.

1.2 Alzheimer´s disease risk genes

In more than 95% of all AD cases, the disease occurs sporadic as a multifactorial disorder, and is thus termed sporadic AD (SAD). However, in less than 5% AD is caused by point mutations, which are genetically inherited. Therefore, this type is referred to as familial AD (FAD) (reviewed in Dorszewska et al., 2016). Further, AD can be classified into early-onset AD (EOAD) (before age 65) and late-onset AD (LOAD) (after age 65) (Seltzer and Sherwin, 1983). Of note, EOAD is associated with a more severe disease progression (Bigio et al., 2002). In the past decades, several Genome-Wide Association Studies (GWAS) revealed risk genes for LOAD and EOAD (Sherva and Farrer, 2011).

For LOAD, *APOE* has been considered as the strongest risk gene due to its high prevalence in numerous studies (Coon et al., 2007; Abraham et al., 2008; Li et al., 2008). The corresponding protein apolipoprotein E (ApoE) mediates appropriate lipolytic processing (Phillips, 2014). In the brain, it is predominantly expressed in astrocytes and transports cholesterol to neurons via ApoE receptors (Jeong et al., 2019). ApoE exists as three isoforms, of which ApoE4 is associated with increased risk for AD as carriers show increased tau pathology and Aβ accumulation (Rannikmäe et al., 2014; Yamazaki et al., 2019). Of note, ApoE is co-deposited in senile plaques and NFTs (Namba et al., 1991).

Another LOAD risk factor gene is *TREM2* (Jonsson et al., 2013; Sims et al., 2017). It encodes the transmembrane glycoprotein triggering receptor expressed on myeloid cells 2 (TREM2) expressed in a subgroup of myeloid cells (Gratuze et al., 2018). In the brain, it is present almost exclusively in microglia and functions as a receptor for apolipoproteins and high- as well as low-density lipoproteins (Yeh et al., 2016; Song et al., 2017). Aβ was also identified as a ligand of TREM2. Upon binding, TREM2 associates with DNAX-activation protein 12 (DAP12) and downstream signaling leads to microglia activation promoting proliferation, cytokine expression and phagocytic ability. This leads to an increased Aβ clearance through uptake by microglia (Zhao et al., 2018). In the past decades, several AD-related single-nucleotide polymorphisms (SNPs) were linked to impaired ligand binding and disturbed signaling of TREM2 (Guerreiro et al., 2013; Jin et al., 2014). In concordance with these findings, TREM2-deficiency in AD mouse models causes elevated plaque abundance at 6-7 months. Contradictory, by the age of 12 months a diminished plaque load was observed in these mice (Meilandt et al., 2020). Thus,

the detailed role of TREM2 for the onset and progression of AD still needs to be further investigated.

EOAD is often a form of familiar AD and predominantly caused by autosomal-dominant inherited variants of APP and PS1 and PS2, which were identified as EOAD risk factors. Several mutations at the secretase sites in APP or within the PSs are associated with increased amyloidogenic APP processing resulting in early AD pathology (reviewed in Dai et al., 2018). Therefore, these familiar AD mutations are the basis for AD mouse models and will be introduced in the next chapter.

1.3 Alzheimer´s disease mouse models

Since the generation of neurofibrillary tangles and Aβ plaques were identified as the hallmarks of AD and closely related to neurotoxicity, the elevation of these pathophysiological events are the basis for AD mouse models. Therefore, AD mouse models overexpressing human tau and APP under the control of strong promotors, such as the prion protein or thymus cell surface antigen 1 promoter, as well as the insertion of pathology associated mutations have been generated (reviewed in Jankowsky and Zheng, 2017). In commonly used mouse models for tau pathology, such as JNPL3 (Lewis et al., 2000) or PS19 (Yoshiyama et al., 2007), the human tau gene *MAPT* containing a point mutation at P301 is expressed under the control of the prion protein promoter. As a result, these mice develop early tau pathology which is accompanied with neuronal loss (Lewis et al., 2000; Yoshiyama et al., 2007). However, mutations in *MAPT* are only associated with a subtype of the dementia form frontotemporal labor degeneration (FTLD), thus, these models represent rather a model for FTLD than AD (Hutton et al., 1998; Spillantini et al., 1998; reviewed in Gendron and Petrucelli, 2009). Therefore, elevating the Aβ pathology has emerged as the more appropriate model for AD (reviewed in Jankowsky and Zheng, 2017). These models usually express human *APP* under the control of a strong neuronal promotor. In order to promote Aβ production, familial APP mutations, identified in EOAD patients, were established in mouse models (reviewed in Esquerda-Canals et al., 2017). The mouse models Tg2576 (Hsiao et al., 1996) and APP23 (Sturchler-Pierrat et al., 1997) were already developed in the 1990s and contain the Swedish APP (APPswe) variant with the mutations K670N and M671L proximal to the β-secretase site. APPswe is cleaved by BACE1 to a very high extend *in vitro* (Li et al., 2015) and *in vivo* (Laird et al., 2005) resulting in increased Aβ1-x levels and early Aβ deposits which results in cognitive deficits after 9-10 months of age (Hsiao et al., 1996). APPswe based models were expanded by the establishment of mutations at the γ-secretase site such as the London APP (APPlon) mutation (V717I) in the TASD-41 model. As a result, the production of predominantly Aβ1-42, which is one of the pathogenic Alzheimer-associated Aβ forms with a high potential to form aggregates,

is elevated (Rockenstein et al., 2001). These mice exhibit cognitive impairments after 6 months of age (Rockenstein et al., 2005). Nowadays, one of the most common used model is the 5xFAD mouse, which contains beyond APPswe and APPlon the Florida APP (APPflo) mutation (I716V) at the γ-secretase site, as well as two mutations (M146L, L286V) in PS1 (Oakley et al., 2006; Jawhar et al., 2012). The ensemble of these mutations leads to an early highly elevated production of predominantly Aβ1-42 resulting in the development of cognitive impairments yet between 3 and 6 months (Jawhar et al., 2012). Recent studies focus on the effects of modulating AD-risk proteins such as TREM2 and ApoE in the AD mouse model 5xFAD. Initial data indicate altered Aβ plaque morphology and cognitive function in these mouse models (Youmans et al., 2012; Liu et al., 2015; Lee et al., 2018). However, to estimate the pathophysiological role of these proteins modulating AD pathology in AD mouse models further investigation is needed.

Of note, almost all Aβ pathology-based AD mouse models contain the APPswe mutations (reviewed in Esquerda-Canals et al., 2017) . This might have contributed to the fact that BACE1 emerged as the most prevalent β-secretase, since APPswe is cleaved to a higher extend by BACE1 than wild-type APP (APPwt) (Li et al., 2015; Schlenzig et al., 2018). However, APPswe was only identified in two Swedish families (Mullan et al., 1992). Thus, investigating these common mouse models might lead to an overestimation of the role of BACE1 and, thus, may not serve as representative AD models. This hypothesis is supported by findings, which show that, although Aβ1-x levels are significantly decreased, total Aβ levels of BACE1-deficient primary neurons expressing APPwt are scarcely diminished (Nishitomi et al., 2006; Schlenzig et al., 2018).

1.4 Alzheimer´s disease treatment

To date, only symptomatic treatments for patients suffering from AD have been clinically approved (Yiannopoulou and Papageorgiou, 2020). It was observed, that cholinergic neurons in AD patient brains progressively malfunction, which results in decreased acetylcholine (ACh) synthesis (Sims et al., 1983). The reduction of ACh correlates with the severity of cognitive decay (Perry et al., 1978). Therefore, cholinesterase inhibitors delaying ACh degradation in the synaptic cleft were successfully approved, since the treatment leads to improved cognitive functions in patients with mild to moderate AD (reviewed in Hampel et al., 2018). For the treatment of moderate to severe AD, the N-methyl-D-aspartate (NMDA) agonist memantine is approved to cause a beneficial effect on cognition (Doody et al., 2007). Memantine binds the NMDA receptor with a low to moderate affinity, partially preventing an association with the neurotransmitter glutamate (Matsunaga et al., 2015). Of note, in AD glutamate levels are increased since Aβ oligomers promote glutamate release (Talantova et al., 2013). As a result,

erratic glutamate signaling promotes neurodegeneration through a process referred to as exitotoxicity, which can be compensated by NMDA agonists (Maragos et al., 1987). Moreover, non-cognitive symptoms such as depression and agitation are treated with widely used antidepressants and anxiolytics (reviewed in Yiannopoulou and Papageorgiou, 2020).
Although symptomatic AD treatment benefits cognition, these therapies do not prevent or decelerate the progression of disease. Therefore, the generation of disease-modifying agents is of great interest (reviewed in Galimberti and Scarpini, 2010). Several compounds have entered clinical trials in the past decades, however, many were declined and so far none is approved (reviewed in Yiannopoulou and Papageorgiou, 2020). In terms of interfering with tau pathology, several approaches including reducing tau expression (NCT03186989), phosphorylation (NCT01350362) and aggregation (NCT03446001) have been tested. However, clinical trials are still on-going or were discontinued due to unaltered cognitive functions of the patients (reviewed in VandeVrede et al., 2020). This also holds true for compounds interfering the Aβ pathology. Aβ targeting antibodies (NCT02477800, NCT01254773) so far did not lead to diminished cognitive impairments. γ-secretase inhibitors failed because of harmful side effects, presumably due to its essential proteolytic role on other substrates (Doody et al., 2013; Coric et al., 2015). Moreover, α-secretase enhancers were considered in clinical trials to promote the non-amyloidogenic pathway. However, the compounds failed due to lack of efficiency (Vellas et al., 2011) or the studies are still on-going (NCT03806478). The inhibition of BACE1 was considered as a promising strategy, since BACE1 deficiency leads to decreased Aβ deposition in 5xFAD mice (Hu et al., 2018) and causes only mild side effects (Roberds et al., 2001; Hu et al., 2006). However, so far all BACE1 inhibitors failed in clinical trials due to no cognitive benefit for AD patients and/or unexpected strong side effects, although Aβ levels were diminished upon administration in several studies (reviewed in Moussa-Pacha et al., 2020; reviewed in Yiannopoulou and Papageorgiou, 2020). This underlines the importance to critically question the idea of BACE1 as the most relevant β-secretase and to further characterize the role of alternative β-secretases.

1.5 The alternative β-secretase meprin β

Several proteases were proposed as alternative β-secretases, e.g. cathepsins. It was shown that cathepsins B, S, and L might be involved in Aβ generation (Schechter and Ziv, 2011; reviewed in Hook et al., 2014), whereas others considered cathepsins as Aβ degrading and thus AD protective enzymes (Mueller-Steiner et al., 2006; Letronne et al., 2016). Therefore, further investigations are necessary to show whether cathepsins play a role in AD.

Apart from cathepsins, the metalloprotease meprin β was identified as capable of cleaving APP and thereby releasing Aβ peptides. Therefore, meprin β has been emerging as a

promising alternative β-secretase in the past years (reviewed in Becker-Pauly and Pietrzik, 2016).

1.5.1 Structural properties

Meprin β is a highly glycosylated type I transmembrane protein. Together with the other meprin metalloprotease meprin α, meprin β belongs to the astacin family of the metzincin-superfamily of zinc-endopeptidases. Meprin metalloproteases consist of an N-terminal signal peptide, a propeptide, an astacin-like protease domain, a meprin A5 protein tyrosine phosphatase μ (MAM) domain and a tumour-necrosis-factor-receptor-associated factor (TRAF) domain, an epidermal growth factor (EGF)-like domain, a transmembrane region and a cytosolic tail (Fig. 4) (reviewed in Sterchi et al., 2008; reviewed in Broder and Becker-Pauly, 2013). Of note, cysteine residues in the MAM domain are responsible for the dimerization of meprin metalloproteases (Arolas et al., 2012). A striking difference between both proteases is that an additional domain, referred to as the inserted domain, is only existent in meprin α. Upon furin cleavage within the inserted domain during the secretory pathway, meprin α is secreted and prone to form large oligomers (Marchand et al., 1995; Bertenshaw et al., 2003). On the contrary, meprin β is predominantly located at the cell membrane (reviewed in Broder and Becker-Pauly, 2013).

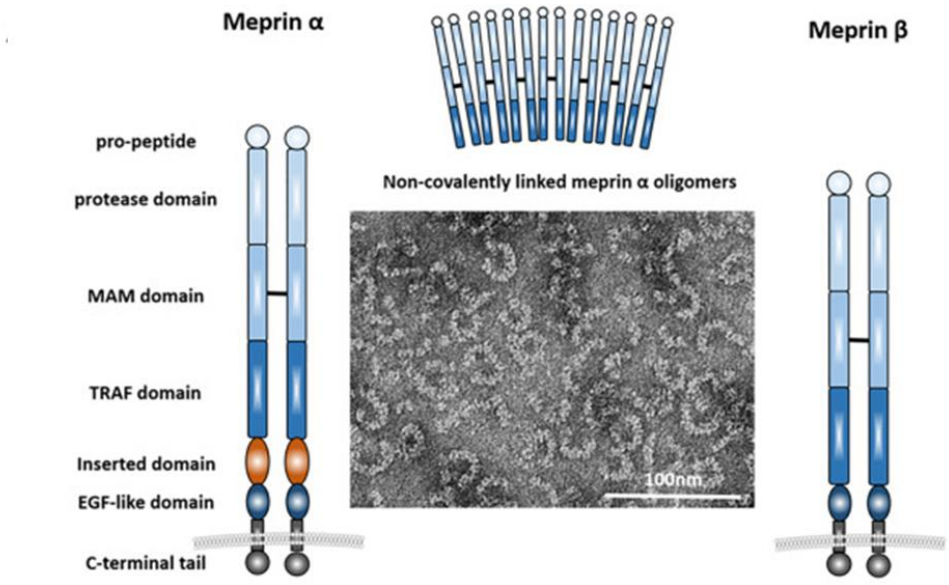

Fig. 4: Structural properties of meprin metalloproteases.

Meprin metalloproteases form dimers and consist of an N-terminal signal peptide, a pro-peptide, an astacin-like protease domain, a meprin A5 protein tyrosine phosphatase μ (MAM) domain and a tumour-necrosis-factor-receptor-associated factor (TRAF) domain, both of which are known to mediate protein–protein interactions, an epidermal growth factor (EGF)-like domain, a transmembrane region and a C-terminal tail. Meprin α exhibits an inserted domain. Since furin cleaves within the inserted domain, meprin α is secreted and prone to form large non-covalently linked oligomers. The figure was adapted from Arnold et al., 2017b.

Meprin β is expressed as a zymogen and requires tryptic activation to exhibit its proteolytic activity (Kounnas et al., 1991; Grünberg et al., 1993). Besides trypsin, matriptase-2 (MT-2) (Jäckle et al., 2015) and several kallikreins (KLKs) (Ohler et al., 2010) were identified as endogenous meprin β activators. The cleavage specificity of meprin β is mainly restricted to acidic amino acids in P1' position (nomenclature according to Schechter and Berger, 1967). This was also observed for other members of the astacin metalloprotease family (Becker-Pauly et al., 2011). With this in line, meprin β contains several positively charged amino acids in the active-site cleft (Broder and Becker-Pauly, 2013). Moreover, meprin β can be shed from the cell surface by ADAM10 and 17 (Hahn et al., 2003; Jefferson et al., 2013), however, only as inactive pro-form. Once shed, soluble pro-meprin β can be activated to obtain proteolytic activity (Wichert et al., 2017). The underlying mechanism how active meprin β escapes from shedding is unknown thus far.

1.5.2 Substrates and function

Due to its high protein expression levels in the intestine (Sterchi et al., 1982; Sterchi et al., 1988, 1988) and kidney (Beynon et al., 1981; Barnes et al., 1989), meprin β was primarily identified in these tissues. Moreover, meprin β is present e.g. in the skin (Becker-Pauly et al., 2007), leukocytes (Crisman et al., 2004) and regions of the brain (reviewed in Sterchi et al., 2008). In the past years, several physiological relevant meprin β substrates have been identified. Interestingly, membrane-bound and shed meprin β partly share a substrate pool, however, several substrates can only be cleaved by one entity. The physiological role of meprin β in the intestine is cleaving mucin-2 (MUC2), which is a main component of the mucus layer in the gut. This cleavage event is of great relevance, as it contributes to mucus homeostasis and prevents from bacterial overgrowth. Of note, only shed meprin β is capable of cleaving MUC2. Thus, diminished shedding of meprin β promotes bacterial invasion in the intestine (Wichert et al., 2017).

Several substrates of meprin β are associated with a pro-inflammatory response such as the interleukine-6 receptor (IL-6R) (Arnold et al., 2017a), which can be shed, and interleukine-18 (IL-18) (Banerjee and Bond, 2008), which can be proteolytically activated by meprin β. Another aspect of meprin β´s pro-inflammatory capacity is the cleavage of CD99 promoting transendothelial migration (TEM), which can be processed by both membrane-bound and soluble meprin β (Bedau et al., 2017).

In the skin, pro-collagen serves as a substrate for meprins, thus, they were considered as collagen maturating enzymes (Kronenberg et al., 2010). Dysregulation of meprin β is often associated with a pathogenic condition such as fibrosis (reviewed in Prox et al., 2015; Biasin

et al., 2017). Interestingly, both meprin metalloproteases are upregulated in fibrotic dermis (Kronenberg et al., 2010). Thus, the upregulation of meprins might contribute to erratic collagen fibril formation in fibrosis due to increased collagen maturation.

1.5.3 Meprin β in AD

Intriguingly, meprin β is upregulated in AD patient brains (Bien et al., 2012; Schlenzig et al., 2018). Moreover, a point mutation in the *Mep1b* gene was identified to be associated with AD (Patel et al., 2018). Therefore, meprin β might be of pathophysiological relevance for AD. It has been demonstrated, that meprin β is capable of cleaving APP at the β-secretase site resulting in Aβ generation (Bien et al., 2012; Schönherr et al., 2016). Interestingly, only membrane-bound meprin β, but not the shed form, serves as an alternative β-secretase, (Fig. 5A) (Bien et al., 2012). Since the α-secretases ADAM10 and 17 represent sheddases of meprin β, they exhibit a dual-protective role in AD by promoting the non-amyloidogenic pathway and reducing meprin β-mediated Aβ release (this aspect was part of a review published in Cellular and Molecular Life Sciences and is attached in the appendix, manuscript 5). Of note, both membrane-bound and shed meprin β are capable of cleaving APP at its N-terminus resulting in non-toxic N-terminal APP fragments (N-APPs), such as N-APP20, which were considered to play no pathophysiological role in AD (Fig. 5A) (Jefferson et al., 2011).

Characterizing the β-secretase activity of meprin β revealed that it cleaves APP independently of BACE1 (Bien et al., 2012). Interestingly, meprin β is capable of cleaving APP between M671 und D672 like BACE1, however, its main cleavage site is between D672 and A673 resulting in a release of N-terminal truncated Aβ2-x (Fig. 5B) (Bien et al., 2012). Several studies provide evidence for a pathophysiological relevance of Aβ2-x in AD, as they are highly elevated in AD patient brains (Wiltfang et al., 2001) and exhibit a strong aggregation potential (Schönherr et al., 2016). Since APPswe is expressed in common AD mouse models (reviewed in Esquerda-Canals et al., 2017), as it serves as a potent substrate for BACE1 (Deng et al., 2013), APPswe procession by meprin β was characterized. Intriguingly, APPswe is only cleaved between L671 und D672 (Fig. 5C) and thus Aβ2-x peptides were completely abolished (Schönherr et al., 2016). These findings further support the hypothesis that APPswe-based mouse models only consider the unilateral view on Aβ1-x peptides generated by BACE1, since Aβ2-x is not generated in these animals. Hence, the development of an AD mouse model considering Aβ2 x by involving meprin β without expressing APPswe is of interest.

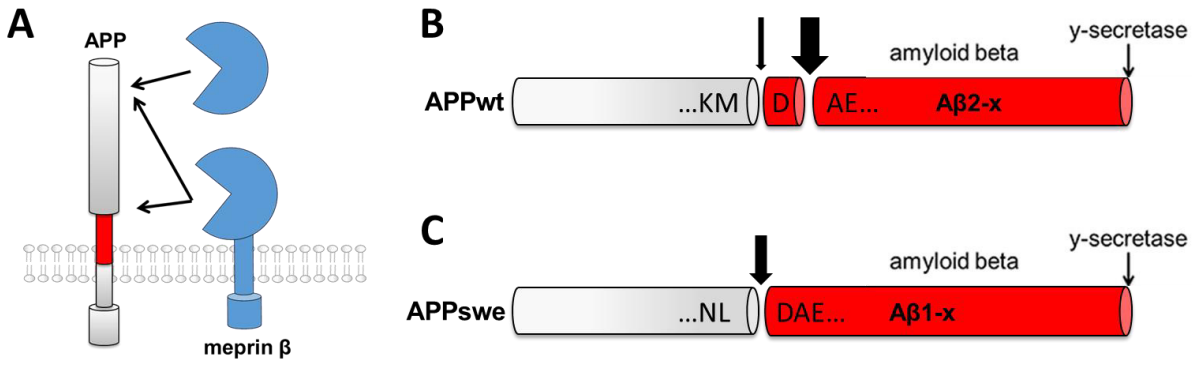

Fig. 5: APP cleavage by meprin β.
(A) Membrane-bound meprin β cleaves APP at the β-secretase site and at the N-terminus, whereas soluble meprin β is only capable of cleaving at the N-terminus. **(B)** Wild type APP (APPwt) is predominantly cleaved by meprin β between D672 and A673 releasing Aβ2-x. **(C)** Swedish APP (APPswe) is only cleaved between M671 and D672 generating Aβ1-x. The figure was adapted from Becker-Pauly and Pietrzik, 2016.

1.6. Aim of this study

It has been demonstrated that meprin β is capable of cleaving APP at the β-secretase site, which results in the release of predominantly N-terminally truncated Aβ2-x peptides (Bien et al., 2012; Schönherr et al., 2016). Since meprin β is upregulated in AD patient brains (Bien et al., 2012) and a point mutation in the *Mep1b* gene was identified to be associated with AD (Patel et al., 2018), a pathophysiological role of meprin β in AD was suggested. Therefore, this thesis aims to provide an insight into the mechanistic regulation of APP cleavage by meprin β and to evaluate the *in vivo* relevance of meprin β for the pathogenesis of AD.

In the first part of this thesis, mechanistic properties of APP cleavage by meprin β were addressed. Since the intracellular regulation of meprin β is scarcely described in literature, cytosolic phosphorylation of meprin β and its biological consequence focussing on APP cleavage were investigated. Moreover, the bacterial meprin β activator arginine-gingipain B (RgpB), which is secreted by the periodontitis-associated bacterium *Porphyromonas gingivalis* (*P. gingivalis*) (Wichert et al., 2017) was characterized with regard to APP cleavage. It has been demonstrated that *P. gingivalis* is able to colonize the brain and is related to AD pathology (Dominy et al., 2019). Therefore, it will be analyzed whether RgpB induces meprin β mediated APP cleavage. All approaches analyzing β-secretase activity of meprin β only considered APP cleavage by meprin β homodimers so far. Due to the existence of meprin α/β heterodimers, the impact of these heterodimers on APP cleavage was analyzed in this thesis. Furthermore, it was addressed whether meprin β is not only involved in the generation of Aβ, but also contributing to Aβ pathology by preventing microglia from Aβ clearance. Therefore, it was

analyzed whether the key mediator of microglial Aβ phagocytosis TREM2, is a substrate of meprin β.

The main aim of this thesis is to evaluate the pathophysiological role of meprin β in AD *in vivo*. Therefore, meprin β-based AD mouse models were generated and characterized. On the one hand, consequences of meprin β deficiency on the Aβ formation and the cognitive function were analyzed in an AD model mouse strain, which overexpresses the human APPlon variant. On the other hand, since meprin β is upregulated in AD patient brains (Bien et al., 2012; Schlenzig et al., 2018), the protease was conditionally overexpressed in wild-type (WT) mouse brains. Due to the observation that astrocytes are rather involved in the release of truncated Aβ2-x peptides than neurons (Oberstein et al., 2015), it was decided to generate a mouse model overexpressing meprin β in astrocytes. By analyzing APP cleavage and Aβ release, this thesis aims to evaluate whether the induced expression of meprin β is directly linked to amyloid pathology and can be considered as a novel AD mouse model.

2. Material and Methods

The Material and Methods section refers to the result of this thesis apart from sections 3.1.1, 3.1.3, 3.2, 3.3.1, since their experimental procedure is described in the method section of the respective attached manuscripts.

Chemicals were purchased from Carl Roth unless otherwise described. Ultrapure water was produced by *Milli-Q® Integral water purification system* and is abbreviated with ddH_2O. Unless otherwise stated, all buffers were prepared in ddH_2O. All buffers and media are summarized in Tab. 1.

Tab. 1: Buffers and media.

5x reducing sample buffer	250 mM Tris-HCl 10% (w/v) Sodium dodecyl sulphate (SDS) 0.5% Bromophenol blue (Merck) 50% (v/v) Glycerol 154 mg Dithiothreitol (DTT) pH 6.8
5x resolving gel buffer	1.5 M Tris-HCl 0.4% (w/v) SDS pH 8.8
5x stacking gel buffer	0.5 M Tris-HCl 0.4% (w/v) SDS pH 6.8
Biotinylation lysis buffer	50 mM Tris-HCl 150 mM NaCl 1% (v/v) Triton-X 100 0.1% (w/v) SDS cOmplete protease inhibitor cocktail (Merck)
BSA blocking solution	3% (w/v) Bovine serum albumine (BSA), Albumin Fraktion V in TBS
Coomassie destaining solution	40% (v/v) Methanol 10% (v/v) Acetic acid
Coomassie staining solution	0.1% (w/v) Coomassie Brilliant Blue R-250 40% (v/v) Methanol 10% (v/v) Acetic acid

ELISA blocking buffer	1% (w/v) BSA in TBS
ELISA incubation buffer	0.1% (w/v) BSA in TBS
Milk blocking solution	5% (w/v) Milk powder in TBS
OBS blocking and permeabilization solution	10% (v/v) FBS 0.5% (v/v) Triton X-100 in PBS
OBS culture medium	45% (v/v) Minimum Essentiell Medium (MEM) 25% (v/v) Horse serum 19% (v/v) HBSS 6.5 mg/mL D-(+)-Glucose 2 mM Glutamine 25 mM HEPES 100 U/mL Penicillin 100 µg/mL Streptomycin pH 7.2
OBS culture medium (serum-free)	45% (v/v) Minimum Essentiell Medium (MEM) 19% (v/v) HBSS 6.5 mg/mL D-(+)-Glucose 2 mM Glutamine 25 mM HEPES 100 U/mL Penicillin 100 µg/mL Streptomycin pH 7.2
OBS cutting medium	10 mM HEPES 100 U/mL Penicillin (Thermo Fisher Scientific) 100 µg/mL Streptomycin (Thermo Fisher Scientific) in Hanks' Balanced Salt Solution (HBSS)
PBS-CM	0.1 mM $CaCl_2$ 1 mM $MgCl_2$ in PBS
PBS	9.2 mM Na_2HPO_4 1.8 mM KH_2PO_4 135 mM NaCl 2.7 mM KCl pH 7.4
Quenching buffer	50 mM Tris-HCl, pH 8.0, in PBS-CM

RIPA lysis buffer	25 mM Tris-HCl 1% (v/v) Nonidet P-40 (NP-40) 0.5%(m/v) Sodium deoxycholate 150 mM Sodium chloride 0.1%(m/v) SDS cOmplete protease inhibitor cocktail, EDTA-free (Merck) pH 7.4
SDS-PAGE running buffer	25 mM Tris-HCl 192 mM Glycine 0.1% (w/v) SDS pH 8.3
Tank-blot buffer	25 mM Tris-HCl 200 mM Gglycine 20% (v/v) Mmethanol pH 8.3
TAE buffer	40 mM Tris-HCl 20 mM Acetic acid 1 mM EDTA pH 8
TBS	20 mM Tris-HCl 137 mM NaCl pH 7.5
TBS-T	20 mM Tris-HCl 100 mM NaCl 0.05% (v/v) Tween20 0.2% (v/v) Triton X-100 pH 7.5
Triton lysis buffer	1% (v/v) Triton-X 100 cOmplete protease inhibitor cocktail (Merck) in PBS pH 7.4
Triton lysis buffer, EDTA-free	1% (v/v) Triton-X 100 cOmplete protease inhibitor cocktail, EDTA-free (Merck) in PBS pH 7.4

IHC incubation buffer	45% (v/v) TBS 5% (v/v) Goat serum (Dianova) 0.1% (v/v) Triton-X 100 in antibody diluent sulution (Zytomed) pH 7.6

2.1 Cell cultivation

HEK (HEK293T, DSMZ), HEK ADAM10/17$^{-/-}$ (ADAM10- and ADAM17-deficient HEK293T), generated by Dr. Björn Rabe, Institute of Biochemistry, Kiel) and SH-SY5Y (DSMZ) cells were cultured under a humidified atmosphere with 5% CO_2 at 37°C. For the cultivation of HEK293T and HEK ADAM10/17$^{-/-}$ cells, Dulbecco's Modified Eagle's Medium (DMEM) (Thermo Fisher Scientific) was used. SH-SY5Y cells were maintained in DMEM/F12 (Thermo Fisher Scientific). Each medium was supplemented with 10% (v/v) fetal bovine serum (FBS) (Thermo Fisher Scientific).

2.1.1 Transient transfection

HEK293T and HEK ADAM10/17$^{-/-}$ cells were transfected with the transfection reagent polyethylenimine (PEI). Therefore, 3 µl PEI (1 mg/ml in ddH_2O, Polysciences) were used per 1 µg plasmid DNA (Tab. 2) in 50 µl serum-free DMEM. Cells cultured in T-25 flasks were transfected with 2 µg of each plasmid, for cells in 10 cm-dishes 4 µg per plasmid were used. After incubation for 30 min at room temperature, the mixture was transferred to the culture medium of selective cells. 24 h after addition of the transfection mixture, the cell culture medium was exchanged with 2 ml serum-free DMEM in case of T-25 flasks or 4 ml in case of 10-cm dishes for up to 24 h.

Tab. 2: Plasmids.

Vector	Inserted gene	Species	Tag
pcDNA3.1	-	-	-
pSG5	*MEP1B*	Human	-
pSG5	*MEP1B* E153A	Human	-
pCMV6	*Mep1b*	Mouse	-
pCIneo	*APP* (isoform 695)	Human	-
pCMV6-Entry	*App* (isoform 695)	Mouse	C-Myc, C-Flag
pJT10	*Lphn3*	Mouse	N-HA, C-Flag

2.1.2 Cell treatment for meprin β activation by RgpB

The RgpB-dependent activation of meprin β was performed in transfected HEK293T cells and 80-90% confluent SHSY5Y cells simultaneously with the change to serum-free medium by addition of 50 nM RgpB (kindly provided by AG Potempa, Louisville) for 30 min. Afterwards, the medium was again exchanged to serum-free DMEM or DMEM/F-12, respectively. In case of meprin β inhibition, 20 µM actinonin (Merck) was added. If RgpB inhibition was required, 5 µM of the cysteine protease inhibitor E-64 (Merck) was included concurrently. Cells were harvested 3 h later.

2.2 Experimental animals

Mice were maintained under a 12-hour light/12-hour dark cycle with access to water and standard mouse diet *ad libitum* in individually ventilated cages (IVCs) in accordance with the ethical standards set by the National Animal Care Committee of Germany.

2.2.1 Generation of mice overexpressing meprin β in astrocytes (GFAP^{Cre};Rosa26$^{Mep1b\text{-}HA}$)

Meprin β knock-in mice were generated in collaboration with Dr. Ronald Naumann and Dr. Michael Haase from the Max Planck Institute of Molecular Cell Biology and Genetics in Dresden as described before (Karimova et al., 2018). In summary, a cDNA coding for C-terminally HA-tagged murine meprin β was cloned into a CAG-Cre-IRES-Rosa26 vector. With the use of this vector, the cDNA was inserted into the Rosa26 locus of C57BL/6N mice by homologous recombination. Homozygous meprin β-knock-in mice are referred to as Rosa26$^{Mep1b\text{-}HA}$. A floxed neomycin-Westphal stop cassette between a CAG promotor and the meprin β cDNA preventing from transcription meprin β cDNA until it is excised by a Cre recombinase (Karimova et al., 2018). In order to achieve meprin β overexpression in astrocytes, Rosa26$^{Mep1b\text{-}HA}$ mice were crossed with mice expressing Cre recombinase under the control of the glial fibrillary acidic protein (GFAP) promoter, specifically active in astrocytes, which were described before (Zhuo et al., 2001). Rosa26$^{Mep1b\text{-}HA}$ mice, which were heterozygous for GFAP-dependent Cre are termed as GFAP$^{Cre+/-}$;Rosa26$^{Mep1b\text{-}HA}$ mice. The respective control animals were Rosa26$^{Mep1b\text{-}HA}$ mice and in this regard were referred to as GFAP$^{Cre-/-}$;Rosa26$^{Mep1b\text{-}HA}$.

2.2.2 Genotyping of GFAP^{Cre};Rosa26$^{Mep1b\text{-}HA}$

Genomic DNA from mice was isolated by digestion of ear or tail biopsies with DirectPCR-Tail (Peqlab Biotechnology GmbH) and Proteinase K (0.2 mg/ml, Thermo Fisher Scientific) over night at 55°C. The Proteinase K was heat inactivated for 1 h at 85°C. The samples were used as templates for genotyping PCRs (Tab. 3 and 4).

Tab. 3: Components of the PCR solution.

Reagents	**Quantity**
Template DNA	2 µl
Forward primer (Merck)	0.4 µM
Reverse primer (Merck)	0.4 µM
Deoxynucleoside triphosphate (dNTP) mix (Thermo Fisher Scientific)	160 µM
10x DreamTaq Buffer (Thermo Fisher Scientific)	1x
DreamTaq Polymerase (Thermo Fisher Scientific)	2.5 U
ad 25 µl with ddH_2O	

Tab. 4: PCR program.

Step	**Duration**	**Temperature**	
Initial Denaturation	1 min	95°C	
Denaturation	30 s	95°C	9x (-1°C per cycle)
Annealing	30 s	65°C	
Synthesis	30 s	72°C	
Denaturation	30 s	95°C	25x
Annealing	30 s	56°C	
Synthesis	30 s	72°C	
Final elongation	3 min	72°C	

Primers for genotyping of Rosa26$^{Mep1b\text{-}HA}$ were designed by Florian Peters (AG Becker-Pauly, Kiel) (Tab. 5). For GFAP^{Cre} genotyping primers were used according to the guidelines from The Jackson Laboratory.

Tab. 5: Genotyping primers.

Primer name	Sequence	Target recognition
Rosa26_fwd	5‘-AAA GTC GCT CTG AGT TGT TAT C-3’	Rosa26$^{Mep1b\text{-HA}}$
Rosa26_wt_rev	5‘-GAT ATG AAG TAC TGG GCT CTT-3’	
Rosa26_tg_rev	5‘-TGT CGC AAA TTA ACT GTG AAT C-3’	
GFAP^{Cre}_fwd	5’-TCC ATA AAG GCC CTG ACA TC-3’	GFAP$^{Cre+/-}$
GFAP^{Cre}_rev	5’-TGC GAA CCT CAT CAC TCG T-3’	

The samples were mixed with 6x Loading Dye (Thermo Fisher Scientific) and analyzed with a 2% (w/v) agarose gel in tris-acetate-EDTA (TAE) buffer supplemented with SYBR™ Safe DNA Gel Stain (Thermo Fisher Scientific) at 100 V for 30 min. Specific amplificates were detected with a UV transilluminator (Intas Science Imaging). Expected band sizes of the PCR products for Rosa26$^{Mep1b\text{-HA}}$ are 570 bp for the wildtype allele and 380 bp for the transgenic allele. A signal for GFAP^{Cre} positive PCR products occurs at 400 bp.

2.2.3 Generation and cultivation of organotypic brain slices

In order to generate organotypic brain slices (OBSs), 7 to 63 weeks old mice were sacrificed by cervical dislocation in accordance with the Guide for the Care and Use of Laboratory Animals (German Animal Welfare Act on Protection of Animals). The head was disinfected in 70% (v/v) ethanol for 1 min and the brain was removed. Afterwards, the brain was sagitally cut in the middle of one hemisphere with a razorblade. The cut side was subsequently glued on the specimen plate of a vibratome (VT1200S, Leica) proximal to a fixed 1 cm³ block of 2% (w/v) agarose with the thalamus facing to the block. The specimen plate was set into its fixture within the vibratome filled with OBS cutting medium. Using the vibratome, 180 µm (for immunofluorescence analysis) or 250 µm (for the generation of lysates) thick sagittal OBSs were generated with a speed of 0.03 mm/s and an amplitude of 3 mm. The OBSs were transferred on a membrane insert with a pore size of 0.4 µm (Greiner AG) in a 6-well plate and cultivated in 1.8 ml OBS culture medium (2 slices per membrane insert) for 14 to 35 days. The brain slices were incubated at 37° in a 5% CO_2 humidified incubator, changing half of the medium every three days. In order to avoid meprin β inhibition by serum components, the OBSs culture medium was substituted by serum-free OBS culture medium for 24 h for several experiments. For meprin β activity measurements and Western Blot analyzes the serum-free medium was applied 24 h prior lysis, except for the Western Blot analyzes of caspase-3. In this case, the medium was changed at day 19 of culture independent of the harvest day. The establishment of the OBS cultivation was part of Kira Bickenbach’s Master thesis. Therefore, the OBS experiments were conducted by her.

2.3 Lysis of cells, whole mouse brains and organotypic brain slices

Cells were washed twice with PBS and subsequently incubated in triton lysis buffer (EDTA-free lysis buffer was used, whenever a meprin β activity assay was applied) for 30 min. Mouse brains were isolated from mice sacrificed with cervical dislocation according to the Guide for the Care and Use of Laboratory Animals (German Animal Welfare Act on Protection of Animals). Afterwards, the brains were homogenized in triton lysis buffer (EDTA-free lysis buffer was used, whenever a meprin β activity assay was applied) using the Precellys® 24 (VWR) for 3 cycles at 3,000 rpm and 4°C. The homogenates were incubated for 1 h at 4°C. OBSs were transferred into reaction tubes and incubated for 1 h at 4°C in triton lysis buffer (EDTA-free lysis buffer was used, whenever a meprin β activity assay was applied). The debris was removed from cell, mouse brain and OBS lysates by centrifugation for 15 min at 16,000 g and 4°C. The protein concentration of all lysates was determined using Pierce™ BCA Protein Assay Kit (Thermo Fisher Scientific) according to the manufacturer´s instructions.

2.4 Cell surface biotinylation assay

In order to label cell surface proteins with biotin, transfected cells in a 10 cm-dish were cultivated in serum-free DMEM for 4 h. After a washing step with PBS-CM, 3 ml of Sulfo-NHS-SS-Biotin (1 mg/ml in PBS-CM; Thermo Fisher Scientific) were applied for 30 min at 4°C. Then, the biotin solution was removed and 10 ml quenching buffer was added for 10 min at 4°C. After washing the cells with PBS-CM, they were lysed in 300 µl biotinylation lysis buffer for 30 min at 4°C. The debris was removed by centrifugation for 15 min at 16,000 g and 4°C. 100 µl of the lysate was used for protein concentration determination using Pierce™ BCA Protein Assay Kit (Thermo Fisher Scientific) and as lysate control in Western blot analyzes. The remaining lysate was incubated with 50 µl of Pierce™ Streptavidin Magnetic Beads (Thermo Fisher Scientific) overnight at 4°C. After washing the beads, they were incubated with 1x sample buffer at 95°C for 10 min as preparation for SDS-PAGE and ensuing Western blot.

2.5 Meprin β activity assay

In order to quantify the enzymatic activity of meprin β, a quenched fluorescent peptide consisting of alternating glutamate and aspartate residues with an N-terminal fluorophore and a C-terminal quencher ((mca)-EDEDED-(K-ε-dnp), Genosphere Biotechnologies; mca - 7-methyloxycoumarin-4-yl, dnp - dinitrophenyl) was used. Due to meprin β's strong preference for acidic amino acids, this peptide is specifically cleaved by the protease (Becker-Pauly et al., 2011; Broder and Becker-Pauly, 2013). For the measurement of the meprin β activity at the cell surface, 5×10^5 transfected HEK293T cells or 1×10^6 SHSY5Y were used after the cultivation in serum-free medium, washed twice with PBS and measured in 300 µl PBS. To

determine the meprin β activity in whole mouse brain lysates, 1 µg was analyzed in 100 µl triton lysis buffer (EDTA-free). For the measurement of meprin β activity in OBSs lysates, 300 µg were prepeared in 100 µl triton lysis buffer (EDTA-free). For each experiment 50 µM of (mca)-EDEDED-(K-ε-dnp) were added. The relative fluorescent units (RFUs) were measured with a fluorescence reader (InfiniteF200Pro or Spark™, Tecan) (emission wave length: 405 nm, excitation wavelength: 320 nm) every 30 s for the duration of 2 h, which is proportional to the meprin β activity. In order to avoid the contribution of photobleaching or other unspecific alterations of the measured fluorescence, RFU values of the respective solvent mixed with 50 µM (mca)-EDEDED-(K-ε-dnp) were determined over 2 h and subtracted from each RFU value of the measured samples. The values for meprin β activity represented in this thesis comprise the slope of the linear range, which were normalized.

2.5 SDS-PAGE

For the sodium dodecyl sulfate polyacrylamide gel electrophoresis (SDS-PAGE) with ensuing Western blot to detect sAPPα, Aβ and N-APP20, the NuPAGE™-system (Thermo Fisher Scientific) with 12% (v/v) acrylamide gels was used (Tab. 6). For all other applications the Mini-PROTEAN® system (Bio-Rad) with 7.5 or 10% (v/v) was applied (Tab. 7).

Tab. 6: Composition of SDS-PAGE gels of the NuPAGE™ system.

Component	**Resolving gel 12% (v/v)**	**Stacking gel 4% (v/v)**
ddH_2O	3.39 ml	1.85 ml
5x Bis-Tris buffer	2.48 ml	790 µl
ROTIPHORESE®Gel 30 (37,5:1)	3.96 ml	390 µl
10% (w/v) Ammonium persulphate (APS)	49.6 µl	30 µl
10% (v/v) Tetramethylethandiamin (TEMED)	165 µl	75 µl

Tab. 7: **Composition of SDS-PAGE gels of the Mini-PROTEAN® system.**

Component	**Resolving gel**		**Stacking gel**
	7.5% (v/v)	**10% (v/v)**	**4% (v/v)**
ddH_2O	3.64 ml	3.21 ml	2.44 ml
5x Resolving gel buffer	2 ml	2 ml	-
5x Stacking gel buffer	-	-	1 ml
ROTIPHORESE®Gel 30 (37,5:1)	2 ml	2,67 ml	510 µl

10% (w/v) APS	80 µl	80 µl	50 µl
10% (v/v) TEMED	80 µl	80 µl	50 µl

Each sample was incubated with 5x sample buffer at 95°C for 10 min prior loading onto SDS gels. 30 µg of cell lysate or 50 µg of mouse brain lysate or OBS lysate was used for SDS-PAGE. The electrophoresis was performed at 90 V for 120 min in MES buffer (Thermo Fisher Scientific) in case of the NuPAGE™ system or Lämmli running buffer, when the mini-PROTEAN® system was used. The separated proteins were stained with Coomassie staining solution for 1 h and destained using Coomassie destaining solution for 8-24 h or transferred to a membrane via Western blot.

2.6 Protein detection by Western blot

After conducting the SDS-PAGE, the separated proteins were transferred onto a polyvinylidene difluoride (PVDF) membrane (Thermo Fisher Scientific) by tank blotting (200 mA per membrane, 2 h, 4°C). Afterwards, the membrane was blocked in milk blocking solution for 1 h and washed with TBS-T. The primary antibody was applied with the respective dilution (Tab. 8) in BSA blocking solution over night at 4°C. After another washing step with TBS-T, the secondary antibody was applied diluted in TBS (Tab. 9). The signal detection was conducted with the LAS-3000 mini system (Fujifilm) using SuperSignal™ West Femto Maximum Sensitivity Substrate (Thermo Fisher Scientific) and SuperSignal™ West Pico PLUS Chemiluminescent Substrate (Thermo Fisher Scientific).

Tab. 8: **Primary antibodies used for Western blot analyzes.**

*The antibody was generated against a peptide from the MAM domain of meprin β. **The sAPPβ+1 antibody was generated against the neo-C-terminus of sAPPβ+1, which is released after APP cleavage by meprin β between D672 and A673. sAPPβ+1 is one amino acid C-terminally extended compared to sAPPβ generated by BACE1.

Antibody	**Source**	**Species**	**Dilution**
Meprin β (Tier1)*	Pineda Antikörper-Service	Rabbit	1:1,000
sAPPβ+1 (Tier3)**	Pineda Antikörper-Service	Rabbit	1:1,000
APP (CT-15)	AG Pietrzik, Mainz	Rabbit	1:5,000
APP (22C11)	Thermo Fisher Scientific	Rabbit	1:1,000
GAPDH (14C10)	Cell Signaling	Rabbit	1:5,000
SEZ6 (14E5)	AG Lichtenthaler, München	Rat	1:1,000
murine Aβ/sAPPα (Poly18058)	Biolegend	Rabbit	1:1,000
BACE1 (A17035K)	Biolegend	Mouse	1:1,000

LPHN3 (B-6)	Santa Cruz	Mouse	1:500
HA-tag (C29F4)	Cell Signaling	Mouse	1:1,000
Caspase-3 (8G10)	Cell Signaling	Rabbit	1:1,000
TFR (ab84036)	Abcam	Mouse	1:1,000

Tab. 9: **Secondary antibodies used for Western blot analyzes.**

Antibody	**Source**	**Species**	**Dilution**
Anti-mouse IgG (H+L)-HRP	Jackson Immuno Research	Sheep	1:10,000
Anti-rabbit IgG (H+L)-HRP	Jackson Immuno Research	Goat	1:10,000
Anti-rat IgG (H+L)-HRP	Jackson Immuno Research	Goat	1:10,000

2.7 Aβ quantification by ELISA

In order to quantify various Aβ species independent of the N-terminus, the Aβx-40 ELISA (LEGEND MAX™ β-Amyloid x-40 ELISA Kit with pre-coated plate; Biolegend) and Aβx-42 ELISA (LEGEND MAX™ β-Amyloid x-42 ELISA Kit with pre-coated plate; Biolegend) were used according to the manufacturer´s instructions diluting the samples 1:10. After the sale of both ELISA Kits was discontinued by Biolegend, an equal Aβx-40 and Aβx-42 sandwich ELISA was developed. For this purpose, 1 µg/ml anti-β-Amyloid, 1-40 (Clone: 11A50-B10; Biolegend) or 1 µg/ml anti-β-Amyloid, 1-42 (Clone: 12F4; Biolegend) diluted in PBS was used as coating antibody and transferred to a Nunc MaxiSorp™ Flat-Bottom Plate (Thermo Fisher Scientific) and incubated overnight at 4°C. Afterwards the wells were washed three times with 300 µl TBS buffer and subsequently incubated with ELISA blocking buffer for 2 h at room temperature. Following another washing step, the samples were applied with a dilution of 1:10 together with 0.5 µg/ml of the detection antibody APP (4G8)-HRP (Biolegend) in a total volume of 100 µl ELISA incubation buffer. After incubating over night at 4°C, the wells were washed five times with 300 µl TBS. The color development was achieved applying 100 µl tetramethylbenzidine (TMB) substrate from the Substrate Reagent Pack (R&D) for 5-10 min. The reaction was stopped with 50 µl of 1 M sulphuric acid.

2.8 Immunohistochemistry of mouse brain sections

The immunohistochemistry (IHC) staining was conducted in collaboration with Hermann Altmeppen (Institute of Neuropathology, Hamburg). Brains were dissected from one-year-old GFAP$^{Cre+/-}$;Rosa26$^{\textit{Mep1b}\text{-HA}}$ and GFAP$^{Cre-/-}$;Rosa26$^{\textit{Mep1b}\text{-HA}}$ mice and fixed in 4% paraformaldehyde (PFA) in PBS overnight. The samples were dehydrated using ethanol

as well as xylene-based solutions and, afterwards, the tissue was embedded in low melting point paraffin according to standard laboratory procedures. 3 µm-thick sections were generated, deparaffinated and immunostained using the Ventana Benchmark XT machine (Ventana, Roche Diagnostics). For this purpose, the sections were boiled in CC1 buffer (Ventana, Roche Diagnostics) for antigen retrieval according to the manufacturer's instructions. The sections were incubated with primary antibodies (Tab. 10) in IHC incubation buffer for 1 h at 4°C. The secondary antibody was applied using the anti-rabbit histofine Simple Stain MAX PO Universal immunoperoxidase polymer (Nichirei) or Mouse Stain Kit (Nichirei) according to the manufacturer's instructions. The detection was conducted with the Ultra View Universal DAB Detection Kit (Ventana, Roche Diagnostics) according to the standard settings of the machine. Sections from GFAP$^{Cre+/-}$;Rosa26$^{Mep1b\text{-}HA}$ and GFAP$^{Cre-/-}$;Rosa26$^{Mep1b\text{-}HA}$ were stained in one run to achieve identical conditions. The counterstaining was also conducted by the machine according to the standard settings.

Tab. 10: **Primary antibodies used for IHC analyzes.**

Antibody	Source	Species	Dilution
GFAP (M0761)	Dako	Mouse	1:200
Iba-1 (019-19741)	Wako	Rabbit	1:500
NeuN (MAB377)	Merck	Mouse	1:50
β-Amyloid (4G8)	Biolegend	Mouse	1:100
HA-tag (C29F4)	Cell Signaling	Rabbit	1:100

2.9 Immunofluorescence microscopy of OBSs

For immunofluorescence staining of OBSs, 180 µm thick slices were cultivated for 14 d. The medium was removed and the OBSs were fixed using 4% (m/v) PFA in PBS at 4°C overnight. Afterwards, the OBS were cut out with a few millimeters of surrounding membrane and transferred to a 24-well plate. The OBSs were washed three times with PBS for 5 min and incubated with OBS blocking and permeabilization solution for 5 h at room temperature. Antibodies against GFAP (ASTRO6, 1:200, Thermo Fisher Scientific) and HA-tag (C29F4, 1:1,000, Cell Signaling) were diluted in PBS and incubated with the OBSs over night at 4°C. After four washing steps for 20 min with PBS, the OBSs were incubated with Donkey anti-Mouse IgG Alexa Fluor® 488 (Thermo Fisher Scientific) and Donkey anti-Rabbit IgG Alexa Fluor® 594 (Thermo Fisher Scientific) diluted 1:300 in PBS for 5 h at room temperature. After another washing step with PBS (four times for 20 min), the slices were incubated with 1 µg/ml DAPI in PBS for 5 min at room temperature followed by another three washing steps for 5 min.

Afterwards, the OBSs were mounted using Fluorescence Mounting Medium (Dako) and analyzed with the confocal microscope FV1000 (Olympus).

2.10 Identification of new meprin β substrates in murine astrocytes

For the identification of new meprin β substrates in murine astrocytes a terminal amine isotopic labeling of substrates (TAILS) analysis was conducted in collaboration with Tomas Koudelka (AG Tholey, Institute of Experimental Medicine, Kiel). For this purpose, the brains of three GFAP$^{Cre+/-}$;Rosa26$^{Mep1b\text{-}HA}$ and GFAP$^{Cre-/-}$;Rosa26$^{Mep1b\text{-}HA}$ mice were isolated and lysed in RIPA lysis buffer. The protein concentration was determined using Pierce™ BCA Protein Assay Kit (Thermo Fisher Scientific) according to the manufacturer´s instructions. 2.5 mg protein of each sample was precipitated by the addition of a 9-fold volume of ethanol. The pellets were incubated for 2 h at -20°C and subsequently centrifuged at 16,000 g for 20 min. 300 µL of 6 M guanidine hydrochloride in 100 mM tris(2-carboxyethyl)phosphine (TCEP) was added to the pellets and these were dissolved on ice with the aid of sonication (5 min). After a centrifugation step at 21,100 g for 5 min at 4°C, the supernatants were removed and BCA analysis was performed to determine the protein concentration. 100 µg of each sample was reduced with 5 mM TCEP for 30 min at 65°C and then alkylated with 12.5 mM iodoacetamide at room temperature for 30 min. The samples were labeled with Tandem Mass Tag (TMT) reagent in equal volume of dimethyl sulfoxide (DMSO). The samples were left to react for 1 h at 25°C and then quenched with 8 µl of 5% (m/v) hydroxylamine for 30 min at 37°C. All channels were combined and the sample was chloroform/methanol/water precipitated. The pellet was washed with methanol and then re-dissolved in 3 M guanidine hydrochloride and then diluted to a final concentration of approximately 0.85 M. The sample was digested with trypsin (approximately 50:1 ratio of protein to enzyme) overnight at 37°C. The sample was cleaned using a C-18 column and eluted with elution buffer (80% (v/v) acetonitrile (ACN) 0.1% (v/v) trifluoracetate (TFA)). Approximately 60 µg of the sample was used for Pre-TAILS, while for the rest of the sample the Hydrophobic Tagging-Assisted N-termini Enrichment strategy (HYTANE) was applied for depleting and the neo-N-termini generated employing trypsin digestion. The samples were dissolved in 200 mM HEPES buffer (pH 7). Then, hexadecanal (500 µL, 10 mg/mL) in isopropanol was added along with 20 mM sodium cyanoborohydride and the reaction left for 4 h at 50°C followed by 37°C overnight. 20 mM sodium cyanoborohydride was added and the sample was dried down. Afterwards, it was resuspended in loading buffer (3% ACN, 0.1% TFA) and cleaned with a C-18 column. The sample was dried down and stored at -20°C prior to analysis. The experiment was performed twice.

For the mass spectrometry (MS) analysis, the samples were injected in duplicates on a Dionex Ultimate 3000 nano-UHPLC coupled to a Q Exactive mass spectrometer (Thermo Scientific, Bremen). The samples were washed on a trap column (Acclaim Pepmap 100 C-18, 5 mm x 300 µm, 5 µm, 100 Å, Dionex) for 4 min with washing solution (3% (v/v) ACN, 0.1% TFA) at a flow rate of 30 µl/min prior to peptide separation using an Acclaim PepMap 100 C18 analytical column (50 cm × 75 µm, 2 µm, 100 Å, Dionex). A flow rate of 300 nl/min using eluent A (0.05% formic acid (FA)) and eluent B (80% ACN,0.04% FA) was used for gradient separation (180-minute gradient, 5-40% eluent B). Spray voltage applied on a metal-coated PicoTip emitter (10 µm tip size, New Objective, Woburn, Massachusetts, US) was 1.7 kV with a source temperature of 250°C. Full scan MS spectra were acquired between 300 and 2,000 m/z at a resolution of 70,000 at m/z 400. The ten most intense precursors with charge states greater than 2+ were selected with an isolation window of 1.4 m/z and fragmented by HCD with normalized collision energies of 33 at a resolution of 17,500. Lock mass (445.120025) and dynamic exclusion (30 seconds) were enabled.

The MS raw files were processed by Proteome Discoverer 2.4 (Thermo, version 2.4.1.15) and MS/MS spectra were searched using the Sequest HT algorithm against a database containing common contaminants and the canonical mouse database. The enzyme specificity was set to semi-ArgC with two missed cleavages allowed. An MS1 tolerance of 10 ppm and a MS2 tolerance of 0.02 Da was implemented. Oxidation (15.995 Da) of methionine residues, acetylation (42.011 Da) and TMT6plex (229.163 Da) on the peptide N-terminus was set as a variable modification while carbamidomethylation (57.02146 Da) on cysteine residues and TMT6plex on lysine residues was set as a static modification. Technical injection replicates were set as fractions. Minimal peptide length was set to 6 amino acids and the peptide false discovery rate (FDR) was set to 1%. Normalized, scaled abundance from Proteome Discoverer were exported, log 2 transformed and statistical analysis (t-test) performed in Perseus (Perseus_1.6.10.43). To compensate for the multiple testing hypothesis, a permutation based FDR value of 0.05 and s0 value of 0.1 (in essence a fold change) value were utilized.

2.11 Statistical analysis and illustrations

All statistical analyzes were performed with the GraphPad Prism 5 software. In case of two data sets, a t-test was applied. For more than two data sets, a one-way analysis of variance (ANOVA) with Tukey post-test was used, when data sets of one independent categorical variable was analyzed. The examination of data sets of two different categorical independent variables of two or more data sets was accomplished with a two-way ANOVA followed by a Bonferroni post-test (ns: $p > 0.05$; *: $p \leq 0.05$; **: $p \leq 0.01$; ***: $p \leq 0.001$; ****: $p \leq 0.0001$).
The figures were created with Microsoft PowerPoint and BioRender.com.

3. Results

3.1 Mechanistic regulation of APP processing by meprin β

3.1.1 Phosphorylation of meprin β leads to its internalization and degradation

Meprin β is an alternative β-secretase capable of cleaving APP at the β-secretase site *in vitro* and *in cellulo*. As a result, the Aβ peptide is released, which is prone to form neurotoxic aggregates (Bien et al., 2012; reviewed in Becker-Pauly and Pietrzik, 2016; Schönherr et al., 2016). Of note, only membrane-bound meprin β, but not its shed form, is able to cleave APP at the β-secretase site (Bien et al., 2012) (Fig. 6A). The extracellular regulation of meprin β has been intensively studied. Thus, activators, such as trypsin (Kounnas et al., 1991), MT-2 (Jäckle et al., 2015) and KLKs (Ohler et al., 2010), sheddases, such as ADAM10 (Herzog et al., 2014) and ADAM17 (Hahn et al., 2003) and inhibitors, including actinonin (Kruse et al., 2004) and fetuin-B (Karmilin et al., 2019) were identified and mechanistically characterized. However, the intracellular regulation of meprin β has been barely analyzed until now. Phosphorylation, as an important intrinsic regulatory event, was only addressed in one publication describing the phosphorylation of S687 in a phorbol 12-myristate 13-acetate (PMA) dependent manner (Hahn et al., 2003) (Fig. 6B). Based on this finding, one aim of this study was to analyze whether meprin β contains more phosphorylation sites apart from S687 and to evaluate consequences of phosphorylation for meprin β biology.

In order to validate meprin β phosphorylation, COLO320 and SH-SY5Y cells, which express meprin β endogenously, were stimulated with PMA. Using a phospho-serine-specific antibody in Western blot analyzes, meprin β phosphorylation was observed (Fig. 6C). Moreover, two meprin β variants were generated by mutating each potential cytosolic phosphorylation site. On the one hand, serine as well as threonine residues were substituted by alanine and, additionally, tyrosine residues were exchanged by phenylalanine in order to obtain a variant with blocked cytosolic phosphorylation. This variant is referred to as eachAF. On the other hand, in a variant, which is termed eachE, all cytoplasmic potential phosphorylation sites were replaced by glutamate residues. Since glutamate side chains contain a negative charge in a similar distance to the backbone as phosphorylated amino acids, this variant mimics constitutive cytosolic phosphorylation. HEK ADAM10/17$^{-/-}$ cells were transiently transfected with these variants and treated with PMA. Of note, ADAM10/17-deficient cells were used to enhance cell surface localization of meprin β by avoiding ectodomain shedding. Cell lysates were analyzed with a phosphate affinity SDS-PAGE. In this type of electrophoresis, phosphorylated proteins constantly interact with an acrylamide-linked Phos-tag™ during migration. Therefore, phosphorylated proteins migrate slower than the corresponding unphosphorylated protein fraction and occur as separate band of higher molecular weight.

Using phosphate affinity electrophoresis, phosphorylation of meprin β was observed ten minutes upon PMA stimulation (Fig. 6D). The meprin β variants eachAF and eachE with substituted cytoplasmic phosphorylation sites remained unphosphorylated. Therefore, phosphorylation is restricted to the cytoplasmic part of meprin β. In addition, the catalytically inactive meprin β variants E153A and R61S were analyzed. While meprin β E153A contains a mutation in the active site preventing from substrate cleavage, the R61S mutations avoids pro-peptide cleavage by proteolytic activators. Of note, phosphorylation of the R61S variant was barely detectable, whereas meprin β WT and E153A were found to be phosphorylated (Fig. 6E). These results indicate that maturated meprin β is more prone to phosphorylation than its inactive zymogen. Moreover, the meprin β variants S687R, S688A and S687R/S688A were analyzed, which were previously characterized (Hahn et al., 2003). In contrast to the results from Hahn *et al*. describing S687 as the only phosphorylation site, in this study, phosphorylation of all variants S687R, S688A and S687R/S688 was observed indicating that meprin β contains more phosphorylation sites than previously expected (Fig. 6F).

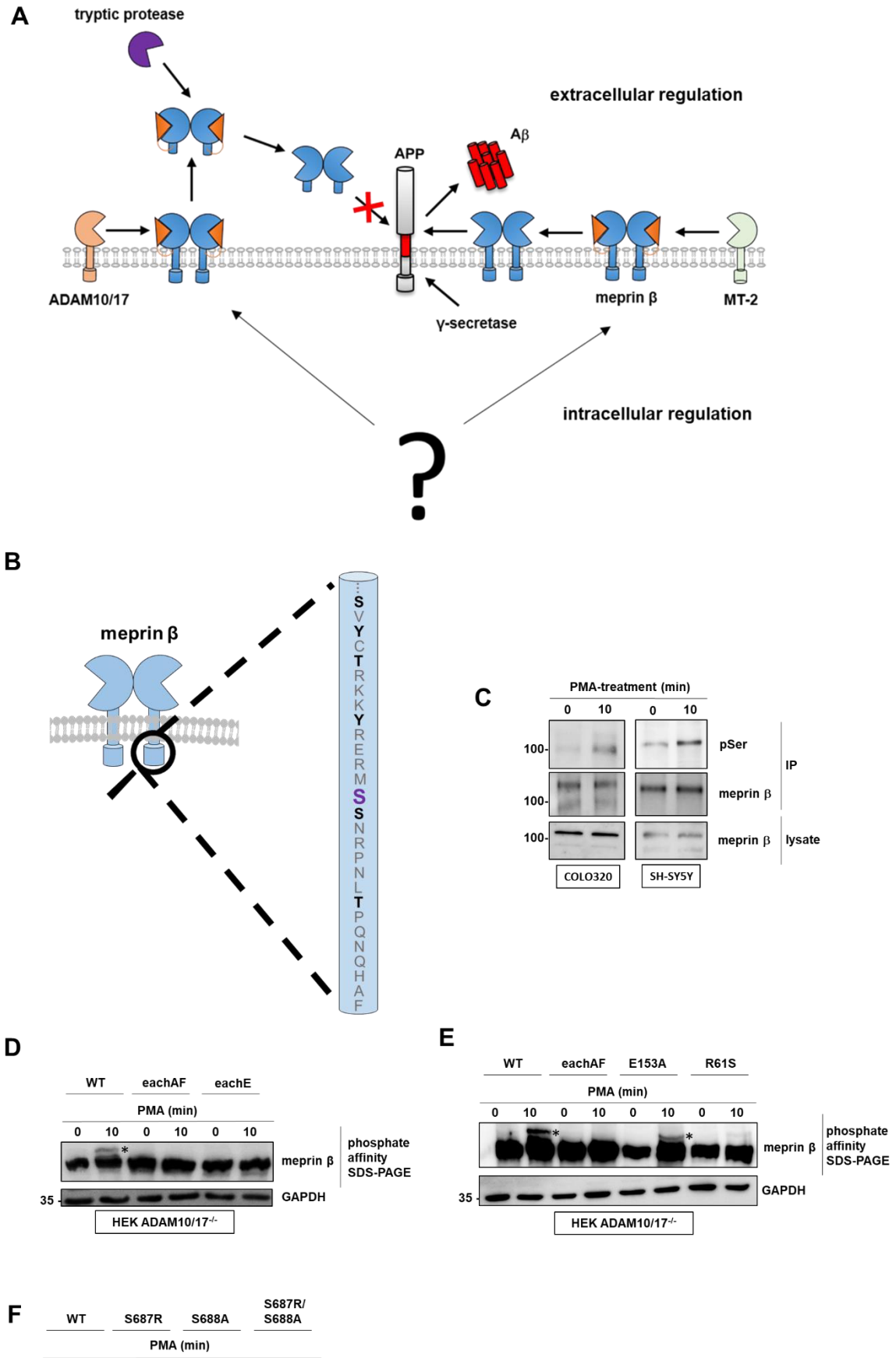
A
tryptic protease
extracellular regulation
APP
Aβ
ADAM10/17
meprin β
MT-2
γ-secretase
intracellular regulation
?
B
meprin β
S V Y C T R K K Y R E R M S S N R P N L T P Q N Q H A F
C
PMA-treatment (min)
0 10 0 10
100
pSer
IP
100
meprin β
100
meprin β
lysate
COLO320
SH-SY5Y
D
WT eachAF eachE
PMA (min)
0 10 0 10 0 10
meprin β
phosphate affinity SDS-PAGE
35
GAPDH
HEK ADAM10/17-/-
E
WT eachAF E153A R61S
PMA (min)
0 10 0 10 0 10 0 10
meprin β
phosphate affinity SDS-PAGE
35
GAPDH
HEK ADAM10/17-/-
F
WT S687R S688A S687R/ S688A
PMA (min)
0 10 0 10 0 10 0 10
meprin β
phosphate affinity SDS-PAGE
35
GAPDH
HEK ADAM10/17-/-

Fig. 6: Meprin β is phosphorylated at its cytoplasmic part in a PMA-dependent manner.
(A) Meprin β is expressed as zymogen at the cell surface. A disintegrin and metalloprotease 10 and 17 (ADAM10/17) act as sheddases of pro-meprin β. Shed meprin β can be activated by tryptic proteases, however, is not capable of cleaving APP at the β-secretase site. Alternatively, inactive membrane-bound meprin β can be maturated by the serine protease matriptase-2 (MT-2). Once activated at the cell surface, membrane-bound meprin β cannot be shed anymore and acts as β-secretase, which contributes to the generation of amyloid-β (Aβ). The scheme was generated based on findings from (Hahn et al., 2003; Bien et al., 2012; Herzog et al., 2014; Jäckle et al., 2015). **(B)** The amino acid sequence of the meprin β C-terminus is depicted. Potential phosphorylation sites are highlighted in back, the previously identified phosphorylation site S687 (according to (Hahn et al., 2003)) is labeled in purple. **(C)** COLO320 and SH-SY5Y cells were cultivated for 24 h in serum-free DMEM and treated with 100 ng/ml PMA for 10 min. After cell lysis, meprin β was immunoprecipitated and analyzed by SDS-PAGE and Western blot using the antibodies pSer (1603) and meprin β (Tier1). **(D)** ADAM10/17-deficient HEK cells were transfected with meprin β WT, eachAF or eachE. After changing the medium to serum-free DMEM for 24 h, the cells were treated with 100 ng/ml PMA for 10 min. After cell lysis, the samples were analyzed by phosphate affinity electrophoresis and Western blot using the antibodies meprin β (Tier1) and GAPDH (14C10). Phosphorylated protein fractions are highlighted with asterisks. **(E)** ADAM10/17-deficient HEK cells were transfected with meprin β WT, eachAF, E153A or R61S. After changing the medium to serum-free DMEM for 24 h, the cells were treated with 100 ng/ml PMA for 10 min. After cell lysis, the samples were analyzed by phosphate affinity electrophoresis and Western blot using the antibodies meprin β (Tier1) and GAPDH (14C10). Phosphorylated protein fractions are highlighted with asterisks. **(F)** ADAM10/17-deficient HEK cells were transfected with meprin β WT, S687R, S688A or S687R/S688A. After changing the medium to serum-free DMEM for 24 h, the cells were treated with 100 ng/ml PMA for 10 min. After cell lysis, the samples were analyzed by phosphate affinity electrophoresis and Western blot using the antibodies meprin β (Tier1) and GAPDH (14C10). Phosphorylated protein fractions are highlighted with asterisks. Adapted from Armbrust et al., submitted (appendix, manuscript 1).

In order to identify C-terminal phosphorylation sites of meprin β in an unbiased approach, liquid chromatography-mass spectrometry (LC-MS) measurements were conducted. To get insight into phosphorylation of endogenously expressed meprin β, COLO320 cells were stimulated with PMA and immunoprecipitated meprin β was analyzed. Of note, a C-terminal peptide from S687 to F701 was identified with phosphorylation sites at S687, S688 and T694 upon digestion with CNBr (Fig. 7A). The extracted ion chromatograph of the phosphopeptide revealed a dominant peak corresponding to phosphorylation at T694 as well as a minor double-peak representing phosphorylation of S687/S688 (Fig. 7B). However, from the spectra, it was not possible to determine whether S687 or S688 were phosphorylated, but due to the double-peak, phosphorylation at both sites is presumable. The digestion of meprin β from PMA-treated COLO320 cells with additional proteases validated T694 as the dominant phosphorylation site. In addition, meprin β from PMA-treated transfected HEK cells were analyzed, since not all C-terminal potential phosphorylation sites were covered by the peptides identified from meprin β from COLO320 cells. Of note, a phosphorylated C-terminal peptide from L672 to L693 was identified covering all potential phosphorylation sites, which were not found in the C-terminal peptides from COLO320 cells (Fig. 7C and D). A separate LC-MS run was performed utilizing an inclusion list to acquire a high number of MS2 spectra of the phosphopeptide. However,

due to insufficient coverage of the respective b- and y-ion series, the phosphorylation site remained ambiguous with phosphorylation possible at Y682 and S687. Phosphorylation at S687 was more presumably as 22 peptide-spectrum matches (PSMs) were identified for this residue (Fig. 7E). However, for Y682 only five PSMs were obtained. In summary, the LC-MS results provide evidence for multiple phosphorylation sites in the cytoplasmic region of meprin β.

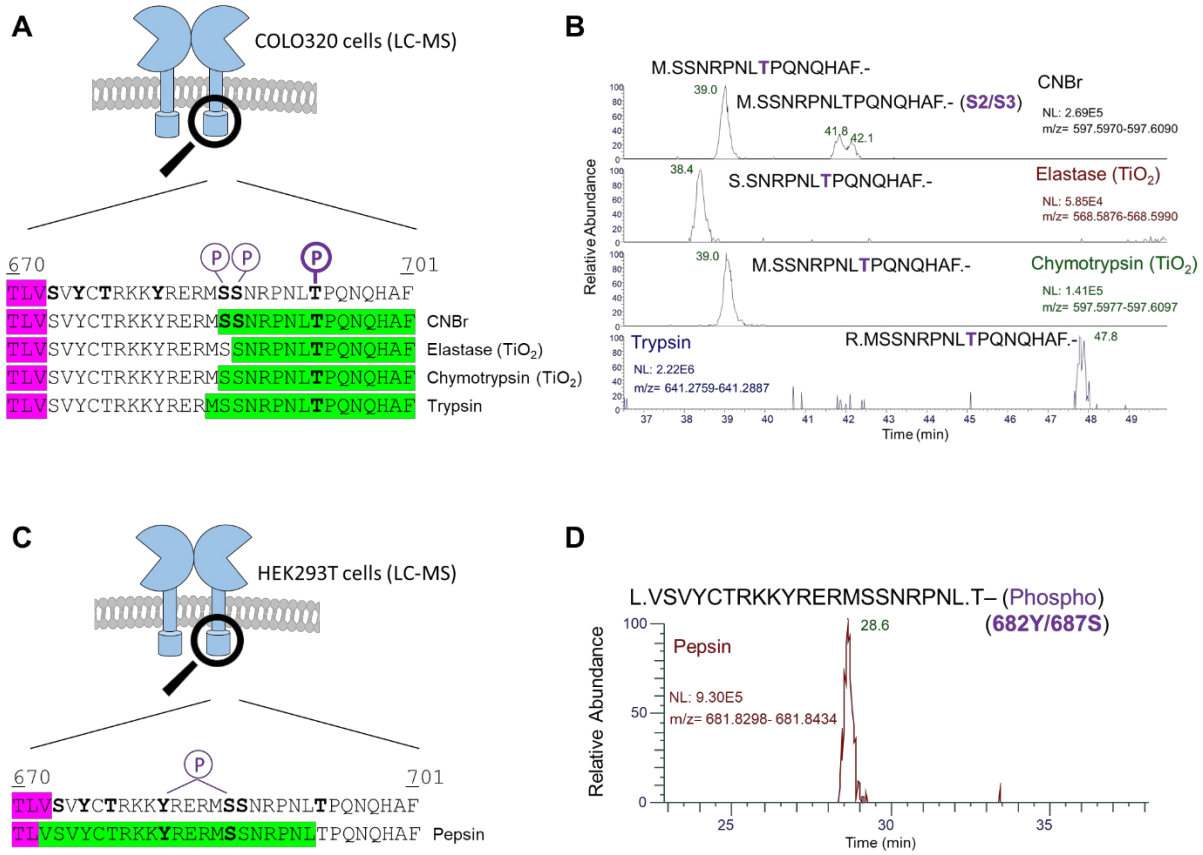

E

Annotated Sequence	Variable modifications	PSMs
[L].VSVYCTRKKYRERMsSNRPNL.[T]	S15(Phospho)	22
[L].VSVYCTRKKyRERMSSNRPNL.[T]	Y10(Phospho)	5

Fig. 7: LC-MS analysis revealed several phosphorylation sites at the C-terminus of meprin β.
(A) The sequence coverage (highlighted in green) of the C-terminus of meprin β from COLO320 cells is depicted. The transmembrane domain is marked in pink. T694 was identified as dominant phosphorylation site, but also S687/S688 were phosphorylated (highlighted in purple). **(B)** The extracted ion chromatograph shows different phosphopeptides obtained upon CNBr, elastase, chymotrypsin or trypsin digestion of meprin β from COLO320 cells. For CNBr, several phosphorylated peptides were identified. The main peak corresponds to a peptide phosphorylated at T694. A minor double peak represents a peptide phosphorylated at S687/S688. **(C)** The sequence coverage (highlighted in green) of the C-terminus of meprin β from HEK cells is depicted. The transmembrane domain is marked in pink. Possible phosphorylation sites are highlighted in purple. **(D)** The extracted ion chromatograph shows different phosphopeptides obtained upon pepsin digestion of meprin β from HEK cells. **(E)** Peptide-spectrum match (PSM) values corresponding to the peptide from (D), phosphorylated either at Y682 or S687. Adapted from Armbrust et al., submitted (appendix, manuscript 1).

Since meprin β is phosphorylated upon application of the protein kinase C (PKC) inducer PMA, it is of interest, which PKC isoforms are involved. Therefore, COLO320 cells were co-transfected with meprin β and the PKC isoforms α, β, γ and ζ. Of note, phosphorylation tends to increase in presence of PKCα and -β (Fig. 8A). Analyzing HEK ADAM10/17$^{-/-}$ cells transfected with meprin β and the PKC isoforms, the previously observed effects were amplified. Meprin β was only phosphorylated upon co-transfection with PKCα or -β, whereas phosphorylation involving PKCγ and -ζ was barely detectable (Fig. 8B). Since residue T694 was the most abundant phosphorylation site in the LC-MS analysis, HEK ADAM10/17$^{-/-}$ cells were transfected with the meprin β T694A variant and analyzed with respect to PKC-dependent phosphorylation. Of note, phosphorylation of meprin β T694A was hardly detectable validating that T694 represents the predominant phosphorylation site of meprin β (Fig. 8C).

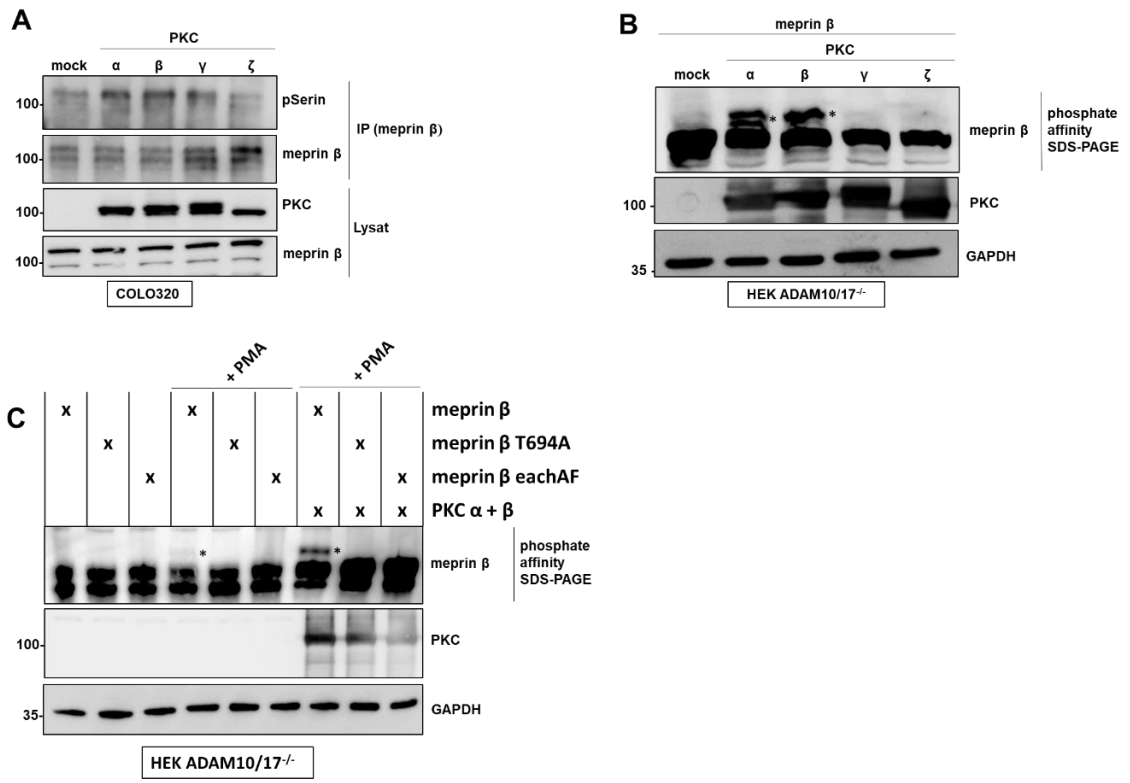

Fig. 8: Meprin β is multi-phosphorylated involving PKCα and -β.

(A) HEK ADAM10/17$^{-/-}$ cells were transfected with meprin β WT and the HA-tagged PKC isoforms α, β, γ, and ζ. After changing the medium to serum-free DMEM for 24 h, the cells were lysed and analyzed by phosphate affinity electrophoresis and Western blot using the antibodies pSer (ab1603), meprin β (Tier1) and HA-tag (C29F4). Phosphorylated protein fractions are highlighted with asterisks. **(B)** ADAM10/17-deficient HEK cells were transfected with meprin β WT, S687R, S688A or S687R/S688A. After changing the medium to serum-free DMEM for 24 h, the cells were treated with 100 ng/ml PMA for 10 min. After cell lysis, the samples were analyzed by phosphate affinity electrophoresis and Western blot using the antibodies meprin β (Tier1), HA-tag (C29F4) and GAPDH (14C10). Phosphorylated protein fractions are highlighted with asterisks. **(C)** HEK ADAM10/17$^{-/-}$ cells were co-transfected with meprin β WT, T694A or eachAF and the HA-tagged PKC isoforms α and β. After changing the medium to serum-free DMEM for 24 h, selective samples were treated with 100 ng/ml PMA for 10 min. The cells were lysed, analyzed by phosphate affinity electrophoresis and Western blot using the antibodies meprin β (Tier1), HA-tag (C29F4) and GAPDH (14C10). Phosphorylated protein fractions are highlighted with asterisks. Adapted from Armbrust et al., submitted (appendix, manuscript 1).

Next, the influence of phosphorylation on the enzymatic activity of meprin β was analyzed. Therefore, a quenched fluorogenic peptide cleavage assay was used, which was previously described (Becker-Pauly et al., 2011; reviewed in Broder and Becker-Pauly, 2013) (Fig. 9A). The peptide consists of alternating glutamate and aspartate residues surrounded by an N-terminal fluorophore (7-methyloxycoumarin-4-yl; mca) and a C-terminal quencher (2,4-dinitrophenyl; dnp), and is specifically cleaved by meprin β. Thus, peptide cleavage by meprin β corresponds to emitted fluorescence. Analyzing the meprin β surface activity on COLO320 cells in a PMA dependent manner revealed a decrease of the activity 60 min after PMA addition (Fig. 9B). This result indicates that the cell surface activity of meprin β is

diminished upon phosphorylation. In order to validate this finding with respect to the individual phosphorylation sites, meprin β variants with substituted C-terminal serine, threonine and/or tyrosine residues were cloned and characterized. On the one hand, single amino acid exchanges to alanine or phenylalanine, respectively, were established to block meprin β phosphorylation. On the other hand, single residues were substituted by glutamate, since it contains a negative charge in similar distance to the backbone compared to phosphorylated residues. Therefore, these variants mimic constitutive phosphorylation of meprin β. Furthermore, the cumulative effect of all potential phosphorylation sites located in the cytoplasmic region of meprin β were investigated. For this purpose, variants, in which all potential phosphorylation sites in the cytoplasmic part are substituted by alanine or phenylalanine (referred to as eachAF) and glutamate (referred to as eachE), respectively, were additionally analyzed. Activity measurements of transfected HEK cells revealed that meprin β variants carrying the S674A, Y676F, T678A or S687A mutation as well as the eachAF variant exhibited increased cell surface activity, whereas the substitutions S688A and T694A did not lead to any change in activity (Fig. 9C). On the contrary, the single mutations Y676E, S688E and T694E led to diminished meprin β activity at the cell surface, whereas variants S674E, T678E, S687E showed no change in activity (Fig. 9D). Intriguingly, the cumulative effect of the single mutations, which was revealed by analyzing the eachE variant, caused a reduction of the meprin β activity at the cell surface by more than 70%. Since LC-MS analyzes showed multiple phosphorylation and the mimicry of phosphorylation at all C-terminal phosphorylation sites led to a strongly diminished cell surface activity, the eachAF and eachE variants were used as proof of concept model to analyze APP cleavage of meprin β with respect to phosphorylation. In concordance with the cell surface activity measurements in line, the cleavage of APP by meprin β is altered, when phosphorylation is mimicked. As described before, meprin β is capable of cleaving APP at the N-terminus releasing non-toxic APP fragments such as N-APP20 (Fig. 9E). Moreover, by cleaving APP at the β-secretase site, meprin β is involved in Aβ formation. Due to the competition of α- and β-secretases for APP cleavage, sAPPα levels are reduced, when meprin β cleaves APP at the β-secretase site. Of note, Western blot and ELISA measurements revealed that upon co-transfection of HEK cells with the eachE variant and APP, sAPPα-levels are increased, whereas N-terminal APP cleavage and Aβ release are reduced in comparison to meprin β WT and eachAF co-transfection (Fig. 9F and G). These data indicate that phosphorylation of meprin β reduces APP processing and Aβ release by meprin β. Of note, diminished substrate cleavage by the eachE variant was also shown for the IL6-R (data shown in the appendix, manuscript 1).

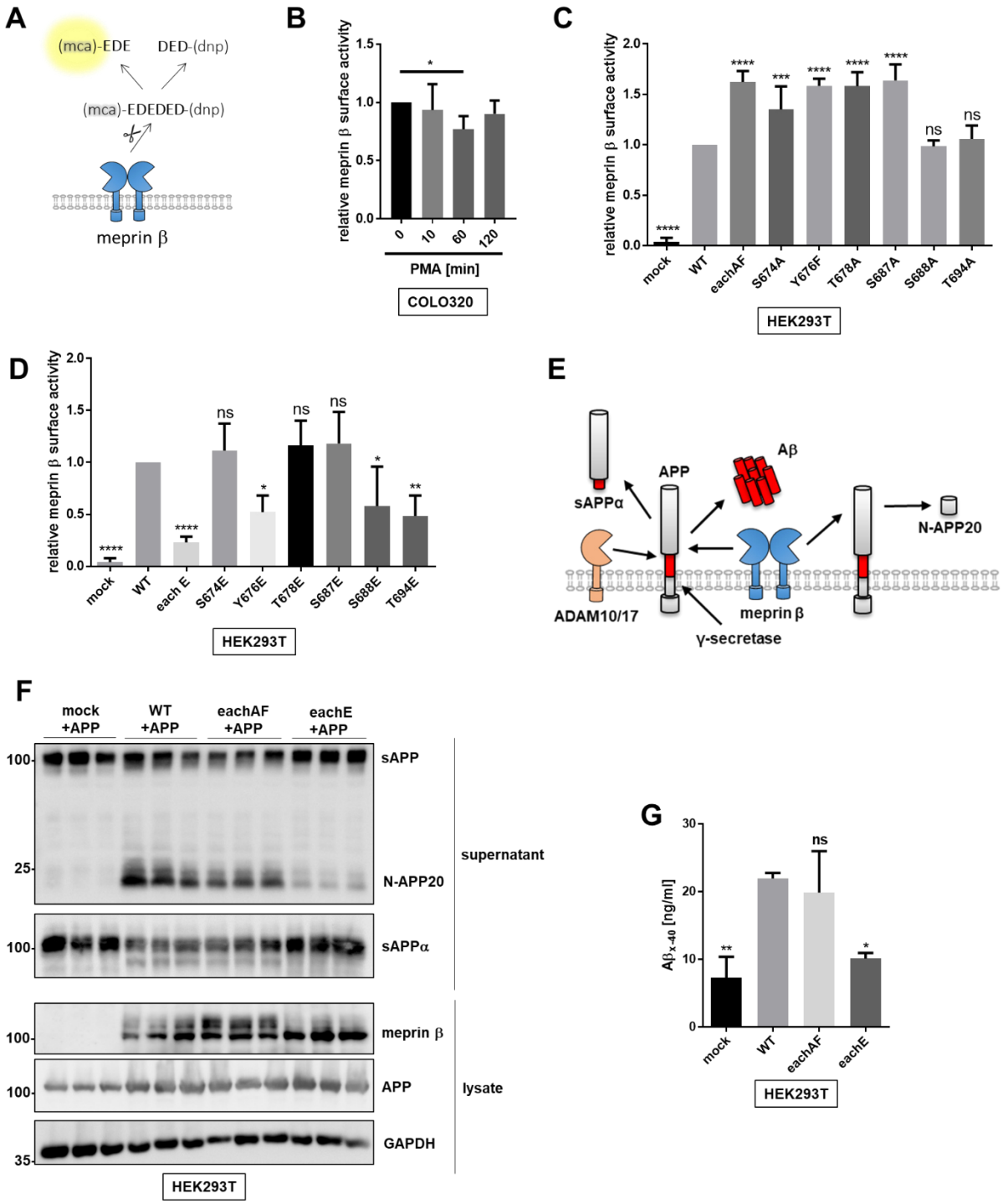

Fig. 9: Meprin β activity at the cell surface is decreased upon phosphorylation leading to diminished Aβ generation.

(A) Principle of the fluorogenic peptide based activity assay. The peptide ((mca)-EDEDED-(K-e-dnp); mca: 7-methyloxycoumarin-4-yl, dnp: 2,4-dinitrophenyl) consists of the fluorophore (mca), alternating glutamate and aspartate residues (EDEDED) and a quencher (dnp). **(B)** COLO320 cells were cultivated in serum-free DMEM for 24 h and subsequently treated with 5 µg/ml trypsin for 30 min. Then, the cells were stimulated with 100 ng/ml PMA for 0, 10, 60 or 120 min. Afterwards, the meprin β-specific surface activity was measured. **(C)** HEK cells were transfected with meprin β mutants carrying single substitutions to alanine or phenylalanine at the C-terminus. Furthermore, a variant, in which all potential phosphorylation sites at the C-terminus are mutated to alanine or phenylalanine, referred to eachAF, was used. The medium was changed to serum-free DMEM 24 h prior measuring

the cell surface activity of meprin β in comparison to an empty vector control and meprin β WT expressing HEK cells. **(D)** HEK cells were transfected with meprin β mutants carrying single substitutions to glutamate at the C-terminus. Furthermore, a variant, in which all potential phosphorylation sites at the C-terminus are mutated to glutamate, referred to eachE, was used. The medium was changed to serum-free DMEM 24 h prior measuring the cell surface activity of meprin β in comparison to an empty vector control and meprin β WT expressing HEK cells. **(E)** Meprin β and ADAM10/17 compete for APP processing at the β/α-secretase site at the cell surface. ADAM10/17-mediated APP cleavage at the α-secretase site leads to sAPPα formation. Upon processing of APP by meprin β at the β-secretase site and subsequent cleavage by the γ-secretase complex, Aβ is generated. Additionally, meprin β cleaves APP at its N-terminus and thereby releasing non-toxic N-APP20 fragments. The scheme was generated based on findings from Hahn et al., 2003; Jefferson et al., 2011; Bien et al., 2012; Herzog et al., 2014. **(F)** HEK cells were transfected with the APP and meprin β WT as well as the phosphovariants eachAF and eachE. After changing the medium to serum-free DMEM for 24 h, the cells were lysed and analyzed by SDS-PAGE and Western blot using the antibodies APP (22C11) for sAPP and N-APP20, 6E10 for sAPPα, APP (CT-15) for APP in the lysate, meprin β (Tier1) and GAPDH (14C10). **(G)** HEK cells were transfected with the APP and meprin β WT as well as the phosphovariants eachAF and eachE. After changing the medium to serum-free DMEM for 24 h, the cell supernatants were analyzed with the Aβx-40 ELISA. Adapted from Armbrust et al., submitted (appendix, manuscript 1).

Due to diminished meprin β activity as a result of phosphorylation, it was hypothesized that meprin β might be internalized and degraded upon phosphorylation (Fig. 10A). Therefore, inhibitors of the proteasome (MG132), endocytosis (cytochalasin D; cytoD), and lysosomal acidification (bafilomycin A1; bafA1) were applied to HEK cells transfected with meprin β WT, eachAF and eachE. Of note, the surface activity of the meprin β variant eachE was significantly increased in the presence of cytoD and bafA1 (Fig. 10B). This indicates that the phosphorylation mimicry of the eachE variant leads to enhanced meprin β internalization and degradation. In summary, the results of this study indicate that multi-phosphorylation of the cytoplasmic part of meprin β involving PKCα and -β promotes its internalization and lysosomal degradation. Due to diminished substrate cleavage at the cell surface, reduced amyloidogenic APP processing leads to diminished Aβ release. For further information, a manuscript is attached (appendix, manuscript 1), which was recently submitted.

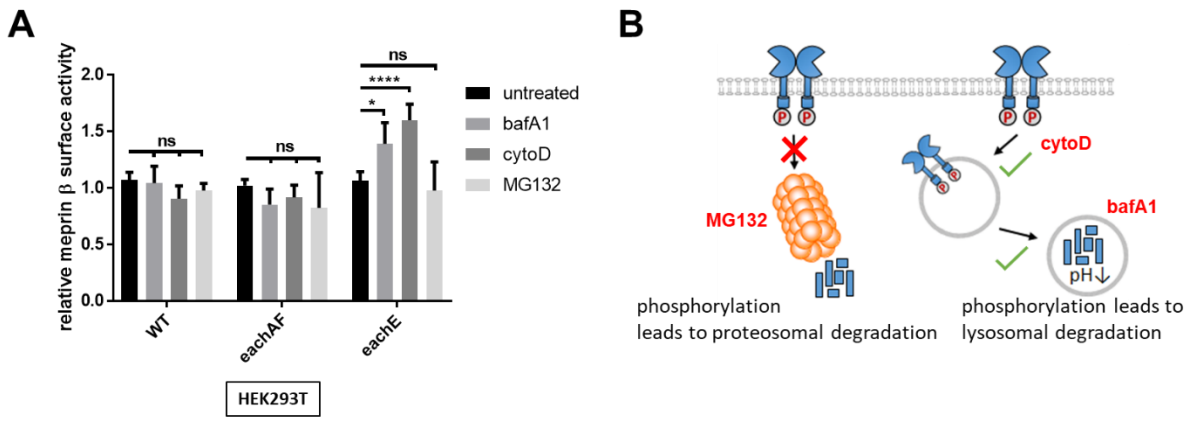

Fig. 10: Meprin β is internalized and degraded upon phosphorylation.

(A) HEK cells were transfected with meprin β WT or the variants eachAF and eachE and treated with trypsin (10 µg/ml) for 30 min and afterwards with baliflomycin A1 (bafA1) (100 nM), cytochalasin D (cyto D) (4 µM) and MG132 (5 µM) for 4 h. The meprin β-specific cell surface activity was measured employing the fluorogenic peptide based activity assay. **(B)** Meprin β is internalized and lysosomal degraded upon phosphorylation. MG132, bafilomycin A1 (bafA1) and cytochalasin D (cytoD) are specific inhibitors for proteasomal degradation, lysosomal degradation and endocytosis, respectively. Adapted from Armbrust et al., submitted (appendix, manuscript 1).

3.1.2 Meprin β activation by RgpB leads to increased Aβ release

To further elucidate the regulation of meprin β, its maturation by the bacterial activator RgpB and the influence on APP cleavage was characterized. RgpB is released by the gram negative bacterium *P. gingivalis*, that is capable of colonizing the gut (Nakajima et al., 2015). In a previous publication it was demonstrated that meprin β can be proteolytically activated by RgpB thereby preventing ectodomain shedding of meprin β (Wichert et al., 2017).

Recently, *P. gingivalis* was identified in AD patient brains assuming that it is also capable of colonizing the brain. Interestingly, mouse experiments confirmed this presumption since *P. gingivalis* was detected in the brain upon oral administration. Further analyzes revealed that RgpB promotes tau pathology and Aβ formation (Dominy et al., 2019). Therefore, it is of interest to investigate whether RgpB-dependent meprin β activation might be responsible for elevated Aβ levels in *P. gingivalis* colonized AD patient brains. Transfecting HEK cells with meprin β and APP (Fig. 11A) revealed increased meprin β activity at the cell surface (Fig. 11B) and elevated N-terminal APP cleavage (Fig. 11C) upon treatment with RgpB. Independent of these observations, RgpB itself emerged as APP degrading enzyme. Therefore, the cysteine protease inhibitor E-64 was applied immediately after meprin β activation by RgpB in the further experiments. Intriguingly, the treatment of APP and meprin β overexpressing HEK cells with RgpB led to elevated Aβ release compared to untreated cells (Fig. 11D). Applying the meprin β inhibitor actinonin, the increased Aβ release upon RgpB treatment was partly

recovered (Fig. 11E). This implies that elevated meprin β activity, as a consequence of maturation by RgpB, is indeed responsible for increased Aβ release upon RgpB application.

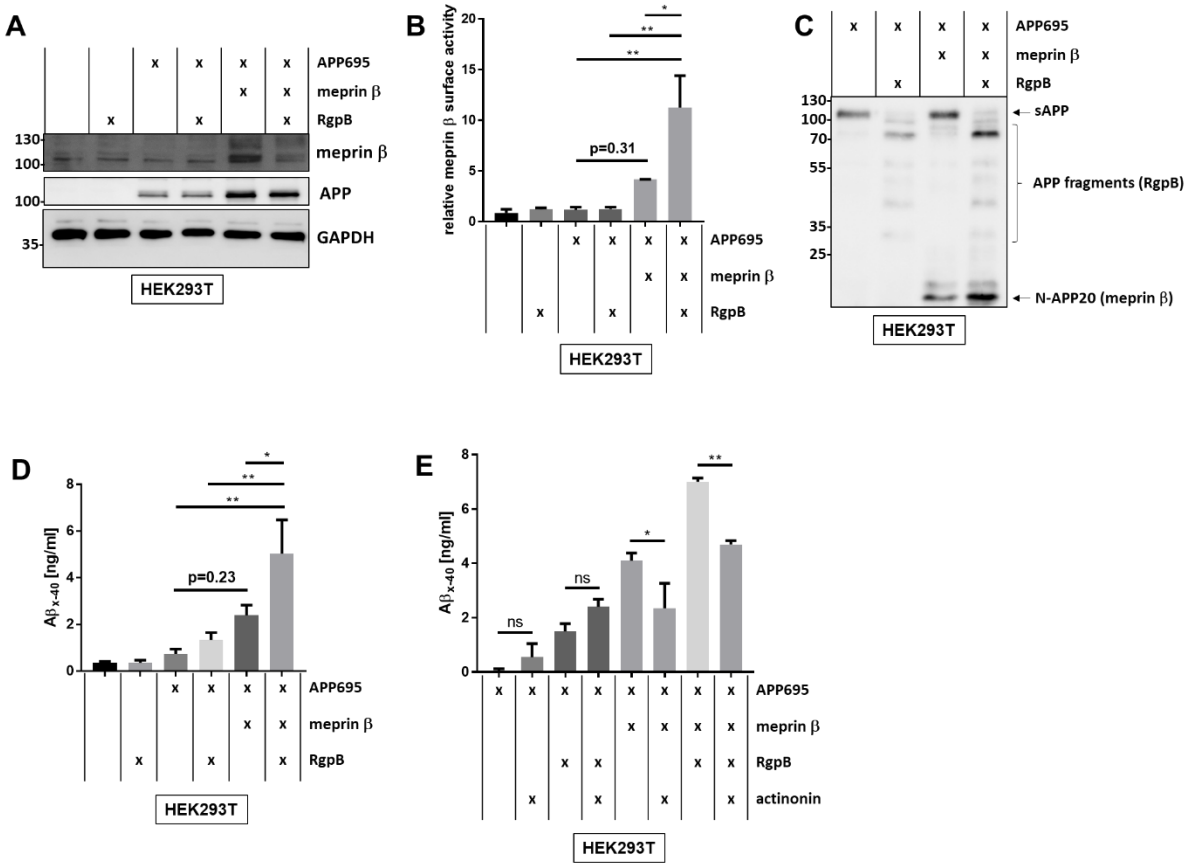

Fig. 11: Meprin β activation by RgpB leads to increased Aβ levels in an overexpression model.
(A) HEK cells were transfected with human APP and/or human meprin β. After 24 h, the medium was changed to serum-free DMEM and the cells were treated with 50 nM RgpB for 30 min. The medium was subsequently changed to serum-free DMEM. Cells were harvested 3 h later and lysed. Proteins were analyzed by Western blot using the antibodies meprin β (Tier1), APP (CT-15) and GAPDH (14C10). **(B)** HEK cells were treated as described in (A), but instead of lysis, the proteolytic activity of meprin β at the cell surface was measured using a meprin β-specific quenched fluorogenic peptide substrate. **(C)** HEK cells were treated as described in (A) and supernatants were analyzed by Western blot using the antibody APP (22C11). **(D)** HEK cells were transfected with human APP and/or human meprin β. After 24 h, the medium was changed to serum-free DMEM and the cells were treated with 50 nM RgpB for 30 min. The medium was subsequently changed to serum-free DMEM and 5 µM of the cysteine protease inhibitor E-64 was added. Cells were harvested 3 h later and lysed. The supernatants were analyzed with the Aβx-40 ELISA. **(E)** HEK cells were treated as described in (D). Together with the E-64 treatment, 20 µM of the meprin β inhibitor, actinonin was added to selective samples and Aβ levels were measured with Aβx-40 ELISA. Adapted from Armbrust et al., pre-print server: www.biorxiv.org (appendix, manuscript 4).

Analyzing the neuroblastoma cell line SH-SY5Y, which expresses meprin β and APP endogenously (Fig. 12A), RgpB treatment led to increased meprin β cell surface activity (Fig. 12B) and elevated Aβ release (Fig. 12C). In summary, the results support the presumption that RgpB from brain colonized *P. gingivalis* might promote Aβ release via

meprin β activation. For further information, a manuscript is attached (appendix, manuscript 4), which is currently published on the pre-print server www.biorxiv.org.

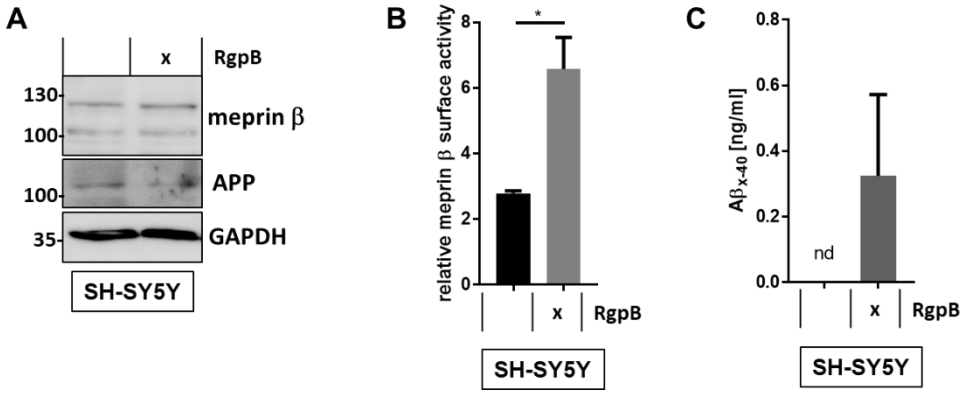

Fig. 12: Meprin β activation by RgpB leads to increased Aβ levels in SH-SY5Y cells.
(A) The medium of cultivated SH-SY5Y cells was changed to serum-free DMEM for 24 h and the cells were simultaneously treated with 50 nM RgpB for 30 min. After cell lysis, the samples were analyzed with SDS-PAGE and Western blot using the antibodies meprin β (Tier1), APP (CT-15) and GAPDH (14C10). **(B)** SH-SY5Y cells were treated as described in (A) and then the meprin β-specific cell surface activity was measured. **(C)** SH-SY5Y cells were treated as described in (A) and Aβx-40 level were measured employing an ELISA. nd – below the detection limit of the ELISA. Adapted from Armbrust et al., pre-print server: www.biorxiv.org (appendix, manuscript 4).

3.1.3 APP cleavage by meprin β is not altered upon homodimer formation with meprin α

In the previous chapters, different mechanisms of meprin β regulation with regard to APP cleavage were characterized in cell culture experiments. For these approaches, transfected HEK cell models, in which meprin β forms homodimers, were primarily used (Bertenshaw et al., 2003). However, it has been observed previously (Johnson and Hersh, 1992) and was validated in this study that meprin β is also capable of forming heterodimers with its close relative meprin α (Fig. 13A). Of note, during the secretory pathway meprin α is cleaved by furin and is, thus, released as secreted enzyme, in contrast to predominantly membrane-bound meprin β (Marchand et al., 1995). In this study, meprin α/β heterodimers were analyzed in detail, observing a covalent disulfide bond between meprin α and meprin β in the MAM domains. As a result, this heterodimer complex tethers soluble meprin α to the cell surface. Of note, meprin β homodimer and meprin α/β heterodimers both can be shed from the surface by ADAM10 and 17. Performing co-immunoprecipitation experiments, the occurrence of heterodimers upon overexpression of both meprin α and β was validated (Fig. 13B). Moreover, brefeldin A was applied to meprin α and meprin β overexpressing cells, which inhibits transport from ER to the Golgi apparatus. Thus, meprin α is not processed by furin and can be precipitated with an antibody binding the N-terminal Strep-tag of meprin α. Co-

immunoprecipitation of meprin β, using a meprin α antibody for the IP, in presence of brefeldin A indicates that dimerization already occurs in the ER. Intriguingly, immunofluorescence stainings of mouse intestine sections of this study were able to validate the occurrence of heterodimers *in vivo*, since in WT mice meprin α colocalizes at the cell surface with meprin β (Fig. 13C). In meprin β knockout mice, meprin α is not detectable at the cell surface.

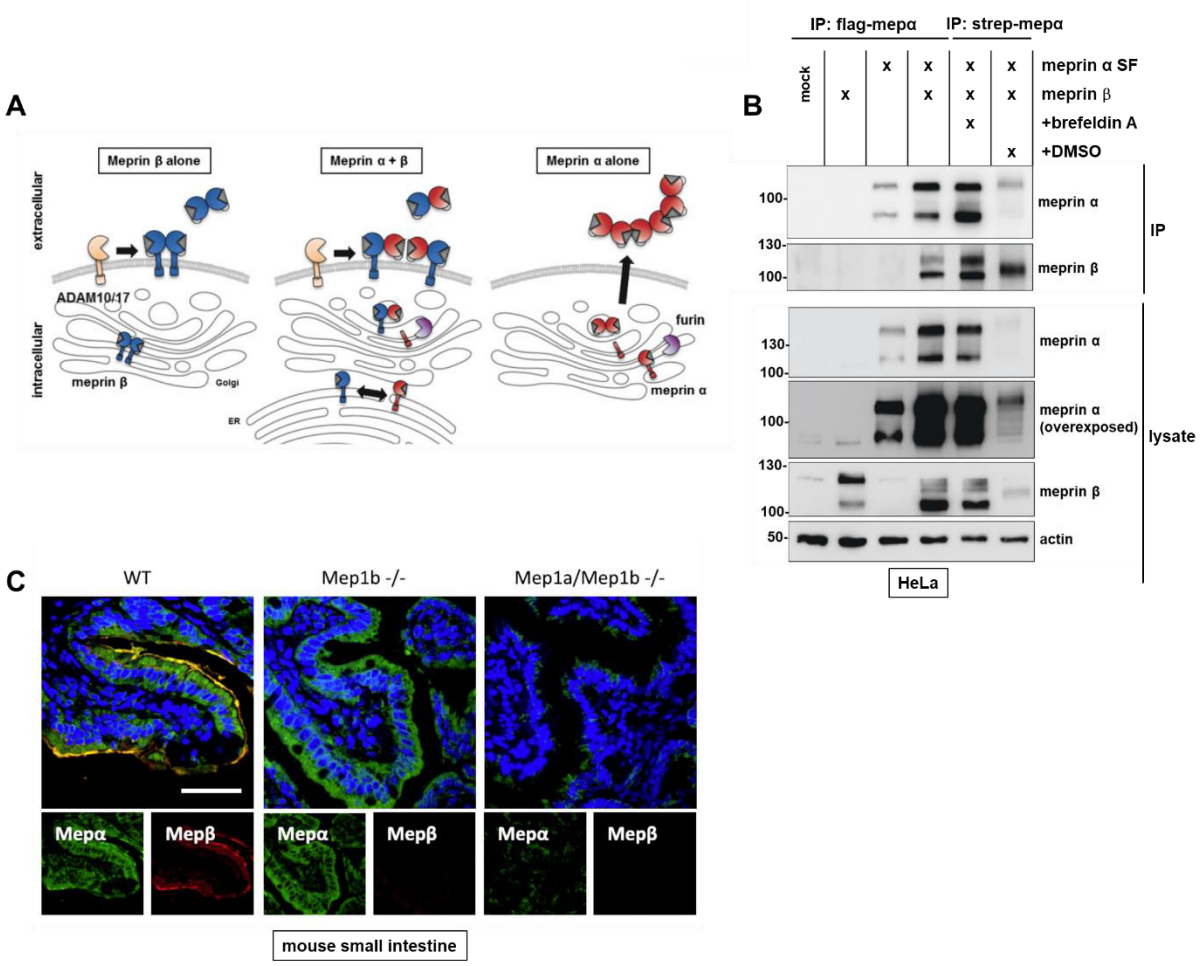

Fig. 13: Meprin α and meprin β form heterodimers *in vitro* and *in vivo*.

(A) Scheme of the secretory pathway of meprin α homodimers, meprin α/β heterodimers, and meprin α homodimers, which form oligomers. Meprin β homodimers translocate to the cell surface and can be shed by ADAM10 and 17. Meprin α/β heterodimers are formed in the ER and meprin α is cleaved by furin in the Golgi apparatus. Translocated to the cell membrane, meprin α is tethered to the cell surface, when covalently linked to meprin β. Heterodimers can also be shed by ADAM10 and 17. Meprin α is processed by furin in the Golgi apparatus, secreted and is then prone to form oligomers. **(B)** HeLa cells were transfected with N-terminal Strep-tagged and C-terminal Flag-tagged meprin α (meprin α SF) and meprin β WT constructs. Selective cells were treated overnight with brefeldin A at 5 µg/ml or DMSO as a control. Co-immunoprecipitation was performed using Flag-tag antibody against meprin α C-terminus or Strep-tag antibody against meprin α N-terminus. Protein fractions were analyzed by Western blot using the antibodies meprin α (Tier1) and meprin β (Tier1). **(C)** Immunofluorescence microscopy of small intestine sections from WT, *Mep1b*$^{-/-}$, and *Mep1a/Mep1b*$^{-/-}$ mice using specific meprin antibodies. Adapted from Peters et al., 2019 (appendix, manuscript 6).

Moreover, the APP cleaving potential of meprin α/β heterodimers was evaluated. Of note, only membrane-bound meprin β is capable of cleaving APP at the β-secretase site, but not shed meprin β (Bien et al., 2012) or secreted meprin α. Since meprin α and meprin β share 41% sequence identity (The UniProt Consortium, 2021, https://www.uniprot.org/uniprot/Q16819, https://www.uniprot.org/uniprot/Q16820) and a preference for acidic amino acids (Becker-Pauly et al., 2011), this study also evaluates whether meprin α is capable of cleaving APP at the β-secretase site, when tethered to the cell membrane as part of a heterodimer (Fig. 14A). Therefore, HeLa cells were transfected with different combinations of APP, meprin α and meprin β to analyze APP cleavage by heterodimers. Meprin α/β heterodimers, which form upon meprin α and meprin β co-transfection, showed a similar APP cleavage pattern compared to meprin β homodimers, as N-APP-20 and Aβ were generated to the same extend (Fig. 14B). In order to evaluate whether meprin α is capable of cleaving APP, when tethered to the membrane, APP and meprin α were co-transfected with the catalytically inactive E153A variant of meprin β. However, heterodimers consisting of inactive meprin β E153A and meprin α did not produce substantially increased levels of N-APP20 or Aβ compared to cells only transfected with APP. Hence, only meprin β in its membrane-bound form acts as alternative β-secretase, but not meprin α, even when tethered to the membrane as part of a meprin α/β heterodimer. For further information, a publication is attached (appendix, manuscript 6), which was published in the FASEB Journal (2019).

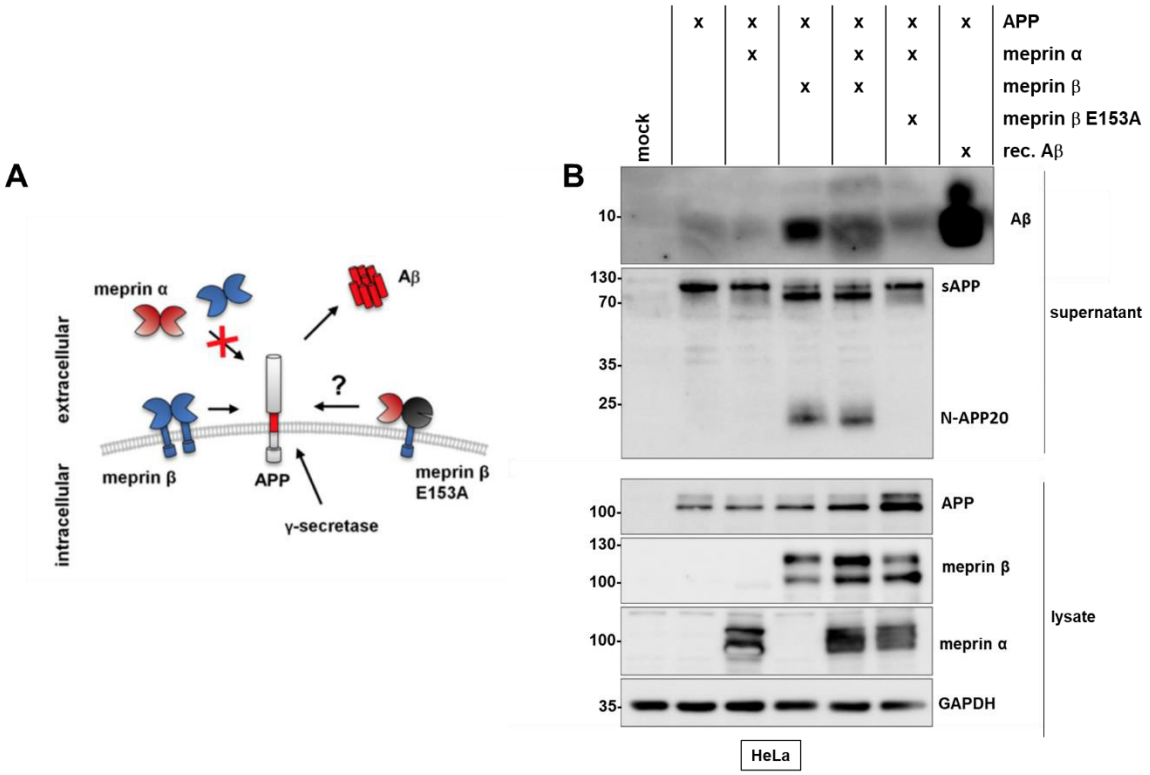

Fig. 14: APP is not cleaved by membrane-tethered meprin α in a meprin α/β heterodimer.
(A) Scheme of APP cleavage by meprins showing processing of membrane-bound meprin β at the β-secretase site of APP, which results in Aβ release upon γ-secretase cleavage. Soluble meprin β and secreted meprin α are note capable of cleaving APP at the β-secretase site. Catalytically inactive meprin β E153A was used for meprin α/β heterodimer formation to exclude meprin β cleavage and analyze APP cleavage by membrane-tethered meprin α. **(B)** HeLa cells were transfected with APP, meprin α, meprin β WT, or the meprin β E153A variant. After 24 h, the medium was changed to serum-free DMEM. Cells were harvested 24 h later and lysed. Proteins were analyzed by Western blot using the antibodies APP (6E10) for Aβ, APP (22C11) for sAPP and N-APP20, polyclonal N-APP for APP in the lysate, meprin β (Tier1), meprin α (Tier1) and GAPDH (14C10). Recombinant Aβ1-40 (rec. Aβ) served as positive control. Adapted from Peters et al., 2019 (appendix, manuscript 6).

3.2 TREM2 is shed and degraded by meprin β

Apart from studying mechanisms of erratic Aβ formation, another branch in the field of AD research is understanding the regulation of Aβ clearance (reviewed in Lee and Landreth, 2010; reviewed in Yoon and Jo, 2012; reviewed in Baranello et al., 2015). In the brain, microglia play a key role in Aβ clearance, as they are capable of taking up Aβ aggregates via phagocytosis (Paresce et al., 1996, 1996). In this regard, TREM2 has emerged as an important receptor on myeloid cells such as microglia, which mediates its activation and thereby promotes the phagocytic ability (Fu et al., 2014). It was published that ADAM10 and 17 are capable of cleaving TREM2 between H157 and S158, thereby releasing the soluble ectodomain of TREM2 (sTREM2) (Schlepckow et al., 2017; Thornton et al., 2017). Of note, increased shedding of TREM2 has emerged as negative regulatory event for phagocytosis signaling (Schlepckow et al., 2017). Due to the overlapping substrate spectrum of meprin β and

ADAM10 (Jefferson et al., 2013), this study should evaluate whether meprin β is also capable of cleaving TREM2. Therefore, recombinant soluble meprin β and TREM2 were incubated and cleavage fragments were analyzed with SDS-PAGE. Coomassie Brilliant Blue staining revealed a dominant cleavage fragment of 25 kDa, when meprin β was applied (Fig. 15A). MS analyzes identified a cleavage site between R136 and D137, which is N-terminal of the ADAM10 and 17 cleavage site between H157 and S158 (Fig. 15B). To further characterize TREM2 cleavage by meprin β, TREM2 transfected HEK ADAM10/17$^{-/-}$ cells were incubated with recombinant meprin β. Upon meprin β application, TREM2 CTFs accumulate in the presence of the γ-secretase inhibitor DAPT (Fig. 15C). However, sTREM2 was barely detectable in meprin β-treated supernatants. Therefore, it was hypothesized that meprin β sheds and degrades the ectodomain of TREM2. In order to validate this hypothesis, conditioned supernatants of HEK cells co-transfected with TREM2 and ADAM10 were collected. Due to ADAM10-mediated shedding, sTREM2 accumulates in the conditioned supernatants. Subsequently, recombinant soluble ADAM10 (sADAM10) or soluble meprin β (smeprin β) was applied, respectively. Upon 4 h of smeprin β co-incubation, TREM2 signals were completely abolished, which was not the case for sADAM10 treatment (Fig. 15D).

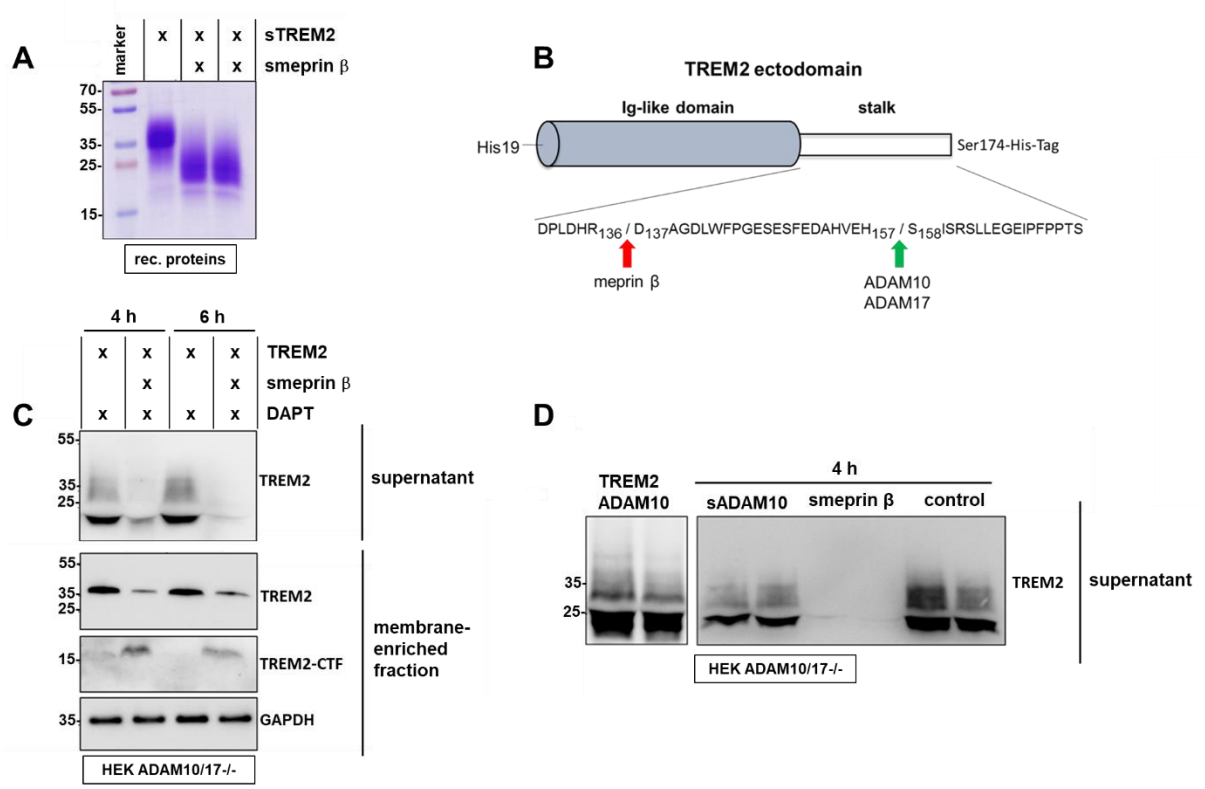

Fig. 15: Meprin β cleaves and degrades TREM2.

(A) Coomassie Brilliant Blue stained SDS gel of recombinant soluble TREM2 (sTREM2) incubated with recombinant soluble meprin β (smeprin β) for 2 hours at 37°C. **(B)** Illustration of the TREM2 ectodomain construct used for cleavage site identification (sTREM2). While TREM2 is cleaved by ADAM10 and ADAM17 between H157 and S158, the major meprin β cleavage site is further N-terminal between R136 and D137. **(C)** HEK ADAM10/17$^{-/-}$ cells were transfected with TREM2 and incubated with smeprin β for 4 or 6 h after changing medium to serum-free DMEM. Proteins from membrane-enriched fractions and cell supernatants were analyzed by SDS-PAGE and Western blot using the antibodies Flag-tag (F1804) for TREM2 and TREM2-CTFs in the membrane-enriched fraction, TREM2 (AF1828) for TREM2 in the supernatant and GAPDH (14C10). **(D)** Conditioned media from TREM2 and ADAM10 transfected HEK ADAM10/17$^{-/-}$ cells was incubated with the smeprin β and recombinant soluble ADAM10 (sADAM10) for 4 hours. sTREM2 levels were analyzed by SDS-PAGE and Western blot using the TREM2 (AF1828) antibody. Adapted from Berner et al., 2020 (appendix, manuscript 3).

Next, it was analyzed whether shedding and degradation of TREM2 by meprin β alters the phagocytic ability, which was measured by fluorescent *E. coli* particle uptake. Therefore, HEK cells were co-transfected with a TREM2-DAP12 fusion protein (Fig. 16A) and meprin β or ADAM10, respectively. Usage of the fusion protein is required to induce signaling, since the adaptor protein DAP12 is not endogenously expressed in HEK cells (Uhlén et al., 2015, https://www.proteinatlas.org/ENSG00000011600-TYROBP/celltype). Upon TREM2 transfection, the phagocytic ability of the HEK cells was significantly increased due to TREM2-mediated signaling (Fig. 16B). However, TREM2 cleavage upon co-transfection with meprin β diminished the phagocytic potential. Intriguingly, the effect of meprin β was even more pronounced compared to ADAM10. Moreover, the phagocytic ability of the monocyte cell

lines THP-1 and U937 was analyzed with respect to meprin β-mediated TREM2 cleavage. These cell lines express DAP12 endogenously. Therefore, they were not transfected with the TREM2-DAP12 fusion protein, but only with TREM2 and/or meprin β. In both cell lines, TREM2 transfection increased the phagocytic ability, which was partly recovered by co-expression of meprin β (Fig. 16C and D).

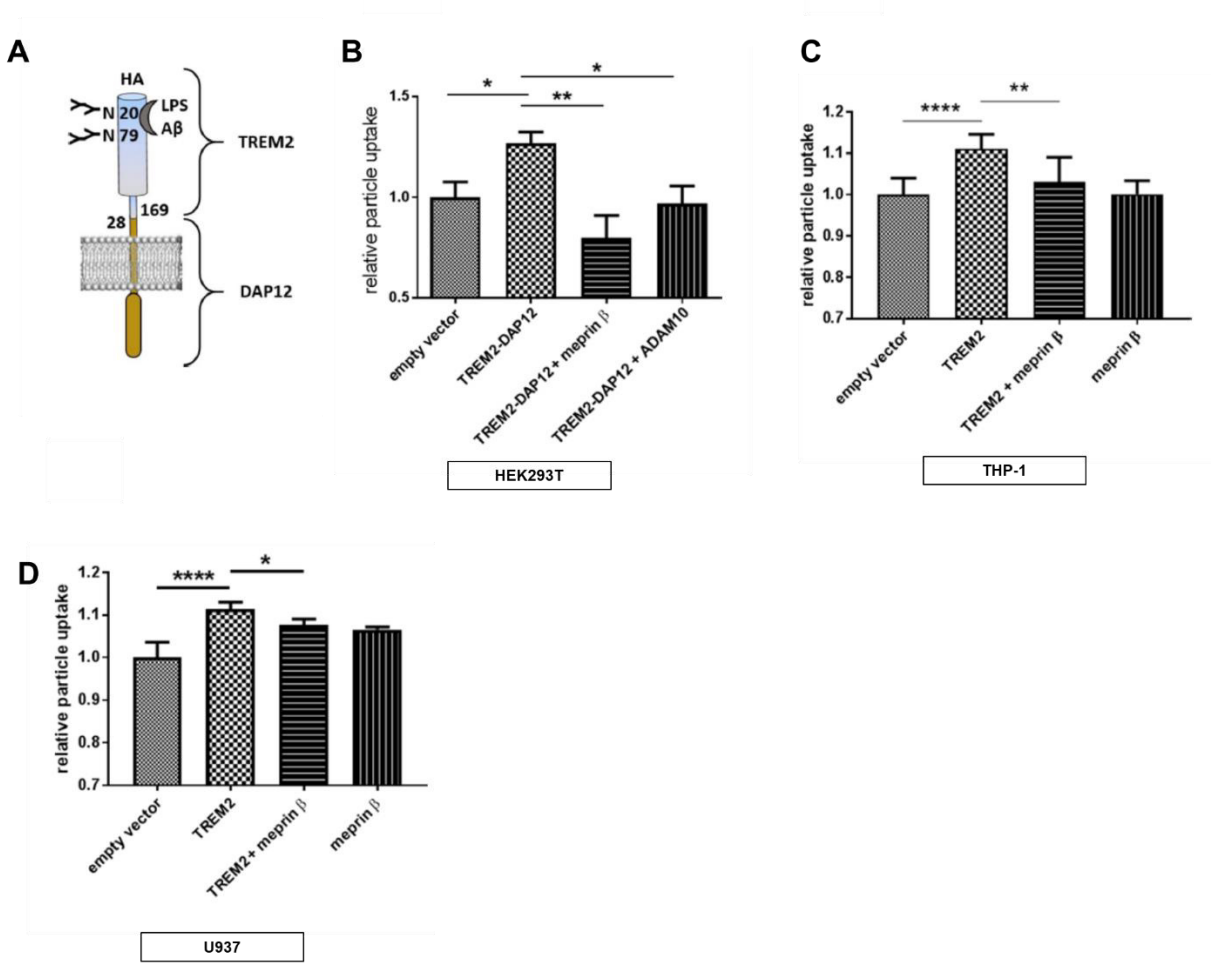

Fig. 16: TREM2 cleavage by meprin β leads to decreased phagocytic activity.
(A) Illustration of the TREM2/DAP12 fusion construct used in (B). The TREM2 ectodomain is glycosylated at N20 and N79 and interacts with, e.g., LPS or Aβ. **(B)** HEK ADAM10/17$^{-/-}$ cells were transfected as labeled in the figure. After 24 h, the medium was changed to serum-free medium for 4 h. Relative particle uptake was analyzed by flow cytometry. Data are represented as means of median fluorescence intensity. **(C)** THP-1 cells were differentiated with 100 ng/ml PMA. After 24 h cells were transfected as labeled in the figure. Another 24 h later, the medium was changed to serum-free for 4h. Relative particle uptake was analyzed using a Tecan fluorescent reader measuring mean fluorescence intensity of a defined number of cells. **(D)** U937 cells were differentiated with 100 ng/ml PMA. After 24 h cells were transfected as labeled in the figure. Another 24 h later, the medium was changed to serum-free for 4h. Relative particle uptake was analyzed using a Tecan fluorescent reader measuring mean fluorescence intensity of a defined number of cells. Adapted from Berner et al., 2020 (appendix, manuscript 3).

In order to analyze the *in vivo* relevance of meprin β-mediated TREM2 cleavage, bone-marrow derived macrophages (BMDMs) of meprin β knockout-out and WT mice were isolated. In meprin β knock-out mice, an approximately 55 kDa band presumably representing full-length

TREM2 was delectable, whereas upon ADAM10 stimulation with lipopolysaccharide (LPS), it was completely abolished (Fig. 17A). However, in WT BMDMs, full-length TREM2 was scarcely detectable independent of LPS stimulation. These findings suggest that meprin β is predominantly responsible for constitutive TREM2 shedding in BMDMs. With this in line, meprin β knock-out BMDMs exhibited a higher phagocytic activity than WT BMDMs due to diminished TREM2 shedding (Fig. 17B). Moreover, sTREM2 levels in the sera of meprin β knock-out mice were significantly diminished (Fig. 17C). In summary, these data show that meprin β is capable of TREM2 shedding and ectodomain degradation (Fig. 17D). As result, the phagocytic ability of monocytic cells is diminished *in vivo* and this might contribute to reduced Aβ uptake by microglia in AD. For further information, a publication is attached (appendix, manuscript 3), which was published in the FASEB Journal (2019).

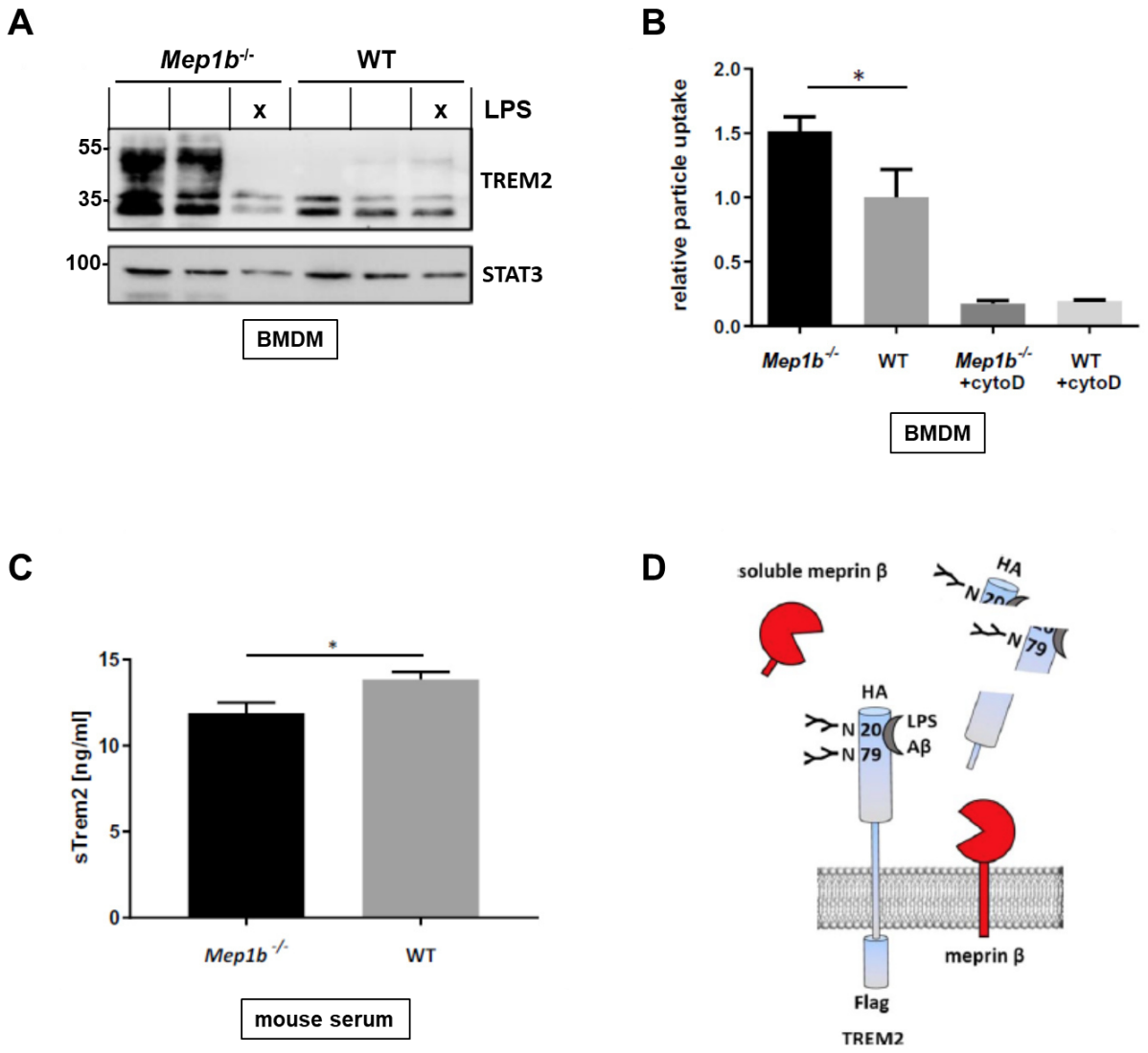

Fig. 17: TREM2 cleavage by meprin β occurs *in vivo*.

(A) Bone marrow derived macrophages (BMDMs) were isolated from *Mep1b*$^{-/-}$ and WT mice and selectively treated with LPS for 6 h. Membrane-enriched fractions were analyzed with SDS-PAGE and Western blot using the antibodies TREM2 (5F4) and STAT3 (124H6). **(B)** BMDMs were isolated and partly treated with cytochalasin D (cytoD) to block endocytosis. Relative particle uptake was measured by FACS and represented as means of median fluorescence intensity. **(C)** Sera from WT and *Mep1b*$^{-/-}$ mice were analyzed with a TREM2 ELISA. **(D)** Cartoon illustrating the shedding and degradation of the TREM2 ectodomain by soluble and membrane bound meprin β. Adapted from Berner et al., 2020 (appendix, manuscript 3).

3.3 The *in vivo* role of the alternative β-secretase meprin β in AD

In the previous chapters, an insight into the mechanistic regulation of meprin β with respect to APP cleavage as well as Aβ formation and degradation was provided. However, the β-secretase activity of meprin β in this study and in general has so far only been substantially analyzed *in vitro* and *in cellulo* (Bien et al., 2012; Schönherr et al., 2016). Therefore, the main aim of this thesis was the generation of AD mouse models to characterize the role of meprin β

in AD *in vivo*. In order to obtain a highly specific tool to detect amyloidogenic APP processing by meprin β, a neo-epitope-specific sAPPβ antibody was generated together with Pineda Antikörper-Service. As described before, meprin β predominantly cleaves APP between D672 and A673, one amino acid shifted towards the C-terminus compared to BACE1 cleavage (Bien et al., 2012). Thus, N-terminally truncated Aβ2-x peptides and C-terminally extended sAPPβ (referred to as sAPPβ+1) are released. To generate an antibody specifically detecting C-terminal extended sAPPβ+1, rabbits were immunized with a peptide consisting of the last five amino acids of sAPPβ+1 coupled to an immunogenic protein. After 120 days, the IgG fraction was purified from the rabbit serum and the neo-epitope-specific antibody was obtained. In order to validate the specificity of this antibody, peptides comprising 46 or 47 amino acids of the C-terminus of different sAPPβ species were analyzed (Fig. 18A). Peptides corresponding to the C-terminus sAPPβ and sAPPβ+1 originating from wild-type APP as well as the previously introduced APPswe variant were loaded onto a SDS gel and detected by Western blot using the neo-epitope-specific sAPPβ antibody as primary antibody. The detection of only sAPPβ+1 resulting from wild-type APP revealed high specificity of the generated antibody (Fig. 18B).

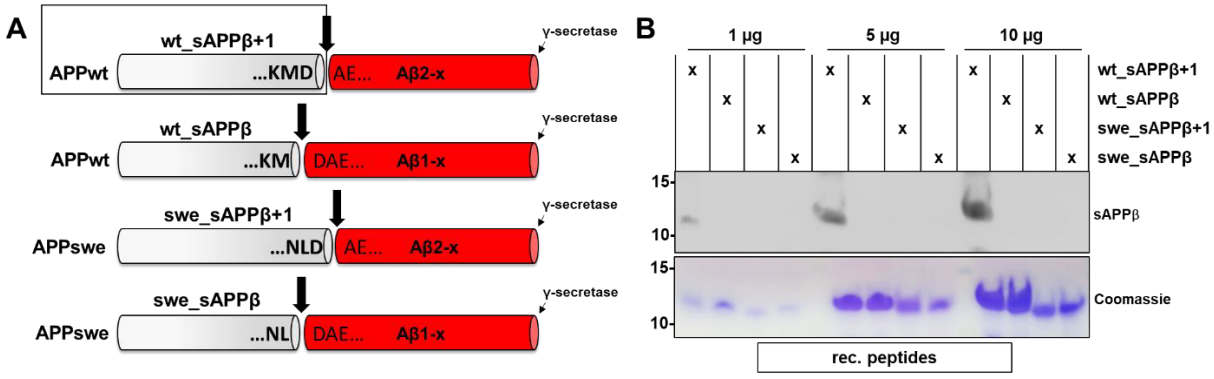

Fig. 18: sAPPβ+1 antibody validation.

(A) The basis for the peptides analyzed in (B) is depicted. The peptides comprise the 46 or 47 C-terminal amino acids of the following sAPPβ species. Upon cleavage between D672 and A673 N-terminally truncated Aβ2-x and C-terminally extended sAPPβ (wt_sAPPβ+1) are generated from wild-type APP (APPwt). When APPwt is cleaved between M671 and D672 Aβ1-x and conventional sAPPβ (wt_sAPPβ) is generated. Both sAPPβ species are also depicted carrying the Swedish APP (APPswe) mutations (swe_sAPPβ+1 and swe_sAPPβ). Wt_sAPPβ, which is specifically detected by the neo-epitope-specific antibody, is highlighted in a black box. **(B)** 1-10 µg of the peptides explained in (A) were analyzed using SDS-PAGE with consecutive Coomassie Brilliant Blue staining and Western blot using the neo-epitope-specific sAPPβ+1 (Tier3) antibody, respectively.

Before analyzing meprin β-mediated APP cleavage in the mouse brain, an evaluation whether murine meprin β is capable of Aβ formation by cleaving murine APP is required. Since common transgenic AD mouse models express human APP to accomplish rapid Aβ formation (reviewed in Esquerda-Canals et al., 2017), the cleavage ability of human APP by murine meprin β is also of interest. Therefore, HEK cells were transfected with each combination of human as well

as murine meprin β and APP. Western blot analyses revealed an equivalent APP cleavage pattern of each combination, because elevated sAPPβ+1, detected with the neo-epitope-specific antibody, and increased N-APP20 as well as diminished sAPPα levels were observed upon meprin β co-transfection with APP compared to APP expression alone (Fig. 19A). Furthermore, an increased release of Aβx-40 (Fig. 19B) and Aβx-42 (Fig. 19C) was detected when meprin β was co-expressed with APP in each combination of murine and human proteins compared to APP expression alone.

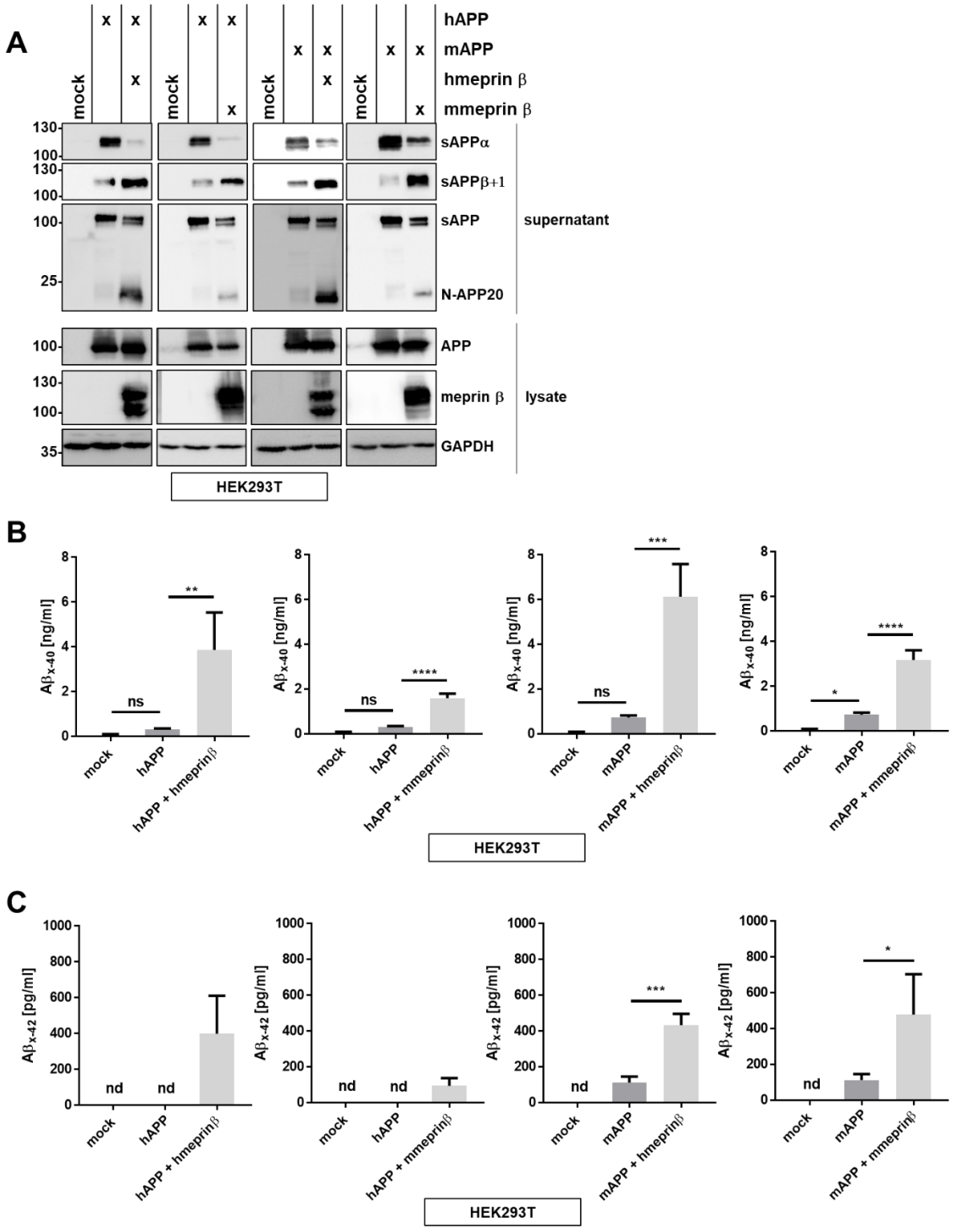

Fig. 19: APP cleavage by meprin β equivalently takes place in the human and murine system.

(A) HEK cells were transfected with each combination of human APP (hAPP) or murine APP (mAPP) and human meprin β (hmeprin β) or murine meprin β (mmeprin β). After 24 h the medium was changed to serum-free DMEM for 24 h. Cell lysates and supernatants were analyzed by SDS-PAGE and Western blot using the antibodies APP (6E10) for human sAPPα detection, murine Aβ/sAPPα (poly18058) for murine sAPPα, sAPPβ+1 (Tier3), APP (22C11) for sAPP and N-APP20, APP (CT-15) for APP in the lysate, meprin β (Tier1) and GAPDH (14C10). **(B)** The supernatants of (A) were analyzed using the Aβx-40 ELISA. **(C)** The supernatants of (A) were analyzed using the Aβx-42 ELISA. nd – below the detection limit of the ELISA.

3.3.1 Meprin β deficiency completely recovered cognitive function in an AD mouse model

In order to evaluate the role of meprin β in AD *in vivo*, a mouse strain overexpressing the human APP695 variant, carrying the familial AD London mutation V642I (using the numbering of APP695 in UniProt (The UniProt Consortium, 2021, https://www.uniprot.org/uniprot/P05067)) close to the γ-secretase site in the *APP* gene, was used in this study. The advantages using APPlon expressing mice are rapid Aβ formation and accelerated plaque deposition (Moechars et al., 1999; van Dorpe et al., 2000).

Evaluating the contribution of meprin β to Aβ formation and cognitive impairment in APPlon expressing mice, in this thesis referred to as APP/lon mice, these mice were crossed with a meprin β knock-out mouse line. The resulting mouse strain was termed as APP/lon x *Mep1b*$^{-/-}$. Analyzing APP/lon in comparison to WT mice in a Morris water maze test, it became obvious that APP/lon mice show reduced cognitive abilities. Intriguingly, cognitive declines of APPlon mice were completely recovered, when meprin β was knocked-out. This was quantified by the average escape latency to find the platform on day 5, which was significantly higher for APP/lon mice in comparison to the controls (Fig. 20A). In an additional experiment on day 5, the platform was removed and platform crossings and latency in finding platform location were measured. Both were significantly reduced for APP/lon x *Mep1b*$^{-/-}$ mice in comparison to APP/lon mice (Fig. 20B and C). Of note, *Mep1b*$^{-/-}$ mice even tended to exhibit a better cognitive ability in contrast to WT mice independent of APPlon expression.

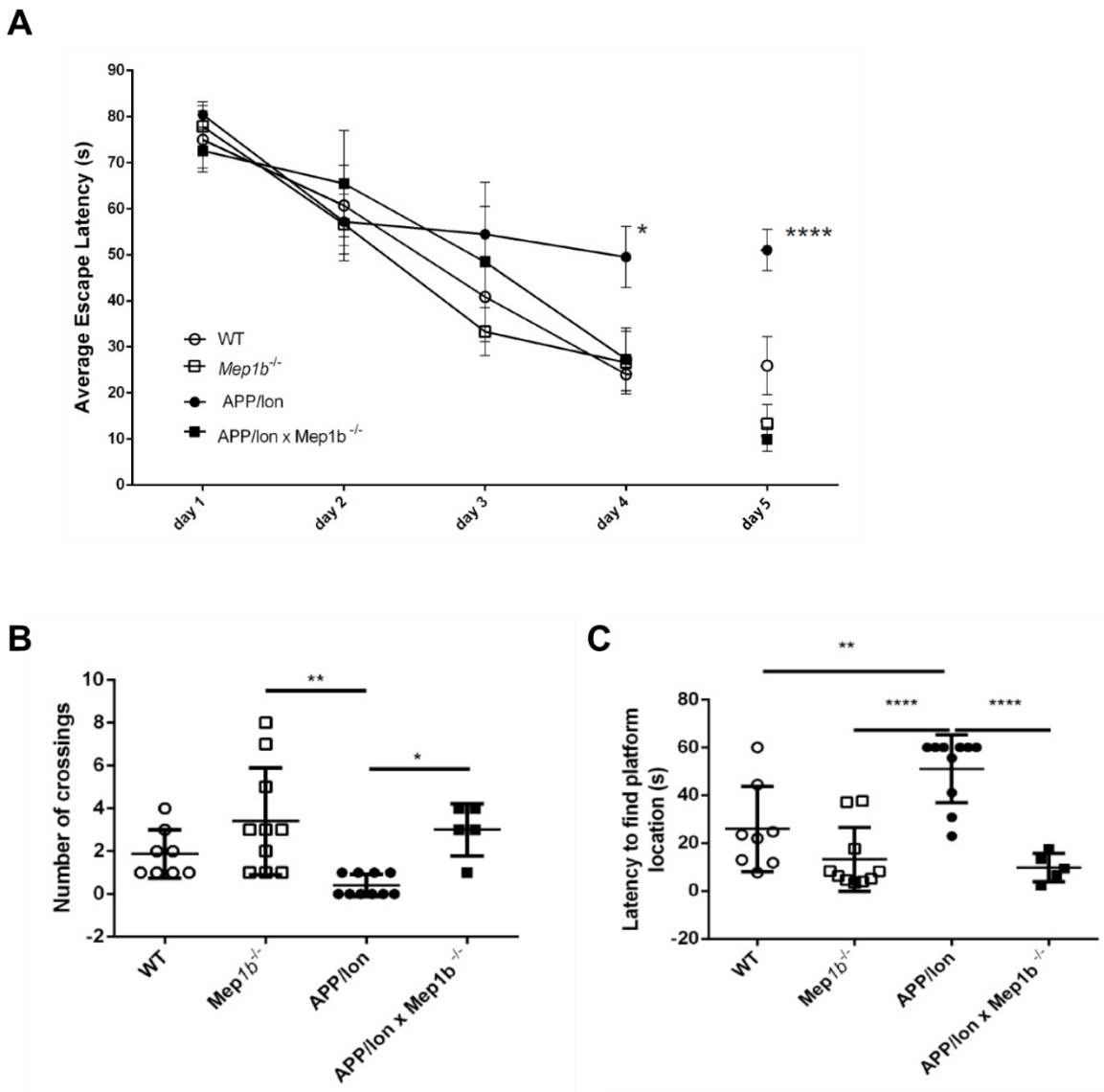

Fig. 20: Meprin β deficiency recovers cognitive functions of APP/lon mice.

(A) A Morris water maze test of WT, *Mep1b*$^{-/-}$, APP/lon and APP/lon x *Mep1b*$^{-/-}$ mice (7 month of age) was performed over 5 days. The time, which the mice needed to find the platform, is represented as average escape latency. **(B)** On day 5 of the Morris water maze test of (A), the platform was removed and the number of crossings quantified**.** **(C)** On day 5 of the Morris water maze test of (A), the platform was removed and the latency to find the platform location was analyzed. Adapted from Marengo et al., submitted (appendix, manuscript 2).

Since cognitive decline is linked to Aβ burden in AD mouse models (Richards et al., 2003; Jawhar et al., 2012), the meprin β-dependent Aβ release and deposition was analyzed. IHC staining revealed a reduced load of Aβ2-x plaques, when APP/lon mice lacked meprin β (Fig. 21A, B, C). However, Aβ1-x plaque deposition was unaltered. In order to analyze soluble Aβ species, these fractions were analyzed by Western blot and ELISA. Of note, decreased Aβ1-42 levels in the soluble fractions were observed, when meprin β was abolished (Fig. 21D, E). Interestingly, also ELISA measurements revealed significantly reduced soluble Aβ1-40 and Aβ1-42 levels in APP/lon x *Mep1b*$^{-/-}$ compared to APP/lon mice (Fig. 21F).

However, the Aβ lowering effects of meprin β deficiency were even more pronounced using Aβx-40 and Aβx-42 ELISAs, which include N-terminal truncated Aβ species such as Aβ2-x predominantly generated by meprin β (Fig. 21G).

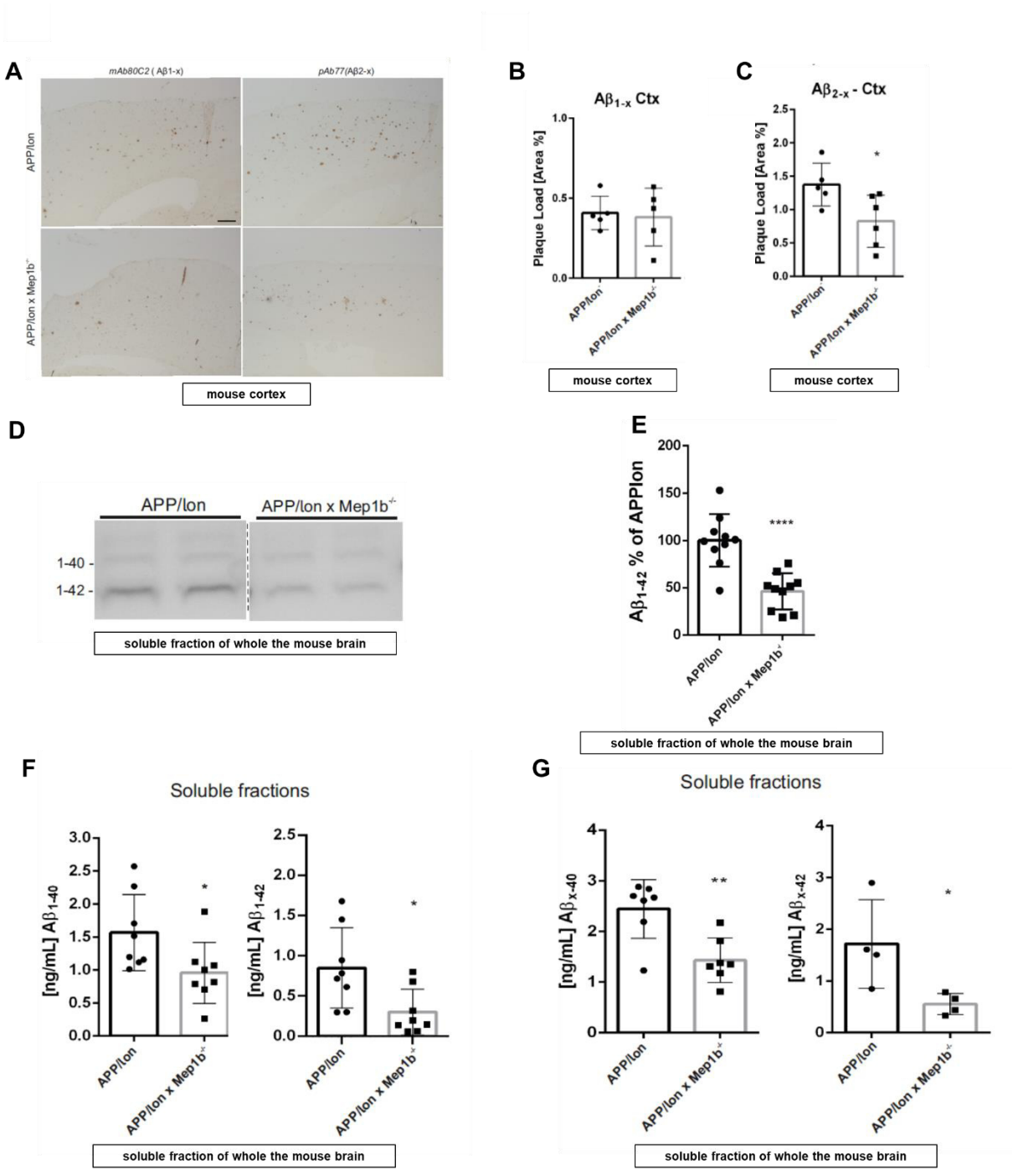

Fig. 21: Meprin β deficiency lowers Aβ burden of APP/lon mice.

(A) Aβ1-x and Aβ2-x were IHC stained in brain sections of APP/lon and APP/lon x *Mep1b*$^{-/-}$ mice using the antibodies mAb80C2 and pAb77, respectively. **(B)** and **(C)** Plaque load was quantified based on (A). **(D)** Total Aβ levels of soluble and insoluble APP/lon and APP/lon x *Mep1b*$^{-/-}$ brain fractions were analyzed with SDS-PAGE and Western blot using the Aβ (IC16) antibody. **(E)** Quantification of (D). **(F)** Soluble fractions of APP/lon and APP/lon x *Mep1b*$^{-/-}$ brains were analyzed with Amyloid-β (1-40) (FL) ELISA and Amyloid-β (1-42) (FL) ELISA. **(G)** Soluble fractions of APP/lon and APP/lon x *Mep1b*$^{-/-}$ brains were analyzed with the Aβx-40 and Aβx-42 ELISA. Adapted from Marengo et al., submitted (appendix, manuscript 2).

Since the ELISA measurements revealed that meprin β deficiency has an impact on Aβ1-x generation in APP/lon mice, which is widely accepted to be predominantly generated by BACE1 (reviewed in Cole and Vassar, 2007; reviewed in Hampel et al., 2020), it was analyzed whether meprin β might be involved in the modulation of BACE1 activity. Therefore, seizure 6 (SEZ6) cleavage in mouse brain lysates were analyzed, which is almost exclusively accomplished by BACE1 (Kuhn et al., 2012). However, SEZ6 levels were not altered between WT and meprin β-deficient mice (Fig. 22A, B), but increased, when BACE1 was additionally knocked out. This finding indicates that meprin β does not induce BACE1 activity. Hence, APP processing and Aβ generation by meprin β seems to occur independently of BACE1.

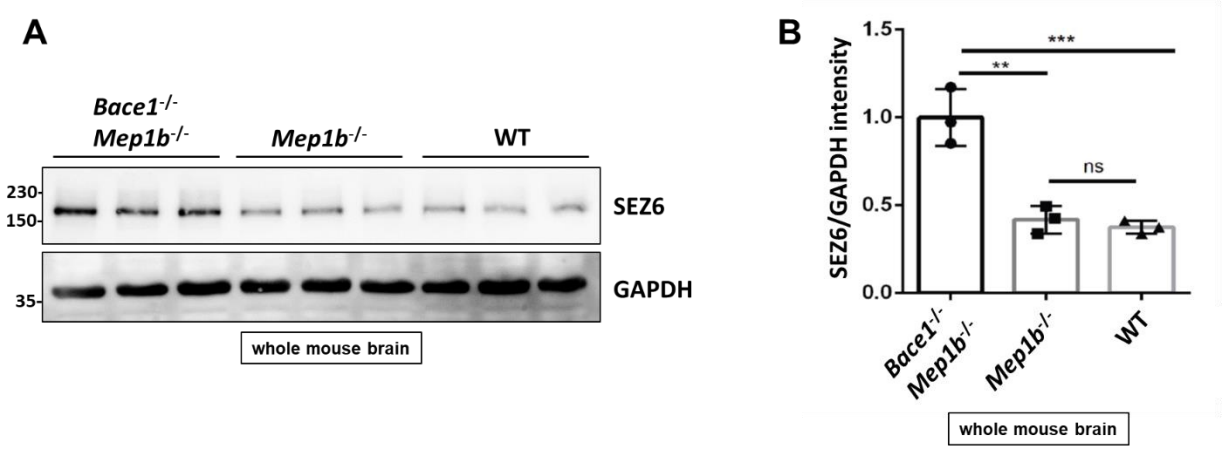

Fig. 22: BACE1 activity is not altered by meprin β.

(A) *Bace1*$^{-/-}$ *Mep1b*$^{-/-}$, *Mep1b*$^{-/-}$ and WT mouse brains were isolated and homogenized. SEZ6 and GAPDH levels were analyzed with SDS-PAGE and Western blot using the SEZ6 (14E5) and GAPDH 14C10) antibody. **(B)** Quantification of (A). Adapted from Marengo et al., submitted (appendix, manuscript 2).

In order to underline the relevance of meprin β for AD, human brain sections of AD patients were analyzed with respect to meprin β expression. Interestingly, IHC stainings revealed a significant increase of meprin β-positive cells in AD patient brains (Fig. 23A, B). As a control, Aβ plaques and phosphorylated tau were stained and only detected in AD patient brain slices. For further information, a manuscript is attached (appendix, manuscript 2), which was recently submitted.

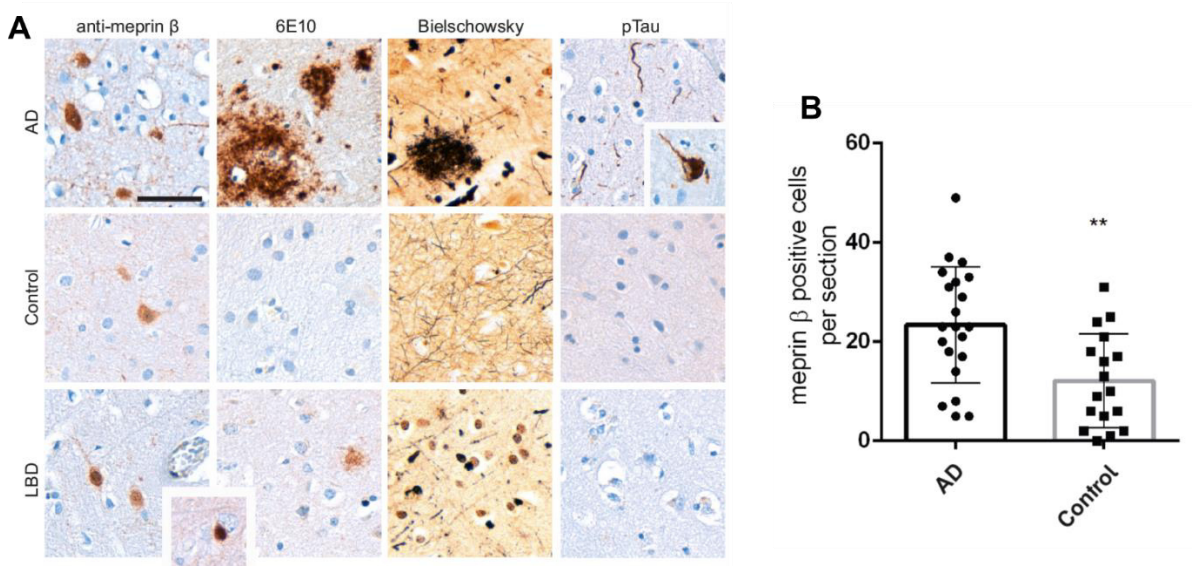

Fig. 23: Meprin β is upregulated in AD patient brains on protein level.
(A) IHC staining of Alzheimer´s disease patient brain sections (AD), healthy donors (control) or Lewy body dementia patient brains (LBD). Aβ plaques were detected using the APP (6E10) antibody; Bieschowsky staining enables visualization of Aβ plaques and neurofibrillary tangles. Phosphorylated tau protein was detected with the phosphorylated tau protein antibody (AT8). **(B)** Quantification of (A). The scale bar indicates 100 µm. Adapted from Marengo et al., submitted (appendix, manuscript 2).

3.3.2. Meprin β overexpression in astrocytes leads to increased Aβ release in mouse brains

In the previous chapter, it was shown that meprin β deficiency significantly lowers Aβ release and completely recovers the cognitive function of APP/Ion mice. Hence, an *in vivo* role for meprin β in AD is suggested. Since elevated meprin β levels in AD patient brains were observed by IHC analyses, the overexpression of the protease in the mouse brain might serve as meprin β-based AD mouse model. Therefore, meprin β knock-in mice were generated by inserting a cDNA coding for HA-tagged murine meprin β in the Rosa26 locus of C57BL/6N mice. A floxed neomycin-Westphal stop cassette between a CAG promoter and the meprin β cDNA prevents from the transcription of meprin β until the stop cassette is excised by a Cre recombinase. Meprin β knock-in mice are referred to as Rosa26$^{Mep1b\text{-HA}}$ in this thesis.

Since astrocytes were observed to be predominantly responsible for Aβ2-42 generation in comparison to neurons and microglia (Oberstein et al., 2015) and Aβ peptides starting at position 2 are the are the dominant species generated by meprin β (Bien et al., 2012), the protease was conditionally overexpressed in astrocytes in this study. Therefore, the Rosa26$^{Mep1b\text{-HA}}$ mice were crossed with Cre expressing mice under control of the GFAP promoter to induce meprin β overexpression in astrocytes. These mice are referred to as GFAP^{Cre};Rosa26$^{Mep1b\text{-HA}}$ mice in this thesis (Fig. 24A) and in the following Cre-heterozygous

GFAP$^{Cre+/-}$;Rosa26$^{Mep1b\text{-}HA}$ mice will be characterized compared to Cre-negative GFAP$^{Cre-/-}$;Rosa26$^{Mep1b\text{-}HA}$ mice. An overexpression of AD-associated human APP variants as it is commonly used in AD models to accelerate Aβ release was not chosen for this approach, since the aim of this trial was to evaluate whether meprin β overexpression is sufficient to observe Aβ release even with endogenous APP levels. GFAP^{Cre};Rosa26$^{Mep1b\text{-}HA}$ mice were sacrificed at the age of 1 y to give sufficient time to potentially develop an amyloidogenic phenotype. The analysis of these mouse brains revealed a meprin β upregulation in the brain of GFAP$^{Cre+/-}$;Rosa26$^{Mep1b\text{-}HA}$ compared to GFAP$^{Cre-/-}$;Rosa26$^{Mep1b\text{-}HA}$ mice using Western blot (Fig. 24B). Measuring the cleavage of a quenched fluorogenic peptide, increased meprin β activity was observed in whole brain lysates of Cre positive mice (Fig. 24C). According to that, overexpressed meprin β in astrocytes is maturated by endogenous activators. In order to validate that meprin β expression is restricted to astrocytes, IHC staining of meprin β as well as markers for astrocytes, neurons and microglia were conducted. The distribution and shape of the meprin β signal revealed meprin β expression in astrocytes exemplarily shown in the cortex and hippocampus (Fig. 24D).

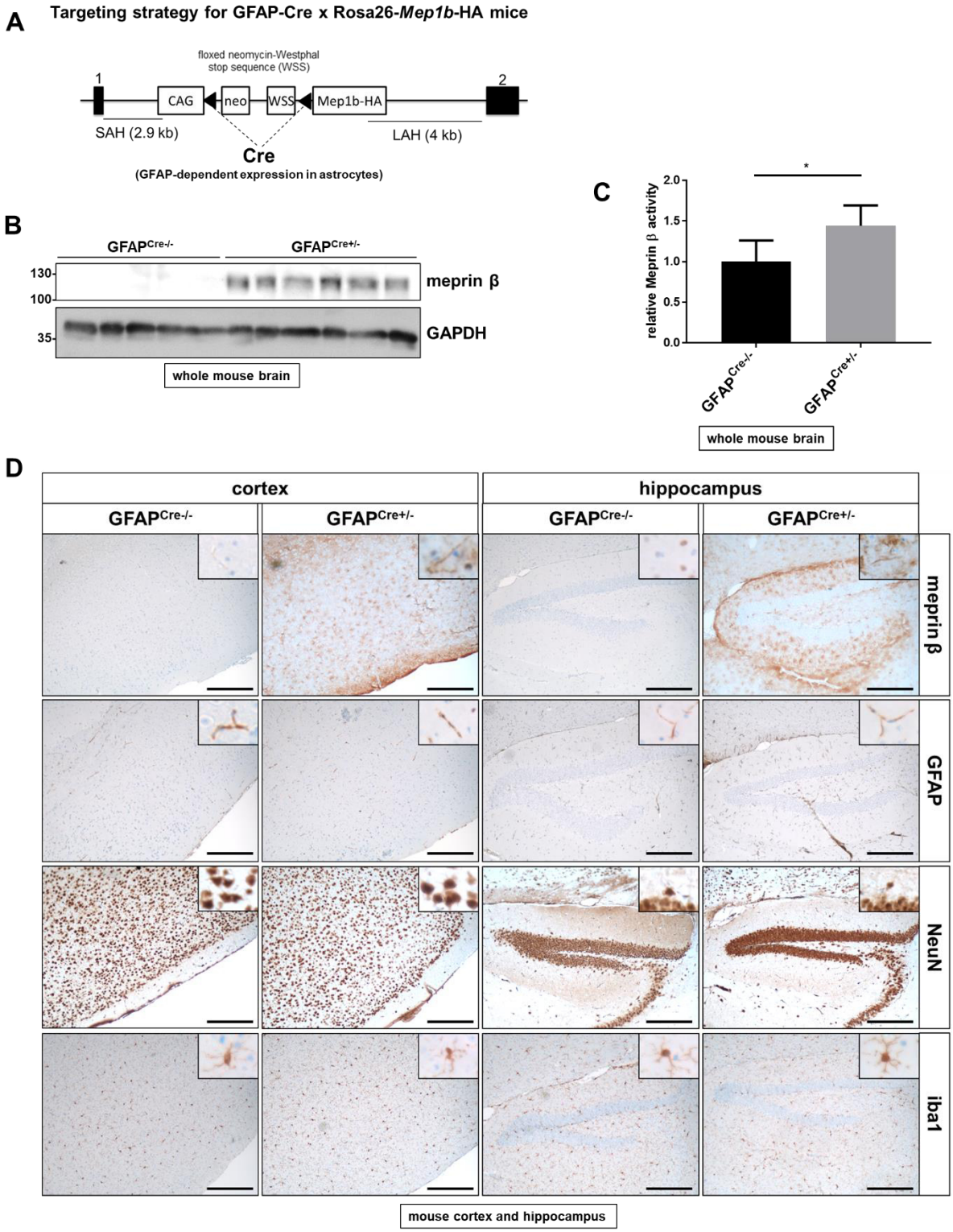

Fig. 24: GFAP$^{Cre+/-}$;Rosa26$^{Mep1b\text{-}HA}$ mice overexpress meprin β in astrocytes.

(A) GFAP$^{Cre+/-}$;Rosa26$^{Mep1b\text{-}HA}$ mice contain a gene coding for C-terminal HA-tagged meprin β (*Mep1b*-HA) under the control of a CAG promotor. Transcription is prevented by a floxed neomycin-Westphal stop sequence (WSS). Only after crossing with GFAP-Cre mice, Cre is expressed in astrocytes and cuts off the floxed neomycin and Westphal stop cassette, thereby inducing meprin β overexpression. SAH – short arm of homology; LAH – long arm of homology. **(B)** Brains from one-year-old GFAP^{Cre};Rosa26$^{Mep1b\text{-}HA}$ were homogenized. Lysates were analyzed with SDS-PAGE and Western blot using the antibodies meprin β (Tier1) and GAPDH (14C10). **(C)** Brains from one-year-old GFAP^{Cre};Rosa26$^{Mep1b\text{-}HA}$ mice were homogenized. Meprin β activity in the lysates was measured using a

quenched fluorogenic peptide assay highly specific for meprin β. **(D)** Brain sections from 1 y old GFAP^{Cre};Rosa26$^{Mep1b\ HA}$ mice were IHC stained. Pictures were taken with the EP50 Kit (Leica) with a 10x objective. Pictures of the cell morphology in the respective upper right corner were taken using the 40x objective. The scale bar indicates 200 µm.

Moreover, APP cleavage fragments in whole brain lysates were analyzed using Western blot. Using the neo-epitope specific sAPPβ+1 antibody, elevated sAPPβ levels were detected in brains of one-year-old GFAP$^{Cre+/-}$;Rosa26$^{Mep1b\text{-}HA}$ mice (Fig. 25A). In Cre-negative control mouse brains, sAPPβ+1 was not observed. In order to validate that meprin β does not induce BACE1 activity, the BACE1 substrate SEZ6 was analyzed. Of note, SEZ6 levels were not altered upon meprin β overexpression in astrocytes, which supports BACE1-independent APP processing by meprin β. Most strikingly, ELISA measurements revealed increased Aβx-40 levels in GFAP^{Cre};Rosa26$^{Mep1b\text{-}HA}$ mouse brains (Fig. 25B). Although Aβ levels were increased, there was no Aβ deposition detectable exemplarily shown in cortex and hippocampus (Fig. 25C).

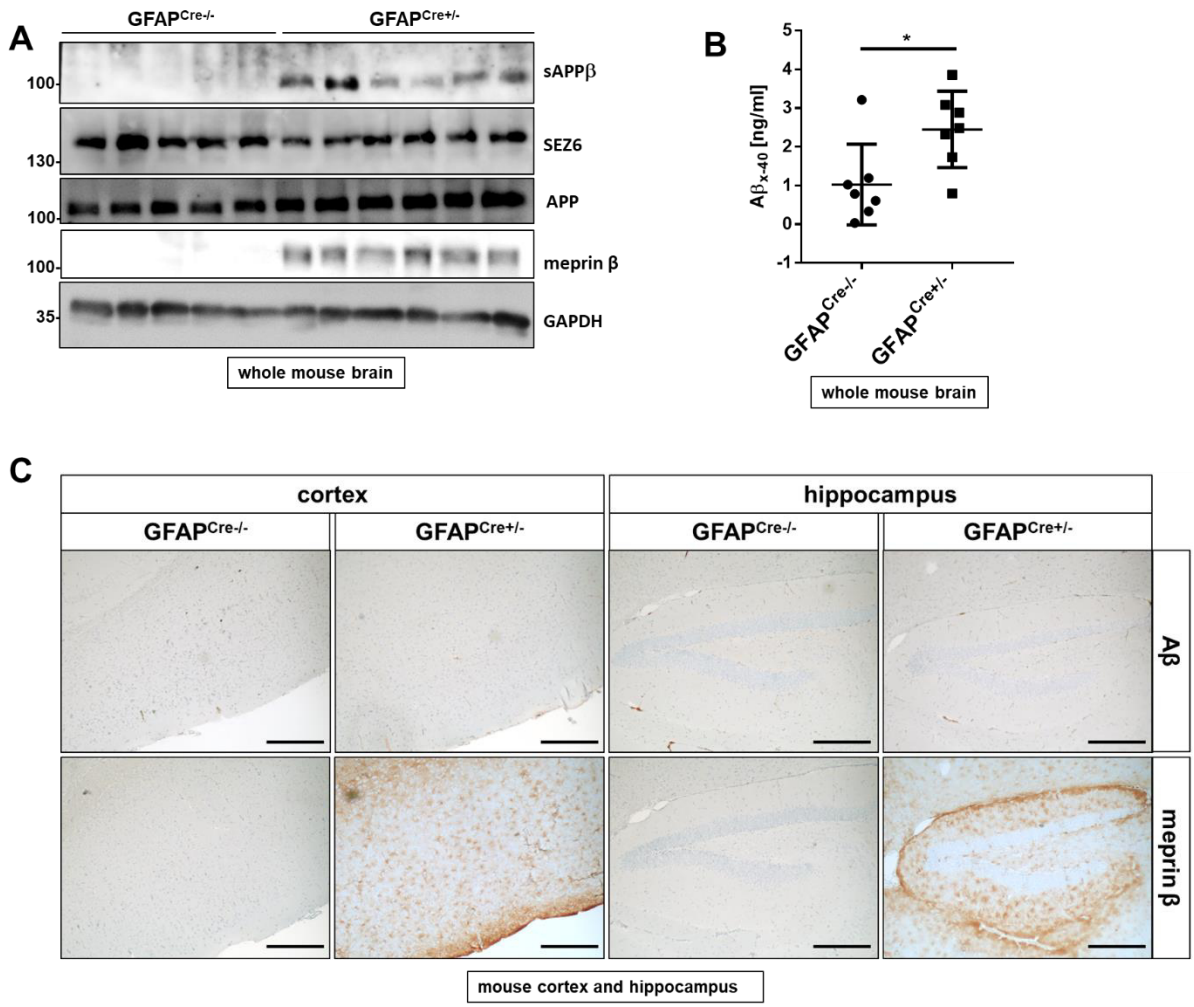

Fig. 25: Meprin β overexpression in astrocytes alters APP cleavage and increases Aβ release.
(A) Brains from one-year-old GFAP^{Cre};Rosa26$^{Mep1b\text{-}HA}$ mice were homogenized. Lysates were analyzed with SDS-PAGE and Western blot using the antibodies sAPPβ+1 (Tier3), SEZ6 (14E5), APP (CT-15), meprin β (Tier1) and GAPDH (14C10). **(B)** Brains from one-year-old GFAP^{Cre};Rosa26$^{Mep1b\text{-}HA}$ mice were homogenized. Aβx-40 levels in the lysates were quantified with ELISA measurements. **(C)** Brain sections from one-year-old GFAP^{Cre};Rosa26$^{Mep1b\text{-}HA}$ mice were IHC stained. Pictures were taken with the EP50 Kit (Leica) with a 10x objective. The scale bar indicates 200 µm.

To further characterize GFAP^{Cre};Rosa26$^{Mep1b\text{-}HA}$ mice, the mouse brains were cut in 180 to 250 µm thick organotypic brain slices (OBS) and cultivated for 14 to 20 days. 24 h before harvesting the OBSs, they were cultivated in serum-free medium to avoid meprin β inhibition by serum components. Immunofluorescence staining revealed meprin β overexpression in astrocytes of GFAP$^{Cre+/-}$;Rosa26$^{Mep1b\text{-}HA}$ mice, as meprin β signals partly co-localize with GFAP staining (Fig. 26A). Since the meprin β activity was increased in meprin β overexpressing OBSs, it is also maturated by endogenous activators in OBSs (Fig. 26B). Of note, time-dependent cultivation of OBSs revealed a high increase of Aβ release by meprin β overexpressing OBSs after 20 d in culture (Fig. 26C). However, Aβ release from OBS of the control mice is barely detectable. Since each OBS was cut from a different brain area, regional

differences of meprin β expression and Aβ generation were analyzed. Hence, OBSs were sequentially cut from one GFAP$^{Cre+/-}$;Rosa26$^{Mep1b\text{-}HA}$ and one GFAP$^{Cre-/-}$;Rosa26$^{Mep1b\text{-}HA}$ mouse. Therefore, 800 µm of the lateral cortex were discarded and the subsequently 16 slices were collected, from which two adjacent slices were co-cultivated for 20 days and referred to as section 1-8 (Fig. 26D). The meprin β expression in GFAP$^{Cre+/-}$;Rosa26$^{Mep1b\text{-}HA}$ OBSs increases from section 1-7 and Aβ release correlates with meprin β expression (Fig. 26E). However, in section 8, representing the medial OBS between both hemispheres, the meprin β expression is low and Aβ release is not detectable. In the Cre-negative OBSs from all the different brain regions, no meprin β expression and Aβ release was observed. APP and SEZ6 were expressed in each OBS, but the levels were not markedly altered between the sections. However, BACE1 was barely detectable in each OBS.

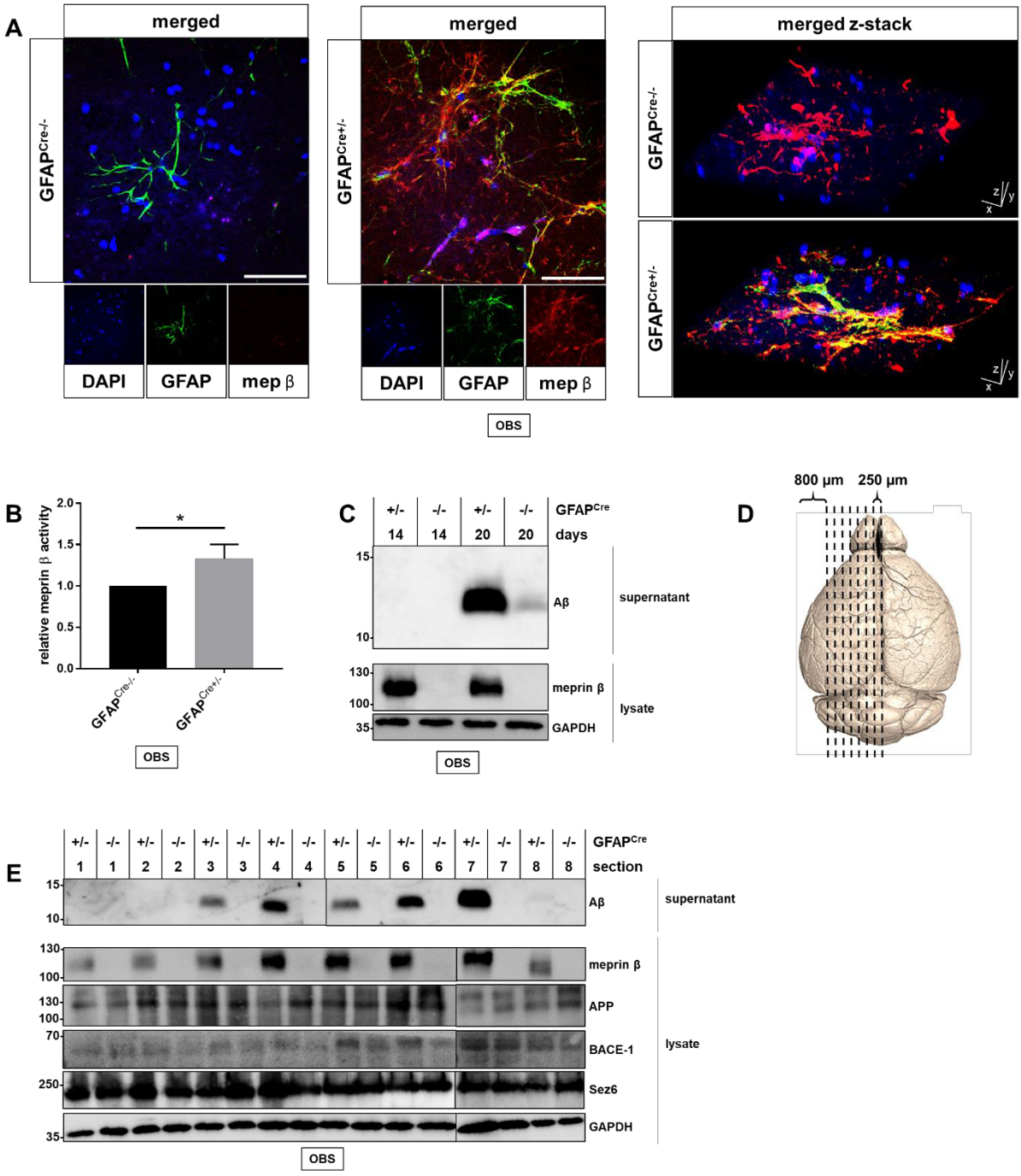

Fig. 26: OBSs of GFAP$^{Cre+/-}$;Rosa26$^{Mep1b\text{-}HA}$ show elevated Aβ release.

(A) Brains from GFAP^{Cre};Rosa26$^{Mep1b\text{-}HA}$ mice were cut into 180 µm thick sections and cultivated for 14 d. 800 µm from the lateral side of each cortex were discarded. The OBSs were subsequently IF stained as indicated. Confocal images and z-stacks are depicted. The scale bar indicates 50 µm. The scale of the z stack is 211 µm in x- and y-direction as well as 15 µm in z-direction. **(B)** Brains from GFAP^{Cre};Rosa26$^{Mep1b\text{-}HA}$ mice were cut into 250 µm thick sections. Each two non-adjacent sections were co-cultivated for 20 d to reduce regional differences. 800 µm from the lateral side of each cortex were discarded. The OBSs were lysed and the meprin β activity was measured using a highly specific quenched fluorogenic substrate. **(C)** Brains from GFAP^{Cre};Rosa26$^{Mep1b\text{-}HA}$ mice were cut into 250 µm thick sections and each two non-adjacent sections were co-cultivated for 14 or 20 d. Lysates and supernatants were lysed and analyzed with SDS-PAGE and Western blot using the murine Aβ/sAPPα (poly18058), meprin β (Tier1) and GAPDH (14C10). **(D)** The cutting procedure for (E) is depicted. From the lateral side of one hemisphere of one GFAP$^{Cre+/-}$;Rosa26$^{Mep1b\text{-}HA}$ and one GFAP$^{Cre-/-}$;Rosa26$^{Mep1b\text{-}HA}$ mouse 800 µm were

discarded. Then, sixteen 250 µm thick slices were cut to obtain OBSs of the entire hemisphere. Each two adjacent slices were co-cultivated and referred to as sections 1-8 **(E)** OBSs were cut as described in (D). Subsequently, the OBSs were cultivated for 20 d. Lysates and supernatants were analyzed with SDS-PAGE and Western blot using the murine Aβ/sAPPα (poly18058), meprin β (Tier1), APP (CT15), BACE1 (A17035K), SEZ6 (14E5) and GAPDH (14C10).

Next, the consequences of Aβ accumulation upon astrocyte-specific overexpression of meprin β were analyzed. Since one of many neurotoxic causes of Aβ is the induction of apoptosis mediated by caspase-3 (Takuma et al., 2004), the activation of caspase-3 was examined. Analyzing caspase-3 levels by Western blot revealed no differences in brain lysates of GFAP$^{Cre+/-}$;Rosa26$^{Mep1b\text{-}HA}$ and GFAP$^{Cre-/-}$;Rosa26$^{Mep1b\text{-}HA}$ mice, as a band slightly below 35 kDa was detected in each sample representing inactive pro-caspase-3 (Fig. 27A). Since aging of OBSs is strongly accelerated compared to living mice (Croft and Noble, 2018) and the results of this thesis revealed OBSs as a suitable model for meprin β-dependent Aβ accumulation, caspase-3 activation was also analyzed in OBSs. Therefore, OBSs were cultivated for 19 days before changing to serum-free medium in order to avoid meprin β inhibition by serum components and induce Aβ release (Fig. 27B). After 24 h, the medium was supplemented with serum and the OBSs were further cultivated to day 24, 30, and 35, respectively. Western blot analyzes revealed a slight time-dependent decrease of pro-caspase-3 levels of GFAP$^{Cre-/-}$;Rosa26$^{Mep1b\text{-}HA}$ OBSs (Fig. 27C). However, pro-caspase-3 levels in GFAP$^{Cre+/-}$;Rosa26$^{Mep1b\text{-}HA}$ OBSs were markedly decreased on day 30 and 35 and, intriguingly, a band of 17 kDa appeared on day 30 and even showed increased intensity on day 35 representing the large subunit p17 of activated capspase-3 (reviewed in Nicholson, 1999). Therefore, these results indicate that meprin β overexpression in astrocytes induces apoptosis in OBSs presumably due to Aβ release.

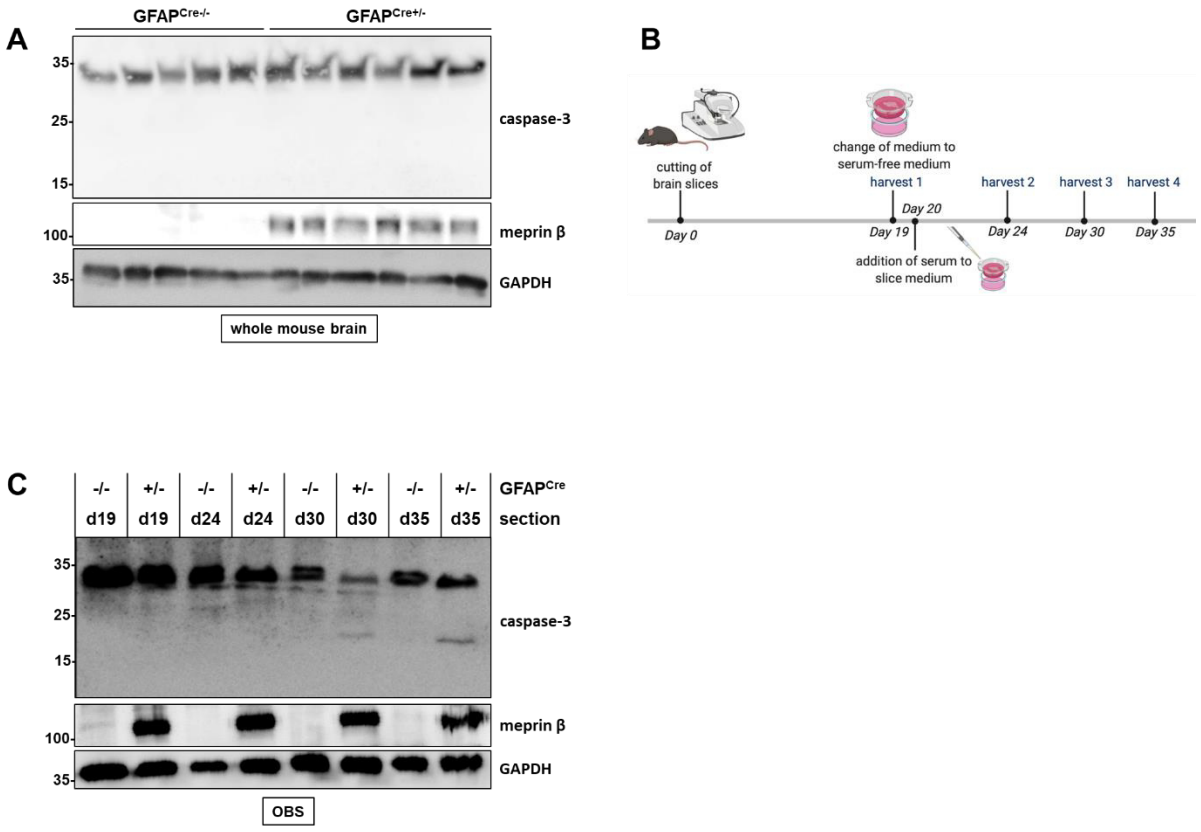

Fig. 27: Caspase-3 is activated upon Aβ release by meprin β in GFAP$^{Cre+/-}$;Rosa26$^{Mep1b\text{-}HA}$ mice OBSs.
(A) Brains from one-year-old GFAPCre;Rosa26$^{Mep1b\text{-}HA}$ mice were homogenized. Lysates were analyzed with SDS-PAGE and Western blot using the antibodies caspase-3 (8G10), meprin β (Tier1) and GAPDH (14C10). **(B)** Cultivation procedure of (C). Brains from GFAP^{Cre};Rosa26$^{Mep1b\text{-}HA}$ mice were cut into 250 µm thick sections and each two non-adjacent sections were co-cultivated for 20 d. 800 µm from the lateral side of each cortex were discarded. On day 19, selective OBSs were harvested. The medium of the remaining OBSs was changed to serum-free medium for 24 h to achieve Aβ release through meprin β activation. Then, the medium was supplemented with serum and the OBSs were further cultivated and harvested on day 24, 30 or 36, respectively. **(C)** Lysates of harvested OBSs cultivated as described in (B) were analyzed with SDS-PAGE and Western blot using the antibodies caspase-3 (8G10), meprin β (Tier1) and GAPDH (14C10).

3.4 Consequences of Meprin β overexpression in astrocytes beyond AD

In order to characterize the effects of meprin β overexpression in astrocytes beyond AD, a TAILS analysis of GFAP^{Cre};Rosa26$^{Mep1b\text{-}HA}$ mouse brain lysates was performed. No significant differences on the respective protein levels could be elucidated for two independent TAILS experiments (Supplementary Fig. S1). Though no changes on the protein level could be observed, the overexpression of meprin β was assessed on the N-terminomics level after TAILS depletion. From the TAILS data, 35 and 19 N-termini were identified as statistically different between GFAP$^{Cre+/-}$;Rosa26$^{Mep1b\text{-}HA}$ and GFAP$^{Cre-/-}$;Rosa26$^{Mep1b\text{-}HA}$ samples for experiments 1 and 2, respectively (Supplementary Fig. S2 and Supplementary Tab. S1 and S2). From this list, several enriched N-termini may derive from meprin β substrates, as

they contain at least one acidic amino acid within the cleavage site (Tab. 11). Of note, seven of the identified substrates play a role in brain development or in neuronal biology. Thus, cleavage of these proteins by meprin β may alter the cognitive function of the astrocyte-specific meprin β overexpressing mice.

Tab. 11: Novel candidate *in vivo* substrates of meprin β overexpressed in astrocytes.

The list only contains substrates cleavage sites with at least one glutamate or aspartate due to meprin β´s preference for acidic amino acids. Functions of substrates, which may alter brain development and neuronal biology, are written in bold. The promising substrate latrophilin 3 is highlighted by a red box, since cell culture experiments experiments validated highly increased cleavage fragments generated by meprin β.

Identified novel substrate	**Uniprot protein accessions**	**Identified cleavage sites**	**Function**
Receptor-type tyrosine-protein phosphatase zeta	B9EKR1	E439/D440	**Negatively regulates oligodendrocyte precursor proliferation in the embryonic spinal cord (Kuboyama et al., 2012)**
Neurocan core protein	P55066	Q24/D25 Q27/D28 D28/T29	**May modulate neuronal adhesion and neurite growth during development by binding to neural cell adhesion molecules (Friedlander et al., 1994)**
Brevican core protein	Q61361	E417/D418 L460/E461 E461/E462 E467/D468 R474/E475 E584/T585	**May inhibit neurite outgrowth (Yamada et al., 1997)**
Chondroitin sulfate proteoglycan-5	Q71M36	E70/D71	**May be involved in neuritogenesis (Nakanishi et al., 2006)**
Latrophilin 3	Q80TS3	D484/S485	**Plays a role in cell-cell adhesion and neuron guidance (Del Toro et al., 2020)**
Probable G-protein coupled receptor-158	Q8C419	R36/E37	**Orphan receptor which influences neuron morphology and controls stress-induced depression (Sutton et al., 2018)**
Hyaluronan and proteoglycan link protein-1	Q9QUP5	S20/D21 D21/S22	**Part of the extracellular matrix in the brain; induce human neocortex folding (Long et al., 2018)**
Protein S100-A5	P63084	R22/E23	Ion-binding protein with unknown function (Schäfer et al., 2000)
CD99 antigen-like protein-2	Q8BIF0	E33/D34	Involved in diapedesis (Bixel et al., 2010)
Beta-actin-like protein-2	Q8BFZ3 P60710 P63260	Y167/E168	Unknown function, presumably involved in cell motility like other actins (Svitkina, 2018)

Amongst the newly identified meprin β substrates, cleavage of the G protein-coupled receptor (GPCR) latrophilin 3 (LPHN3) may be of potential biological relevance, since cleavage leads to the release of the two extracellular domains of LPHN3: the sea urchin egg lectin (SUEL)-type lectin and olfactomedin-like domain (The UniProt Consortium, 2021, https://www.uniprot.org/uniprot/Q80TS3) (Fig. 28A). Besides these domains, LPHN3 contains a hormone-binding domain and a highly glycosylated GPCR autoproteolysis inducing (GAIN) domain (Araç et al., 2012; O'Sullivan et al., 2014). At the C-terminal part of the GAIN domain, LPHN3 is cleaved by autoproteolysis resulting in a membrane-bound C-terminal fragment (LPHN3-CTF) and a non-covalently linked N-terminal fragment (LPHN3-NTF) (Araç et al., 2012; reviewed in Moreno-Salinas et al., 2019). As a result, the so-called stachel sequence located at the new N-terminus of the LPHN3-CTF is exposed and may acts as tethered agonist for the GPCR activity of LPHN3 (Röthe et al., 2019). In whole brain lysates of GFAP$^{Cre-/-}$;Rosa26$^{Mep1b\text{-}HA}$ mice, an intensive LPHN3 band slightly above 130 kDa was detected, which was reduced in GFAP$^{Cre+/-}$;Rosa26$^{Mep1b\text{-}HA}$ mouse brain lysates (Fig. 28B). These bands presumably represent the highly glycosylated LPHN3-NTF. In astrocyte-specific meprin β overexpressing mice, an additional band occurred around 100 kDa and most likely represents the C-terminal part of LPHN3-NTF cleaved by meprin β, however, in control mice this fragment was barely detectable. Moreover, LPHN3-NTF cleavage was also observed in OBSs. In GFAP$^{Cre+/-}$;Rosa26$^{Mep1b\text{-}HA}$ OBSs the 130 kDa signal of LPHN-NTF was reduced compared to the control mice, whereas the 100 kDa signal was increased (Fig. 28C).

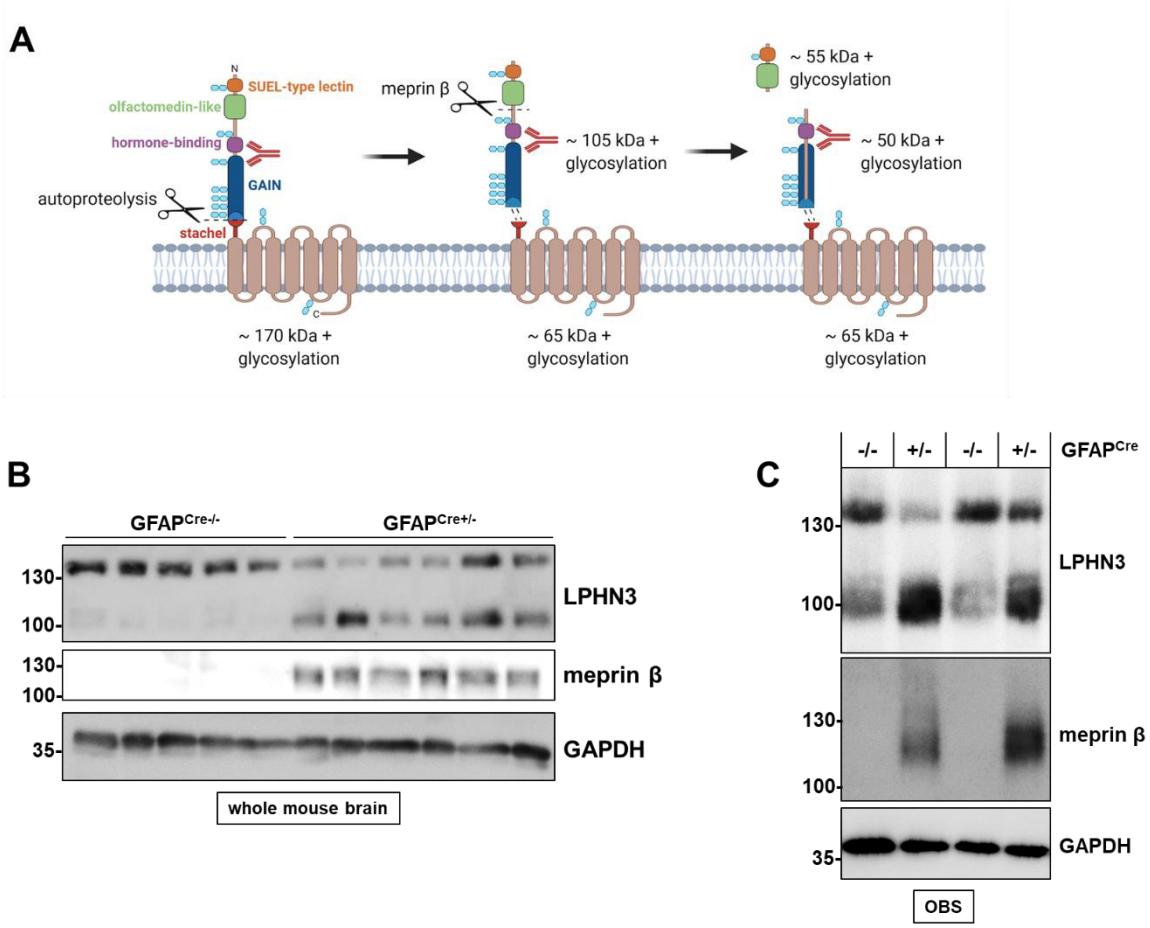

Fig. 28: LPHN3 cleavage by meprin β in mouse brains.

(A) LPHN3 consists of a short C-terminal part, a seven-pass transmembrane domain, a GPCR autoproteolysis inducing (GAIN) domain with N-terminally adjacent hormone-binding domain and a C-terminally included stachel sequence, an olfactomedin-like domain and a sea urchin egg lectin (SUEL)-type lectin domain. Upon autoproteolysis, LPHN3 is cleaved into a membrane-bound C-terminal fragment (LPHN3-CTF) and a non-covalently linked N-terminal fragment (LPHN3-NTF). Meprin β cleaves within the LPHN3 ectodomain releasing a fragment containing the SUEL-type lectin and olfactomedin-like domain. The used LPHN3 (B-6) antibody (red) binds between the GAIN and the olfactomedin-like domain as indicated. Glycosylation sites are highlighted in light blue. The molecular weight of LPHN3 and its cleavage fragments are depicted based on the amino acid sequence, however, the actual molecular mass is presumably higher than calculated due to glycosylated side chains. The figure was created based on results from Araç et al., 2012; O'Sullivan et al., 2014; Moreno-Salinas et al., 2019; The UniProt Consortium, 2021. **(B)** Brains from one-year-old GFAP^{Cre};Rosa26$^{Mep1b\text{-}HA}$ mice were homogenized. Lysates were analyzed with SDS-PAGE and Western blot using the antibodies LPHN3 (B-6), meprin β (Tier1) and GAPDH (14C10). **(C)** Brains from GFAP^{Cre};Rosa26$^{Mep1b\text{-}HA}$ mice were cut to 250 µm thick sections. 800 µm from the lateral side of each cortex were discarded. The OBSs were cultivated for 20 d. Lysates and supernatants analyzed with SDS-PAGE and Western blot using the antibodies LPHN3 (B-6), meprin β (Tier1) and GAPDH (14C10).

The cleavage of LPHN3 by meprin β was validated in an overexpression model, transfecting HEK cells with human meprin β as well as N-terminal HA-tagged murine LPHN3. Due to a biotinylation step prior to the lysis, cell surface proteins were purified using streptavidin beads. Using an N-terminal HA-tag antibody, single transfected LPHN3 occurred as two signals above

130 kDa in the lysate (Fig. 29A). As a control the catalytically inactive meprin β variant E153A was co-transfected with LPHN3, however, the band pattern was not markedly altered compared to LPHN3 transfection alone. Since the lower band was abolished in the biotinylated fraction, it might represent a minor glycosylated ER form. However, the higher band can presumably be assigned to the fully glycosylated non-covalently linked LPHN3-NTF, as only this signal was dominantly detectable in the biotinylated fraction. Interestingly, upon co-transfection with meprin β WT, membrane-bound LPHN3-NTF was hardly detectable at the cell surface with the HA-tag antibody due to ectodomain cleavage by meprin β. This finding was supported by the accumulation of a 55 kDa fragment in the supernatant, which probably represents the cleaved part of the ectodomain, when meprin β WT was present. Using a LPHN3 antibody binding to LPHN3-NTF C-terminal of the potential meprin β cleavage site, LPHN3-NTF occurred as double band between 100 and 150 kDa in the lysate as well as in the biotinylated fraction, when transfected alone or together with meprin β E153A. The lower band was not detectable using the HA antibody indicating that this signal represents an N-terminal truncated LPHN3-NTF fragment. When meprin β WT was co-transfected, both LPHN3-NTF bands were markedly reduced, whereas a dominant membrane-bound cleavage fragment at 100 kDa and minor fragments at around 50-60 kDa occurred. Since the effect of meprin β WT on LPHN3 was more pronounced in the biotinylated fraction than in the lysate, it can be concluded that LPHN3 cleavage by meprin β predominantly occurs at the cell surface.

In summary, the results indicate that LPHN3-NTF, which is covalently linked to the membrane-bound LPHN3-CTF, occurs partly N-terminally truncated in the HEK cell-based overexpression model (Fig. 29B). Both LPHN-NTF forms were efficiently cleaved by meprin β between the GAIN and the hormone-binding domain and thereby the olfactomedin-like and the SUEL-type lectin domains were released from the remaining LPHN3-NTF.

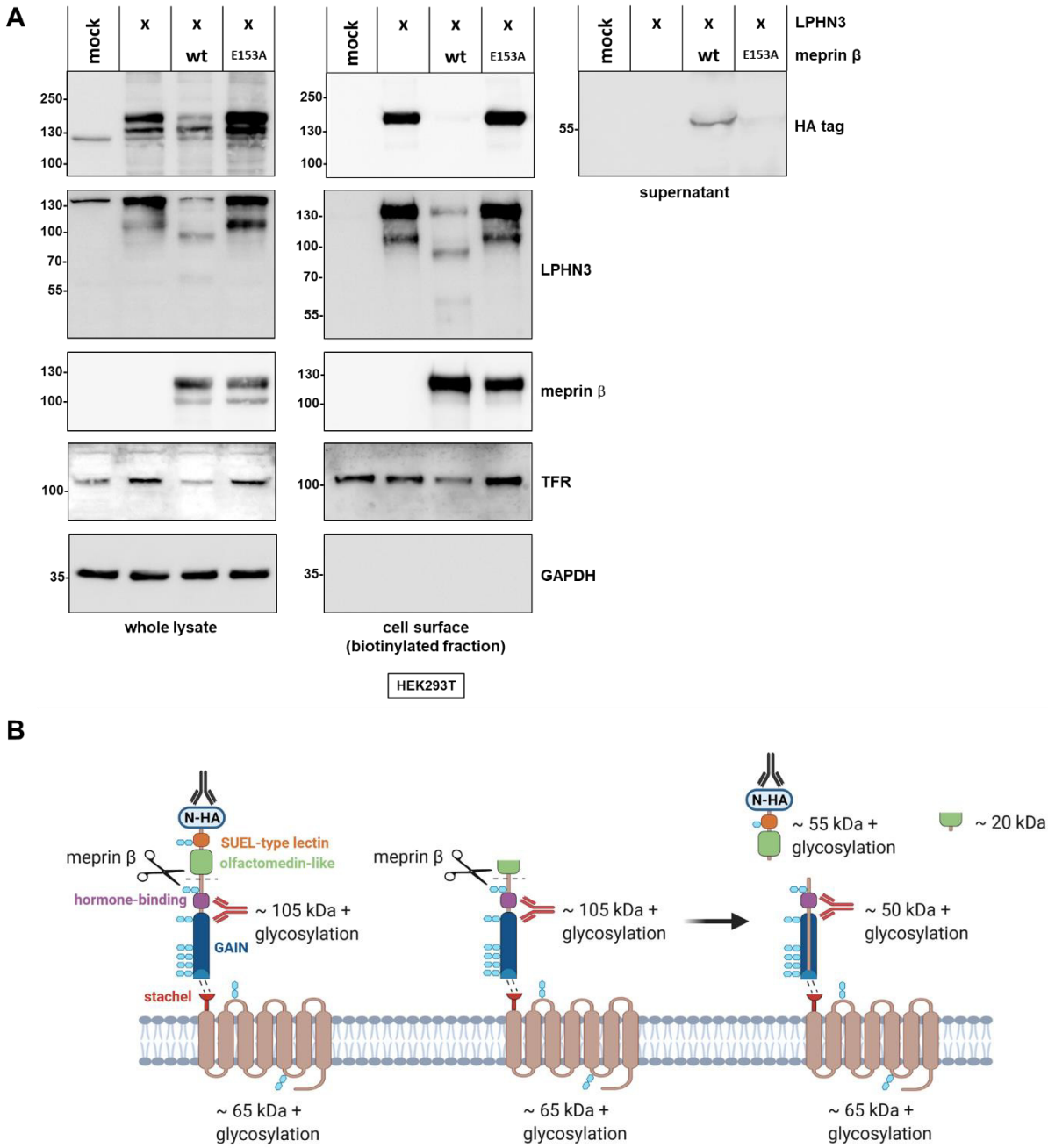

Fig. 29: LPHN3 cleavage by meprin β in a HEK cells-based overexpression model.

(A) HEK cells were transfected with human meprin β, meprin β E153A and LPHN3. After 24 h, the medium was changed to serum-free DMEM for 4 h. Cells were biotinylated, harvested and lysed. The whole lysate, the biotinylated fraction, as well as supernatants were analyzed by SDS-PAGE and Western blot using the antibodies HA-tag (C29F4), LPHN3 (B-6), meprin β (Tier1) and TFR (ab84036) and GAPDH (14C10). **(B)** As a consequence of autoproteolytic processing, LPHN3 occurs as a membrane-bound C-terminal fragment (LPHN3-CTF) consisting of a short C-terminal part, a seven-pass transmembrane domain and the exposed stachel sequence, as well as a non-covalently linked N-terminal fragment (LPHN3-NTF) comprising a GPCR autoproteolysis inducing (GAIN) domain, a hormone-binding domain, an olfactomedin-like domain and a sea urchin egg lectin (SUEL)-type lectin domain. In HEK cell-based overexpression, the LPHN3-NTF is partly N-terminally truncated. Meprin β cleaves both LPHN3-NTF entities within the LPHN3 ectodomain removing the SUEL-type lectin and olfactomedin-like domain entirely from the non-covalently bound LPHN3-NTF. The used HA-tag (C29F4) antibody (black) binds to the N-

terminal HA-tag of LPHN3-NTF. The used LPHN3 (B-6) antibody (red) binds between the GAIN and the olfactomedin domain as indicated. Glycosylation sites are highlighted in light blue. The molecular weight of the LPHN3 fragments are depicted based on the amino acid sequence, however, the actual molecular mass is presumably higher than calculated due to glycosylated side chains. The figure was created based on results from Araç et al., 2012; O'Sullivan et al., 2014; Moreno-Salinas et al., 2019; The UniProt Consortium, 2021, https://www.uniprot.org/ uniprot/Q80TS3.

4. Discussion

Meprin β is a metalloprotease capable of cleaving APP at the β-secretase site. As a result, Aβ peptides are released, which are prone to aggregate and form neurotoxic oligomers as well as senile plaques (Bien et al., 2012; reviewed in Becker-Pauly and Pietrzik, 2016). Hence, amyloidogenic APP cleavage plays a major role for the pathobiochemistry of AD (reviewed in Castro et al., 2019). In contrast to BACE1, which has been considered as the most relevant β-secretase from the AD research field (reviewed in Cole and Vassar, 2008), the cleavage site of meprin β is shifted one amino acid towards the C-terminus of APP, thus, N-terminal truncated Aβ peptides are released (Bien et al., 2012). These truncated Aβ2-x species are elevated in AD patient brains (Wiltfang et al., 2001) and exhibit a higher potential to aggregate than Aβ1-x (Schönherr et al., 2016). Of note, BACE1 is not capable of generating Aβ2-x, therefore, the formation of Aβ2-x is thought to involve an alternative β-secretase (Wiltfang et al., 2001; Schieb et al., 2010). Moreover, several BACE1 inhibitors have been failing in clinical trials as treatment for AD (reviewed in Moussa-Pacha et al., 2020; reviewed in Yiannopoulou and Papageorgiou, 2020). Therefore, alternative β secretases, such as meprin β emerged as promising targets in AD research. Since meprin β is upregulated in AD patient brains (Bien et al., 2012; Schlenzig et al., 2018) and an AD-associated genetic variant of meprin β was identified (Patel et al., 2018), an involvement of meprin β in the pathogenesis of AD is hypothesized. This is further supported by recent findings, which revealed meprin β as member of a high-molecular-weight cluster consisting of AD-associated proteins such as APP, ADAM10 and the γ-secretase complex. Of note, BACE1 was present in this protein cluster to a minor extend. Upon *in vitro* cultivation of *ex vivo* isolated microvesicles from the mouse brain comprising this cluster of proteins, it is capable of releasing Aβ (Liu et al., 2019). Therefore, it was investigated in this thesis whether the alternative β-secretase meprin β and the generation of Aβ2-x peptides might play a role in AD.

4.1 Mechanistic regulation of APP cleavage by meprin β

4.1.1 Phosphorylation of meprin β controls its β-secretase activity

In the first part of this thesis, aspects of the intracellular and extracellular regulation of meprin β with regard to APP cleavage were analyzed in different cell-based *in vitro* models. Since intracellular regulation of meprin β is barely addressed in the literature, the phosphorylation of meprin β was characterized. Using phospho-specific antibodies, phosphate-affinity SDS-PAGE and mass spectrometry analyzes, multiple phosphorylation sites at the cytoplasmic part of meprin β were identified, the most prevalent being T694. A previous study from 2003 also described meprin β phosphorylation in a PMA-dependent manner. However, the authors

claimed that phosphorylation only occurs at Ser287 (Hahn et al., 2003). This discrepancy might occur due to a broader spectrum of more sensitive methods available nowadays to identify phosphorylation sites. Furthermore, the aim of this study was to identify PKC isoforms, which are involved in meprin β phosphorylation. Out of four analyzed isoforms, only PKCα and -β were identified as candidate kinases, both representing conventional PKC subtypes capable of phosphorylating serine and threonine residues in a PMA-dependent manner (reviewed in Steinberg, 2008). Since the LC-MS analyzes revealed predominant phosphorylation of cytoplasmic serine and threonine residues, a direct phosphorylation of the PKCs is likely. However, also Y682 was identified as possible phosphorylation site. Thus, other kinases may also be involved in meprin β phosphorylation. Moreover, this study focused on the biological consequences of meprin β phosphorylation. Therefore, a meprin β variant mimicking constitutive phosphorylation due to substituting all potential cytoplasmic phosphorylation sites with a glutamate residue was analyzed. Inhibitor studies revealed that this meprin β variant mimicking constitutive phosphorylation is internalized and lysosomally degraded. Therefore, it was hypothesized that this is the consequence of meprin beta phosphorylation. Endocytosis as a consequence of phosphorylation is a frequently observed phenomenon, since many transmembrane receptors become internalized upon phosphorylation (Filippova et al., 1999; Sergé et al., 2011). Furthermore, the proteasomal, but also the lysosomal degradation of proteins marked with phosphorylation motifs, which was observed for meprin β in this study, is often reported in the literature (Liu et al., 2002; Thompson et al., 2009; Varedi K et al., 2010; Zemoura et al., 2019). As a result of protein internalization, the cell surface abundance of meprin β is reduced. Therefore, meprin β activity at the cell surface is diminished and substrate cleavage is reduced, in this study exemplarily shown for APP and IL-6R. Analyzing APP processing by meprin β revealed that phosphorylation causes decreased Aβ generation. Hence, it can be concluded that PKC-mediated meprin β phosphorylation counteracts the amyloidogenic pathway by promoting internalization of meprin β and may represent a promising therapeutic target for AD. Of note, AD preventing properties of PKC activity are extensively described in the literature (Savage et al., 1998; Etcheberrigaray et al., 2004; reviewed in Talman et al., 2016). *Inter alia*, PKC is capable of activating gelosin, which inhibits Aβ fibrillization (Ji et al., 2010). Another target of PKCs are the embryonic lethal abnormal vision (ELAV)-like RNA-binding proteins that regulate the stability and translation of mRNAs involved in synaptic remodeling connected to cognitive processes. These RNA-binding proteins are upregulated upon PKC-mediated phosphorylation (reviewed in Talman et al., 2016). However, some studies attribute PKC AD promoting properties (Alfonso et al., 2016). Therefore, the detailed role of PKCs in AD is still elusive and requires further investigation. However, with regard to the interplay of meprin β and the α-secretase ADAM17, PKC activity can be assigned anti-amyloidogenic properties (Fig. 30). ADAM17 can be activated by PKC

activity and acts as meprin β sheddase (Hahn et al., 2003). Since shed meprin β is not capable of cleaving APP at the β-secretase site (Bien et al., 2012), this event prevents from Aβ formation. Moreover, ADAM17 itself acts as α-secretase upon activation by PKCs, thereby also preventing from amyloidogenic APP processing (Buxbaum et al., 1998; Kuhn et al., 2010). In this study, another AD preventing event, the internalization and degradation of the alternative β-secretase meprin β, was observed induced by multi-phosphorylation of its C-terminus involving PKCα and -β.

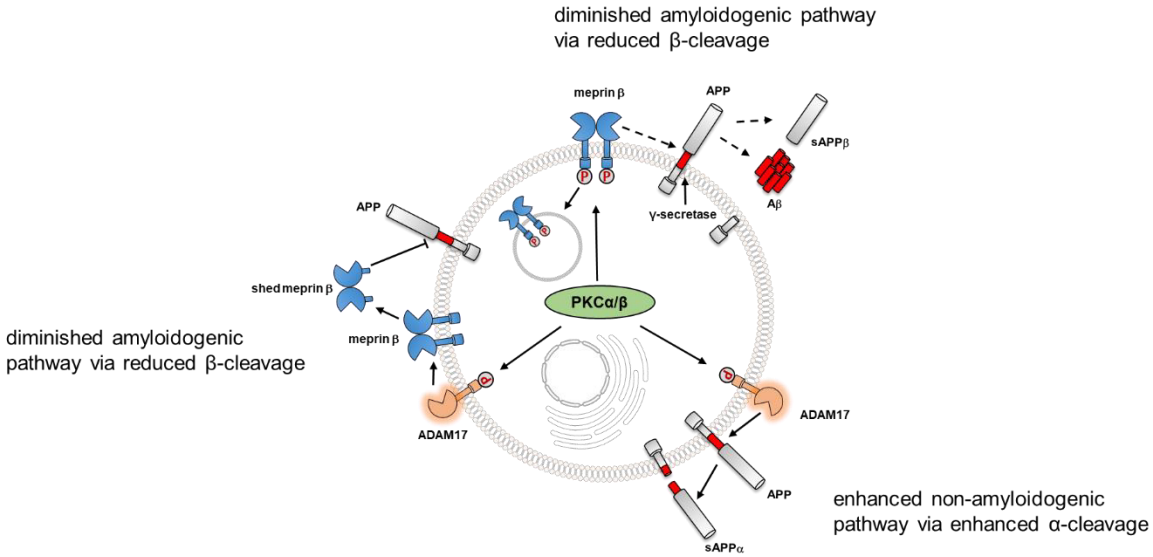

Fig. 30: PKC-mediated phosphorylation events prevent from Aβ release.

PKCα and -β are involved in meprin β phosphorylation. As a consequence, meprin β is internalized and degraded. Thus, APP cleavage by meprin β is diminished. Also ADAM17 can be phosphorylated by PKCs leading to its activation. ADAM17 prevents from Aβ release by cleaving APP at the α-secretase site and shedding the ectodomain of meprin β from the cell surface. Shed meprin β is not able to act as β-secretase. The figure was generated based on findings from this study and Buxbaum et al., 1998; Hahn et al., 2003; Kuhn et al., 2010; Bien et al., 2012.

4.1.2 RgpB-mediated meprin β activation causes elevated Aβ release

To further characterize the regulation of meprin β with regard to APP cleavage, the bacterial meprin β activator RgpB was analyzed. RgpB is a virulence factor secreted by *P. gingivalis*, a gram negative bacterium responsible for periodontitis (reviewed in Curtis et al., 2001). However, *P. gingivalis* is also capable of colonizing the gut through saliva flow and may influence meprin β biology in the intestine (Nakajima et al., 2015). In a previous study, it was observed that RgpB serves as an activator of meprin β. Since activation of meprin β prevents from its ectodomain shedding, the presence of RgpB diminishes shed meprin β levels. In the intestine, shed meprin β plays an important physiological role by cleaving MUC2, one essential component of the mucus barrier, which cannot be accomplished by membrane-bound meprin β. Hence, this mechanism promotes mucus homeostasis and the release of the

virulence factor RgpB induces bacterial overgrowth and intestinal inflammation by preventing from MUC2 cleavage by meprin β activation (Wichert et al., 2017).

Recently, a publication described that *P. gingivalis* is capable of colonizing the brain, which was predominantly observed in AD patients (Dominy et al., 2019). Correlation studies revealed a coherence between levels of RgpB and tau. Further mouse experiments showed that upon oral administration of P*. gingivalis*, it colonizes the brain and causes elevated Aβ levels (Dominy et al., 2019). Therefore, one aim of this thesis was to analyze whether the Aβ increase upon brain infection with *P. gingivalis* might occur as a result of meprin β activation. To address this assumption, the Aβ release was quantified upon meprin β activation with RgpB in a HEK cell-based overexpression model. Interestingly, the Aβ levels were significantly increased in presence of RgpB. The application of the meprin inhibitor actinonin led to diminished Aβ levels. Hence, meprin β activation by RgpB indeed caused increased β-secretase activity and elevated Aβ production. However, the *in vivo* relevance of meprin β as mediator of RgpB-dependent Aβ accumulation still needs to be investigated. Nevertheless, the data of this thesis suggest that a brain infection with *P. gingivalis* may contribute to AD pathology via meprin β activation.

Apart from the pathological consequences of Aβ generation, the upregulation of Aβ upon brain infection might support the innate immune system, since Aβ serves as an antimicrobial peptide, thereby contributing to the defense against pathogens (reviewed in Gosztyla et al., 2018). Several publications described the antimicrobial properties of Aβ, as it entraps viruses (Eimer et al., 2018), exerts antibiotic and antimycotic activity against bacteria as well as yeast (Soscia et al., 2010; Kumar et al., 2016), and has the ability to disrupt lipid membrane integrity (Bode et al., 2019). Of note, the presence of Aβ confers the resistance against pathogens in primary brain cells (Lukiw et al., 2010) and mice (Kumar et al., 2016). Moreover, pathogens such as herpes simplex virus-1 (HSV-1) (Wozniak et al., 2009) or the spirochete *Borrelia burgdorferi* (Miklossy, 2016) were identified in Aβ plaques of AD patients. Due to the association of pathogens and Aβ, a role of pathogens for the onset or progression of AD is suggested in the literature, but not substantially proven (reviewed in Miklossy, 2011).

4.1.3 Meprin α as part of a meprin α/β heterodimer does not exhibit β-secretase activity

The characterization of meprin β as alternative β-secretase in the previous chapters only considered meprin β homodimers, which are formed in cell-based overexpression models (Bertenshaw et al., 2003). However, the existence of meprin α/β heterodimers, which are formed presence of the other meprin metalloprotease meprin α were already described

decades ago (Johnson and Hersh, 1992). In contrast to predominantly membrane-bound meprin β, meprin α is secreted due to furin cleavage during the secretory pathway (Marchand et al., 1995). By analyzing meprin α/β heterodimers in this study, it was observed that, when meprin α and meprin β form heterodimers via a disulfide bond in the MAM domain, meprin α is tethered to the plasma membrane. This was shown in a cell-based overexpression model as well as in mouse intestine in this study.

Meprin α and meprin β share 41% sequence identity (The UniProt Consortium, 2021, https://www.uniprot.org/uniprot/Q16819, https://www.uniprot.org/uniprot/Q16820) and both have a cleavage preference for acidic amino acids (Becker-Pauly et al., 2011). However, secreted meprin α was not observed to cleave APP thus far. Of note, membrane-bound meprin β was shown to exhibit an altered substrate spectrum compared to soluble meprin β (Bien et al., 2012; Arnold et al., 2017a). With regard to APP as a substrate, only membrane-bound meprin β is capable of cleaving at the β-secretase site (Bien et al., 2012). Therefore, one aim of this study was to analyze whether meprin α is capable of cleaving APP, when tethered to the membrane as part of a heterodimer. For this purpose, APP cleavage of HEK cells overexpressing a catalytically inactive meprin β variant and meprin α WT, which form heterodimers in this experimental setup, was analyzed. However, amyloidogenic APP cleavage by the heterodimers was not was observed. The overexpression of meprin α and meprin β WT led to amyloidogenic APP cleavage to a similar extend as meprin β alone. Therefore, it can be concluded that meprin α is not capable of cleaving APP, even when tethered to the membrane as part of a meprin α/β heterodimer. This is not in discrepancy with previous studies as meprin α has not been identified as APP cleaving enzyme.

4.2 Shedding and degradation of TREM2 by meprin β might impair Aβ phagocytosis by microglia

The accumulation of Aβ is widely accepted as a key pathological event in AD (reviewed in Murphy and LeVine, 2010). While AD research at an earlier stage mainly examined the Aβ generation (Sisodia et al., 1990; Haass et al., 1995), nowadays Aβ clearance mechanisms have become a novel focus in scientific research (reviewed in Lee and Landreth, 2010; reviewed in Xin et al., 2018), and it is assumed that both the production and clearance of Aβ contribute to a dyshomeostasis of Aβ, which leads to the pathogenesis of AD (reviewed in Selkoe and Hardy, 2016). Several Aβ clearance mechanisms were identified and discussed in the literature such as the degradation of Aβ by secreted proteases, e.g. angiotensin-converting enzyme (ACE) (Hu et al., 2001; Bernstein et al., 2014) or insulin-degrading enzyme (IDE) (Chesneau et al., 2000; Leissring et al., 2003), as well as the transport of Aβ out of the brain across the blood-brain barrier for systemic clearance (reviewed in Bates et al., 2009).

Furthermore, microglia emerged as promising cells, which are capable of internalizing Aβ (reviewed in Lee and Landreth, 2010). Several clinical trials targeting the induction of Aβ uptake by microglia such as small molecules (NCT02254369) and antibodies (NCT04592874) are on-going, which promote the Aβ uptake by microglia. In context of microglia-mediated Aβ clearance, the transmembrane receptor TREM2 came into focus of research, as it was identified as AD risk gene in several GWAS studies (Jonsson et al., 2013; Sims et al., 2017) and plays a major role in the signaling induction promoting microglia activation and consequently phagocytosis (N'Diaye et al., 2009). Several ligands for the TREM2 ectodomain were identified (Daws et al., 2003; Zhong et al., 2015; Yeh et al., 2016) as for example Aβ (Zhao et al., 2018). The recognition of Aβ by TREM2 leads to the association with adaptor protein DAP12 and a signaling cascade including phosphorylation of spleen tyrosine kinase (SYK) and glycogen synthase kinase 3β (GSK3β) is initiated promoting microglia activation (Zhao et al., 2018). Of note, TREM2 was considered as AD risk gene, since several GWAS studies identified TREM2 SNPs in AD patient brains (Jonsson et al., 2013; Sims et al., 2017). Interestingly, it has been observed that ectodomain shedding of TREM2 by ADAM10 and 17 between H157 and S158 diminishes phagocytosis-activating signaling (Schlepckow et al., 2017; Thornton et al., 2017). In line with these findings, the TREM2 H157Y variant, which is shed to a high extend compared to wild-type TREM2, was identified as risk factor for AD. In this study, meprin β was identified as another TREM2 sheddase cleaving between R136 and D137, which is further N-terminal compared to the ADAM10/17 cleavage site. Additionally, meprin β was observed to subsequently degrade the shed TREM2 ectodomain. This degradation substantially distinguishes meprin β-mediated from ADAM-mediated TREM2 shedding, since the secreted sTREM2 by ADAM cleavage is still capable of inducing microglia activation (Zhong et al., 2017). The injection of sTREM2 into the brain of AD model mice even causes a cognitive benefit (Zhong et al., 2019). Meprin β-mediated shedding and degradation, however, also prevents sTREM2 signaling induction, which attributes meprin β shedding and subsequent degradation of sTREM2 a more severe impact on myeloid cell activation than the release of sTREM2 by ADAM10 and 17. The relevance of meprin β-mediated TREM2 shedding was demonstrated analyzing WT and meprin β knock-out mice, which revealed accumulation of TREM2 levels in BMDMs from meprin β knock-out compared to WT controls. Of note, ADAM stimulation with LPS also led to reduced TREM2 levels in meprin β-knock-out mice. This finding indicates that meprin β acts as constitutive TREM2 sheddase, whereas ADAM-mediated TREM2 shedding rather requires a stimulus. Moreover, meprin β-mediated TREM2 shedding and degradation led to diminished phagocytosis, which was observed in different monocytic cell lines and *ex vivo* isolated BMDMs. Hence, these results show that TREM2 cleavage by meprin β reduces the phagocytotic ability of myeloid cells and, thus, suggest a reduction of the phagocytic ability of microglia to internalize Aβ in the brain. However,

detailed studies of the interplay between meprin β and TREM2 in microglia need to be conducted. Furthermore, it would be of interest to develop an AD mouse model, to analyze whether meprin β-mediated TREM2 shedding and degradation diminishes Aβ uptake by microglia *in vivo*. If this was confirmed, meprin β might be attributed a dual AD promoting role by preventing Aβ clearance through TREM2 cleavage and elevating Aβ formation as alternative β-secretase.

4.3 Meprin β is involved in the AD pathogenesis *in vivo*

4.3.1 Meprin β and truncated Aβ2-x peptides play a so far underestimated role in APPlon mice

So far, meprin β as alternative β-secretase was only characterized *in vitro* and *in cellulo* (Bien et al., 2012; Schönherr et al., 2016). Therefore, the main aim of this thesis was the evaluation of the role of meprin β in AD *in vivo*. For this purpose, an AD mouse model was developed, that enables meprin β-dependent Aβ formation and analysis of cognitive impairments. Common AD mouse models overexpress human APP with mutations at β- and γ-secretase sites to accelerate Aβ production (reviewed in Esquerda-Canals et al., 2017). One of the most prevalent mutations in commonly used AD mouse models such as Tg2576 (Hsiao et al., 1996) or 5xFAD (Oakley et al., 2006) are the APPswe mutations K670N and M671L located N-terminal to the β-secretase site, which have a strong influence on BACE1 cleavage (Deng et al., 2013; Schönherr et al., 2016). APPswe is a much more potent BACE1 substrate than wild-type APP and highly prone to be cleaved between L671 and D672 (Deng et al., 2013), thus, representing a model to study BACE1-mediated Aβ1-x release. However, APPswe is not cleaved between D672 and A673, hence, Aβ2-x is not generated from this APP variant (Schönherr et al., 2016). Of note, the APPswe mutations were only observed in two families from Sweden, whose members were prone to develop EOAD (Mullan et al., 1992). Studying APPswe processing *in vitro* and *in vivo*, it became evident that in these families, BACE1-dependent Aβ1-x generation is the origin for their susceptibility for EOAD (Deng et al., 2013; Schönherr et al., 2016; Hu et al., 2018). However, the APPswe mutations were not observed in any AD case apart from these two families. Taken into account that APPswe is prone to be cleaved by BACE1 to a high extend (Deng et al., 2013) and truncated Aβ species cannot derive from APPswe (Schönherr et al., 2016), the use of APPswe-based mouse models needs to be reconsidered for an unbiased view on β-secretases and truncated Aβ species. Since the main APP cleavage site of meprin β is between D672 and A673 (Bien et al., 2012), and as a result Aβ2-x peptides are released, APPswe-based mouse models are not suitable for our research objectives. Therefore, APPlon expressing mice were used in this study. In this mouse model the accelerated Aβ production is accomplished only through the APPlon mutation V171I at the

γ-secretase site (Moechars et al., 1999; van Dorpe et al., 2000). Since the sequence around the β-secretase is not altered in APPlon-based mouse models, it allows the generation of Aβ2-x peptides, whose consideration is crucial, as Aβ2-x peptides are highly abundant in AD patient brains (Wiltfang et al., 2001) and exhibit an increased potential for aggregation (Schönherr et al., 2016). Therefore, this approach is more suitable for our research objectives than commonly used AD mouse models.

In order to analyze influences of meprin β deficiency on the Aβ generation and cognitive function, *Mep1b*$^{-/-}$ mice were crossed with APPlon mice. Of note, the meprin β knock-out in APPlon mice led to diminished soluble Aβ and reduced plaque load as well as completely recovered cognitive impairments. These findings provide evidence that meprin β plays an *in vivo* role in AD. Interestingly, only Aβ plaques consisting of Aβ2-x peptides were diminished in meprin β-deficient mice, whereas the Aβ1-x plaque load was unaltered. This finding validates the generation of Aβ2-x by meprin β *in vivo*, which was previously observed *in vitro* and *in cellulo* studies (Bien et al., 2012; Schlenzig et al., 2018). Furthermore, the occurrence of plaques consisting of Aβ2-x validate the strong ability of Aβ2-x to aggregate and form plaques, which was so far only suggested based on *in vitro* data (Schönherr et al., 2016). Surprisingly, also Aβ1-x levels were diminished, when meprin β was knocked-out. Since BACE1 activity was shown to be not affected by meprin β deficiency, altered Aβ levels of both Aβ1-x and Aβ2-x occurred due to cleavage by meprin β independent of BACE1. Therefore, these results validate *in vivo* APP cleavage at both meprin β cleavage sites between M671 and D672 and as well as D672 and A673, which were identified so far only in *in vitro* studies (Bien et al., 2012; Schlenzig et al., 2018). A previous study characterizing BACE1-mediated Aβ formation in APPlon mice showed that also BACE1 contributes to the formation of Aβ1-x in APPlon mice, as the injection of a BACE1 inhibitor caused diminished Aβ levels (Jacobsen et al., 2014). Furthermore, the overexpression of BACE1 in APPlon mice leads to increased Aβ formation (Willem et al., 2004). However, in both studies, the impact of BACE1 dysregulation on the cognitive function was not addressed. Nevertheless, it can be concluded that both BACE1 and meprin β independently act as β-secretases in APPlon mice.

Interestingly, several studies showed that truncated Aβ2-x cannot be generated by BACE1 (Schieb et al., 2010; Oberstein et al., 2015), neither by APPswe nor APPwt, which has been promoting the quest to identify alternative β-secretases capable of generating these truncated species. Meprin β was identified in this study as alternative β-secretase responsible for Aβ2-x generation *in vivo*. As meprin β deficiency completely recovers the cognitive decline, the data of this study suggest a crucial role for meprin β and Aβ2-x for the pathogenesis of AD. Therefore, a critical view on APPswe-based mouse models and further research on mouse

models considering Aβ2-x is needed to evaluate whether Aβ2-x plays a so far underestimated role for the onset and progression of AD.

4.3.2 The overexpression of meprin β in astrocytes is a suitable mouse model to promote amyloidogenic APP processing

Since cognitive deficits of APPlon mice were completely recovered, when meprin β was abolished, the data provide first evidence that meprin β plays a crucial *in vivo* role in AD. However, in order to reproduce the disease in a mouse model, the overexpression of meprin β in the brain is closer to the diseased state, since meprin β was observed to be upregulated in AD patient brains (Bien et al., 2012; Schlenzig et al., 2018). For this purpose, a conditional meprin β overexpressing mouse line was generated. Since a previous publication described that particularly Aβ2-42 is secreted in a higher amount by astrocytes than neurons or microglia (Oberstein et al., 2015), it was decided to express meprin β under the control of the GFAP promotor, which is specifically active in astrocytes (Brenner et al., 1994). In order to analyze whether meprin β overexpression is sufficient to cause an AD-like phenotype without human APP overexpression, which is used in common mouse models, endogenous APP expression was maintained in these mice. Interestingly, the overexpression of meprin β in astrocytes led to increased amyloidogenic APP procession and to a significant increase of Aβ levels in whole brain lysates. However, no plaque deposition was detected. Intriguingly, the existence of amyloid plaques does not entail neurodegeneration or cognitive decline (reviewed in Sengupta et al., 2016). It has been shown that the brains of mice from the AD model Tg2576, which is based on the overexpression of APPswe, exhibit a rapid increase of plaque deposition at the age of 12 months. Interestingly, at this time point an intact memory function was detected (Lesné et al., 2008). Instead, impaired cognitive function was observed to be associated with a soluble oligomeric Aβ form of 56 kDa (Lesné et al., 2006; Lesné et al., 2008). This finding suggest that Aβ oligomers are rather neurotoxic than amyloid plaques. The neurotoxic effects of oligomeric Aβ independent of plaque formation are extensively described in the literature (reviewed in Sakono and Zako, 2010; reviewed in Cline et al., 2018). Two independent studies revealed that mutating E693 of APP695 in Tg2576 leads to a loss of plaque deposition. Instead, soluble Aβ oligomers were observed to cause cognitive impairments in these mice (Gandy et al., 2010; Tomiyama et al., 2010). As in this thesis also increased soluble Aβ levels were detected, whereas plaque load was abolished, this mouse model of astrocyte-specific meprin β overexpression has the potential to serve as mouse model for characterizing the consequences of soluble Aβ release independent of plaque formation. Cultivating *ex vivo* organotypic brain slices of the mouse brains overexpressing meprin β in astrocytes, high levels of soluble Aβ were observed to be released into the supernatant. As a consequence, caspase-3 activation was detected. Induction of apoptosis by Aβ-mediated caspase-3

activation was previously described in primary neurons (Harada and Sugimoto, 1999; Marín et al., 2000) and found to cause neuronal loss *in vivo* (Takuma et al., 2004). Therefore, behavioral studies are on-going to analyze the cognitive ability of meprin β overexpressing mice and to evaluate whether these mice may serve as an AD mouse model without manipulated APP expression.

The effect of BACE1 overexpression on endogenous APP cleavage in the mouse brain is barely addressed in the literature. In one single study, elevated sAPPβ levels were observed upon BACE1 overexpression in neurons. However, Aβ generation was only analyzed when these mice were crossed with APPswe overexpressing mice. Surprisingly, the Aβ formation was observed to negatively correlate with the quantity of overexpressed BACE1 (Lee et al., 2005). Hence, the meprin β-based mouse model from this study is the only existing mouse model achieving increased Aβ levels from endogenous APP.

4.4 The astrocyte-specific overexpression of meprin β leads to increased ectodomain cleavage of LPHN3

Moreover, it was aimed to characterize the consequences of meprin β overexpression in astrocytes apart from APP processing. Interestingly, it was observed in this study that meprin β knock-out mice, also without a transgenic APP background, tend to exhibit an increased memory function in the Morris-water maze test compared to WT mice. Therefore, it was hypothesized that meprin β expression might negatively correlate with cognitive function independent of APP processing. This hypothesis is supported by a study, which revealed *MEP1B* to be associated with severe cognitive disabilities by diagnostic exome sequencing, as the mutation T324A in meprin β was identified to be related with a low IQ (Ligt et al., 2012). Therefore, it was aimed to identify candidate meprin β substrates in the brain potentially involved in cognitive function. Hence, mice overexpressing meprin β in astrocytes were used for a TAILS analysis. Interestingly, several new candidate substrates were identified, of which seven are related to neuronal biology or brain development. This further supports the hypothesis that elevated meprin β expression might influence cognitive function. However, a validation of these potential substrates using other detection methods and further research of the consequences caused by the cleavage of the new identified substrates is needed.

The identified substrate LPHN3 emerged as a candidate of potential *in vivo* relevance, since the results revealed a dominant cleavage by meprin β and the release of two extracellular domains of LPHN3. Of note, LPHN3 is a GPCR highly expressed on neurons and astrocytes (Zhang et al., 2016; reviewed in Moreno-Salinas et al., 2019) and was identified in several genetic studies as associated with attention-deficit/hyperactivity disorder (ADHD) (Arcos-

Burgos et al., 2010; Domené et al., 2011; Ribasés et al., 2011; Choudhry et al., 2012). With this in line, LPHN3 knock-out mice exhibit altered neurotransmitter levels and hyperactivity (Wallis et al., 2012). However, the detailed functions of LPHN3 are yet to be investigated. It has been shown that LPHNs undergo autoproteolysis (Araç et al., 2012). As a result, the so-called stachel sequence is exposed, which is thought to serve as tethered agonist, capable to induce signaling leading to decreased cyclic adenosine monophosphate (cAMP) and increased serum response element (SRE) levels (Nazarko et al., 2018; Röthe et al., 2019). In pancreatic β-cells, LPHN3 signaling causes decreased insulin secretion, however, signaling induced by the alternative splice variant expressed in the brain was not observed so far (Röthe et al., 2019). During brain development, LPHN3 is expressed at the surface of neurons and progenitor glia cells and interacts in *trans* with neuronal expressed members of the fibronectin leucine rich transmembrane proteins (FLRT) and the teneurin (TEN) family. This interaction is important for the axonal guidance during neuronal development (Del Toro et al., 2020). It was observed that binding of FLRT3 involves the olfactomedin-like domain, whereas TEN1 interaction requires the olfactomedin-like as well as the SUEL-type lectin domain (O'Sullivan et al., 2014), which both are released upon cleavage by meprin β. Therefore, further research is needed to analyze whether meprin β-dependent LPHN3 cleavage and the release of the olfactomedin-like and the SUEL-type lectin domains may alter LPHN3 signaling or impedes neuronal development (Fig. 31).

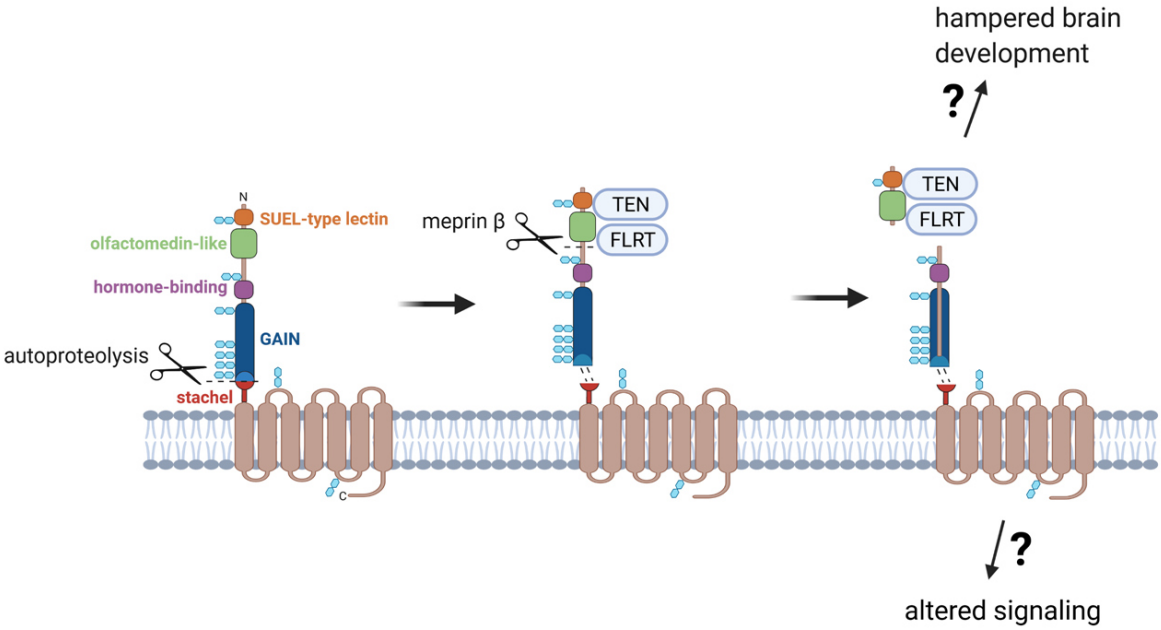

Fig. 31: LPHN3 cleavage by meprin β may alter LPHN3 biology.

As a consequence of autoproteolytic processing, LPHN3 occurs as a membrane-bound C-terminal fragment (LPHN3-CTF) consisting of a short C-terminal part, a seven-pass transmembrane domain and the exposed stachel sequence, as well as a non-covalently linked N-terminal fragment (LPHN3-NTF) comprising a GPCR autoproteolysis inducing (GAIN) domain, SUEL-type lectin and olfactomedin-like domain entirely from the non-covalently bound LPHN3-NTF. Members of the fibronectin leucine rich transmembrane proteins (FLRT) and the teneurin (TEN) family are interaction partners of the olfactomedin and SUEL-type lectin domain. Upon meprin β cleavage, the olfactomedin and SUEL-type lectin domain are released, which may alter LPHN3 signaling or hamper brain development. The figure was created based on results from Araç et al., 2012; O'Sullivan et al., 2014; Moreno-Salinas et al., 2019; The UniProt Consortium, 2021, https://www.uniprot.org/uniprot/Q80TS3.

5. References

Abraham, R., Moskvina, V., Sims, R., Hollingworth, P., Morgan, A., Georgieva, L., Dowzell, K., Cichon, S., Hillmer, A.M., and O'Donovan, M.C., et al. (2008). A genome-wide association study for late-onset Alzheimer's disease using DNA pooling. BMC Med Genomics *1*, 2112.

Alfonso, S.I., Callender, J.A., Hooli, B., Antal, C.E., Mullin, K., Sherman, M.A., Lesné, S.E., Leitges, M., Newton, A.C., and Tanzi, R.E., et al. (2016). Gain-of-function mutations in protein kinase Cα (PKCα) may promote synaptic defects in Alzheimer's disease. Science signaling *9*, ra47.

Alzheimer, A. (1907). Über eine eigenartige Erkrankung der Hirnrinde. Allgemeine Zeitschrift fur Psychiatrie und Psychisch-gerichtliche Medizin *64*, 146-148.

Anderson, J.J., Holtz, G., Baskin, P.P., Wang, R., Mazzarelli, L., Wagner, S.L., and Menzaghi, F. (1999). Reduced cerebrospinal fluid levels of α-secretase-cleaved amyloid precursor protein in aged rats. Correlation with spatial memory deficits. Neuroscience *93*, 1409-1420.

Araç, D., Boucard, A.A., Bolliger, M.F., Nguyen, J., Soltis, S.M., Südhof, T.C., and Brunger, A.T. (2012). A novel evolutionarily conserved domain of cell-adhesion GPCRs mediates autoproteolysis. The EMBO Journal *31*, 1364-1378.

Arcos-Burgos, M., Jain, M., Acosta, M.T., Shively, S., Stanescu, H., Wallis, D., Domené, S., Vélez, J.I., Karkera, J.D., and Balog, J., et al. (2010). A common variant of the latrophilin 3 gene, LPHN3, confers susceptibility to ADHD and predicts effectiveness of stimulant medication. Molecular psychiatry *15*, 1053-1066.

Arnold, P., Boll, I., Rothaug, M., Schumacher, N., Schmidt, F., Wichert, R., Schneppenheim, J., Lokau, J., Pickhinke, U., and Koudelka, T., et al. (2017a). Meprin Metalloproteases Generate Biologically Active Soluble Interleukin-6 Receptor to Induce Trans-Signaling. Scientific reports *7*, 44053.

Arnold, P., Otte, A., and Becker-Pauly, C. (2017b). Meprin metalloproteases. Molecular regulation and function in inflammation and fibrosis. Biochimica et biophysica acta. Molecular cell research *1864*.

Arolas, J.L., Broder, C., Jefferson, T., Guevara, T., Sterchi, E.E., Bode, W., Stöcker, W., Becker-Pauly, C., and Gomis-Rüth, F.X. (2012). Structural basis for the sheddase function of human meprin β metalloproteinase at the plasma membrane. Proceedings of the National Academy of Sciences of the United States of America *109*, 16131-16136.

Bancher, C., Brunner, C., Lassmann, H., Budka, H., Jellinger, K., Wiche, G., Seitelberger, F., Grundke-Iqbal, I., Iqbal, K., and Wisniewski, H.M. (1989). Accumulation of abnormally

phosphorylated τ precedes the formation of neurofibrillary tangles in Alzheimer's disease. Brain Research *477*, 90-99.

Banerjee, S., and Bond, J.S. (2008). Prointerleukin-18 is activated by meprin beta in vitro and in vivo in intestinal inflammation. The Journal of biological chemistry *283*, 31371-31377.

Baranello, R.J., Bharani, K.L., Padmaraju, V., Chopra, N., Lahiri, D.K., Greig, N.H., Pappolla, M.A., and Sambamurti, K. (2015). Amyloid-beta protein clearance and degradation (ABCD) pathways and their role in Alzheimer's disease. CAR *12*, 32-46.

Barbier, P., Zejneli, O., Martinho, M., Lasorsa, A., Belle, V., Smet-Nocca, C., Tsvetkov, P.O., Devred, F., and Landrieu, I. (2019). Role of Tau as a Microtubule-Associated Protein. Structural and Functional Aspects. Frontiers in aging neuroscience *11*, 204.

Barger, S.W., Fiscus, R.R., Ruth, P., Hofmann, F., and Mattson, M.P. (1995). Role of cyclic GMP in the regulation of neuronal calcium and survival by secreted forms of beta-amyloid precursor. Journal of neurochemistry *64*, 2087-2096.

Barnes, K., Ingram, J., and Kenny, A.J. (1989). Proteins of the kidney microvillar membrane. Structural and immunochemical properties of rat endopeptidase-2 and its immunohistochemical localization in tissues of rat and mouse. The Biochemical journal *264*, 335-346.

Bates, K.A., Verdile, G., Li, Q.-X., Ames, D., Hudson, P., Masters, C.L., and Martins, R.N. (2009). Clearance mechanisms of Alzheimer's amyloid-beta peptide. Implications for therapeutic design and diagnostic tests. Molecular psychiatry *14*, 469-486.

Becker-Pauly, C., Barré, O., Schilling, O., dem Keller, U. auf, Ohler, A., Broder, C., Schütte, A., Kappelhoff, R., Stöcker, W., and Overall, C.M. (2011). Proteomic analyses reveal an acidic prime side specificity for the astacin metalloprotease family reflected by physiological substrates. Molecular & cellular proteomics : MCP *10*, M111.009233.

Becker-Pauly, C., Höwel, M., Walker, T., Vlad, A., Aufenvenne, K., Oji, V., Lottaz, D., Sterchi, E.E., Debela, M., and Magdolen, V., et al. (2007). The alpha and beta subunits of the metalloprotease meprin are expressed in separate layers of human epidermis, revealing different functions in keratinocyte proliferation and differentiation. The Journal of investigative dermatology *127*, 1115-1125.

Becker-Pauly, C., and Pietrzik, C.U. (2016). The Metalloprotease Meprin β Is an Alternative β-Secretase of APP. Frontiers in molecular neuroscience *9*, 159.

Bedau, T., Peters, F., Prox, J., Arnold, P., Schmidt, F., Finkernagel, M., Köllmann, S., Wichert, R., Otte, A., and Ohler, A., et al. (2017). Ectodomain shedding of CD99 within highly conserved

regions is mediated by the metalloprotease meprin β and promotes transendothelial cell migration. Federation of American Societies for Experimental Biology *31*, 1226-1237.

Beher, D., Hesse, L., Masters, C.L., and Multhaup, G. (1996). Regulation of amyloid protein precursor (APP) binding to collagen and mapping of the binding sites on APP and collagen type I. The Journal of biological chemistry *271*, 1613-1620.

Belyaev, N.D., Kellett, K.A.B., Beckett, C., Makova, N.Z., Revett, T.J., Nalivaeva, N.N., Hooper, N.M., and Turner, A.J. (2010). The transcriptionally active amyloid precursor protein (APP) intracellular domain is preferentially produced from the 695 isoform of APP in a {beta}-secretase-dependent pathway. The Journal of biological chemistry *285*, 41443-41454.

Bernstein, K.E., Koronyo, Y., Salumbides, B.C., Sheyn, J., Pelissier, L., Lopes, D.H.J., Shah, K.H., Bernstein, E.A., Fuchs, D.-T., and Yu, J.J.-Y., et al. (2014). Angiotensin-converting enzyme overexpression in myelomonocytes prevents Alzheimer's-like cognitive decline. The Journal of clinical investigation *124*, 1000-1012.

Bertenshaw, G.P., Norcum, M.T., and Bond, J.S. (2003). Structure of homo- and hetero-oligomeric meprin metalloproteases. Dimers, tetramers, and high molecular mass multimers. The Journal of biological chemistry *278*, 2522-2532.

Beynon, R.J., Shannon, J.D., and Bond, J.S. (1981). Purification and characterization of a metallo-endoproteinase from mouse kidney. The Biochemical journal *199*, 591-598.

Biasin, V., Wygrecka, M., Marsh, L.M., Becker-Pauly, C., Brcic, L., Ghanim, B., Klepetko, W., Olschewski, A., and Kwapiszewska, G. (2017). Meprin β contributes to collagen deposition in lung fibrosis. Scientific reports *7*, 39969.

Bien, J., Jefferson, T., Causević, M., Jumpertz, T., Munter, L., Multhaup, G., Weggen, S., Becker-Pauly, C., and Pietrzik, C.U. (2012). The metalloprotease meprin β generates amino terminal-truncated amyloid β peptide species. The Journal of biological chemistry *287*, 33304-33313.

Bigio, E.H., Hynan, L.S., Sontag, E., Satumtira, S., and White, C.L. (2002). Synapse loss is greater in presenile than senile onset Alzheimer disease. Implications for the cognitive reserve hypothesis. Neuropathology and applied neurobiology *28*, 218-227.

Bixel, M.G., Li, H., Petri, B., Khandoga, A.G., Khandoga, A., Zarbock, A., Wolburg-Buchholz, K., Wolburg, H., Sorokin, L., and Zeuschner, D., et al. (2010). CD99 and CD99L2 act at the same site as, but independently of, PECAM-1 during leukocyte diapedesis. Blood *116*, 1172-1184.

Bode, D.C., Freeley, M., Nield, J., Palma, M., and Viles, J.H. (2019). Amyloid-β oligomers have a profound detergent-like effect on lipid membrane bilayers, imaged by atomic force and electron microscopy. The Journal of biological chemistry *294*, 7566-7572.

Brenner, M., Kisseberth, W.C., Su, Y., Besnard, F., and Messing, A. (1994). GFAP promoter directs astrocyte-specific expression in transgenic mice. J. Neurosci. *14*, 1030-1037.

Broder, C., and Becker-Pauly, C. (2013). The metalloproteases meprin α and meprin β. Unique enzymes in inflammation, neurodegeneration, cancer and fibrosis. The Biochemical journal *450*, 253-264.

Buxbaum, J.D., Liu, K.N., Luo, Y., Slack, J.L., Stocking, K.L., Peschon, J.J., Johnson, R.S., Castner, B.J., Cerretti, D.P., and Black, R.A. (1998). Evidence that tumor necrosis factor alpha converting enzyme is involved in regulated alpha-secretase cleavage of the Alzheimer amyloid protein precursor. The Journal of biological chemistry *273*, 27765-27767.

Castro, M.A., Hadziselimovic, A., and Sanders, C.R. (2019). The vexing complexity of the amyloidogenic pathway. Protein Science *28*, 1177-1193.

Chesneau, V., Vekrellis, K., Rosner, M.R., and Selkoe, D.J. (2000). Purified recombinant insulin-degrading enzyme degrades amyloid beta-protein but does not promote its oligomerization. The Biochemical journal *351 Pt 2*, 509-516.

Choi, M.C., Raviv, U., Miller, H.P., Gaylord, M.R., Kiris, E., Ventimiglia, D., Needleman, D.J., Kim, M.W., Wilson, L., and Feinstein, S.C., et al. (2009). Human microtubule-associated-protein tau regulates the number of protofilaments in microtubules. A synchrotron x-ray scattering study. Biophysical journal *97*, 519-527.

Chong, F.P., Ng, K.Y., Koh, R.Y., and Chye, S.M. (2018). Tau Proteins and Tauopathies in Alzheimer's Disease. Cellular and molecular neurobiology *38*, 965-980.

Choudhry, Z., Sengupta, S.M., Grizenko, N., Fortier, M.-E., Thakur, G.A., Bellingham, J., and Joober, R. (2012). LPHN3 and attention-deficit/hyperactivity disorder. Interaction with maternal stress during pregnancy. Journal of child psychology and psychiatry, and allied disciplines *53*, 892-902.

Clarris, H.J., Cappai, R., Heffernan, D., Beyreuther, K., Masters, C.L., and Small, D.H. (1997). Identification of heparin-binding domains in the amyloid precursor protein of Alzheimer's disease by deletion mutagenesis and peptide mapping. Journal of neurochemistry *68*, 1164-1172.

Cline, E.N., Bicca, M.A., Viola, K.L., and Klein, W.L. (2018). The Amyloid-β Oligomer Hypothesis. Beginning of the Third Decade. Journal of Alzheimer's disease : JAD *64*, S567-S610.

Cole, S.L., and Vassar, R. (2007). The Alzheimer's disease beta-secretase enzyme, BACE1. Molecular neurodegeneration *2*, 22.

Cole, S.L., and Vassar, R. (2008). The role of amyloid precursor protein processing by BACE1, the beta-secretase, in Alzheimer disease pathophysiology. The Journal of biological chemistry *283*, 29621-29625.

Coon, K.D., Myers, A.J., Craig, D.W., Webster, J.A., Pearson, J.V., Lince, D.H., Zismann, V.L., Beach, T.G., Leung, D., and Bryden, L., et al. (2007). A high-density whole-genome association study reveals that APOE is the major susceptibility gene for sporadic late-onset Alzheimer's disease. The Journal of clinical psychiatry *68*, 613-618.

Coric, V., Salloway, S., van Dyck, C.H., Dubois, B., Andreasen, N., Brody, M., Curtis, C., Soininen, H., Thein, S., and Shiovitz, T., et al. (2015). Targeting Prodromal Alzheimer Disease With Avagacestat. JAMA Neurol *72*, 1324.

Coronel, R., Bernabeu-Zornoza, A., Palmer, C., Muñiz-Moreno, M., Zambrano, A., Cano, E., and Liste, I. (2018). Role of Amyloid Precursor Protein (APP) and Its Derivatives in the Biology and Cell Fate Specification of Neural Stem Cells. Molecular neurobiology *55*, 7107-7117.

Crisman, J.M., Zhang, B., Norman, L.P., and Bond, J.S. (2004). Deletion of the mouse meprin beta metalloprotease gene diminishes the ability of leukocytes to disseminate through extracellular matrix. Journal of immunology (Baltimore, Md. : 1950) *172*, 4510-4519.

Croft, C.L., and Noble, W. (2018). Preparation of organotypic brain slice cultures for the study of Alzheimer's disease. F1000Research *7*, 592.

Curtis, M.A., Aduse-Opoku, J., and Rangarajan, M. (2001). Cysteine proteases of Porphyromonas gingivalis. Critical reviews in oral biology and medicine *12*, 192-216.

Dai, M.-H., Zheng, H., Zeng, L.-D., and Zhang, Y. (2018). The genes associated with early-onset Alzheimer's disease. Oncotarget *9*, 15132-15143.

Daws, M.R., Sullam, P.M., Niemi, E.C., Chen, T.T., Tchao, N.K., and Seaman, W.E. (2003). Pattern recognition by TREM-2. Binding of anionic ligands. Journal of immunology (Baltimore, Md. : 1950) *171*, 594-599.

Del Toro, D., Carrasquero-Ordaz, M.A., Chu, A., Ruff, T., Shahin, M., Jackson, V.A., Chavent, M., Berbeira-Santana, M., Seyit-Bremer, G., and Brignani, S., et al. (2020). Structural Basis of Teneurin-Latrophilin Interaction in Repulsive Guidance of Migrating Neurons. Cell *180*, 323-339.e19.

Deng, Y., Wang, Z., Wang, R., Zhang, X., Zhang, S., Wu, Y., Staufenbiel, M., Cai, F., and Song, W. (2013). Amyloid-β protein (Aβ) Glu11 is the major β-secretase site of β-site amyloid-

β precursor protein-cleaving enzyme 1(BACE1), and shifting the cleavage site to Aβ Asp1 contributes to Alzheimer pathogenesis. The European journal of neuroscience *37*, 1962-1969.

Domené, S., Stanescu, H., Wallis, D., Tinloy, B., Pineda, D.E., Kleta, R., Arcos-Burgos, M., Roessler, E., and Muenke, M. (2011). Screening of human LPHN3 for variants with a potential impact on ADHD susceptibility. American journal of medical genetics. Part B, Neuropsychiatric genetics *156B*, 11-18.

Dominy, S.S., Lynch, C., Ermini, F., Benedyk, M., Marczyk, A., Konradi, A., Nguyen, M., Haditsch, U., Raha, D., and Griffin, C., et al. (2019). Porphyromonas gingivalis in Alzheimer's disease brains. Evidence for disease causation and treatment with small-molecule inhibitors. Science advances *5*, eaau3333.

Donoviel, D.B., Hadjantonakis, A.K., Ikeda, M., Zheng, H., Hyslop, P.S., and Bernstein, A. (1999). Mice lacking both presenilin genes exhibit early embryonic patterning defects. Genes & development *13*, 2801-2810.

Doody, R.S., Raman, R., Farlow, M., Iwatsubo, T., Vellas, B., Joffe, S., Kieburtz, K., He, F., Sun, X., and Thomas, R.G., et al. (2013). A Phase 3 Trial of Semagacestat for Treatment of Alzheimer's Disease. The New England journal of medicine *369*, 341-350.

Doody, R.S., Tariot, P.N., Pfeiffer, E., Olin, J.T., and Graham, S.M. (2007). Meta-analysis of six-month memantine trials in Alzheimer's disease. Alzheimer's & Dementia *3*, 7-17.

Dorszewska, J., Prendecki, M., Oczkowska, A., Dezor, M., and Kozubski, W. (2016). Molecular Basis of Familial and Sporadic Alzheimer's Disease. CAR *13*, 952-963.

Edbauer, D., Winkler, E., Haass, C., and Steiner, H. (2002). Presenilin and nicastrin regulate each other and determine amyloid beta-peptide production via complex formation. Proceedings of the National Academy of Sciences of the United States of America *99*, 8666-8671.

Eimer, W.A., Vijaya Kumar, D.K., Navalpur Shanmugam, N.K., Rodriguez, A.S., Mitchell, T., Washicosky, K.J., György, B., Breakefield, X.O., Tanzi, R.E., and Moir, R.D. (2018). Alzheimer's Disease-Associated β-Amyloid Is Rapidly Seeded by Herpesviridae to Protect against Brain Infection. Neuron *99*, 56-63.e3.

Esch, F.S., Keim, P.S., Beattie, E.C., Blacher, R.W., Culwell, A.R., Oltersdorf, T., McClure, D., and Ward, P.J. (1990). Cleavage of amyloid beta peptide during constitutive processing of its precursor. Science (New York, N.Y.) *248*, 1122-1124.

Esquerda-Canals, G., Montoliu-Gaya, L., Güell-Bosch, J., and Villegas, S. (2017). Mouse Models of Alzheimer's Disease. Journal of Alzheimer's disease : JAD *57*, 1171-1183.

Etcheberrigaray, R., Tan, M., Dewachter, I., Kuipéri, C., van der Auwera, I., Wera, S., Qiao, L., Bank, B., Nelson, T.J., and Kozikowski, A.P., et al. (2004). Therapeutic effects of PKC activators in Alzheimer's disease transgenic mice. Proceedings of the National Academy of Sciences of the United States of America *101*, 11141-11146.

Fá, M., Puzzo, D., Piacentini, R., Staniszewski, A., Zhang, H., Baltrons, M.A., Li Puma, D.D., Chatterjee, I., Li, J., and Saeed, F., et al. (2016). Extracellular Tau Oligomers Produce An Immediate Impairment of LTP and Memory. Scientific reports *6*, 19393.

Fellgiebel, A., Kojro, E., Müller, M.J., Scheurich, A., Schmidt, L.G., and Fahrenholz, F. (2009). CSF APPs alpha and phosphorylated tau protein levels in mild cognitive impairment and dementia of Alzheimer's type. Journal of geriatric psychiatry and neurology *22*, 3-9.

Filippova, N., Dudley, R., and Weiss, D.S. (1999). Evidence for phosphorylation-dependent internalization of recombinant human rho1 GABAC receptors. The Journal of physiology *518 (Pt 2)*, 385-399.

Friedlander, D.R., Milev, P., Karthikeyan, L., Margolis, R.K., Margolis, R.U., and Grumet, M. (1994). The neuronal chondroitin sulfate proteoglycan neurocan binds to the neural cell adhesion molecules Ng-CAM/L1/NILE and N-CAM, and inhibits neuronal adhesion and neurite outgrowth. The Journal of cell biology *125*, 669-680.

Fu, R., Shen, Q., Xu, P., Luo, J.J., and Tang, Y. (2014). Phagocytosis of microglia in the central nervous system diseases. Molecular neurobiology *49*, 1422-1434.

Fukumoto, H., Rosene, D.L., Moss, M.B., Raju, S., Hyman, B.T., and Irizarry, M.C. (2004). Beta-secretase activity increases with aging in human, monkey, and mouse brain. The American journal of pathology *164*, 719-725.

Fymat, A.L. (2018). Dementia. A Review. Journal of Clinical Psychiatry and Neuroscience *1*.

Galimberti, D., and Scarpini, E. (2010). Treatment of Alzheimers Disease. Symptomatic and Disease-Modifying Approaches. CAS *3*, 46-56.

Gandy, S., Simon, A.J., Steele, J.W., Lublin, A.L., Lah, J.J., Walker, L.C., Levey, A.I., Krafft, G.A., Levy, E., and Checler, F., et al. (2010). Days to criterion as an indicator of toxicity associated with human Alzheimer amyloid-beta oligomers. Annals of neurology *68*, 220-230.

Gendron, T.F., and Petrucelli, L. (2009). The role of tau in neurodegeneration. Molecular neurodegeneration *4*, 13.

Goedert, M., and Jakes, R. (1990). Expression of separate isoforms of human tau protein. Correlation with the tau pattern in brain and effects on tubulin polymerization. The EMBO Journal *9*, 4225-4230.

Goodman, Y., and Mattson, M.P. (1994). Secreted forms of beta-amyloid precursor protein protect hippocampal neurons against amyloid beta-peptide-induced oxidative injury. Experimental neurology *128*, 1-12.

Gosztyla, M.L., Brothers, H.M., and Robinson, S.R. (2018). Alzheimer's Amyloid-β is an Antimicrobial Peptide. A Review of the Evidence. Journal of Alzheimer's disease : JAD *62*, 1495-1506.

Gratuze, M., Leyns, C.E.G., and Holtzman, D.M. (2018). New insights into the role of TREM2 in Alzheimer's disease. Molecular neurodegeneration *13*, 66.

Grünberg, J., Dumermuth, E., Eldering, J.A., and Sterchi, E.E. (1993). Expression of the alpha subunit of PABA peptide hydrolase (EC 3.4.24.18) in MDCK cells. FEBS Letters *335*, 376-379.

Grundke-Iqbal, I., Iqbal, K., Tung, Y.C., Quinlan, M., Wisniewski, H.M., and Binder, L.I. (1986). Abnormal phosphorylation of the microtubule-associated protein tau (tau) in Alzheimer cytoskeletal pathology. Proceedings of the National Academy of Sciences of the United States of America *83*, 4913-4917.

Gu, Y., Misonou, H., Sato, T., Dohmae, N., Takio, K., and Ihara, Y. (2001). Distinct intramembrane cleavage of the beta-amyloid precursor protein family resembling gamma-secretase-like cleavage of Notch. The Journal of biological chemistry *276*, 35235-35238.

Guerreiro, R., Wojtas, A., Bras, J., Carrasquillo, M., Rogaeva, E., Majounie, E., Cruchaga, C., Sassi, C., Kauwe, J.S.K., and Younkin, S., et al. (2013). TREM2 variants in Alzheimer's disease. The New England journal of medicine *368*, 117-127.

Guo, Q., Li, H., Gaddam, S.S.K., Justice, N.J., Robertson, C.S., and Zheng, H. (2012). Amyloid precursor protein revisited. Neuron-specific expression and highly stable nature of soluble derivatives. The Journal of biological chemistry *287*, 2437-2445.

Gustke, N., Trinczek, B., Biernat, J., Mandelkow, E.M., and Mandelkow, E. (1994). Domains of tau protein and interactions with microtubules. Biochemistry *33*, 9511-9522.

Haass, C., Lemere, C.A., Capell, A., Citron, M., Seubert, P., Schenk, D., Lannfelt, L., and Selkoe, D.J. (1995). The Swedish mutation causes early-onset Alzheimer's disease by beta-secretase cleavage within the secretory pathway. Nature medicine *1*, 1291-1296.

Hahn, D., Pischitzis, A., Roesmann, S., Hansen, M.K., Leuenberger, B., Luginbuehl, U., and Sterchi, E.E. (2003). Phorbol 12-myristate 13-acetate-induced ectodomain shedding and phosphorylation of the human meprinbeta metalloprotease. The Journal of biological chemistry *278*, 42829-42839.

Hampel, H., Mesulam, M.-M., Cuello, A.C., Farlow, M.R., Giacobini, E., Grossberg, G.T., Khachaturian, A.S., Vergallo, A., Cavedo, E., and Snyder, P.J., et al. (2018). The cholinergic system in the pathophysiology and treatment of Alzheimer's disease. Brain *141*, 1917-1933.

Hampel, H., Vassar, R., Strooper, B. de, Hardy, J., Willem, M., Singh, N., Zhou, J., Yan, R., Vanmechelen, E., and Vos, A. de, et al. (2020). The β-Secretase BACE1 in Alzheimer's Disease. Biological psychiatry.

Harada, J., and Sugimoto, M. (1999). Activation of caspase-3 in β-amyloid-induced apoptosis of cultured rat cortical neurons. Brain Research *842*, 311-323.

Hérard, A.S., Besret, L., Dubois, A., Dauguet, J., Delzescaux, T., Hantraye, P., Bonvento, G., and Moya, K.L. (2006). siRNA targeted against amyloid precursor protein impairs synaptic activity in vivo. Neurobiology of aging *27*, 1740-1750.

Heron, M. (2019). Deaths: Leading Causes for 2017. National vital statistics reports *68*, 1-77.

Herzog, C., Haun, R.S., Ludwig, A., Shah, S.V., and Kaushal, G.P. (2014). ADAM10 is the major sheddase responsible for the release of membrane-associated meprin A. The Journal of biological chemistry *289*, 13308-13322.

Hippius, H., and Neundörfer, G. (2003). The discovery of Alzheimer's disease. Dialogues in Clinical Neuroscience *5*, 101-108.

Hook, G., Yu, J., Toneff, T., Kindy, M., and Hook, V. (2014). Brain pyroglutamate amyloid-β is produced by cathepsin B and is reduced by the cysteine protease inhibitor E64d, representing a potential Alzheimer's disease therapeutic. Journal of Alzheimer's disease : JAD *41*, 129-149.

Hsiao, K., Chapman, P., Nilsen, S., Eckman, C., Harigaya, Y., Younkin, S., Yang, F., and Cole, G. (1996). Correlative memory deficits, Abeta elevation, and amyloid plaques in transgenic mice. Science (New York, N.Y.) *274*, 99-102.

Hu, J., Igarashi, A., Kamata, M., and Nakagawa, H. (2001). Angiotensin-converting enzyme degrades Alzheimer amyloid beta-peptide (A beta); retards A beta aggregation, deposition, fibril formation; and inhibits cytotoxicity. The Journal of biological chemistry *276*, 47863-47868.

Hu, X., Das, B., Hou, H., He, W., and Yan, R. (2018). BACE1 deletion in the adult mouse reverses preformed amyloid deposition and improves cognitive functions. The Journal of experimental medicine *215*, 927-940.

Hu, X., Hicks, C.W., He, W., Wong, P., Macklin, W.B., Trapp, B.D., and Yan, R. (2006). Bace1 modulates myelination in the central and peripheral nervous system. Nature neuroscience *9*, 1520-1525.

Huse, J.T., Pijak, D.S., Leslie, G.J., Lee, V.M., and Doms, R.W. (2000). Maturation and endosomal targeting of beta-site amyloid precursor protein-cleaving enzyme. The Alzheimer's disease beta-secretase. The Journal of biological chemistry *275*, 33729-33737.

Hutton, M., Lendon, C.L., Rizzu, P., Baker, M., Froelich, S., Houlden, H., Pickering-Brown, S., Chakraverty, S., Isaacs, A., and Grover, A., et al. (1998). Association of missense and 5'-splice-site mutations in tau with the inherited dementia FTDP-17. Nature *393*, 702-705.

Iqbal, K., Liu, F., Gong, C.-X., and Grundke-Iqbal, I. (2010). Tau in Alzheimer disease and related tauopathies. Current Alzheimer research *7*, 656-664.

Jäckle, F., Schmidt, F., Wichert, R., Arnold, P., Prox, J., Mangold, M., Ohler, A., Pietrzik, C.U., Koudelka, T., and Tholey, A., et al. (2015). Metalloprotease meprin β is activated by transmembrane serine protease matriptase-2 at the cell surface thereby enhancing APP shedding. The Biochemical journal *470*, 91-103.

Jacobsen, H., Ozmen, L., Caruso, A., Narquizian, R., Hilpert, H., Jacobsen, B., Terwel, D., Tanghe, A., and Bohrmann, B. (2014). Combined treatment with a BACE inhibitor and anti-Aβ antibody gantenerumab enhances amyloid reduction in APPLondon mice. J. Neurosci. *34*, 11621-11630.

Jankowsky, J.L., and Zheng, H. (2017). Practical considerations for choosing a mouse model of Alzheimer's disease. Molecular neurodegeneration *12*, 89.

Jawhar, S., Trawicka, A., Jenneckens, C., Bayer, T.A., and Wirths, O. (2012). Motor deficits, neuron loss, and reduced anxiety coinciding with axonal degeneration and intraneuronal Aβ aggregation in the 5XFAD mouse model of Alzheimer's disease. Neurobiology of aging *33*, 196.e29-40.

Jefferson, T., Čaušević, M., dem Keller, U. auf, Schilling, O., Isbert, S., Geyer, R., Maier, W., Tschickardt, S., Jumpertz, T., and Weggen, S., et al. (2011). Metalloprotease meprin beta generates nontoxic N-terminal amyloid precursor protein fragments in vivo. The Journal of biological chemistry *286*, 27741-27750.

Jefferson, T., dem Keller, U. auf, Bellac, C., Metz, V.V., Broder, C., Hedrich, J., Ohler, A., Maier, W., Magdolen, V., and Sterchi, E., et al. (2013). The substrate degradome of meprin metalloproteases reveals an unexpected proteolytic link between meprin β and ADAM10. Cellular and molecular life sciences : CMLS *70*, 309-333.

Jeong, W., Lee, H., Cho, S., and Seo, J. (2019). ApoE4-Induced Cholesterol Dysregulation and Its Brain Cell Type-Specific Implications in the Pathogenesis of Alzheimer's Disease. Molecules and cells *42*, 739-746.

Ji, L., Chauhan, A., and Chauhan, V. (2010). Upregulation of cytoplasmic gelsolin, an amyloid-beta-binding protein, under oxidative stress conditions. Involvement of protein kinase C. Journal of Alzheimer's disease : JAD *19*, 829-838.

Jin, S.C., Benitez, B.A., Karch, C.M., Cooper, B., Skorupa, T., Carrell, D., Norton, J.B., Hsu, S., Harari, O., and Cai, Y., et al. (2014). Coding variants in TREM2 increase risk for Alzheimer's disease. Human molecular genetics *23*, 5838-5846.

Johnson, G.D., and Hersh, L.B. (1992). Cloning a rat meprin cDNA reveals the enzyme is a heterodimer. The Journal of biological chemistry *267*, 13505-13512.

Jonsson, T., Stefansson, H., Steinberg, S., Jonsdottir, I., Jonsson, P.V., Snaedal, J., Bjornsson, S., Huttenlocher, J., Levey, A.I., and Lah, J.J., et al. (2013). Variant of TREM2 associated with the risk of Alzheimer's disease. The New England journal of medicine *368*, 107-116.

Jorissen, E., Prox, J., Bernreuther, C., Weber, S., Schwanbeck, R., Serneels, L., Snellinx, A., Craessaerts, K., Thathiah, A., and Tesseur, I., et al. (2010). The disintegrin/metalloproteinase ADAM10 is essential for the establishment of the brain cortex. J. Neurosci. *30*, 4833-4844.

Karimova, M., Baker, O., Camgoz, A., Naumann, R., Buchholz, F., and Anastassiadis, K. (2018). A single reporter mouse line for Vika, Flp, Dre, and Cre-recombination. Scientific reports *8*, 14453.

Karmilin, K., Schmitz, C., Kuske, M., Körschgen, H., Olf, M., Meyer, K., Hildebrand, A., Felten, M., Fridrich, S., and Yiallouros, I., et al. (2019). Mammalian plasma fetuin-B is a selective inhibitor of ovastacin and meprin metalloproteinases. Scientific reports *9*, 546.

Kempf, M., Clement, A., Faissner, A., Lee, G., and Brandt, R. (1996). Tau Binds to the Distal Axon Early in Development of Polarity in a Microtubule- and Microfilament-Dependent Manner. J. Neurosci. *16*, 5583-5592.

Kibbey, M.C., Jucker, M., Weeks, B.S., Neve, R.L., van Nostrand, W.E., and Kleinman, H.K. (1993). beta-Amyloid precursor protein binds to the neurite-promoting IKVAV site of laminin. Proceedings of the National Academy of Sciences of the United States of America *90*, 10150-10153.

Kinoshita, A., Fukumoto, H., Shah, T., Whelan, C.M., Irizarry, M.C., and Hyman, B.T. (2003). Demonstration by FRET of BACE interaction with the amyloid precursor protein at the cell surface and in early endosomes. Journal of cell science *116*, 3339-3346.

Koike, H., Tomioka, S., Sorimachi, H., Saido, T.C., Maruyama, K., Okuyama, A., Fujisawa-Sehara, A., Ohno, S., Suzuki, K., and Ishiura, S. (1999). Membrane-anchored metalloprotease

MDC9 has an alpha-secretase activity responsible for processing the amyloid precursor protein. The Biochemical journal *343 Pt 2*, 371-375.

Kojro, E., and Fahrenholz, F. (2005). The Non-Amyloidogenic Pathway. Structure and Function of α-Secretases. In Alzheimer' s Disease. Cellular and Molecular Aspects of Amyloid beta, J.R. Harris and F. Fahrenholz, eds. (s.l.: Springer Science + Business Media), pp. 105–127.

Koo, E.H., and Squazzo, S.L. (1994). Evidence that production and release of amyloid beta-protein involves the endocytic pathway. The Journal of biological chemistry *269*, 17386-17389.

Kopan, R. (2012). Notch signaling. Cold Spring Harbor perspectives in biology *4*.

Kosik, K.S., Joachim, C.L., and Selkoe, D.J. (1986). Microtubule-associated protein tau (tau) is a major antigenic component of paired helical filaments in Alzheimer disease. Proceedings of the National Academy of Sciences of the United States of America *83*, 4044-4048.

Kounnas, M.Z., Wolz, R.L., Gorbea, C.M., and Bond, J.S. (1991). Meprin-A and -B. Cell surface endopeptidases of the mouse kidney. The Journal of biological chemistry *266*, 17350-17357.

Kronenberg, D., Bruns, B.C., Moali, C., Vadon-Le Goff, S., Sterchi, E.E., Traupe, H., Böhm, M., Hulmes, D.J.S., Stöcker, W., and Becker-Pauly, C. (2010). Processing of procollagen III by meprins. New players in extracellular matrix assembly? The Journal of investigative dermatology *130*, 2727-2735.

Kruse, M.-N., Becker, C., Lottaz, D., Köhler, D., Yiallouros, I., Krell, H.-W., Sterchi, E.E., and Stöcker, W. (2004). Human meprin alpha and beta homo-oligomers. Cleavage of basement membrane proteins and sensitivity to metalloprotease inhibitors. The Biochemical journal *378*, 383-389.

Kuboyama, K., Fujikawa, A., Masumura, M., Suzuki, R., Matsumoto, M., and Noda, M. (2012). Protein tyrosine phosphatase receptor type z negatively regulates oligodendrocyte differentiation and myelination. PloS one *7*, e48797.

Kuhn, A.J., Abrams, B.S., Knowlton, S., and Raskatov, J.A. (2020). Alzheimer's Disease "Non-amyloidogenic" p3 Peptide Revisited. A Case for Amyloid-α. ACS chemical neuroscience *11*, 1539-1544.

Kuhn, P.-H., Koroniak, K., Hogl, S., Colombo, A., Zeitschel, U., Willem, M., Volbracht, C., Schepers, U., Imhof, A., and Hoffmeister, A., et al. (2012). Secretome protein enrichment identifies physiological BACE1 protease substrates in neurons. The EMBO Journal *31*, 3157-3168.

Kuhn, P.-H., Wang, H., Dislich, B., Colombo, A., Zeitschel, U., Ellwart, J.W., Kremmer, E., Rossner, S., and Lichtenthaler, S.F. (2010). ADAM10 is the physiologically relevant,

constitutive alpha-secretase of the amyloid precursor protein in primary neurons. The EMBO Journal *29*, 3020-3032.

Kumar, D.K.V., Choi, S.H., Washicosky, K.J., Eimer, W.A., Tucker, S., Ghofrani, J., Lefkowitz, A., McColl, G., Goldstein, L.E., and Tanzi, R.E., et al. (2016). Amyloid-β peptide protects against microbial infection in mouse and worm models of Alzheimer's disease. Science translational medicine *8*, 340ra72.

Laird, F.M., Cai, H., Savonenko, A.V., Farah, M.H., He, K., Melnikova, T., Wen, H., Chiang, H.-C., Xu, G., and Koliatsos, V.E., et al. (2005). BACE1, a major determinant of selective vulnerability of the brain to amyloid-beta amyloidogenesis, is essential for cognitive, emotional, and synaptic functions. J. Neurosci. *25*, 11693-11709.

Lee, C.Y.D., Daggett, A., Gu, X., Jiang, L.-L., Langfelder, P., Li, X., Wang, N., Zhao, Y., Park, C.S., and Cooper, Y., et al. (2018). Elevated TREM2 Gene Dosage Reprograms Microglia Responsivity and Ameliorates Pathological Phenotypes in Alzheimer's Disease Models. Neuron *97*, 1032-1048.e5.

Lee, C.Y.D., and Landreth, G.E. (2010). The role of microglia in amyloid clearance from the AD brain. Journal of neural transmission (Vienna, Austria : 1996) *117*, 949-960.

Lee, E.B., Zhang, B., Liu, K., Greenbaum, E.A., Doms, R.W., Trojanowski, J.Q., and Lee, V.M.-Y. (2005). BACE overexpression alters the subcellular processing of APP and inhibits Abeta deposition in vivo. The Journal of cell biology *168*, 291-302.

Leissring, M.A., Farris, W., Chang, A.Y., Walsh, D.M., Wu, X., Sun, X., Frosch, M.P., and Selkoe, D.J. (2003). Enhanced Proteolysis of β-Amyloid in APP Transgenic Mice Prevents Plaque Formation, Secondary Pathology, and Premature Death. Neuron *40*, 1087-1093.

Lesné, S., Koh, M.T., Kotilinek, L., Kayed, R., Glabe, C.G., Yang, A., Gallagher, M., and Ashe, K.H. (2006). A specific amyloid-beta protein assembly in the brain impairs memory. Nature *440*, 352-357.

Lesné, S., Kotilinek, L., and Ashe, K.H. (2008). Plaque-bearing mice with reduced levels of oligomeric amyloid-beta assemblies have intact memory function. Neuroscience *151*, 745-749.

Letronne, F., Laumet, G., Ayral, A.-M., Chapuis, J., Demiautte, F., Laga, M., Vandenberghe, M.E., Malmanche, N., Leroux, F., and Eysert, F., et al. (2016). ADAM30 Downregulates APP-Linked Defects Through Cathepsin D Activation in Alzheimer's Disease. EBioMedicine *9*, 278-292.

Lewis, J., McGowan, E., Rockwood, J., Melrose, H., Nacharaju, P., van Slegtenhorst, M., Gwinn-Hardy, K., Paul Murphy, M., Baker, M., and Yu, X., et al. (2000). Neurofibrillary tangles,

amyotrophy and progressive motor disturbance in mice expressing mutant (P301L) tau protein. Nature genetics *25*, 402-405.

Li, H., Wetten, S., Li, L., St Jean, P.L., Upmanyu, R., Surh, L., Hosford, D., Barnes, M.R., Briley, J.D., and Borrie, M., et al. (2008). Candidate single-nucleotide polymorphisms from a genomewide association study of Alzheimer disease. Arch Neurol *65*, 45-53.

Li, J., Fici, G.J., Mao, C.-A., Myers, R.L., Shuang, R., Donoho, G.P., Pauley, A.M., Himes, C.S., Qin, W., and Kola, I., et al. (2003). Positive and negative regulation of the gamma-secretase activity by nicastrin in a murine model. The Journal of biological chemistry *278*, 33445-33449.

Li, S., Hou, H., Mori, T., Sawmiller, D., Smith, A., Tian, J., Wang, Y., Giunta, B., Sanberg, P.R., and Zhang, S., et al. (2015). Swedish mutant APP-based BACE1 binding site peptide reduces APP β-cleavage and cerebral Aβ levels in Alzheimer's mice. Scientific reports *5*, 11322.

Ligt, J. de, Willemsen, M.H., van Bon, B.W.M., Kleefstra, T., Yntema, H.G., Kroes, T., Vulto-van Silfhout, A.T., Koolen, D.A., Vries, P. de, and Gilissen, C., et al. (2012). Diagnostic exome sequencing in persons with severe intellectual disability. The New England journal of medicine *367*, 1921-1929.

Lindwall, G., and Cole, R.D. (1984). Phosphorylation affects the ability of tau protein to promote microtubule assembly. The Journal of biological chemistry *259*, 5301-5305.

Liu, C., Li, Y., Semenov, M., Han, C., Baeg, G.-H., Tan, Y., Zhang, Z., Lin, X., and He, X. (2002). Control of β-Catenin Phosphorylation/Degradation by a Dual-Kinase Mechanism. Cell *108*, 837-847.

Liu, D.-s., Pan, X.-d., Zhang, J., Shen, H., Collins, N.C., Cole, A.M., Koster, K.P., Ben Aissa, M., Dai, X.-m., and Zhou, M., et al. (2015). APOE4 enhances age-dependent decline in cognitive function by down-regulating an NMDA receptor pathway in EFAD-Tg mice. Molecular neurodegeneration *10*, 7.

Liu, L., Ding, L., Rovere, M., Wolfe, M.S., and Selkoe, D.J. (2019). A cellular complex of BACE1 and γ-secretase sequentially generates Aβ from its full-length precursor. The Journal of cell biology *218*, 644-663.

Long, K.R., Newland, B., Florio, M., Kalebic, N., Langen, B., Kolterer, A., Wimberger, P., and Huttner, W.B. (2018). Extracellular Matrix Components HAPLN1, Lumican, and Collagen I Cause Hyaluronic Acid-Dependent Folding of the Developing Human Neocortex. Neuron *99*, 702-719.e6.

Lukiw, W.J., Cui, J.G., Yuan, L.Y., Bhattacharjee, P.S., Corkern, M., Clement, C., Kammerman, E.M., Ball, M.J., Zhao, Y., and Sullivan, P.M., et al. (2010). Acyclovir or Aβ42

peptides attenuate HSV-1-induced miRNA-146a levels in human primary brain cells. Neuroreport *21*, 922-927.

Ma, G., Li, T., Price, D.L., and Wong, P.C. (2005). APH-1a is the principal mammalian APH-1 isoform present in gamma-secretase complexes during embryonic development. J. Neurosci. *25*, 192-198.

Maragos, W.F., Greenamyre, J.T., Penney, J.B., and Young, A.B. (1987). Glutamate dysfunction in Alzheimer's disease. An hypothesis. Trends in Neurosciences *10*, 65-68.

Marchand, P., Tang, J., Johnson, G.D., and Bond, J.S. (1995). COOH-terminal proteolytic processing of secreted and membrane forms of the alpha subunit of the metalloprotease meprin A. Requirement of the I domain for processing in the endoplasmic reticulum. The Journal of biological chemistry *270*, 5449-5456.

Marín, N., Romero, B., Bosch-Morell, F., Llansola, M., Felipo, V., Romá, J., and Romero, F.J. (2000). β-Amyloid-induced activation of Caspase-3 in primary cultures of rat neurons. Mechanisms of Ageing and Development *119*, 63-67.

Matsunaga, S., Kishi, T., Iwata, N., and Quinn, T.J. (2015). Memantine Monotherapy for Alzheimer’s Disease. A Systematic Review and Meta-Analysis. PLoS ONE *10*, e0123289.

Meilandt, W.J., Ngu, H., Gogineni, A., Lalehzadeh, G., Lee, S.-H., Srinivasan, K., Imperio, J., Wu, T., Weber, M., and Kruse, A.J., et al. (2020). Trem2 Deletion Reduces Late-Stage Amyloid Plaque Accumulation, Elevates the Aβ42:Aβ40 Ratio, and Exacerbates Axonal Dystrophy and Dendritic Spine Loss in the PS2APP Alzheimer's Mouse Model. J. Neurosci. *40*, 1956-1974.

Miklossy, J. (2011). Emerging roles of pathogens in Alzheimer disease. Expert reviews in molecular medicine *13*, e30.

Miklossy, J. (2016). Bacterial Amyloid and DNA are Important Constituents of Senile Plaques. Further Evidence of the Spirochetal and Biofilm Nature of Senile Plaques. Journal of Alzheimer's Disease *53*, 1459-1473.

Moechars, D., Dewachter, I., Lorent, K., Reversé, D., Baekelandt, V., Naidu, A., Tesseur, I., Spittaels, K., Haute, C.V., and Checler, F., et al. (1999). Early phenotypic changes in transgenic mice that overexpress different mutants of amyloid precursor protein in brain. The Journal of biological chemistry *274*, 6483-6492.

Mondragón-Rodríguez, S., Basurto-Islas, G., Santa-Maria, I., Mena, R., Binder, L.I., Avila, J., Smith, M.A., Perry, G., and García-Sierra, F. (2008). Cleavage and conformational changes of tau protein follow phosphorylation during Alzheimer's disease. International journal of experimental pathology *89*, 81-90.

Moreno-Salinas, A.L., Avila-Zozaya, M., Ugalde-Silva, P., Hernández-Guzmán, D.A., Missirlis, F., and Boucard, A.A. (2019). Latrophilins. A Neuro-Centric View of an Evolutionary Conserved Adhesion G Protein-Coupled Receptor Subfamily. Frontiers in neuroscience *13*, 700.

Moussa-Pacha, N.M., Abdin, S.M., Omar, H.A., Alniss, H., and Al-Tel, T.H. (2020). BACE1 inhibitors. Current status and future directions in treating Alzheimer's disease. Medicinal research reviews *40*, 339-384.

Mueller-Steiner, S., Zhou, Y., Arai, H., Roberson, E.D., Sun, B., Chen, J., Wang, X., Yu, G., Esposito, L., and Mucke, L., et al. (2006). Antiamyloidogenic and neuroprotective functions of cathepsin B. Implications for Alzheimer's disease. Neuron *51*, 703-714.

Mullan, M., Crawford, F., Axelman, K., Houlden, H., Lilius, L., Winblad, B., and Lannfelt, L. (1992). A pathogenic mutation for probable Alzheimer's disease in the APP gene at the N-terminus of beta-amyloid. Nature genetics *1*, 345-347.

Murphy, M.P., and LeVine, H. (2010). Alzheimer's disease and the amyloid-beta peptide. Journal of Alzheimer's disease : JAD *19*, 311-323.

Nakajima, M., Arimatsu, K., Kato, T., Matsuda, Y., Minagawa, T., Takahashi, N., Ohno, H., and Yamazaki, K. (2015). Oral Administration of P. gingivalis Induces Dysbiosis of Gut Microbiota and Impaired Barrier Function Leading to Dissemination of Enterobacteria to the Liver. PloS one *10*, e0134234.

Nakanishi, K., Aono, S., Hirano, K., Kuroda, Y., Ida, M., Tokita, Y., Matsui, F., and Oohira, A. (2006). Identification of neurite outgrowth-promoting domains of neuroglycan C, a brain-specific chondroitin sulfate proteoglycan, and involvement of phosphatidylinositol 3-kinase and protein kinase C signaling pathways in neuritogenesis. The Journal of biological chemistry *281*, 24970-24978.

Nalivaeva, N.N., and Turner, A.J. (2013). The amyloid precursor protein. A biochemical enigma in brain development, function and disease. FEBS Letters *587*, 2046-2054.

Namba, Y., Tomonaga, M., Kawasaki, H., Otomo, E., and Ikeda, K. (1991). Apolipoprotein E immunoreactivity in cerebral amyloid deposits and neurofibrillary tangles in Alzheimer's disease and kuru plaque amyloid in Creutzfeldt-Jakob disease. Brain Research *541*, 163-166.

Näslund, J., Jensen, M., Tjernberg, L.O., Thyberg, J., Terenius, L., and Nordstedt, C. (1994). The metabolic pathway generating p3, an A beta-peptide fragment, is probably non-amyloidogenic. Biochemical and Biophysical Research Communications *204*, 780-787.

Nazarko, O., Kibrom, A., Winkler, J., Leon, K., Stoveken, H., Salzman, G., Merdas, K., Lu, Y., Narkhede, P., and Tall, G., et al. (2018). A Comprehensive Mutagenesis Screen of the Adhesion GPCR Latrophilin-1/ADGRL1. iScience *3*, 264-278.

N'Diaye, E.-N., Branda, C.S., Branda, S.S., Nevarez, L., Colonna, M., Lowell, C., Hamerman, J.A., and Seaman, W.E. (2009). TREM-2 (triggering receptor expressed on myeloid cells 2) is a phagocytic receptor for bacteria. The Journal of cell biology *184*, 215-223.

Nicholson, D.W. (1999). Caspase structure, proteolytic substrates, and function during apoptotic cell death. Cell death and differentiation *6*, 1028-1042.

Nishitomi, K., Sakaguchi, G., Horikoshi, Y., Gray, A.J., Maeda, M., Hirata-Fukae, C., Becker, A.G., Hosono, M., Sakaguchi, I., and Minami, S.S., et al. (2006). BACE1 inhibition reduces endogenous Abeta and alters APP processing in wild-type mice. Journal of neurochemistry *99*, 1555-1563.

Nunan, J., and Small, D.H. (2000). Regulation of APP cleavage by α-, β- and γ-secretases. FEBS Letters *483*, 6-10.

Oakley, H., Cole, S.L., Logan, S., Maus, E., Shao, P., Craft, J., Guillozet-Bongaarts, A., Ohno, M., Disterhoft, J., and van Eldik, L., et al. (2006). Intraneuronal beta-amyloid aggregates, neurodegeneration, and neuron loss in transgenic mice with five familial Alzheimer's disease mutations. Potential factors in amyloid plaque formation. J. Neurosci. *26*, 10129-10140.

Oberstein, T.J., Spitzer, P., Klafki, H.-W., Linning, P., Neff, F., Knölker, H.-J., Lewczuk, P., Wiltfang, J., Kornhuber, J., and Maler, J.M. (2015). Astrocytes and microglia but not neurons preferentially generate N-terminally truncated Aβ peptides. Neurobiology of disease *73*, 24-35.

O'Brien, R.J., and Wong, P.C. (2011). Amyloid precursor protein processing and Alzheimer's disease. Annual review of neuroscience *34*, 185-204.

Ohler, A., Debela, M., Wagner, S., Magdolen, V., and Becker-Pauly, C. (2010). Analyzing the protease web in skin. Meprin metalloproteases are activated specifically by KLK4, 5 and 8 vice versa leading to processing of proKLK7 thereby triggering its activation. Biological chemistry *391*, 455-460.

O'Sullivan, M.L., Martini, F., Daake, S. von, Comoletti, D., and Ghosh, A. (2014). LPHN3, a presynaptic adhesion-GPCR implicated in ADHD, regulates the strength of neocortical layer 2/3 synaptic input to layer 5. Neural development *9*, 7.

Paresce, D.M., Ghosh, R.N., and Maxfield, F.R. (1996). Microglial Cells Internalize Aggregates of the Alzheimer's Disease Amyloid β-Protein Via a Scavenger Receptor. Neuron *17*, 553-565.

Pastorino, L., Ikin, A.F., Nairn, A.C., Pursnani, A., and Buxbaum, J.D. (2002). The carboxyl-terminus of BACE contains a sorting signal that regulates BACE trafficking but not the formation of total A(beta). Molecular and cellular neurosciences *19*, 175-185.

Patel, T., Brookes, K.J., Turton, J., Chaudhury, S., Guetta-Baranes, T., Guerreiro, R., Bras, J., Hernandez, D., Singleton, A., and Francis, P.T., et al. (2018). Whole-exome sequencing of the

BDR cohort. Evidence to support the role of the PILRA gene in Alzheimer's disease. Neuropathology and applied neurobiology *44*, 506-521.

Perry, E.K., Tomlinson, B.E., Blessed, G., Bergmann, K., Gibson, P.H., and Perry, R.H. (1978). Correlation of cholinergic abnormalities with senile plaques and mental test scores in senile dementia. British medical journal *2*, 1457-1459.

Phillips, M.C. (2014). Apolipoprotein E isoforms and lipoprotein metabolism. IUBMB life *66*, 616-623.

Pike, C.J., Burdick, D., Walencewicz, A.J., Glabe, C.G., and Cotman, C.W. (1993). Neurodegeneration induced by beta-amyloid peptides in vitro. The role of peptide assembly state. J. Neurosci. *13*, 1676-1687.

Porat, Y., Kolusheva, S., Jelinek, R., and Gazit, E. (2003). The human islet amyloid polypeptide forms transient membrane-active prefibrillar assemblies. Biochemistry *42*, 10971-10977.

Prasansuklab, A., and Tencomnao, T. (2013). Amyloidosis in Alzheimer's Disease. The Toxicity of Amyloid Beta (A β), Mechanisms of Its Accumulation and Implications of Medicinal Plants for Therapy. Evidence-based complementary and alternative medicine : eCAM *2013*, 413808.

Prox, J., Arnold, P., and Becker-Pauly, C. (2015). Meprin α and meprin β. Procollagen proteinases in health and disease. Matrix biology : journal of the International Society for Matrix Biology *44-46*, 7-13.

Qi-Takahara, Y., Morishima-Kawashima, M., Tanimura, Y., Dolios, G., Hirotani, N., Horikoshi, Y., Kametani, F., Maeda, M., Saido, T.C., and Wang, R., et al. (2005). Longer forms of amyloid beta protein. Implications for the mechanism of intramembrane cleavage by gamma-secretase. J. Neurosci. *25*, 436-445.

Rannikmäe, K., Kalaria, R.N., Greenberg, S.M., Chui, H.C., Schmitt, F.A., Samarasekera, N., Al-Shahi Salman, R., and Sudlow, C.L.M. (2014). APOE associations with severe CAA-associated vasculopathic changes. Collaborative meta-analysis. Journal of neurology, neurosurgery, and psychiatry *85*, 300-305.

Ribasés, M., Ramos-Quiroga, J.A., Sánchez-Mora, C., Bosch, R., Richarte, V., Palomar, G., Gastaminza, X., Bielsa, A., Arcos-Burgos, M., and Muenke, M., et al. (2011). Contribution of LPHN3 to the genetic susceptibility to ADHD in adulthood. A replication study. Genes, brain, and behavior *10*, 149-157.

Richards, J.G., Higgins, G.A., Ouagazzal, A.-M., Ozmen, L., Kew, J.N.C., Bohrmann, B., Malherbe, P., Brockhaus, M., Loetscher, H., and Czech, C., et al. (2003). PS2APP Transgenic

Mice, Coexpressing hPS2mut and hAPPswe, Show Age-Related Cognitive Deficits Associated with Discrete Brain Amyloid Deposition and Inflammation. J. Neurosci. *23*, 8989-9003.

Roberds, S.L., Anderson, J., Basi, G., Bienkowski, M.J., Branstetter, D.G., Chen, K.S., Freedman, S.B., Frigon, N.L., Games, D., and Hu, K., et al. (2001). BACE knockout mice are healthy despite lacking the primary beta-secretase activity in brain. Implications for Alzheimer's disease therapeutics. Human molecular genetics *10*, 1317-1324.

Rockenstein, E., Mallory, M., Mante, M., Sisk, A., and Masliaha, E. (2001). Early formation of mature amyloid-beta protein deposits in a mutant APP transgenic model depends on levels of Abeta(1-42). Journal of neuroscience research *66*, 573-582.

Rockenstein, E., Mante, M., Alford, M., Adame, A., Crews, L., Hashimoto, M., Esposito, L., Mucke, L., and Masliah, E. (2005). High beta-secretase activity elicits neurodegeneration in transgenic mice despite reductions in amyloid-beta levels. Implications for the treatment of Alzheimer disease. The Journal of biological chemistry *280*, 32957-32967.

Röthe, J., Thor, D., Winkler, J., Knierim, A.B., Binder, C., Huth, S., Kraft, R., Rothemund, S., Schöneberg, T., and Prömel, S. (2019). Involvement of the Adhesion GPCRs Latrophilins in the Regulation of Insulin Release. Cell reports *26*, 1573-1584.e5.

Sakono, M., and Zako, T. (2010). Amyloid oligomers. Formation and toxicity of Abeta oligomers. The FEBS journal *277*, 1348-1358.

Sastre, M., Steiner, H., Fuchs, K., Capell, A., Multhaup, G., Condron, M.M., Teplow, D.B., and Haass, C. (2001). Presenilin-dependent gamma-secretase processing of beta-amyloid precursor protein at a site corresponding to the S3 cleavage of Notch. EMBO reports *2*, 835-841.

Savage, M.J., Trusko, S.P., Howland, D.S., Pinsker, L.R., Mistretta, S., Reaume, A.G., Greenberg, B.D., Siman, R., and Scott, R.W. (1998). Turnover of amyloid beta-protein in mouse brain and acute reduction of its level by phorbol ester. J. Neurosci. *18*, 1743-1752.

Schäfer, B.W., Fritschy, J.M., Murmann, P., Troxler, H., Durussel, I., Heizmann, C.W., and Cox, J.A. (2000). Brain S100A5 is a novel calcium-, zinc-, and copper ion-binding protein of the EF-hand superfamily. The Journal of biological chemistry *275*, 30623-30630.

Schechter, I., and Berger, A. (1967). On the size of the active site in proteases. I. Papain. Biochemical and Biophysical Research Communications *27*, 157-162.

Schechter, I., and Ziv, E. (2011). Cathepsins S, B and L with aminopeptidases display β-secretase activity associated with the pathogenesis of Alzheimer's disease. Biological chemistry *392*, 555-569.

Schieb, H., Weidlich, S., Schlechtingen, G., Linning, P., Jennings, G., Gruner, M., Wiltfang, J., Klafki, H.-W., and Knölker, H.-J. (2010). Structural design, solid-phase synthesis and activity of membrane-anchored β-secretase inhibitors on Aβ generation from wild-type and Swedish-mutant APP. Chemistry *16*, 14412-14423.

Schlenzig, D., Cynis, H., Hartlage-Rübsamen, M., Zeitschel, U., Menge, K., Fothe, A., Ramsbeck, D., Spahn, C., Wermann, M., and Roßner, S., et al. (2018). Dipeptidyl-Peptidase Activity of Meprin β Links N-truncation of Aβ with Glutaminyl Cyclase-Catalyzed pGlu-Aβ Formation. Journal of Alzheimer's disease : JAD *66*, 359-375.

Schlepckow, K., Kleinberger, G., Fukumori, A., Feederle, R., Lichtenthaler, S.F., Steiner, H., and Haass, C. (2017). An Alzheimer-associated TREM2 variant occurs at the ADAM cleavage site and affects shedding and phagocytic function. EMBO molecular medicine *9*, 1356-1365.

Schönherr, C., Bien, J., Isbert, S., Wichert, R., Prox, J., Altmeppen, H., Kumar, S., Walter, J., Lichtenthaler, S.F., and Weggen, S., et al. (2016). Generation of aggregation prone N-terminally truncated amyloid β peptides by meprin β depends on the sequence specificity at the cleavage site. Molecular neurodegeneration *11*, 19.

Selkoe, D.J., and Hardy, J. (2016). The amyloid hypothesis of Alzheimer's disease at 25 years. EMBO molecular medicine *8*, 595-608.

Seltzer, B., and Sherwin, I. (1983). A Comparison of Clinical Features in Early- and Late-Onset Primary Degenerative Dementia. One Entity or Two? Arch Neurol *40*, 143-146.

Sengupta, U., Nilson, A.N., and Kayed, R. (2016). The Role of Amyloid-β Oligomers in Toxicity, Propagation, and Immunotherapy. EBioMedicine *6*, 42-49.

Sergé, A., Keijzer, S. de, van Hemert, F., Hickman, M.R., Hereld, D., Spaink, H.P., Schmidt, T., and Snaar-Jagalska, B.E. (2011). Quantification of GPCR internalization by single-molecule microscopy in living cells. Integrative biology : quantitative biosciences from nano to macro *3*, 675-683.

Sherva, R., and Farrer, L.A. (2011). Power and pitfalls of the genome-wide association study approach to identify genes for Alzheimer's disease. Current psychiatry reports *13*, 138-146.

Sims, N.R., Bowen, D.M., Allen, S.J., Smith, C.C.T., Neary, D., Thomas, D.J., and Davison, A.N. (1983). Presynaptic Cholinergic Dysfunction in Patients with Dementia. Journal of neurochemistry *40*, 503-509.

Sims, R., van der Lee, S.J., Naj, A.C., Bellenguez, C., Badarinarayan, N., Jakobsdottir, J., Kunkle, B.W., Boland, A., Raybould, R., and Bis, J.C., et al. (2017). Rare coding variants in PLCG2, ABI3, and TREM2 implicate microglial-mediated innate immunity in Alzheimer's disease. Nature genetics *49*, 1373-1384.

Sisodia, S.S., Koo, E.H., Beyreuther, K., Unterbeck, A., and Price, D.L. (1990). Evidence that beta-amyloid protein in Alzheimer's disease is not derived by normal processing. Science (New York, N.Y.) *248*, 492-495.

Skovronsky, D.M., Moore, D.B., Milla, M.E., Doms, R.W., and Lee, V.M. (2000). Protein kinase C-dependent alpha-secretase competes with beta-secretase for cleavage of amyloid-beta precursor protein in the trans-golgi network. The Journal of biological chemistry *275*, 2568-2575.

Slack, B.E., Ma, L.K., and Seah, C.C. (2001). Constitutive shedding of the amyloid precursor protein ectodomain is up-regulated by tumour necrosis factor-alpha converting enzyme. The Biochemical journal *357*, 787-794.

Song, W., Hooli, B., Mullin, K., Jin, S.C., Cella, M., Ulland, T.K., Wang, Y., Tanzi, R.E., and Colonna, M. (2017). Alzheimer's disease-associated TREM2 variants exhibit either decreased or increased ligand-dependent activation. Alzheimer's & Dementia *13*, 381-387.

Soscia, S.J., Kirby, J.E., Washicosky, K.J., Tucker, S.M., Ingelsson, M., Hyman, B., Burton, M.A., Goldstein, L.E., Duong, S., and Tanzi, R.E., et al. (2010). The Alzheimer's disease-associated amyloid beta-protein is an antimicrobial peptide. PloS one *5*, e9505.

Spillantini, M.G., Murrell, J.R., Goedert, M., Farlow, M.R., Klug, A., and Ghetti, B. (1998). Mutation in the tau gene in familial multiple system tauopathy with presenile dementia. Proceedings of the National Academy of Sciences of the United States of America *95*, 7737-7741.

Steinberg, S.F. (2008). Structural basis of protein kinase C isoform function. Physiological reviews *88*, 1341-1378.

Steiner, H., Fluhrer, R., and Haass, C. (2008). Intramembrane proteolysis by gamma-secretase. The Journal of biological chemistry *283*, 29627-29631.

Steiner, H., Fukumori, A., Tagami, S., and Okochi, M. (2018). Making the final cut. Pathogenic amyloid-β peptide generation by γ-secretase. Cell stress *2*, 292-310.

Stéphan, A., Laroche, S., and Davis, S. (2001). Generation of Aggregated β-Amyloid in the Rat Hippocampus Impairs Synaptic Transmission and Plasticity and Causes Memory Deficits. J. Neurosci. *21*, 5703-5714.

Sterchi, E.E., Green, J.R., and Lentze, M.J. (1982). Non-pancreatic hydrolysis of N-benzoyl-l-tyrosyl-p-aminobenzoic acid (PABA-peptide) in the human small intestine. Clinical science (London, England : 1979) *62*, 557-560.

Sterchi, E.E., Naim, H.Y., Lentze, M.J., Hauri, H.-P., and Fransen, J.A.M. (1988). N-benzoyl-l-tyrosyl-p-aminobenzoic acid hydrolase. A metalloendopeptidase of the human intestinal

microvillus membrane which degrades biologically active peptides. Archives of Biochemistry and Biophysics *265*, 105-118.

Sterchi, E.E., Stöcker, W., and Bond, J.S. (2008). Meprins, membrane-bound and secreted astacin metalloproteinases. Molecular aspects of medicine *29*, 309-328.

Sturchler-Pierrat, C., Abramowski, D., Duke, M., Wiederhold, K.H., Mistl, C., Rothacher, S., Ledermann, B., Bürki, K., Frey, P., and Paganetti, P.A., et al. (1997). Two amyloid precursor protein transgenic mouse models with Alzheimer disease-like pathology. Proceedings of the National Academy of Sciences of the United States of America *94*, 13287-13292.

Sutton, L.P., Orlandi, C., Song, C., Oh, W.C., Muntean, B.S., Xie, K., Filippini, A., Xie, X., Satterfield, R., and Yaeger, J.D.W., et al. (2018). Orphan receptor GPR158 controls stress-induced depression. eLife *7*.

Svitkina, T. (2018). The Actin Cytoskeleton and Actin-Based Motility. Cold Spring Harbor perspectives in biology *10*.

Takasugi, N., Tomita, T., Hayashi, I., Tsuruoka, M., Niimura, M., Takahashi, Y., Thinakaran, G., and Iwatsubo, T. (2003). The role of presenilin cofactors in the gamma-secretase complex. Nature *422*, 438-441.

Takuma, H., Tomiyama, T., Kuida, K., and Mori, H. (2004). Amyloid beta peptide-induced cerebral neuronal loss is mediated by caspase-3 in vivo. Journal of neuropathology and experimental neurology *63*, 255-261.

Talantova, M., Sanz-Blasco, S., Zhang, X., Xia, P., Akhtar, M.W., Okamoto, S.-i., Dziewczapolski, G., Nakamura, T., Cao, G., and Pratt, A.E., et al. (2013). A induces astrocytic glutamate release, extrasynaptic NMDA receptor activation, and synaptic loss. Proceedings of the National Academy of Sciences of the United States of America *110*, E2518-E2527.

Talman, V., Pascale, A., Jäntti, M., Amadio, M., and Tuominen, R.K. (2016). Protein Kinase C Activation as a Potential Therapeutic Strategy in Alzheimer's Disease. Is there a Role for Embryonic Lethal Abnormal Vision-like Proteins? Basic & clinical pharmacology & toxicology *119*, 149-160.

Tanaka, S., Shiojiri, S., Takahashi, Y., Kitaguchi, N., Ito, H., Kameyama, M., Kimura, J., Nakamura, S., and Ueda, K. (1989). Tissue-specific expression of three types of β-protein precursor mRNA. Enhancement of protease inhibitor-harboring types in Alzheimer's disease brain. Biochemical and Biophysical Research Communications *165*, 1406-1414.

The UniProt Consortium (2021). UniProt. The universal protein knowledgebase in 2021. Nucleic acids research *49*, D480-D489.

Thinakaran, G., Borchelt, D.R., Lee, M.K., Slunt, H.H., Spitzer, L., Kim, G., Ratovitsky, T., Davenport, F., Nordstedt, C., and Seeger, M., et al. (1996). Endoproteolysis of Presenilin 1 and Accumulation of Processed Derivatives In Vivo. Neuron *17*, 181-190.

Thompson, L.M., Aiken, C.T., Kaltenbach, L.S., Agrawal, N., Illes, K., Khoshnan, A., Martinez-Vincente, M., Arrasate, M., O'Rourke, J.G., and Khashwji, H., et al. (2009). IKK phosphorylates Huntingtin and targets it for degradation by the proteasome and lysosome. The Journal of cell biology *187*, 1083-1099.

Thornton, P., Sevalle, J., Deery, M.J., Fraser, G., Zhou, Y., Ståhl, S., Franssen, E.H., Dodd, R.B., Qamar, S., and Gomez Perez-Nievas, B., et al. (2017). TREM2 shedding by cleavage at the H157-S158 bond is accelerated for the Alzheimer's disease-associated H157Y variant. EMBO molecular medicine *9*, 1366-1378.

Tomiyama, T., Matsuyama, S., Iso, H., Umeda, T., Takuma, H., Ohnishi, K., Ishibashi, K., Teraoka, R., Sakama, N., and Yamashita, T., et al. (2010). A mouse model of amyloid beta oligomers. Their contribution to synaptic alteration, abnormal tau phosphorylation, glial activation, and neuronal loss in vivo. J. Neurosci. *30*, 4845-4856.

Uhlén, M., Fagerberg, L., Hallström, B.M., Lindskog, C., Oksvold, P., Mardinoglu, A., Sivertsson, Å., Kampf, C., Sjöstedt, E., and Asplund, A., et al. (2015). Proteomics. Tissue-based map of the human proteome; https://www.proteinatlas.org/ENSG00000011600-TYROBP/celltype. Science (New York, N.Y.) *347*, 1260419.

van Dorpe, J., Smeijers, L., Dewachter, I., Nuyens, D., Spittaels, K., van den Haute, C., Mercken, M., Moechars, D., Laenen, I., and Kuiperi, C., et al. (2000). Prominent Cerebral Amyloid Angiopathy in Transgenic Mice Overexpressing the London Mutant of Human APP in Neurons. The American journal of pathology *157*, 1283-1298.

Vandersteen, A., Hubin, E., Sarroukh, R., Baets, G. de, Schymkowitz, J., Rousseau, F., Subramaniam, V., Raussens, V., Wenschuh, H., and Wildemann, D., et al. (2012). A comparative analysis of the aggregation behavior of amyloid-β peptide variants. FEBS Letters *586*, 4088-4093.

VandeVrede, L., Boxer, A.L., and Polydoro, M. (2020). Targeting tau. Clinical trials and novel therapeutic approaches. Neuroscience letters *731*, 134919.

Varedi K, S.M., Ventura, A.C., Merajver, S.D., and Lin, X.N. (2010). Multisite phosphorylation provides an effective and flexible mechanism for switch-like protein degradation. PloS one *5*, e14029.

Vassar, R., Bennett, B.D., Babu-Khan, S., Kahn, S., Mendiaz, E.A., Denis, P., Teplow, D.B., Ross, S., Amarante, P., and Loeloff, R., et al. (1999). Beta-secretase cleavage of Alzheimer's

amyloid precursor protein by the transmembrane aspartic protease BACE. Science (New York, N.Y.) *286*, 735-741.

Vellas, B., Sol, O., J. Snyder, P., Ousset, P.-J., Haddad, R., Maurin, M., Lemarie, J.-C., Desire, L., and P. Pando, M. (2011). EHT0202 in Alzheimers Disease. A 3-Month, Randomized, Placebo- Controlled, Double-Blind Study. CAR *8*, 203-212.

Wallis, D., Hill, D.S., Mendez, I.A., Abbott, L.C., Finnell, R.H., Wellman, P.J., and Setlow, B. (2012). Initial characterization of mice null for Lphn3, a gene implicated in ADHD and addiction. Brain Research *1463*, 85-92.

Walter, J., Fluhrer, R., Hartung, B., Willem, M., Kaether, C., Capell, A., Lammich, S., Multhaup, G., and Haass, C. (2001). Phosphorylation regulates intracellular trafficking of beta-secretase. The Journal of biological chemistry *276*, 14634-14641.

Wang, Z., Wang, B., Yang, L., Guo, Q., Aithmitti, N., Songyang, Z., and Zheng, H. (2009). Presynaptic and postsynaptic interaction of the amyloid precursor protein promotes peripheral and central synaptogenesis. J. Neurosci. *29*, 10788-10801.

Weidemann, A., Eggert, S., Reinhard, F.B.M., Vogel, M., Paliga, K., Baier, G., Masters, C.L., Beyreuther, K., and Evin, G. (2002). A novel epsilon-cleavage within the transmembrane domain of the Alzheimer amyloid precursor protein demonstrates homology with Notch processing. Biochemistry *41*, 2825-2835.

Wichert, R., Ermund, A., Schmidt, S., Schweinlin, M., Ksiazek, M., Arnold, P., Knittler, K., Wilkens, F., Potempa, B., and Rabe, B., et al. (2017). Mucus Detachment by Host Metalloprotease Meprin β Requires Shedding of Its Inactive Pro-form, which Is Abrogated by the Pathogenic Protease RgpB. Cell reports *21*, 2090-2103.

Willem, M., Dewachter, I., Smyth, N., van Dooren, T., Borghgraef, P., Haass, C., and van Leuven, F. (2004). β-Site Amyloid Precursor Protein Cleaving Enzyme 1 Increases Amyloid Deposition in Brain Parenchyma but Reduces Cerebrovascular Amyloid Angiopathy in Aging BACE × APP[V717I] Double-Transgenic Mice. The American journal of pathology *165*, 1621-1631.

Wiltfang, J., Esselmann, H., Cupers, P., Neumann, M., Kretzschmar, H., Beyermann, M., Schleuder, D., Jahn, H., Rüther, E., and Kornhuber, J., et al. (2001). Elevation of beta-amyloid peptide 2-42 in sporadic and familial Alzheimer's disease and its generation in PS1 knockout cells. The Journal of biological chemistry *276*, 42645-42657.

Wolfe, M.S., Xia, W., Ostaszewski, B.L., Diehl, T.S., Kimberly, W.T., and Selkoe, D.J. (1999). Two transmembrane aspartates in presenilin-1 required for presenilin endoproteolysis and gamma-secretase activity. Nature *398*, 513-517.

Wozniak, M.A., Mee, A.P., and Itzhaki, R.F. (2009). Herpes simplex virus type 1 DNA is located within Alzheimer's disease amyloid plaques. The Journal of pathology *217*, 131-138.

Xin, S.-H., Tan, L., Cao, X., Yu, J.-T., and Tan, L. (2018). Clearance of Amyloid Beta and Tau in Alzheimer's Disease. From Mechanisms to Therapy. Neurotoxicity research *34*, 733-748.

Yamada, H., Fredette, B., Shitara, K., Hagihara, K., Miura, R., Ranscht, B., Stallcup, W.B., and Yamaguchi, Y. (1997). The Brain Chondroitin Sulfate Proteoglycan Brevican Associates with Astrocytes Ensheathing Cerebellar Glomeruli and Inhibits Neurite Outgrowth from Granule Neurons. J. Neurosci. *17*, 7784-7795.

Yamazaki, Y., Zhao, N., Caulfield, T.R., Liu, C.-C., and Bu, G. (2019). Apolipoprotein E and Alzheimer disease. Pathobiology and targeting strategies. Nature reviews. Neurology *15*, 501-518.

Yeh, F.L., Wang, Y., Tom, I., Gonzalez, L.C., and Sheng, M. (2016). TREM2 Binds to Apolipoproteins, Including APOE and CLU/APOJ, and Thereby Facilitates Uptake of Amyloid-Beta by Microglia. Neuron *91*, 328-340.

Yiannopoulou, K.G., and Papageorgiou, S.G. (2020). Current and Future Treatments in Alzheimer Disease. An Update. Journal of central nervous system disease *12*, 19-33.

Yoon, S.-S., and Jo, S.A. (2012). Mechanisms of Amyloid-β Peptide Clearance. Potential Therapeutic Targets for Alzheimer's Disease. Biomolecules & therapeutics *20*, 245-255.

Yoshiyama, Y., Higuchi, M., Zhang, B., Huang, S.-M., Iwata, N., Saido, T.C., Maeda, J., Suhara, T., Trojanowski, J.Q., and Lee, V.M.-Y. (2007). Synapse loss and microglial activation precede tangles in a P301S tauopathy mouse model. Neuron *53*, 337-351.

Youmans, K.L., Tai, L.M., Nwabuisi-Heath, E., Jungbauer, L., Kanekiyo, T., Gan, M., Kim, J., Eimer, W.A., Estus, S., and Rebeck, G.W., et al. (2012). APOE4-specific changes in Aβ accumulation in a new transgenic mouse model of Alzheimer disease. The Journal of biological chemistry *287*, 41774-41786.

Yu, C., Kim, S.H., Ikeuchi, T., Xu, H., Gasparini, L., Wang, R., and Sisodia, S.S. (2001). Characterization of a presenilin-mediated amyloid precursor protein carboxyl-terminal fragment gamma. Evidence for distinct mechanisms involved in gamma -secretase processing of the APP and Notch1 transmembrane domains. The Journal of biological chemistry *276*, 43756-43760.

Zemoura, K., Balakrishnan, K., Grampp, T., and Benke, D. (2019). Ca2+/Calmodulin-Dependent Protein Kinase II (CaMKII) β-Dependent Phosphorylation of GABAB1 Triggers Lysosomal Degradation of GABAB Receptors via Mind Bomb-2 (MIB2)-Mediated Lys-63-Linked Ubiquitination. Molecular neurobiology *56*, 1293-1309.

Zhang, Y., Sloan, S.A., Clarke, L.E., Caneda, C., Plaza, C.A., Blumenthal, P.D., Vogel, H., Steinberg, G.K., Edwards, M.S.B., and Li, G., et al. (2016). Purification and Characterization of Progenitor and Mature Human Astrocytes Reveals Transcriptional and Functional Differences with Mouse. Neuron *89*, 37-53.

Zhao, G., Cui, M.-Z., Mao, G., Dong, Y., Tan, J., Sun, L., and Xu, X. (2005). gamma-Cleavage is dependent on zeta-cleavage during the proteolytic processing of amyloid precursor protein within its transmembrane domain. The Journal of biological chemistry *280*, 37689-37697.

Zhao, Y., Wu, X., Li, X., Jiang, L.-L., Gui, X., Liu, Y., Sun, Y., Zhu, B., Piña-Crespo, J.C., and Zhang, M., et al. (2018). TREM2 Is a Receptor for β-Amyloid that Mediates Microglial Function. Neuron *97*, 1023-1031.e7.

Zheng, H., Jiang, M., Trumbauer, M.E., Sirinathsinghji, D.J.S., Hopkins, R., Smith, D.W., Heavens, R.P., Dawson, G.R., Boyce, S., and Conner, M.W., et al. (1995). β-amyloid precursor protein-deficient mice show reactive gliosis and decreased locomotor activity. Cell *81*, 525-531.

Zhong, L., Chen, X.-F., Wang, T., Wang, Z., Liao, C., Wang, Z., Huang, R., Wang, D., Li, X., and Wu, L., et al. (2017). Soluble TREM2 induces inflammatory responses and enhances microglial survival. The Journal of experimental medicine *214*, 597-607.

Zhong, L., Chen, X.-F., Zhang, Z.-L., Wang, Z., Shi, X.-Z., Xu, K., Zhang, Y.-W., Xu, H., and Bu, G. (2015). DAP12 Stabilizes the C-terminal Fragment of the Triggering Receptor Expressed on Myeloid Cells-2 (TREM2) and Protects against LPS-induced Pro-inflammatory Response. The Journal of biological chemistry *290*, 15866-15877.

Zhong, L., Xu, Y., Zhuo, R., Wang, T., Wang, K., Huang, R., Wang, D., Gao, Y., Zhu, Y., and Sheng, X., et al. (2019). Soluble TREM2 ameliorates pathological phenotypes by modulating microglial functions in an Alzheimer's disease model. Nature communications *10*, 1365.

Zhuo, L., Theis, M., Alvarez-Maya, I., Brenner, M., Willecke, K., and Messing, A. (2001). hGFAP-cre transgenic mice for manipulation of glial and neuronal function in vivo. Genesis *31*, 85-94.

6. Supplementary Information

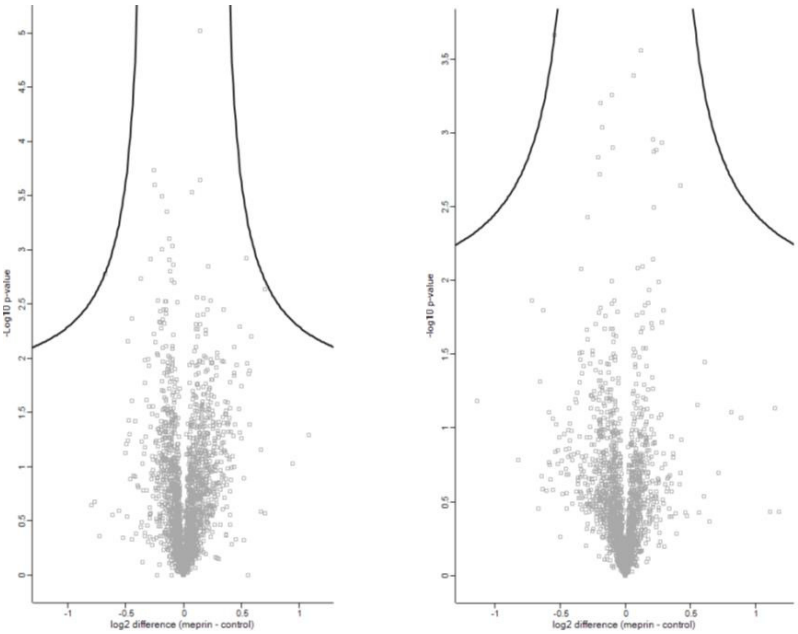

Supplementary Fig. S1: Protein level t-test data from Pre-TAILS experiments 1 (left) and 2 (right).

Brains of GFAP$^{Cre+/-}$;Rosa26$^{Mep1b\text{-}HA}$ and GFAP$^{Cre-/-}$;Rosa26$^{Mep1b\text{-}HA}$ were dissected and prepeared for TAILS analyisis. A t-test of the protein levels obtained from the two Pre-TAILS analyses revealed in no significant protein level changes. Black lines represent p-value adjusted cut-offs (FDR of 5% and s0 of 0.1).

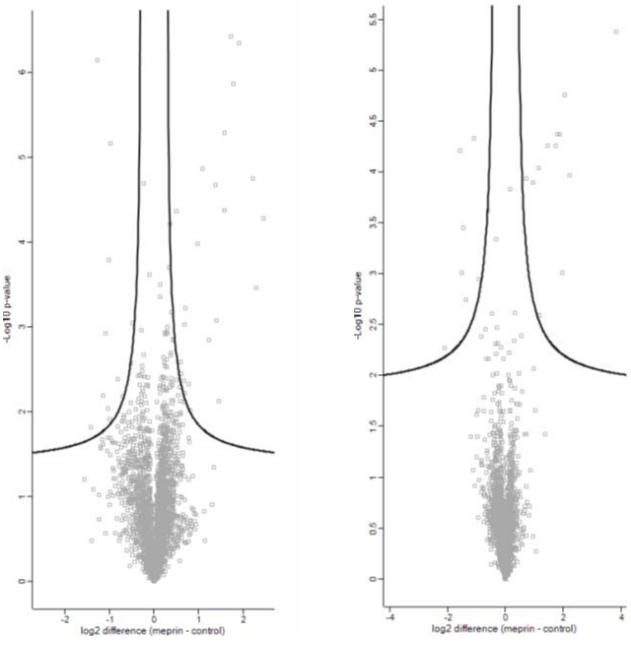

Supplementary Fig. S2: N-termini peptide abundance t-test data from TAILS experiments 1 (left) and 2 (right).

Brains of GFAP$^{Cre+/-}$;Rosa26$^{Mep1b\text{-}HA}$ and GFAP$^{Cre-/-}$;Rosa26$^{Mep1b\text{-}HA}$ were dissected and prepeared for TAILS analyisis. A t-test of the N-terminal peptide abundance obtained from the two TAILS experiments revealed 35 and 19 statistically different N-termini between the GFAP$^{Cre+/-}$;Rosa26$^{Mep1b\text{-}HA}$ and GFAP$^{Cre-/-}$;Rosa26$^{Mep1b\text{-}HA}$ samples, respectively. Black lines represent p-value adjusted cut-offs (FDR of 5% and s0 of 0.1).

Supplementary Tab. S1: N-termini significant hits identified from TAILS experiment 1.

Brains of GFAP$^{Cre+/-}$;Rosa26$^{Mep1b\text{-}HA}$ and GFAP$^{Cre-/-}$;Rosa26$^{Mep1b\text{-}HA}$ were dissected and prepeared for TAILS analyisis. A t-test of the N-terminal peptide abundance obtained from the first TAILS experiments revealed 35 statistically different N-termini between the GFAP$^{Cre+/-}$;Rosa26$^{Mep1b\text{-}HA}$ and GFAP$^{Cre-/-}$;Rosa26$^{Mep1b\text{-}HA}$ samples depicted in the table. A positive value indicates the N-terminus was more abundant in GFAP$^{Cre+/-}$;Rosa26$^{Mep1b\text{-}HA}$ compared to GFAP$^{Cre-/-}$;Rosa26$^{Mep1b\text{-}HA}$.

log_{10} p-value (Cre+/- vs. Cre-/-)	**log_2 diff. (Cre+/- vs. Cre-/-)**	**Annotated Sequence**	**Description**	**Master Protein Accessions**	**Pos.**	**Mass**
3.22	0.70	[E].DTGLNPGRDSVTNQIR.[K]	Receptor-type tyrosine-protein phosphatase zeta	B9EKR1	[440-455]	1972.041
2.22	0.69	[M].AASSSQVSEMKGVEDSSKTQTEGPR.[H]	Proline-rich transmembrane protein 2	E9PUL5	[2-26]	3096.552
1.91	-0.99	[Y].SLHVDIPR.[W]	Dihydropyrimidinase-related protein 4	O35098	[136-143]	1165.689
2.19	-1.13	[R].HGFLPR.[H]	Myelin basic protein	P04370	[158-163]	955.5675
2.01	0.81	[M].ASTEGANNMPKQVEVR.[M]	Excitatory amino acid transporter 2	P43006	[2-17]	2002.023
2.58	0.60	[M].ASTEGANNMPKQVEVR.[M]	Excitatory amino acid transporter 2	P43006	[2-17]	2205.17
1.91	-0.99	[R].SPAGLRR.[A]	Rabphilin-3A	P47708	[262-268]	985.6104
6.35	1.90	[Q].DTQDTTATEKGLR.[M]	Neurocan core protein	P55066	[25-37]	1894.028
5.87	1.78	[Q].DTTATEKGLR.[M]	Neurocan core protein	P55066	[28-37]	1549.895
4.38	1.56	[D].TTATEKGLR.[M]	Neurocan core protein	P55066	[29-37]	1434.868
4.75	2.21	[L].EEEKEQEDLWVWPR.[E]	Brevican core protein	Q61361	[461-474]	2331.202
4.27	2.44	[E].TPSEEKSGR.[T]	Brevican core protein	Q61361	[585-593]	1448.811
5.29	1.58	[E].EEKEQEDLWVWPR.[E]	Brevican core protein	Q61361	[462-474]	2202.16
4.86	1.09	[E].DPAEAPR.[T]	Brevican core protein	Q61361	[418-424]	984.5312
2.84	1.23	[E].DLWVWPR.[E]	Brevican core protein	Q61361	[468-474]	1200.673
5.17	-0.97	[E].DGGGGSSTPEDPAEAPR.[T]	Brevican core protein	Q61361	[408-424]	1828.851
6.15	-1.26	[A].DDLKEDSSEDR.[A]	Brevican core protein	Q61361	[23-33]	1766.881
2.92	-1.08	[A].AGAGLPESVIWAVNAGGEAHVDVHGIHFR.[K]	Malectin	Q6ZQI3	[39-67]	3195.665
3.03	0.68	[E].DETSWTER.[G]	Chondroitin sulfate proteoglycan 5	Q71M36	[71-78]	1252.601
1.81	-1.41	[R].TEGHEETPLPPAQSQTQEGGPAAGKASGADER.[D]	Microtubule-associated protein 6	Q7TSJ2	[340-371]	3661.809
4.68	1.38	[D].SELERPPVR.[G]	Latrophilin-3	Q80TS3	[485-493]	1311.758
3.08	1.39	[Y].EGYAILR.[L]	Beta-actin-like protein 2	Q8BFZ3;P60710;P63260	[168-178]	1468.847
2.04	-1.02	[R].SAPKEDDASASTSQSSR.[A]	Eukaryotic translation initiation factor 4B	Q8BGD9	[340-356]	2182.099

3.79	-1.01	[G].DTDGFNLEDALKETSSVKQR.[W]	CD99 antigen-like protein 2	Q8BIF0	[26-45]	2940.588
2.33	0.77	[M].AAGAGARPAPR.[W]	Cholinephosphotransferase 1	Q8C025	[2-12]	1223.717
3.46	2.29	[L].DPPGRPDSPR.[E]	Probable G-protein coupled receptor 158	Q8C419	[27-36]	1322.701
2.38	-0.81	[R].SPSQEPSAPGKAEAVGEQAR.[G]	Eukaryotic translation initiation factor 3 subunit B	Q8JZQ9	[88-107]	2454.299
2.36	0.67	[M].SSLHKSR.[I]	TBC1 domain family member 13	Q8R3D1	[2-8]	1085.626
3.05	-0.47	[A].LAFSDETLDKVTKSEGYCSR.[I]	Spondin-1	Q8VCC9	[27-46]	2993.586
2.18	-0.70	[R].SHAQKNENAR.[Q]	Myosin-9	Q8VDD5	[1771-1780]	1612.892
2.13	1.44	[M].GEIKVSPDYNWFR.[S]	Maspardin	Q9CQC8	[2-14]	1881.97
2.45	0.62	[P].LGTTAKEEMER.[F]	Succinate dehydrogenase cytochrome b560 subunit, mitochondrial	Q9CZB0	[30-40]	1722.946
4.37	0.50	[A].FHMTKDMLPGSYPR.[T]	NADH dehydrogenase [ubiquinone] 1 β subcomplex subunit 8, mitochondrial	Q9D6J5	[30-43]	2138.129
6.42	1.71	[S].DSYTPPDQDR.[V]	Hyaluronan and proteoglycan link protein 1	Q9QUP5	[21-30]	1422.67
3.98	0.97	[D].SYTPPDQDR.[V]	Hyaluronan and proteoglycan link protein 1	Q9QUP5	[22-30]	1307.643

Supplementary Tab. S2: N-termini significant hits identified from TAILS experiment 2.

Brains of GFAP$^{Cre+/-}$;Rosa26$^{Mep1b\text{-HA}}$ and GFAP$^{Cre-/-}$;Rosa26$^{Mep1b\text{-HA}}$ were dissected and prepeared for TAILS analyisis. A t-test of the N-terminal peptide abundance obtained from the second TAILS experiments revealed 19 statistically different N-termini between the GFAP$^{Cre+/-}$;Rosa26$^{Mep1b\text{-HA}}$ and GFAP$^{Cre-/-}$;Rosa26$^{Mep1b\text{-HA}}$ samples depicted in the table. A positive value indicates the N-terminus was more abundant in GFAP$^{Cre+/-}$;Rosa26$^{Mep1b\text{-HA}}$ compared to GFAP$^{Cre-/-}$;Rosa26$^{Mep1b\text{-HA}}$.

log_{10} p-value (Cre+/- vs. Cre-/-)	**log_2 diff. (Cre+/- vs. Cre-/-)**	**Annotated Sequence**	**Description**	**Master Protein Accessions**	**Pos.**	**Mass**
3.97	2.23	[Q].DTQDTTATEKGLR.[M]	Neurocan core protein	P55066	[25-37]	1894.028
4.26	1.74	[D].TTATEKGLR.[M]	Neurocan core protein	P55066	[29-37]	1434.868
3.94	0.72	[-].METPLEKALTTMVTTFHKYSGR.[E]	Protein S100-A5	P63084	[1-22]	3041.62
5.38	3.83	[E].TPSEEKSGR.[T]	Brevican core protein	Q61361	[585-593]	1448.811
4.37	1.89	[E].EEKEQEDLWVWPR.[E]	Brevican core protein	Q61361	[462-474]	2202.16
3.01	1.97	[E].DLWVWPR.[E]	Brevican core protein	Q61361	[468-474]	1200.673

4.26	1.45	[L].EEEKEQEDLWVWPR.[E]	Brevican core protein	Q61361	[461-474]	2331.202
3.90	0.95	[E].DPAEAPR.[T]	Brevican core protein	Q61361	[418-424]	984.5312
4.21	-1.57	[A].DDLKEDSSEDR.[A]	Brevican core protein	Q61361	[23-33]	1766.881
2.27	-2.11	[D].GGGGSSTPEDPAEAPR.[T]	Brevican core protein	Q61361	[409-424]	1713.824
2.59	1.18	[E].DETSWTER.[G]	Chondroitin sulfate proteoglycan 5	Q71M36	[71-78]	1252.601
2.95	-0.92	[V].PARETGSAIEAEELVR.[S]	Chondroitin sulfate proteoglycan 5	Q71M36	[32-47]	1957.055
3.45	-1.44	[A].IEAEELVR.[S]	Chondroitin sulfate proteoglycan 5	Q71M36	[40-47]	1187.683
3.01	-1.52	[A].VPARETGSAIEAEELVR.[S]	Chondroitin sulfate proteoglycan 5	Q71M36	[31-47]	2056.124
4.38	1.80	[E].DALKETSSVKQR.[W]	CD99 antigen-like protein 2	Q8BIF0	[34-45]	2049.227
4.33	-1.08	[G].DTDGFNLEDALKETSSVKQR.[W]	CD99 antigen-like protein 2	Q8BIF0	[26-45]	2940.588
2.74	-1.38	[R].AGEEAADSPELPRDVVNVVFVDR.[S]	Ferredoxin-2, mitochondrial	Q9CPW2	[44-66]	2713.399
4.76	2.06	[S].DSYTPPDQDR.[V]	Hyaluronan and proteoglycan link protein 1	Q9QUP5	[21-30]	1422.67
4.04	1.13	[D].SYTPPDQDR.[V]	Hyaluronan and proteoglycan link protein 1	Q9QUP5	[22-30]	1307.643

Declaration of Authorship/Eidesstattliche Erklärung

I hereby declare that I have written this dissertation independently, exclusively based on the indicated tools and literature. Furthermore, I confirm that this thesis was generated according to the rules of good scientific praxis of the German Research Foundation. This document has not previously been and will not be submitted to any other institution than to the University of Kiel to receive an academic grade. Furthermore, no academic degree has been withdrawn from me.

Hiermit erkläre ich, dass die Abhandlung nach Inhalt und Form die eigene Arbeit ist und keine anderen als die angegebenen Quellen und Hilfsmittel verwendet wurden. Weiterhin versichere ich, dass diese Arbeit unter Einhaltung der Regeln guter wissenschaftlicher Praxis der Deutschen Forschungsgemeinschaft entstanden ist und noch nicht als Abschlussarbeit an anderer Stelle vorgelegen hat. Mir wurde des Weiteren kein akademischer Grad entzogen.

Kiel, 30.04.2021 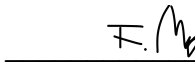

(Date/Datum) (Fred Armbrust)

Acknowledgments

Christoph Becker-Pauly möchte ich für die Möglichkeit danken, in seiner Arbeitsgruppe promovieren zu dürfen. Durch die optimale Mischung zwischen „mich als Betreuer in die richtige Richtung zu lenken“ und „mich eigenverantwortlich handeln zu lassen“ habe ich sehr viel gelernt und bin immer gerne zur Arbeit gekommen. Auch für die vielen lustigen Arbeitsgruppen-Aktionen nach Feierabend bin ich sehr dankbar.

Thomas Roeder danke ich herzlich für die Übernahme des Zweitgutachtens für diese Thesis.

Insbesondere Kira Bickenbach möchte ich für die mittlerweile fast dreijährige Zusammenarbeit danken. Sowohl die praktische Unterstützung, als auch die wissenschaftlichen Diskussionen haben mir sehr oft weitergeholfen.

Auch Anne Winkelmann und Marion Mengel danke ich für ihre Hilfe.

Des Weiteren danke ich allen ehemaligen und derzeitigen Mitgliedern der AG Becker-Pauly, insbesondere Saschi, Lui, Cynthi, Flo, Kriti, und Franka für das freundschaftliche Arbeitsklima, die nicht selbstverständliche Hilfsbereitschaft und viele produktive wissenschaftliche Diskussionen…und natürlich für den ganzen Spaß, den wir neben der Arbeit noch hatten.

Ferner möchte ich mich bei allen Mitgliedern des Biochemischen Institutes für ihre Hilfsbereitschaft bedanken, insbesondere Gamze, Petra, Jessi, Micha, Detlef und Christine.

Hermann Altmeppen danke ich für die Beratung und Durchführung der IHC-Färbungen.

Liana Marengo und Claus Pietrzik danke ich für ihre Unterstützung und die tolle Kooperation.

Tomas Koudelka und Andreas Tholey danke ich für die Durchführung der massenspektrometrischen Analysen.

Phipsi, Nico und Hauke möchte ich für die wertvollen Ratschläge danken.

Schließlich möchte ich auch meiner Familie, meinen Freundinnen und Freunden (insbesondere Anni für die Verpflegung) und Luzie für die Unterstützung in jeder Lebenslage danken.

Appendix

I. Abbreviations

ACE	angiotensin-converting enzyme
ACh	acetylcholine
ACN	acetonitrile
AD	Alzheimer's disease
ADAM	a disintegrin and metalloprotease
ADHD	attention-deficit/hyperactivity disorder
AICD	amyloid precursor protein intracellular domain
ANOVA	analysis of variance
APH-1	anterior pharynx-defective 1
ApoE	apolipoprotein E
APP	amyloid precursor protein
APPflo	Florida amyloid precursor protein
APPlon	London amyloid precursor protein
APPswe	Swedish amyloid precursor protein
APPwt	wild-type amyloid precursor protein
APS	ammonium persulphate
Aβ	amyloid-β
BACE1	β-site of APP cleaving enzyme
bafA1	bafilomycin A1
BMDM	bone-marrow derived macrohages
BSA	bovine serum albumin
CD	cluster of differentiation
CSF	cerebrospinal fluid
CTF	C-terminal fragment
cyto D	cytochalasin D
DAP12	DNAX-activation protein 12
DMEM	Dulbecco's Modified Eagle's Medium
DMSO	dimethyl sulfoxide
dnp	dinitrophenyl
EDTA	ethylenediaminetetraacetic acid
EGF	epidermal growth factor
ELAV	embryonic lethal abnormal vision
EOAD	early-onset Alzheimer's disease
FA	formic acid

FAD	familial Alzheimer’s disease
FDR	false discovery rate
FLRT	fibronectin leucine rich transmembrane protein
FTLD	frontotemporal labor degeneration
GAIN	G protein-coupled receptor autoproteolysis inducing
GFAP	glial fibrillary acidic protein
GPCR	G protein-coupled receptor
HSV-1	herpes simplex virus-1
IDE	insulin-degrading enzyme
IL-18	interleukin-18
IL-6R	interleukin-6 receptor
IQ	intelligence quotient
IVC	individually ventilated cage
KLK	kallikrein
LAH	long arm of homology
LBD	Lewy body dementia patient brains
LC-MS	liquid chromatography-mass spectrometry
LOAD	late-onset Alzheimer’s disease
LPHN	latrophilin
LPHN3-CTF	C-terminal fragment of latrophilin 3
LPHN3-NTF	N-terminal fragment of latrophilin 3
LPS	lipoplysaccharide
MAM	meprin A5 protein tyrosine phosphatase μ
mca	7-methyloxycoumarin-4-yl
MS	mass spectrometry
MT-2	matriptase-2
MUC2	mucin 2
N-APP	N-terminal amyloid precursor protein fragment
NFT	neurofibrillary tangle
NICD	notch intracellular domain
NMDA	N-methyl-D-aspartate
OBS	organotypic brain slice
P. gingivalis	*Porphyromonas gingivalis*
PBS	phosphate buffered saline
PEI	polyethylenimine
PEN-2	presinilin enhancer 2
PFA	paraformaldehyde

PKC	protein kinase C
PMA	phorbol 12-myristate 13-acetate
PS	presinilin
PSM	peptide-spectrum match
PVDF	polyvenylidene difluoride
RFU	Relative fluorescence units
RgpB	arginine-gingipain B
SAD	sporadic Alzheimer's disease
sADAM10	soluble a disintegrin and metalloprotease
SAH	short arm of homology
sAPP	souluble APP
SDS	sodium dodecyl sulphate
SEZ6	seizure 6
smeprin beta	soluble meprin beta
SNP	single-nucleotide polymorphism
SRE	serum response element
sTREM2	soluble triggering receptor expressed on myeloid cells 2
SUEL	sea urchin egg lectin
SYK	spleen tyrosin kinase
TAE	Tris-acetat-EDTA
TAILS	terminal amine isotopic labeling of substrates
TBS	tris-buffered saline
TCEP	tris(2-carboxyethyl)phosphine
TEMED	tetramethylethandiamin
TEN	teneurin
TFA	trifluoracetate
TFR	transferrin receptor
TGN	trans-Golgi network
TRAF	tumour-necrosis-factor-receptor-associated factor
TREM2	triggering receptor expressed on myeloid cells 2
WSS	Westphal stop cassette
WT	wild-type

II. Manuscripts

1. **Armbrust, F.**, Bickenbach, K., Kodelka, T., Tholey, A., Pietrzik, C.U., and Becker-Pauly, C. (2021). Phosphorylation of meprin β at the C-terminus controls its enzymatic activity at the cell surface. submitted

2. Marengo, L., **Armbrust, F.**, Schoenherr, C., Storck, S.E., Schmitt, U., Zampar, S., Wirths, O., Altmeppen, H., Glatzel, M., Weggen, S., Becker-Pauly, C., and Pietrzik, C.U. (2021). Meprin β knockout reduces brain Aβ levels and rescues learning and memory impairments in the APP/lon mouse model for Alzheimer's disease. submitted

3. Berner, D.K.*, Wessolowski, L.*, **Armbrust, F.**, Schneppenheim, J., Schlepckow, K., Koudelka, T., Scharfenberg, F., Lucius, R., Tholey, A., Kleinberger, G., Haass, C., Arnold, P., and Becker-Pauly, C. (2020). Meprin β cleaves TREM2 and controls its phagocytic activity on macrophages. Federation of American Societies for Experimental Biology 34, 6675-6687. doi: 10.1096/fj.201902183R
*These Authors contributed equally to this work.

4. **Armbrust, F.**, Colmorgen, C., Pietrzik, C.U., and Becker-Pauly, C. (2019). The Alzheimer's disease associated bacterial protease RgpB from P. gingivalis activates the alternative β-secretase meprin β thereby increasing Aβ generation. Pre-print-server: www.biorxiv.com. doi: 10.1101/748814

5. Scharfenberg, F., **Armbrust, F.**, Marengo, L., Pietrzik, C., and Becker-Pauly, C. (2019). Regulation of the alternative β-secretase meprin β by ADAM-mediated shedding. Cellular and molecular life sciences 76, 3193-3206. doi: 10.1007/s00018-019-03179-1

6. Peters, F., Scharfenberg, F., Colmorgen, C., **Armbrust, F.**, Wichert, R., Arnold, P., Potempa, B., Potempa, J., Pietrzik, C.U., Häsler, R., Rosenstiel, P., and Becker-Pauly, C. (2019). Tethering soluble meprin α in an enzyme complex to the cell surface affects IBD-associated genes. Federation of American Societies for Experimental Biology 33, 7490-7504. doi: 10.1096/fj.201802391R

Phosphorylation of meprin β at the C-terminus controls its enzymatic activity at the cell surface

Fred Armbrust[1], Kira Bickenbach[1], Tomas Koudelka[2], Andreas Tholey[2], Claus Pietrzik[3] and Christoph Becker-Pauly[1]

[1]Biochemical Institute, Unit for Degradomics of the Protease Web, University of Kiel, Kiel, Germany
[2]Systematic Proteomics & Bioanalytics, Institute for Experimental Medicine, University of Kiel, Kiel, Germany
[3]Institute for Pathobiochemistry, University Medical Center of the Johannes Gutenberg-University Mainz, Mainz, Germany

* Correspondence should be addressed to:
Prof. Dr. Christoph Becker-Pauly, Biochemical Institute, Unit for Degradomics of the Protease Web, University of Kiel, Otto-Hahn-Platz 9, 24118 Kiel, Germany, Tel: 0049-431-880 7118, Fax: 0049-431-880 2238, E-mail: cbeckerpauly@biochem.uni-kiel.de

Abstract

Meprin β is a zinc-dependent metalloprotease exhibiting a unique cleavage specificity with strong preference for acidic amino acids at the cleavage site. Proteomic studies revealed a diverse substrate pool of meprin β including the interleukin-6 receptor (IL-6R) and the amyloid precursor protein (APP). Dysregulation of meprin β is often associated with pathological conditions such as chronic inflammation, fibrosis or Alzheimer´s disease (AD). The extracellular regulation of meprin β including interactors, sheddases and activators has been intensively investigated while intracellular regulation has been barely addressed in the literature. This study aimed to analyze C-terminal phosphorylation of meprin β with regard to cell surface expression and proteolytic activity. By immunoprecipitation of endogenous meprin β from the colon cancer cell line Colo320 and subsequent LC-MS analysis, we identified several phosphorylation sites in its C-terminal region. Here, T694 in the C-terminus of meprin β was the most preferred residue after phorbol-12-myristate-13-acetate (PMA) stimulation. We further demonstrated the role of protein kinase C (PKC) isoforms for meprin β phosphorylation and identified the involvement of PKC-α and PKC-β. As a result of phosphorylation, the meprin β activity at the cell surface is reduced and, consequently, the extent of substrate cleavage is diminished. Our data indicate that this decrease of the surface activity is caused by the internalization and degradation of meprin β.

Introduction

The metalloprotease meprin β belongs to the astacin family of proteinases and is highly expressed in the kidney as well as the intestine (1). By cleaving mucin 2 (MUC2), which is a major component of the mucus layer in the intestine, meprin β contributes to physiological mucus detachment and bacterial defense (2, 3). Apart from its high abundance in the kidney and intestine, meprin β is also expressed in many other tissues such as the skin (4), lung (5) or brain (6). Of note, in many cases dysregulation of meprin β is associated with

pathological conditions. For instance, meprin β is described as collagen maturating enzyme, and plays a crucial role for the pathogenesis of skin and lung fibrosis due to erratic collagen fibril formation and deposition (7, 8). Furthermore, we and others demonstrated that meprin β is upregulated in Alzheimer´s disease (AD) patient brains (9, 10). As meprin β is capable of cleaving APP at the β-secretase site and thereby releasing neurotoxic Aβ peptides, a pathophysiological role for meprin β in AD is suggested (9–12). Apart from that, meprin β was identified as a sheddase of the interleukin-6 receptor (IL-6R), thereby releasing the soluble IL-6R (sIL-6R) ectodomain, which is capable of inducing pro-inflammatory trans-signaling (13).

Meprin β is regulated within a complex protease web (Fig. 1A). It is expressed as a zymogen and requires tryptic activation to get rid of the inhibitory propeptide. Matriptase-2 (MT-2), several human tissue related kallikreins (KLKs) and trypsin were identified as potent activators of meprin β (1, 12, 14, 15). We and others revealed ectodomain shedding of meprin β as a key regulatory event, mediated by a disintegrin and metalloproteinase 10 and 17 (ADAM10 and 17) (16, 17). Importantly, only the inactive pro-form of meprin β can be shed from the cell surface, whereas shedding of activated membrane bound meprin β is completely abolished (3, 14). Membrane-bound and shed meprin β differ in their substrate spectrum (3, 9, 13). Of note, only membrane-bound meprin β is capable of IL-6R shedding (13) and cleaving APP at the β-secretase cleavage site (9). Despite the identification of several extracellular regulators of meprin β activity, intracellular modifications are almost elusive. Therefore, we investigated meprin β phosphorylation as an intracellular regulatory event, which has only been addressed in one previous publication (18). In this study by Hahn *et al.*, the authors focused on the amino acid residues Ser687 and Ser688, which are located in the cytoplasmic tail of meprin β within a protein kinase C (PKC)-consensus sequence. Of note, phosphorylation of Ser687 but not Ser688 was observed upon stimulation with the PKC activator PMA (Fig. 1B). However, investigation of other potential phosphorylation sites and the biological consequence of meprin β phosphorylation were not addressed in that study. Therefore, we aimed to investigate meprin β phosphorylation in detail to reveal subsequent consequences for its cell surface localization and proteolytic activity.

Results

Meprin β is phosphorylated at multiple sites of its cytoplasmic part

In order to validate meprin β phosphorylation, we analyzed endogenously expressed meprin β in colon carcinoma-derived COLO320 and neuroblastoma-derived SH-SY5Y cells with or without PMA stimulation. In both cell lines, meprin β phosphorylation was detectable 10 min after PMA treatment with an antibody specific for phosphorylated serine residues (Fig. 1C). To additionally visualize protein phosphorylation on other sites, we employed a phosphate affinity electrophoresis. For this purpose, SDS gels were supplemented with the Phos-tag™ compound that interacts with phosphorylated proteins during electrophoresis resulting in a diminished migration velocity. As a result, phosphorylated species of one distinct protein appear as bands above the non-phosphorylated protein fraction (Fig. S1). Using phosphate affinity electrophoresis, we validated PMA-dependent meprin β phosphorylation in transient transfected HEK ADAM10/17$^{-/-}$ cells (Fig. 1D). Of note, ADAM10/17-deficient cells were used to avoid ectodomain shedding of meprin β and thus achieving a higher surface expression. Additionally, we cloned and biochemically analyzed meprin β variants with mutations at all potential phosphorylation sites in the cytoplasmic part. The eachAF variant contains alanine instead of serine and threonine or phenylalanine instead of tyrosine residues at each potential phosphorylation site to block

phosphorylation. For the eachE variant, we inserted glutamate at the potential phosphorylation sites in the cytoplasmic part in order to mimic constitutive phosphorylation, as glutamate residues contain a negative charge in similar distance to the peptide backbone compared to phosphorylated residues. Both variants served as negative controls for the phosphate affinity SDS-PAGE approach and did not show altered migration velocity. In addition, we analyzed the catalytically inactive meprin β variants E153A and R61S. Meprin β E153A is characterized by a mutation at the catalytic site that prevents hydrolysis of substrate peptide bonds, whereas meprin β R61S contains a mutation at the activation site preventing from propeptide cleavage by proteolytic activators. We observed no alteration in PMA-dependent phosphorylation for the meprin β E153A variant (Fig. 1E). However, phosphorylation of meprin β R61S was barely detectable indicating that mature meprin β is more prone to phosphorylation than the inactive zymogen. Next, we analyzed the meprin β variants S687R, S688A and S687R/S688A, which were previously characterized by Hahn *et al.* (18), using phosphate affinity electrophoresis. In contrast to the previous results showing phosphorylation only at S687, we observed hardly any differences in the amount of phosphorylation between the variants S687R, S688A and S687R/S688A and wild-type meprin β indicating that meprin β contains several phosphorylation sites in the cytoplasmic part (Fig. 1F).

In order to screen for potential C-terminal phosphorylation sites in meprin β with an unbiased approach, we conducted a LC-MS analysis. For this purpose, COLO320 cells were stimulated with PMA to obtain an insight into phosphorylation of endogenously expressed meprin β. Using cyanogen bromide (CNBr), which hydrolyse peptide bonds C-terminal to methionine, a C-terminal peptide of meprin β from S687 to F701, which contains three potential phosphorylation sites (S687, S688 and T694), was found to be mono-phosphorylated (Fig. 1G). The extracted ion chromatograph of the phosphopeptide revealed a mixture of monophosphorylated peptides with the dominant peak identified as the peptide phosphorylated at T694 and a minor double peak belonging to phosphorylation at S687/S688 (Fig. 1H and Fig. S2A and B). From the MS2 spectra it was not possible to determine, whether S687 or S688 were phosphorylated but due to a presence of a double peak, it is likely that both are phosphorylated to some extent. Digestion of meprin β from Colo320 cells with various enzymes confirmed that T694 was the dominant phosphorylated species. Additionally, PMA-dependent phosphorylation of meprin β from transfected HEK cells were also analyzed. Here, we identified a peptide containing all potential phosphorylation sites within the cytoplasmic tail of meprin β, which were not covered by the peptides identified from COLO320 cells (Fig. S3A). A peptide from L672 to L693 was identified as a monophosphorylated peptide species (Fig. S3B). A separate LC-MS run was performed utilizing an inclusion list to acquire a high number of MS2 spectra of the phosphopeptide. However, due to insufficient coverage of the respective b- and y-ion series, the phosphorylation site remained ambiguous with phosphorylation possible at Y682 and S687, though phosphorylation at S687 was more likely with 5 PSMs and 22 PSMs identified for Y682 and S687, respectively (Fig. S3C). Overall, these data provide evidence for multiple phosphorylation sites in the cytoplasmic region of meprin β.

PKC-α and PKC-β are involved in meprin β phosphorylation

PMA-dependent phosphorylation events suggest the involvement of PKCs. In order to analyze which PKC isoforms are responsible for meprin β phosphorylation, we transfected COLO320 cells with the PKC isoforms α, β, γ,

and ζ and observed increased serine phosphorylation of endogenously expressed meprin β, particularly for PKC-α or PKC-β (Fig. 2A). Additionally, we cotransfected ADAM10 and 17-deficient HEK cells with meprin β and the different PKC isoforms. With phosphate affinity electrophoresis, we observed high amounts of phosphorylated meprin β only when cells were transfected with PKC-α and PKC-β (Fig. 2B). The bands representing phosphorylated meprin β seem to occur as multiple bands supporting the LC-MS data that meprin β is phosphorylated at several sites in the cytoplasmic part. As a control, HEK ADAM10/17-/- cells were again co-transfected with meprin β and PKC-α or -β, respectively, but either treated with the pan-PKC inhibitor Gouml6983 before cell lysis or the cell lysate was treated with alkaline phosphatase (AP) (Fig. 2C). Of note, phosphorylated bands were completely abolished under these conditions and phosphorylation was only detected in samples of untreated cells. In order to validate that T694 is predominantly phosphorylated, HEK ADAM10/17-/- cells were co-transfected with PKC-α and -β as well as meprin β WT, T694A, and eachAF. As described before, in the meprin β variant each AF, all potential phosphorylation sites at the C-terminus are blocked by the substitution with an alanine or phenylalanine. Of note, using the phosphate affinity SDS-PAGE, there is hardly any phosphorylated species detected for the T694A variant indicating that T694 represents a major phosphorylation site (Fig. 2D).

Meprin β activity at the cell surface is decreased upon phosphorylation

In order to analyze the functional consequence of phosphorylation, we examined whether meprin β activity on the surface of COLO320 cells is altered upon phosphorylation. Of note, meprin β phosphorylation follows a typical protein phosphorylation curve with a maximum at 10 minutes after PMA application (Fig. S4). We analyzed the meprin β activity up to 120 min after PMA treatment using a well described fluorogenic peptide-based cleavage assay (Fig. 3A) (1). Interestingly, 60 minutes after PMA application the meprin β surface activity was significantly decreased (Fig. 3B). Of note, the meprin β sheddase ADAM17 is also activated by PMA-dependent phosphorylation. Therefore, the experiment was repeated applying the ADAM10/17 inhibitor GW to exclude that diminished cell surface activity of meprin β is caused by ectodomain shedding. However, despite the ADAM inhibition, meprin β activity was still significantly decreased at the cell surface upon PMA stimulation (Fig. 3C). This finding indicates diminished meprin β activity at the plasma membrane of COLO320 cells as a result of its phosphorylation. In order to validate this finding with respect to the individual phosphorylation sites, meprin β variants with substituted C-terminal serine, threonine and/or tyrosine residues were cloned and biochemically characterized. On the one hand, we established single amino acid exchanges to alanine or phenylalanine, respectively, to block meprin β phosphorylation. On the other hand, single residues were substituted by glutamate, since it contains a negative charge in similar distance to the backbone compared to phosphorylated residues. Therefore, these variants mimic constitutive phosphorylation of meprin β. In order to investigate the cumulative effect of all potential phosphorylation sites located in the cytoplasmic region of meprin β, we additionally analyzed variants, in which each potential phosphorylation site is substituted either by alanine or phenylalanine or glutamate. Activity measurements of transfected HEK cells revealed that meprin β variants carrying the S674A, Y676F, T678A or S687A mutation as well as the eachAF variant exhibited increased cell surface activity, whereas the substitutions S688A and T694A caused no alteration (Fig. 3D). On the contrary, the single mutations Y676E, S688E and T694 led to significantly diminished meprin β activity at the cell surface, whereas variants S674E, T678E, S687E were comparable to the

wild-type enzyme (Fig. 3E). Intriguingly, the cumulative effect of the single mutations, which is revealed by analyzing the eachE variant, caused a reduction of the meprin β activity at the cell surface by more than 70%. Conducting a protein-biotinylation assay, a comparable cell surface abundance of meprin β and the variants eachAF and eachE, representative for all the used mutants, could be demonstrated (Fig. 3F). Of note, the meprin β eachE variant showed a slightly different band pattern compared to wild-type meprin β. A PNGase F digestion revealed a different glycosylation pattern of the eachE variant (Fig. S5) that obviously does not seem to alter trafficking to the cell surface. Additionally, we confirmed similar cellular distribution of the meprin β variants eachAF and eachE employing immunofluorescence (IF) microscopy (Fig. S6). In sum, these data provide evidence that phosphorylation of meprin β results in decreased cell surface activity of the protease.

Decreased meprin activity at the cell surface leads to diminished substrate cleavage

Next, we investigated, whether the phosphorylation-induced decrease of meprin β activity at the cell surface is crucial for cleavage of its protein substrates. Therefore, we characterized phosphorylation-dependent processing of APP and IL-6R by meprin β. Since we could demonstrate by LC-MS analyzes and phosphate affinity electrophoresis that meprin β contains multiple phosphorylation sites and that the induced negative charge in the cytoplasmic region leads to strongly diminished activity at the cell surface, we decided to use the eachAF and eachE variant as proof of concept model to study substrate cleavage alterations with respect to phosphorylation. It has been shown that meprin β is involved in the generation of Aβ peptides by cleaving APP at the β-secretase site. Hence, meprin β competes with α-secretases for APP processing, which cleave within the Aβ sequence (Fig. 4A) (9, 11). Moreover, meprin β cleaves APP in its N-terminal region releasing non-toxic N-APP fragments (20). Analyzing APP processing in transfected HEK cells revealed that no altered cleavage pattern between wild-type meprin β and the eachAF variant (Fig. 4B). However, upon expression of the meprin β eachE variant we observed diminished N-APP20 levels as well as increased sAPPα levels compared to meprin β WT and the eachAF variant. Of note, $A\beta_{x-40}$ levels generated by the eachE variant were significantly decreased compared to meprin β WT and eachAF (Fig. 4C). Moreover, we aimed to address the cleavage of the IL-6R by meprin β (Fig. 4D). Western blot analyzes of IL-6R cleavage by the meprin β variants with mutated phosphorylation sites revealed effects similar to those observed for APP processing. While the eachAF variant showed no alterations in IL-6R cleavage compared to wild-type meprin β, the eachE variant caused diminished soluble IL-6R (sIl-6R) release (Fig. 4E). Of note, the band at 55 kDa represents the IL6-R ectodomain released by meprin β, whereas the upper band around 70 kDa represents ADAM17-mediated sIL-6R (21). Since APP and IL-6R processing by the meprin β eachE variant mimicking constitutive phosphorylation was decreased, these results support the hypothesis that diminished meprin β surface activity as a consequence of phosphorylation alters substrate cleavage.

Meprin β is internalized and degraded upon phosphorylation

After demonstrating that phosphorylation of meprin β leads to diminished proteolytic activity at the cell surface, we investigated possible molecular mechanism responsible for this effect: (1) increased ectodomain shedding of meprin β or its release via microvesicles (Fig. 5A); (2) diminished proteolytic activation of meprin β (Fig. 5B), or (3) internalization and degradation of meprin β (Fig. 5C). In order to test the first hypothesis, we transfected HEK cells with the meprin β variants eachAF and eachE, and applied PMA and/or ionomycin to

stimulate ADAM17- and/or ADAM10-mediated shedding, respectively. Of note, the meprin β variants eachAF and eachE are unresponsive to PMA, which under these conditions should only induce an ADAM17-specific effect. However, the eachE variant mimicking constitutive phosphorylation did not accumulate in the supernatant upon stimulation of ADAM activity (Fig. 5D). Accordingly, in the supernatants of cells transfected with the eachE variant no increased meprin β activity was detectable (Fig. S7). Moreover, we transfected ADAM10/17-deficient HEK cells with meprin β WT and the variants eachAF and eachE and measured cell surface activity that was strongly reduced for the eachE variant as observed in HEK293T wild-type cells (Fig. S8). Therefore, we conclude that ectodomain shedding of meprin β by ADAM10/17 is not altered by phosphorylation. Next, we investigated, whether phosphorylation may disturb proteolytic activation of meprin β (Fig. 5B). Co-immunoprecipitation experiments revealed that the interaction of meprin β and its activator MT-2 was not altered for the meprin β variants eachAF and eachE (Fig. 5E). Further, both meprin β variants could be activated by MT-2 to a similar extend (Fig. 5F). Thus, proteolytic activation of meprin β by MT-2 was not altered by phosphorylation. Finally, we investigated, whether meprin β is internalized and degraded upon phosphorylation. Therefore, transfected HEK cells were treated with the endocytosis inhibitor cytochalasin D (cytoD), the proteasome inhibitor MG132 and the inhibitor of lysosomal degradation bafilomycin A1 (bafA1) (Fig. 5C). Western Blot analyses showed that meprin β levels were not significantly affected by inhibitor-treatment (Fig. 5G). However, the meprin β eachE variant mimicking a constitutive phosphorylation tends to accumulate upon bafA1 and cytoD treatment. Since our experiments revealed that predominantly maturated meprin β is phosphorylated, we additionally analyzed meprin β activity at the cell surface. Of note, the surface activity of the eachE variant was significantly increased upon inhibition of endocytosis and lysosomal degradation (Fig. 5H). However, the applied inhibitors did not affect the surface activity of meprin β WT and eachAF. These results indicate that predominantly activated meprin β is internalized and degraded upon phosphorylation via the lysosomal pathway.

Discussion

Dysregulation of meprin β expression and proteolytic activity can be associated with pathological conditions, due to altered substrate cleavage (1, 8, 12). Therefore, studying the regulation of meprin β may help to reveal new therapeutic strategies. The extracellular regulation of meprin β activity has been studied in detail (1, 22). The most decisive posttranslational modifications of meprin β are its shedding from the cell surface by ADAM10/17 as zymogen and its proteolytic activation by tryptic enzymes (15, 16). However, the intracellular regulation of the membrane anchored meprin β is poorly understood. Based on findings by Hahn et al. (18) showing that Ser687 is phosphorylated in a PMA-dependent manner, we focused on further potential phosphorylation sites at the cytoplasmic part and the functional consequences of meprin β phosphorylation. In this study, we could verify meprin β phosphorylation with three distinct methods using phosphate affinity electrophoresis, Western Blot analyses with phospho-specific antibodies, and by LC-MS measurements. In contrast to Hahn et al., we detected T694A as the predominant phosphorylation site of meprin β. However, our experiments show that the C-terminus of meprin β contains several potential additional phosphorylation sites besides T694. Discrepancies between these studies may be due to different cell culture conditions and stimulation time points, but employment of latest available methods used herein are obviously much more sensitive to detect potential phosphorylation sites in

meprin β. Furthermore, we analyzed the involvement of certain PKC isotypes including PKC-α, PKC-β and PKC-γ as conventional PKCs as well as the atypical isoform PKC-ζ (23). Our data show that predominantly PKC-α and PKC-β play a role in meprin β phosphorylation. However, PKCs have a variety of substrates including other kinases (24, 25). Hence, it is still uncertain, if PKC-α and PKC-β directly phosphorylate meprin β, or if other kinases activated by PKCs subsequently modify the protease. Of note, using catalytically inactive meprin β variants, we observed that mature meprin β is more prone to phosphorylation than its zymogen. We further focused on the consequences of meprin β phosphorylation and detected decreased meprin β activity at the cell surface upon phosphorylation. This finding was observed employing a meprin β-specific fluorogenic peptide cleavage assay and characterizing the cleavage of the meprin β substrates APP and IL-6R. Therefore, our findings indicate that phosphorylation emerges as an intrinsic regulator of meprin β activity at the cell surface.

Using suitable inhibitors, we could show that a meprin β variant mimicking constitutive C-terminal phosphorylation is endocytosed and degraded in lysosomes. Therefore, our data indicate that phosphorylation of meprin β leads to its internalization and degradation. Endocytosis as a consequence of phosphorylation is well-described for many receptors (26–28). Furthermore, it is reported that phosphorylated and consequently internalized proteins can be ubiquitinated for proteasomal degradation (29, 30). This crosstalk between phosphorylation, ubiquitination and proteasomal degradation was e.g. observed for β-catenin (31). Besides proteasomal degradation, also phosphorylation-induced lysosomal degradation is reported, as we observed for meprin β. However, the exact regulation of this cellular pathway is so far unknown (32, 33).

As described above, meprin β is upregulated in diseases such as AD (9, 10) and fibrosis (7). Therefore, elevated meprin β activity is thought to promote the onset and progression of these diseases due to increased Aβ generation (12) and collagen fibril formation (8), respectively. Since we identified phosphorylation as a mechanism, which reduces the cell surface activity of meprin β, this might represent a target for therapeutic intervention. Accordingly, activators of PKC may serve as compounds to treat pathologies promoted by upregulated meprin β expression by counteracting elevated meprin β activity. With regard to AD, our data fit into a variety of publications demonstrating an AD protective role of PKC activity (33–36). For instance, PKC can activate gelosin which inhibits Aβ fibrillization (35, 36). Other targets of PKCs are the embryonic lethal abnormal vision-like RNA-binding proteins that regulate the stability and translation of mRNAs involved in synaptic remodeling connected to cognitive processes (37). Of note, PKC activators were shown to direct APP processing towards cleavage at the α-secretase site, located within the Aβ sequence, by modulating α-secretases and thereby reducing Aβ levels (38).

In conclusion, we identified multiple phosphorylation sites in the cytoplasmic region of meprin β modified by PKC-α and -β. As a consequence, phosphorylation leads to diminished enzymatic activity of meprin β at the cell surface (Fig. 6). Thus, substrate cleavage of meprin β at the cell surface is reduced upon phosphorylation, as demonstrated for APP and the IL-6R. Based on the characterization of a meprin β variant mimicking constitutive phosphorylation, we propose that phosphorylation of meprin β leads to its internalization and lysosomal degradation. Therefore, regulation of meprin β phosphorylation may provide new therapeutic options for the treatment of associated diseases.

Experimental procedures

Cell culture and transfection

HEK 293T, HEK ADAM10/17-/-, HeLa and COLO320 cells were maintained at 37°C under an atmosphere of 5% CO2 in Dulbecco´s modified Eagles´s medium (DMEM; Thermo Fisher Scientific) supplemented with 10% fetal bovine serum (FBS; Thermo Fisher Scientific), 100 units/ml penicillin and 100 µg/ml streptomycin (Thermo Fisher Scientific). Transfection was performed at 80-90% cell confluence. HEK and HeLa cells were transfected with plasmid-DNA, pre-mixed with polyethylenimine (PEI) (1:3) in serum-free medium and incubated for 30 min at room temperature. COLO320 were transfected with plasmid-DNA, pre-mixed with XtremeGene (Thermo Fisher Scientific) (1:3) in serum-free medium and incubated for 15 min at room temperature. Plasmid DNA with APP695, human meprin β variants (WT, eachAF, eachE, S674A, S674E, Y676F, Y676E, T678A, T678E, Y682F, S687A, S687R, S687E, S687R/S688A, S688A, S688E, T694A, T694E, E153A, R61S), PKC isoforms (α, β, γ, ζ), IL-6R, matriptase-2 (MT-2), and pcDNA3.1 as empty vector control in different combinations were added together with transfection reagent to the cell medium. After 24 h the cell medium was changed to serum-free DMEM.

Cell treatment and stimulation

Transfected cells were treated 48 after addition of the transfection pre-mix; untransfected cells were grown to 90% confluency before stimulation. Cells were stimulated for 10 to 120 min with 100 ng/ml PMA (Merck) and/or 1 µM ionomycin (Merck). In case of GW280264X (GW) (Merck) treatment, 3 µM GW were added 30 min prior PMA addition. In case of cell surface activity measurements, meprin β was activated with 5 µg/ml trypsin (Merck) for 30 min prior to PMA stimulation, when indicated in the respective figure caption. Selective samples were incubated with 20 nM of the pan-PKC inhibitor Gouml6983 (abcam) 2 h prior to cell lysis. The inhibitor treatment with 100 nM bafilomycin A1 (Merck), 15 µM MG132 (Merck) or 1 µM cytochalasin D (Merck) took place for 3 h.

Immunoprecipitation (IP)

Harvested cells were lysed in 450 µl IP lysis buffer (50 mM Tris-HCl pH 7,4, 120 mM NaCl, 0,5% (v/v) NP-40, cOmplete protease inhibitor cocktail (Roche)). 50 µl of the lysate were separated for bicinchoninic acid (BCA) assay (Thermo Fisher Scientific) and as lysate control for the SDS-PAGE. The remaining sample was incubated over night with 5 µg anti-meprin β antibody (polyclonal antibody, generated against the ectodomain (Pineda)) and 20 µl Protein G Agarose (Thermo Fisher Scientific). After washing the beads, the proteins were removed and denatured by addition of sample buffer (50 mM Tris/HCl (pH 6,8), 2% (w/v) SDS, 10% (v/v) glycerin, 0,1% (w/v) bromphenol blue, 20 mM dithiothreitol), for 10 min at 95 °C. The samples were analyzed by SDS-PAGE and Western Blot.

Immunofluorescence (IF)

For immunofluorescence analyses, transfected HeLa cells were incubated for 24 h and then washed with PBS. Afterwards, the cells were fixed with 4% (w/v) paraformaldehyde in PBS for 10 min at room temperature. For permeabilization, the cells were incubated with 0.12% (w/v) glycine and 0.2% (w/v) saponin in PBS for 10 min and subsequently blocked with blocking buffer (10% (v/v) FCS and 0.2% (w/v) saponin in PBS). A polyclonal antibody generated against the ectodomain of meprin β (Pineda) was applied 1:1000 in blocking buffer for 1 h. After washing with 0.2% (w/v) saponin in PBS, the Alexa Fluor 594-conjugated secondary antibody was applied (1:300 in blocking buffer; Thermo Scientific). The coverslips were washed again with 0.2% (w/v) saponin in PBS and then mounted onto slides with Mowiol/1,4-diazabicyclo(2.2.2)octane (DABCO; Sigma-Aldrich) solution (7% (w/v)

Mowiol, 33% (v/v) glycerol, and 50 mg/ml DABCO), including 1 µg/ml DAPI for nuclear staining. A Leica DMi8 inverted microscope was used to acquire images of the fluorescence-labeled cells. For the imaging of internalized meprin β, the primary antibody was applied during cell cultivation for 30 min. Afterwards, cells were washed and further cultivated for 3 h. The cells were subsequently fixed, permeabilized and incubated with the secondary antibody as described above.

Cell lysates, SDS-PAGE and Western Blot analysis

For SDS-PAGE and Western Blot analyses, harvested cells were washed with phosphate-buffered saline (PBS) and then 30 min at 4°C incubated in lysis buffer (cOmplete protease inhibitor cocktail (Roche), 1% (v/v) Triton X-100 in PBS (pH 7,4)). For each experiment, in which phosphorylation was analyzed, the phosphatase inhibitor cocktail PhosSTOP™ (Roche) was added. The lysate was centrifuged at 15.000 x g at 4°C and the cell debris was discarded. When highlighted in a figure, 10 U alkaline phosphatase (Thermo Fisher Scientific) was added to the cell lysate (without phosphatase inhibitor cocktail) for 1 h at 37°C. The protein concentration in the lysate was determined using the BCA protein assay kit (Thermo Fisher Scientific) according to manufacturer's instructions. As preparation for the SDS-PAGE the samples were incubated with sample buffer. The protein separation was performed by SDS-PAGE (120 V, 90 min) using the Lämmli conditions in the Mini-PROTEAN® system(Bio-Rad) or the Nu-Page system (Thermo Fisher Scientific). For phosphate affinity SDS-PAGE Phos-tag™ (Wako) and 10 µM ZnCl were added to Lämmli gels according to the manufacturer's instructions. The Western blot was accomplished with a Tank-Blot system (Bio-Rad) onto PVDF membranes (0.8 A, 2 h, 4°C). Afterwards, the membranes were blocked with 3% (w/v) BSA in Tris-buffered saline (TBS) or 5% milk (w/v) in TBS for 1 h at room temperature. The primary antibodies against meprin β (polyclonal antibody, generated against peptide from the ectodomain (Pineda)), myc-tag (2276C, Cell Signaling), HA-tag (C29F4, Cell Signaling), pSer (ab1603, Merck), APP (N-APP, Thermo Fisher Scientific), APP (6E10, Biolegend), APP (22C11, eBioscience), hIL6-R (4-11, AG Rose-John, Kiel; described previously (19)) transferrin receptor (ab84036, abcam), GAPDH (14C10, Cell Signaling) were incubated using a dilution of 1:1000 with the membrane over night at 4°C. Horseradish peroxidase-conjugated secondary antibodies (Thermo Fisher Scientific) were diluted in TBS-T (TBS with 0.1% (v/v) Tween20) and incubated with the membranes for 1 h at room temperature. The chemoluminescence signal was detected in the Intelligent Dark Box (Fujifilm) using the Super Signal® West Pico/Femto Kit (Thermo Fisher Scientific) according to manufacturer's instructions.

Sample preparation for mass spectrometry (MS) analysis

For the MS analysis, COLO320 cells and HEK cells transfected with meprin β WT were lysed and meprin β was immunoprecipitated. Afterwards, the immunoprecipitated meprin β was analyzed using SDS-PAGE and subsequent Coomassie staining. The gel bands were excised and destained with 100 mM ammonium bicarbonate (ABC), 30% acetonitrile (ACN), 50 mM ABC and 100% ACN, respectively. Samples were reduced with dithiotheritol (10 mM) at 56°C for 30 min and then alkylated with iodoacetamide (55 mM final) in the dark at room temperature for 30 min. Gel bands were washed with 50 mM ABC in 30% ACN. Samples were dehydrated with ACN and dried by vacuum centrifugation. Gel bands were incubated with 50 ng pepsin, 6mM cyanogen bromide (CNBR) or 50 ng trypsin in triethylammonium bicarbonate (TEAB) buffer overnight. For pepsin, the digestion was performed at low pH (≈pH2) using 0.1% trifluoroacetic acid (TFA) at 37°C. For CNBR

digestions, gel bands were incubated with 6 mM of CNBR in 70% TFA and incubate at 20 °C. Peptides were extracted from the gel band using 1% formic acid (FA), 50% ACN, 1% FA and 100% ACN with the aid of sonication, respectively. Pooled supernatants were dried down by vacuum centrifugation. For CNBR, samples were diluted 5 fold in water, prior to peptide extraction (as above) and the pooled supernatant lypholized. For TiO2 enrichment, immunoprecipitated samples were made up to 1% SDS in ABC buffer, reduced and alkylated as above and precipitated onto Speedbead Magnetic Carboxylate modified beads (bead:protein, 10:1, GE healthcare) by adding ethanol up to a final concentration of 80%. The sample was incubated with the beads for 20 min to initiate binding and then washed twice with 80% ethanol. The beads were resuspended in TEAB buffer at a protein concentration of 1 mg/mL and then digested with chymotrypsin or elastase (40:1). For chymotrypsin digestion the buffer was supplemented with 0.5 mM $CaCl_2$. Peptides were removed from the SP3 beads with the aid of a magnet. Samples were dried by vacuum centrifugation and resuspended in 3% ACN and 0.1% TFA. The sample was enriched with 10:1 (TiO2 beads: protein).

LC-MS analysis

The samples were suspended in loading buffer (3% ACN, 0.1% TFA) and a fraction injected on a Dionex Ultimate 3000 nano-UHPLC coupled to a Q Exactive plus mass spectrometer (Thermo Scientific, Bremen). The samples were washed on a trap column (Acclaim Pepmap 100 C-18, 5 mm × 300 µm, 5 µm, 100 Å, Dionex) for 4 min with 3% ACN/0.1% TFA at a flow rate of 30 µl/min prior to peptide separation using an Acclaim PepMap 100 C-18 analytical column (50 cm × 75 µm, 2 µm, 100 Å, Dionex). A flow rate of 300 nL/min using eluent A (0.05% FA) and eluent B (80% ACN/0.04% FA) was used for gradient separation (5-40% B). Spray voltage applied on a metal-coated PicoTip emitter (10 µm tip size, New Objective, Woburn, Massachusetts, US) was 1.6-1.7 kV, with a source temperature of 250°C. Full scan MS spectra were acquired between 300 and 1,800 m/z at a resolution of 70,000 at m/z 200. The ten most intense precursors with charge states greater than 2+ were selected for fragmentation by HCD with normalized collision energies (NCE) of 27 at a resolution of 17,500. Lock mass (445.120025) and dynamic exclusion (15-30 seconds) were enabled. A separate run with an inclusion list containing the m/z of the phosphopeptide was also performed, here, dynamic exclusion was not utilized.

Database Search and Statistics of the MS results

The MS raw files were processed by Proteome Discoverer 2.2 and MS/MS spectra were searched using the Sequest HT algorithm against a database containing common contaminants and the canonical and reviewed human database. Oxidation (+15.995 Da) of methionine residues and phosphorylation of serine, threonine and tyrosine residues (+79.966 Da) was set as a dynamic modification while carbamidomethylation (+57.021 Da) of cysteine residues was set as a static modification. In addition, several dynamic protein terminal modifications were allowed: acetylation (+42.011 Da), Met-loss (-131.040 Da), and Met-loss + acetyl (-89.030 Da). Minimal peptide length was set to 6 amino acids and the peptide false discovery rate (FDR) was set to 1% at the peptide and protein level. For trypsin digestion up to two missed cleavages were allowed. For CNBR up to 2 missed cleavages were allowed; for pepsin and elastase no enzyme search was utilized. For chymotrypsin up to 5 missed cleavages were allowed.

Cell surface biotinylation assay

Harvested cells for the cell surface biotinylation assay were washed with PBS-CM (0.1 mM $CaCl_2$, 1 mM $MgCl_2$ in PBS) and incubated with biotin solution (1 mg/ml Sulfo-NHS-SS-Biotin (Thermo Fisher Scientific)) in

PBS-CM. Subsequently, cells were incubated with quenching buffer (50 mM Tris-HCl, pH 8.0 in PBS-CM) for 10 min. Afterwards, cells were lysed in 450 µl biotinylation lysis buffer (50 mM Tris-HCl (pH 7.4), 150 mM NaCl, 1% (v/v) Triton-X 100, 0.1% (w/v) SDS, complete protease inhibitor cocktail (Roche)) for 30 min. 50 µl were separated as a lysate control. Streptavidin agarose resin beads (Thermo Fisher Scientific) were added to the remaining lysate and incubated for 1 h. Afterwards, the beads were washed with biotinylation lysis buffer and the proteins were removed and denaturated by addition of sample buffer for 10 min at 95°C. The samples were analyzed by SDS-PAGE and Western Blot.

PNGase F digestion

PNGase F digestion was performed with PNGase F Digestion Kit (Thermo Fisher Scientific) according to the manufacturer's instructions. 10 µg lysate was used for deglycosylation and analyzed with SDS-PAGE and Western-Blot.

Fluorogenic peptide based activity assay

The activity of meprin β at the cell surface or in the supernatant was measured with a well-established highly specific quenched fluorogenic peptide substrate ((mca)-EDEDED-(K-e-dnp); mca: 7-methyloxycoumarin-4-yl, dnp: dinitrophenyl) (1). For cell surface activity measurements, 5 x 10^6 cells were transferred into 48-well plates in a total volume of 300 µl PBS. To analyze the activity in the supernatant adjusted amounts of supernatants were transferred in 96-well plates in a total volume of 100 µl serum-free DMEM. As controls, PBS or serum-free DMEM only were used. Supernatants were pre-incubated 30 min with 10 µg/ml trypsin to activate meprin β. Immediately before the measurement, 50 µM quenched fluorogenic peptide substrate was added. The measurement was performed at 37°C for 2 h, thereby each 30 s the fluorescence at λ_{ex} = 320 nm and λ_{em} = 405 nm was monitored. The bar graphs display the slope of the linear gain of fluorescence within the first 30 minutes. Relative fluorescent units (RFUs) were normalized to the control samples.

Aβ enzyme-linked immunosorbent assay (ELISA)

$A\beta_{x-40}$ ELISA was performed with LEGEND MAX™ β-Amyloid x-40 ELISA Kit with pre-coated plate (Biolegend) according to manufacturer's instructions. Cell supernatants were diluted 1:100 in incubation buffer.

Statistical analysis

All statistical analyses were performed with GraphPad Prism using one- or two-way ANOVA followed by a Tukey's test (*$p < 0.05$, **$p < 0.01$, ***$p < 0.001$, ****$p<0.0001$). Values were normalized and are shown as mean ± SD.

Acknowledgements

The authors thank Dirk Schmidt-Arras (Biochemical Institute, Kiel) for providing the PKC subunits containing vectors.

Author contribution

FA designed and performed experiments, analyzed data and wrote the manuscript. KB carried out experiments. TK and AT conducted and analyzed the MS experiments. CP provided material and edited the manuscript. CBP conceived and supervised the project and edited the manuscript.

Funding

This work was supported by the Deutsche Forschungsgemeinschaft (DFG) Project-number 125440785 SFB 877 (Proteolysis as a Regulatory Event in Pathophysiology, Projects A9 (to C.B.-P.), A15 (to C.B.-P. and C.U.P.) and Z2 (to T.K and A.T.), and by the Alzheimer Forschungsinitiative e.V. (AFI) project 18007 (to C.B.-P. and C.U.P.).

References

1. Broder, C. and Becker-Pauly, C. (2013) The metalloproteases meprin α and meprin β. Unique enzymes in inflammation, neurodegeneration, cancer and fibrosis. *The Biochemical journal* **450**, 253–264.
2. Schütte, A., Ermund, A., Becker-Pauly, C., Johansson, M. E. V., Rodriguez-Pineiro, A. M., Bäckhed, F., Müller, S., Lottaz, D., Bond, J. S., and Hansson, G. C. (2014) Microbial-induced meprin β cleavage in MUC2 mucin and a functional CFTR channel are required to release anchored small intestinal mucus. *Proceedings of the National Academy of Sciences of the United States of America* **111**, 12396–12401.
3. Wichert, R., Ermund, A., Schmidt, S., Schweinlin, M., Ksiazek, M., Arnold, P., Knittler, K., Wilkens, F., Potempa, B., Rabe, B., Stirnberg, M., Lucius, R., Bartsch, J. W., Nikolaus, S., Falk-Paulsen, M., Rosenstiel, P., Metzger, M., Rose-John, S., Potempa, J., Hansson, G. C., Dempsey, P. J., and Becker-Pauly, C. (2017) Mucus Detachment by Host Metalloprotease Meprin β Requires Shedding of Its Inactive Pro-form, which Is Abrogated by the Pathogenic Protease RgpB. *Cell reports* **21**, 2090–2103.
4. Becker-Pauly, C., Höwel, M., Walker, T., Vlad, A., Aufenvenne, K., Oji, V., Lottaz, D., Sterchi, E. E., Debela, M., Magdolen, V., Traupe, H., and Stöcker, W. (2007) The alpha and β subunits of the metalloprotease meprin are expressed in separate layers of human epidermis, revealing different functions in keratinocyte proliferation and differentiation. *The Journal of investigative dermatology* **127**, 1115–1125.
5. Biasin, V., Wygrecka, M., Marsh, L. M., Becker-Pauly, C., Brcic, L., Ghanim, B., Klepetko, W., Olschewski, A., and Kwapiszewska, G. (2017) Meprin β contributes to collagen deposition in lung fibrosis. *Scientific reports* **7**, 39969.
6. Sterchi, E. E., Stöcker, W., and Bond, J. S. (2008) Meprins, membrane-bound and secreted astacin metalloproteinases. *Molecular aspects of medicine* **29**, 309–328.
7. Kronenberg, D., Bruns, B. C., Moali, C., Vadon-Le Goff, S., Sterchi, E. E., Traupe, H., Böhm, M., Hulmes, D. J. S., Stöcker, W., and Becker-Pauly, C. (2010) Processing of procollagen III by meprins. New players in extracellular matrix assembly? *The Journal of investigative dermatology* **130**, 2727–2735.
8. Prox, J., Arnold, P., and Becker-Pauly, C. (2015) Meprin α and meprin β. Procollagen proteinases in health and disease. *Matrix biology : journal of the International Society for Matrix Biology* **44-46**, 7–13.
9. Bien, J., Jefferson, T., Causevic, M., Jumpertz, T., Munter, L., Multhaup, G., Weggen, S., Becker-Pauly, C., and Pietrzik, C. U. (2012) The metalloprotease meprin β generates amino terminal-truncated amyloid β peptide species. *The Journal of biological chemistry* **287**, 33304–33313.
10. Schlenzig, D., Cynis, H., Hartlage-Rübsamen, M., Zeitschel, U., Menge, K., Fothe, A., Ramsbeck, D., Spahn, C., Wermann, M., Roßner, S., Buchholz, M., Schilling, S., and Demuth, H.-U. (2018) Dipeptidyl-Peptidase Activity of Meprin β Links N-truncation of Aβ with Glutaminyl Cyclase-Catalyzed pGlu-Aβ Formation. *Journal of Alzheimer's disease : JAD* **66**, 359–375.
11. Schönherr, C., Bien, J., Isbert, S., Wichert, R., Prox, J., Altmeppen, H., Kumar, S., Walter, J., Lichtenthaler, S. F., Weggen, S., Glatzel, M., Becker-Pauly, C., and Pietrzik, C. U. (2016) Generation of aggregation prone N-terminally truncated amyloid β peptides by meprin β depends on the sequence specificity at the cleavage site. *Molecular neurodegeneration* **11**, 19. https://molecularneurodegeneration.biomedcentral.com/track/pdf/10.1186/s13024-016-0084-5.
12. Becker-Pauly, C. and Pietrzik, C. U. (2016) The Metalloprotease Meprin β Is an Alternative β-Secretase of APP. *Frontiers in molecular neuroscience* **9**, 159.
13. Arnold, P., Boll, I., Rothaug, M., Schumacher, N., Schmidt, F., Wichert, R., Schneppenheim, J., Lokau, J., Pickhinke, U., Koudelka, T., Tholey, A., Rabe, B., Scheller, J., Lucius, R., Garbers, C., Rose-John, S., and Becker-Pauly, C. (2017) Meprin Metalloproteases Generate Biologically Active Soluble Interleukin-6 Receptor to Induce Trans-Signaling. *Scientific reports* **7**, 44053.

14. Ohler, A., Debela, M., Wagner, S., Magdolen, V., and Becker-Pauly, C. (2010) Analyzing the protease web in skin. Meprin metalloproteases are activated specifically by KLK4, 5 and 8 vice versa leading to processing of proKLK7 thereby triggering its activation. *Biological chemistry* **391**, 455–460.
15. Jäckle, F., Schmidt, F., Wichert, R., Arnold, P., Prox, J., Mangold, M., Ohler, A., Pietrzik, C. U., Koudelka, T., Tholey, A., Gütschow, M., Stirnberg, M., and Becker-Pauly, C. (2015) Metalloprotease meprin β is activated by transmembrane serine protease matriptase-2 at the cell surface thereby enhancing APP shedding. *The Biochemical journal* **470**, 91–103.
16. Herzog, C., Haun, R. S., Ludwig, A., Shah, S. V., and Kaushal, G. P. (2014) ADAM10 is the major sheddase responsible for the release of membrane-associated meprin A. *The Journal of biological chemistry* **289**, 13308–13322.
17. Jefferson, T., dem Keller, U. auf, Bellac, C., Metz, V. V., Broder, C., Hedrich, J., Ohler, A., Maier, W., Magdolen, V., Sterchi, E., Bond, J. S., Jayakumar, A., Traupe, H., Chalaris, A., Rose-John, S., Pietrzik, C. U., Postina, R., Overall, C. M., and Becker-Pauly, C. (2013) The substrate degradome of meprin metalloproteases reveals an unexpected proteolytic link between meprin β and ADAM10. *Cellular and molecular life sciences : CMLS* **70**, 309–333.
18. Hahn, D., Pischitzis, A., Roesmann, S., Hansen, M. K., Leuenberger, B., Luginbuehl, U., and Sterchi, E. E. (2003) Phorbol 12-myristate 13-acetate-induced ectodomain shedding and phosphorylation of the human meprinβ metalloprotease. *The Journal of biological chemistry* **278**, 42829–42839.
19. Chalaris, A., Rabe, B., Paliga, K., Lange, H., Laskay, T., Fielding, C. A., Jones, S. A., Rose-John, S., and Scheller, J. (2007) Apoptosis is a natural stimulus of IL6R shedding and contributes to the proinflammatory trans-signaling function of neutrophils. *Blood* **110**, 1748–1755.
20. Jefferson, T., Čaušević, M., dem Keller, U. auf, Schilling, O., Isbert, S., Geyer, R., Maier, W., Tschickardt, S., Jumpertz, T., Weggen, S., Bond, J. S., Overall, C. M., Pietrzik, C. U., and Becker-Pauly, C. (2011) Metalloprotease meprin β generates nontoxic N-terminal amyloid precursor protein fragments in vivo. *The Journal of biological chemistry* **286**, 27741–27750.
21. Sammel, M., Peters, F., Lokau, J., Scharfenberg, F., Werny, L., Linder, S., Garbers, C., Rose-John, S., and Becker-Pauly, C. (2019) Differences in Shedding of the Interleukin-11 Receptor by the Proteases ADAM9, ADAM10, ADAM17, Meprin α, Meprin β and MT1-MMP. *International journal of molecular sciences* **20**.
22. Scharfenberg, F., Armbrust, F., Marengo, L., Pietrzik, C., and Becker-Pauly, C. (2019) Regulation of the alternative β-secretase meprin β by ADAM-mediated shedding. *Cellular and molecular life sciences : CMLS* **76**, 3193–3206.
23. Webb, B. L., Hirst, S. J., and Giembycz, M. A. (2000) Protein kinase C isoenzymes. A review of their structure, regulation and role in regulating airways smooth muscle tone and mitogenesis. *British journal of pharmacology* **130**, 1433–1452.
24. Tatin, F., Varon, C., Génot, E., and Moreau, V. (2006) A signalling cascade involving PKC, Src and Cdc42 regulates podosome assembly in cultured endothelial cells in response to phorbol ester. *Journal of cell science* **119**, 769–781. https://jcs.biologists.org/content/joces/119/4/769.full.pdf.
25. Amin, A. R. M. R., Ichigotani, Y., Oo, M. L., Biswas, M. H. U., Yuan, H., Huang, P., Mon, N. N., and Hamaguchi, M. (2003) The PLC-PKC cascade is required for IL-1β-dependent Erk and Akt activation. Their role in proliferation. *International journal of oncology* **23**, 1727–1731.
26. Filippova, N., Dudley, R., and Weiss, D. S. (1999) Evidence for phosphorylation-dependent internalization of recombinant human rho1 GABAC receptors. *The Journal of physiology* **518 (Pt 2)**, 385–399.
27. Bian, J., Zhang, S., Yi, M., Yue, M., and Liu, H. (2018) The mechanisms behind decreased internalization of angiotensin II type 1 receptor. *Vascular Pharmacology* **103-105**, 1–7.
28. Sergé, A., Keijzer, S. d., van Hemert, F., Hickman, M. R., Hereld, D., Spaink, H. P., Schmidt, T., and Snaar-Jagalska, B. E. (2011) Quantification of GPCR internalization by single-molecule microscopy in living cells. *Integr. Biol.* **3**, 675–683. https://pubs.rsc.org/en/content/articlepdf/2011/ib/c0ib00121j.

29. Varedi K., S. M., Ventura, A. C., Merajver, S. D., and Lin, X. N. (2010) Multisite Phosphorylation Provides an Effective and Flexible Mechanism for Switch-Like Protein Degradation. *PLoS ONE* **5**, e14029.
30. Skowyra, D., Craig, K. L., Tyers, M., Elledge, S. J., and Harper, J. W. (1997) F-box proteins are receptors that recruit phosphorylated substrates to the SCF ubiquitin-ligase complex. *Cell* **91**, 209–219.
31. Liu, C., Li, Y., Semenov, M., Han, C., Baeg, G. H., Tan, Y., Zhang, Z., Lin, X., and He, X. (2002) Control of β-catenin phosphorylation/degradation by a dual-kinase mechanism. *Cell* **108**, 837–847.
32. Zemoura, K., Balakrishnan, K., Grampp, T., and Benke, D. (2019) Ca2+/Calmodulin-Dependent Protein Kinase II (CaMKII) β-Dependent Phosphorylation of GABAB1 Triggers Lysosomal Degradation of GABAB Receptors via Mind Bomb-2 (MIB2)-Mediated Lys-63-Linked Ubiquitination. *Molecular neurobiology* **56**, 1293–1309.
33. Thompson, L. M., Aiken, C. T., Kaltenbach, L. S., Agrawal, N., Illes, K., Khoshnan, A., Martinez-Vincente, M., Arrasate, M., O'Rourke, J. G., Khashwji, H., Lukacsovich, T., Zhu, Y.-Z., Lau, A. L., Massey, A., Hayden, M. R., Zeitlin, S. O., Finkbeiner, S., Green, K. N., LaFerla, F. M., Bates, G., Huang, L., Patterson, P. H., Lo, D. C., Cuervo, A. M., Marsh, J. L., and Steffan, J. S. (2009) IKK phosphorylates Huntingtin and targets it for degradation by the proteasome and lysosome. *The Journal of cell biology* **187**, 1083–1099.
34. Etcheberrigaray, R., Tan, M., Dewachter, I., Kuipéri, C., van der Auwera, I., Wera, S., Qiao, L., Bank, B., Nelson, T. J., Kozikowski, A. P., van Leuven, F., and Alkon, D. L. (2004) Therapeutic effects of PKC activators in Alzheimer's disease transgenic mice. *Proceedings of the National Academy of Sciences of the United States of America* **101**, 11141–11146.
35. Ji, L., Chauhan, A., and Chauhan, V. (2010) Upregulation of cytoplasmic gelsolin, an amyloid-β-binding protein, under oxidative stress conditions. Involvement of protein kinase C. *Journal of Alzheimer's disease : JAD* **19**, 829–838.
36. Choi, D.-S., Wang, D., Yu, G.-Q., Zhu, G., Kharazia, V. N., Paredes, J. P., Chang, W. S., Deitchman, J. K., Mucke, L., and Messing, R. O. (2006) PKCepsilon increases endothelin converting enzyme activity and reduces amyloid plaque pathology in transgenic mice. *Proceedings of the National Academy of Sciences of the United States of America* **103**, 8215–8220.
37. Talman, V., Pascale, A., Jäntti, M., Amadio, M., and Tuominen, R. K. (2016) Protein Kinase C Activation as a Potential Therapeutic Strategy in Alzheimer's Disease. Is there a Role for Embryonic Lethal Abnormal Vision-like Proteins? *Basic & clinical pharmacology & toxicology* **119**, 149–160.
38. Kuhn, P.-H., Wang, H., Dislich, B., Colombo, A., Zeitschel, U., Ellwart, J. W., Kremmer, E., Rossner, S., and Lichtenthaler, S. F. (2010) ADAM10 is the physiologically relevant, constitutive alpha-secretase of the amyloid precursor protein in primary neurons. *The EMBO journal* **29**, 3020–3032.

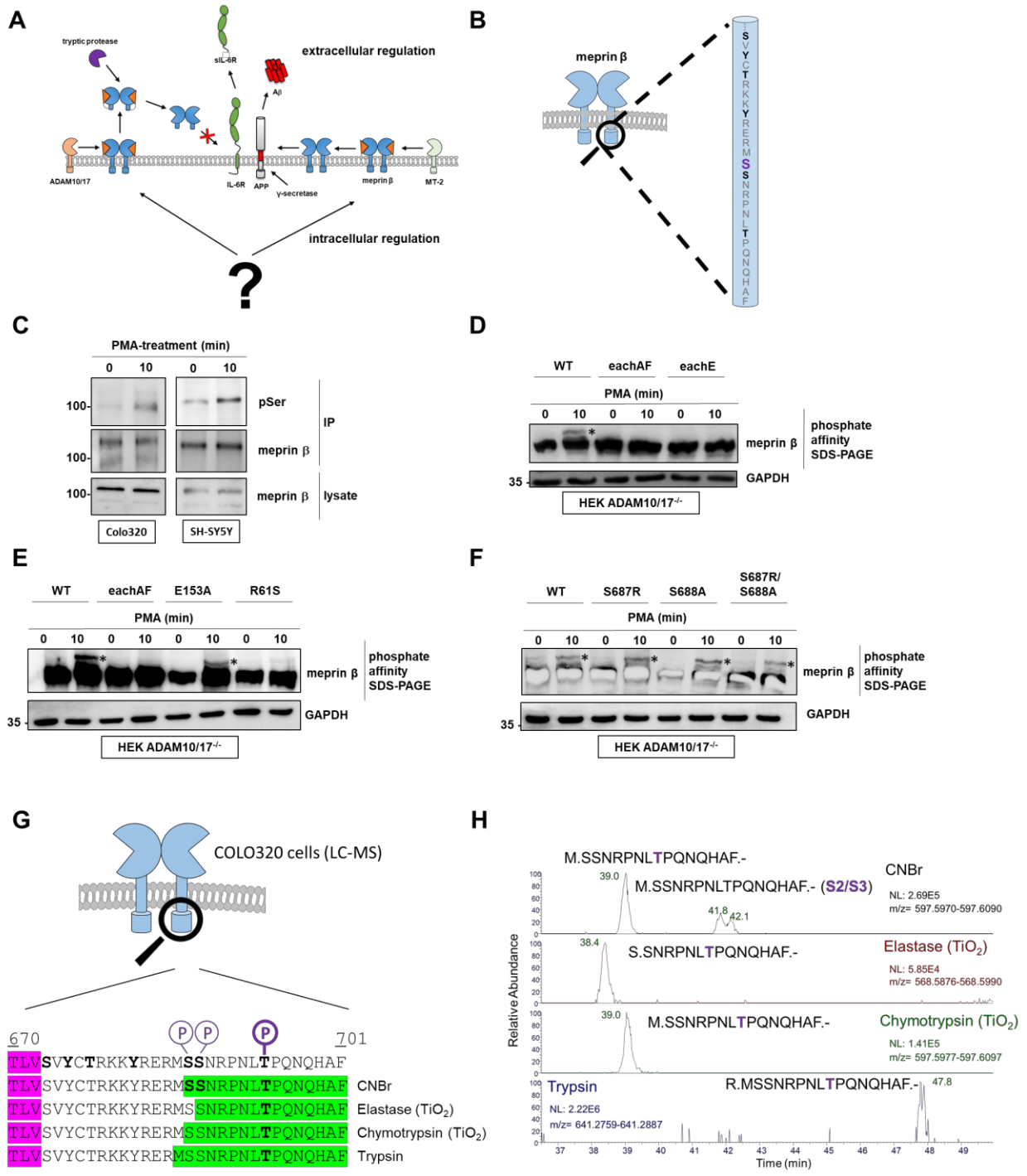

Figure 1: Meprin β is multi-phosphorylated at its cytoplasmic part in a PMA-dependent manner. (A) Meprin β is expressed as zymogen at the cell surface. A disintegrin and metalloprotease 10 and 17 (ADAM10/17) act as sheddases of pro-meprin β. Shed meprin β can be activated by tryptic proteases. Of note, as soluble protease, meprin β is not capable of cleaving IL6-R and APP at the β-secretase site. Alternatively, inactive membrane-bound meprin β can be maturated by the serine protease matriptase-2 (MT-2). Once activated at the cell surface, membrane-bound meprin β cannot be shed any more and cleaves its substrates such as APP at β-secretase site and thereby contributing to the generation of amyloid-β (Aβ). Moreover, IL6-R is only shed by membrane-bound meprin β. As a result, soluble IL6-R (sIL6-R) is released. (B) The

amino acid sequence of the meprin β C-terminus is displayed. Potential phosphorylation sites are highlighted in back, the previously identified phosphorylation site S687 (according to (18)) is labeled in purple. (C) COLO320 and SH-SY5Y cells were treated with 100 ng/ml PMA for 10 min. After cell lysis, meprin β was immunoprecipitated and analyzed by SDS-PAGE and Western Blot. (D) ADAM10/17-deficient HEK cells were transfected with meprin β WT, eachAF or eachE and treated with 100 ng/ml PMA for 10 min. After cell lysis, the samples were analyzed by phosphate affinity electrophoresis and Western Blot. (E) ADAM10/17-deficient HEK cells were transfected with meprin β WT, eachAF, E153A or R61S and treated with 100 ng/ml PMA for 10 min. After cell lysis, the samples were analyzed by phosphate affinity electrophoresis and Western Blot. (F) ADAM10/17-deficient HEK cells were transfected with meprin β WT, S687R, S688A or S687R/S688A and treated with 100 ng/ml PMA for 10 min. After cell lysis, the samples were analyzed by phosphate affinity electrophoresis and Western Blot. (G) LC-MS analysis of meprin ß from COLO320 cells stimulated with PMA. The scheme shows the sequence coverage of the C-terminus of meprin β with identified phosphopeptides highlighted in green. The TMD is highlighted in pink. Identified phosphorylation sites are highlighted in purple. T694A was identified as the predominant phosphorylation site. (H) Extracted ion chromatograph of the different phosphopeptides identified in the CNBr, elastase, chymotrypsin and trypsin digestions, respectively, of meprin β from COLO320 cells. For CNBr, several mono-phosphorylated peptides were identified, with the main peak originating from the peptide carrying the main phosphorylation site at T694, and two minor peaks of peptides modified at serine residues 687/688, respectively.

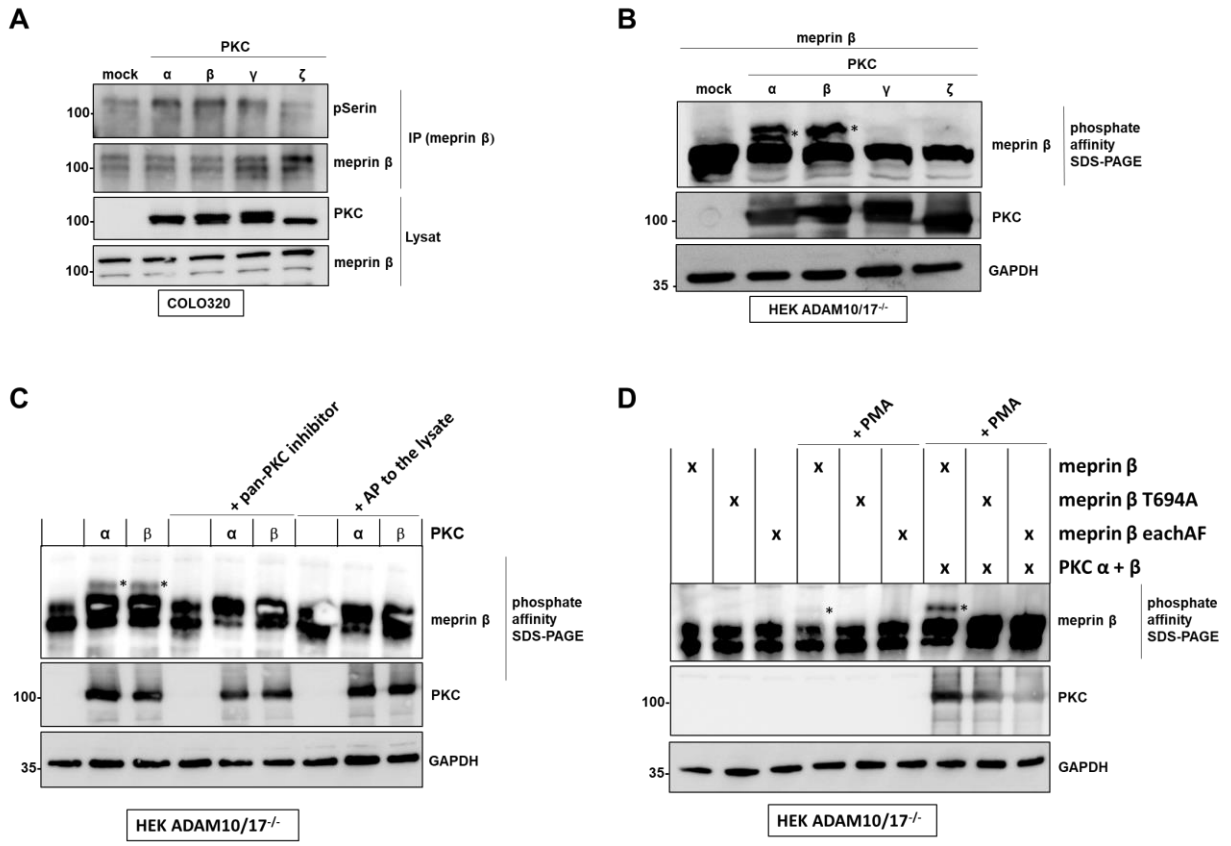

Figure 2: PKC-α and PKC-β are involved in meprin β phosphorylation. (A) COLO320 cells were transfected with the HA-tagged PKC isoforms α, β, γ, and ζ. After cell lysis, meprin β was immunoprecipitated and analyzed by SDS-PAGE and Western Blot. (B) ADAM10/17-deficient HEK cells were transfected with meprin β WT and the HA-tagged PKC isoforms α, β, γ, and ζ. After cell lysis, the samples were analyzed by phosphate affinity electrophoresis and Western Blot. (C) ADAM10/17-deficient HEK cells were transfected with meprin β WT and the HA-tagged PKC isoforms α and β. Either the cells were treated with 20 nM of the pan-PKC inhibitor Gouml6983 2 h prior to the cell lysis, or 10 U alkaline phosphatase (AP) was added to the lysate for 1 h. The samples were analyzed by phosphate affinity electrophoresis and Western Blot. (D) ADAM10/17-deficient HEK cells were either transfected with meprin β WT, meprin β T694A or meprin β eachAF alone, or co-transfected with the HA-tagged PKC isoforms α and β. Selective cells were stimulated with 100 ng/ml PMA for 10 min and subsequently lysed. The samples were analyzed by phosphate affinity electrophoresis and Western Blot.

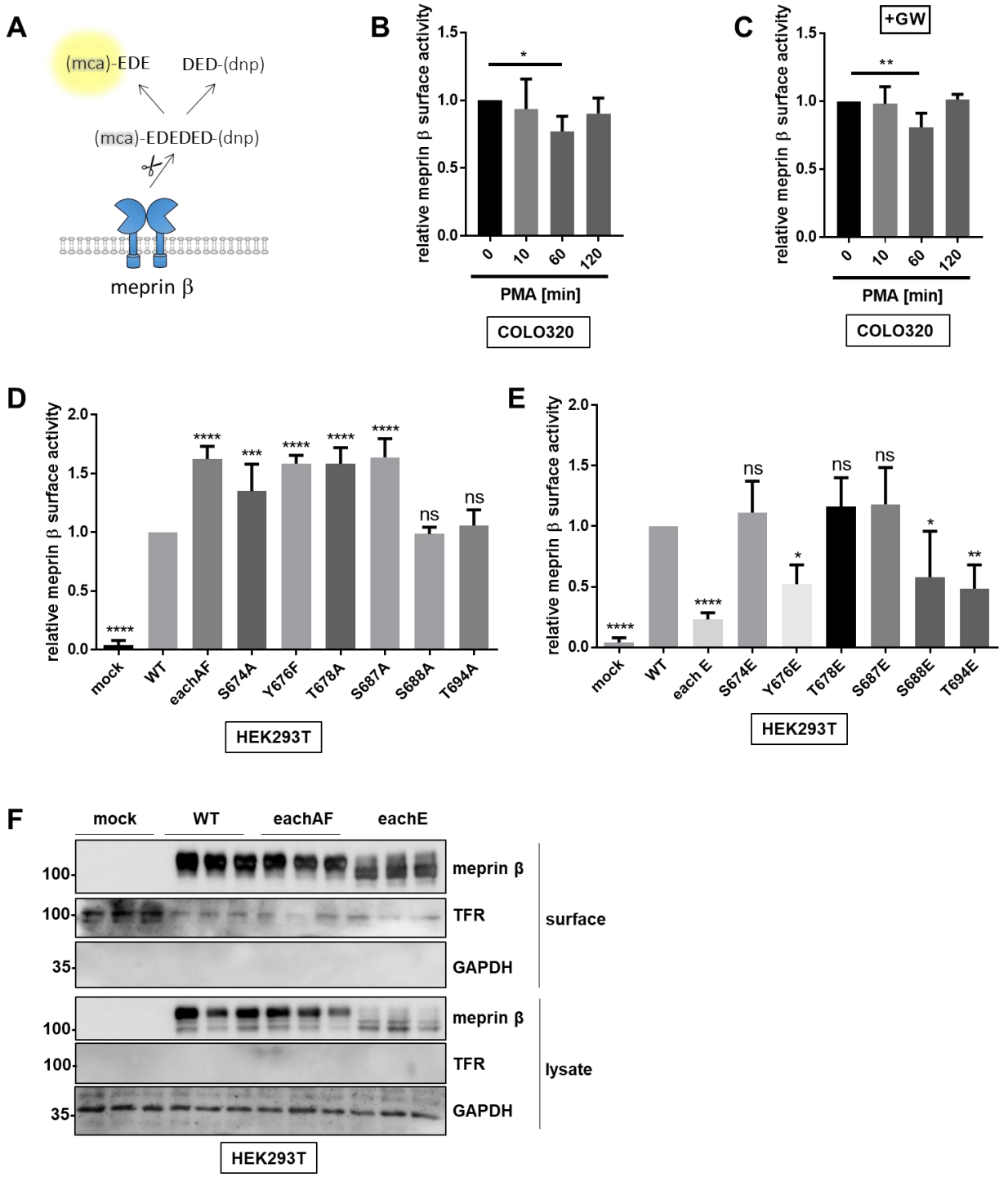

Figure 3: Meprin β activity at the cell surface is decreased upon phosphorylation. (A) Principle of the fluorogenic peptide based activity assay. The peptide ((mca)-EDEDED-(K-e-dnp); mca: 7-methyloxycoumarin-4-yl, dnp: dinitrophenyl) consists of the fluorophore (mca), alternating glutamate and aspartate residues (EDEDED) and a quencher (dnp). Upon cleavage, fluorescence is emitted. (B) COLO320 cells were treated with 5 µg/ml trypsin for 30 min to activate meprin β and afterwards stimulated with 100 ng/ml PMA for 0, 10, 60, and 120 min. Afterwards, the meprin β-specific surface activity was measured. (C) COLO320 cells were treated

with 5 µg/ml trypsin for 30 min to activate meprin β in the presence of 3 µM GW to block shedding by ADAM17. The cells were subsequently stimulated with 100 ng/ml PMA for 0, 10, 60, and 120 min. Afterwards, the meprin β-specific surface activity was measured. (D) HEK cells were transfected with meprin β mutants carrying single substitutions to alanine or phenylalanine at the C-terminus. Furthermore, a variant, in which all potential phosphorylation sites at the C-terminus are mutated to alanine or phenylalanine, referred to eachAF, was used. The meprin β-specific surface activity was measured in comparison to an empty vector control and meprin β WT expressing HEK cells. (E) HEK cells were transfected with meprin β mutants carrying single substitutions to glutamate at the C-terminus. Furthermore, a variant, in which all potential phosphorylation sites at the C-terminus are mutated to glutamate, referred to eachE, was used. The meprin β-specific surface activity was measured in comparison to an empty vector control and meprin β WT expressing HEK cells. (F) Cell surface biotinylation assay of HEK cells transfected with pcDNA3.1 (mock), meprin β WT, eachAF or eachE. After cell lysis, samples were analyzed by SDS-PAGE and Western Blot.

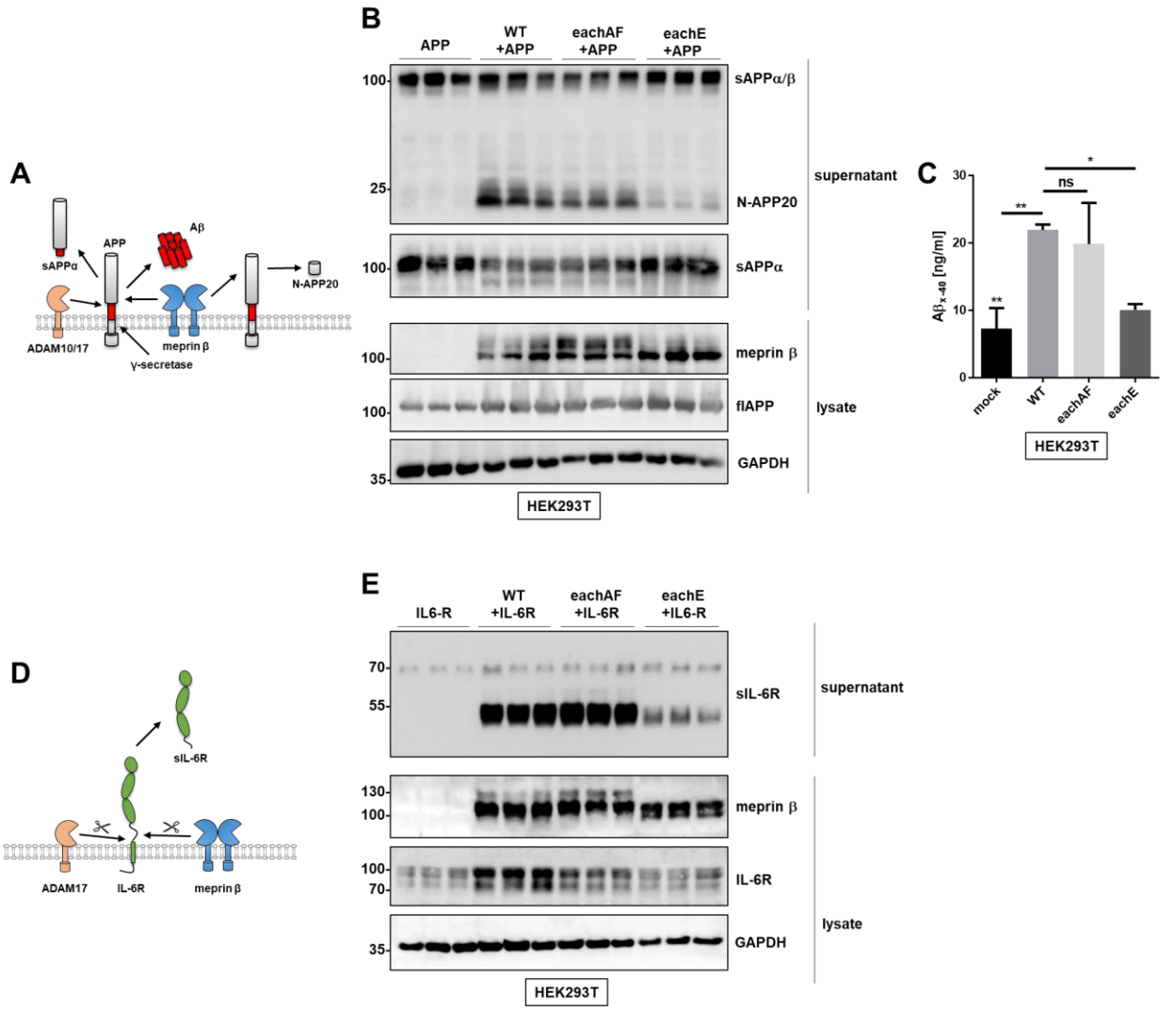

Figure 4: Decreased cell surface activity of the meprin β eachE variant leads to diminished substrate cleavage. (A) Meprin β and ADAM10/17 compete for APP processing at the α/β secretase site. ADAM10/17-mediated APP cleavage leads to sAPPα formation. Upon APP processing by meprin β at the β-site and subsequent cleavage by the γ-secretase complex Aβ is generated. Additionally, meprin β cleaves APP more N-terminally releasing non-toxic N-APP20 fragments. (B) HEK cells were transfected with the APP and meprin β WT as well as the meprin β variants eachAF and eachE. After cell lysis, samples were analyzed by SDS-PAGE and Western Blot using the APP antibodies 22C11 for N-APP20 (supernatant), 6E10 for sAPPα (supernatant) and N-APP for APP (lysate) detection. (C) The cell supernatants were analyzed with $Aβ_{x-40}$ ELISA (LEGEND MAX™ β-Amyloid x-40 ELISA Kit with pre-coated plate). (D) ADAM17 is the main sheddase of the IL6-R. However, also meprin β is capable of IL-6R ectodomain shedding, thereby cleaving N-terminal of the ADAM17 cleavage site. As a result, soluble IL-6R (sIL-6) is released. (E) HEK cells were transfected with the IL-6R and meprin β WT as well as the meprin β variants eachAF and eachE. After cell lysis, the samples were analyzed by SDS-PAGE and Western Blot.

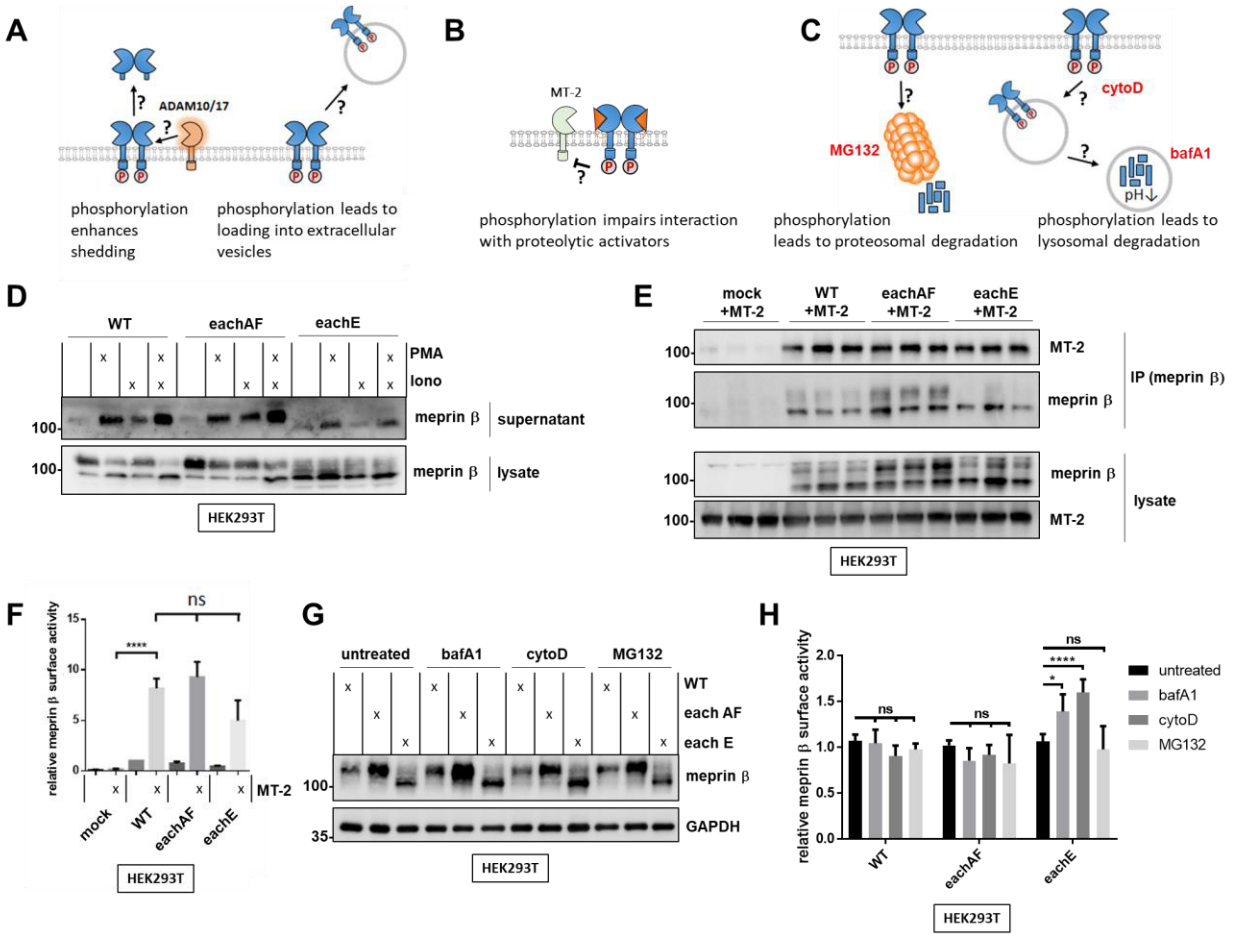

Figure 5: Meprin β is internalized and degraded upon phosphorylation. (A) Scheme of the hypothesis that meprin β shedding by ADAM10/17 and its release via extracellular vesicles are altered by phosphorylation. (B) A cartoon is depicted illustrating the hypothesis that meprin β phosphorylation may block its activation by matriptase-2 (MT-2). (C) Scheme of phosphorylation-induced meprin β internalization and proteasomal as well as lysosomal degradation. MG132, bafilomycin A1 (bafA1) and cytochalasin D (cytoD) are specific inhibitors for proteasomal degradation, lysosomal degradation and endocytosis, respectively. (D) HEK cells were transfected with meprin β WT or the variants eachAF or eachE, respectively, and stimulated with PMA (100 ng/ml) and/or ionomycin (1 µM) for 2 h. After cell lysis, lysates und corresponding supernatants were analyzed by SDS-PAGE and Western Blot. (E) HEK cells were cotransfected with myc-tagged MT-2 and either meprin β WT or the variants eachAF or eachE, respectively. After cell lysis, immunoprecipitation was performed using an antibody against meprin β. Lysate controls and immunoprecipitates were analyzed by SDS-PAGE and Western Blot. (F) HEK cells were cotransfected with myc-tagged MT-2 and either meprin β WT or the variants eachAF or eachE, respectively. Meprin β-specific cell surface activity was measured with the fluorogenic peptide based activity assay. (G) HEK cells were transfected with meprin β WT or the variants eachAF or eachE, respectively, and treated with trypsin (10 µg/ml) for 30 min and afterwards with bafA1 (100 nM), cyto D (4 µM) and MG132 (5 µM) for 4 h. After cell lysis, the samples were analyzed by SDS-PAGE and Western Blot. (H) Cells were treated as described in G and meprin β-specific cell surface activity was measured employing the fluorogenic peptide based activity assay.

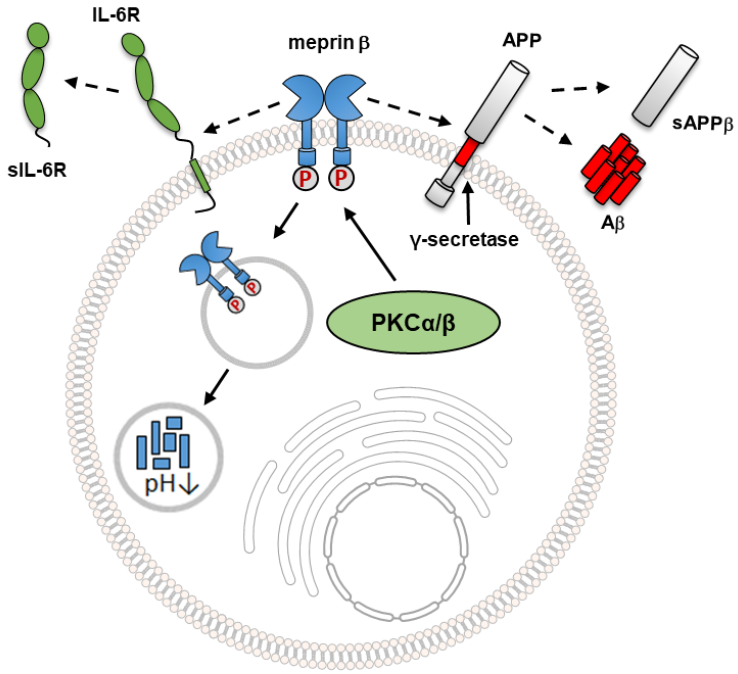

Figure 6: PKC-mediated phosphorylation of meprin β controls its cell surface activity. PKC-α and -β are involved in meprin β phosphorylation. As a consequence, meprin β is internalized and degraded. Thus, meprin β substrates such as APP and IL6-R are cleaved to a lesser extent upon meprin β phosphorylation.

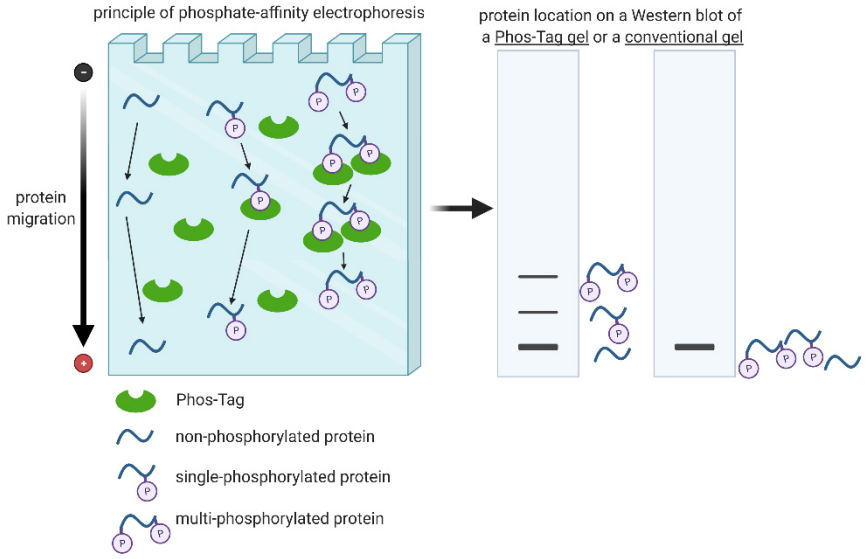

Supplementary Figure S1: Principle of a phosphate affinity SDS-PAGE. The Phos-tag™ compound is added to a SDS-gel during casting. The immobilized Phos-tag™ interacts with phosphorylated proteins throughout protein migration. Therefore, unphosphorylated proteins migrate faster than phosphorylated proteins depending on the number of phosphorylated residues. As a result, the higher the phosphorylation state of a protein is, the higher it is located in the gel after migration. The figure was created with BioRender.com based on information from the manual of the Phos-tag™ (Wako).

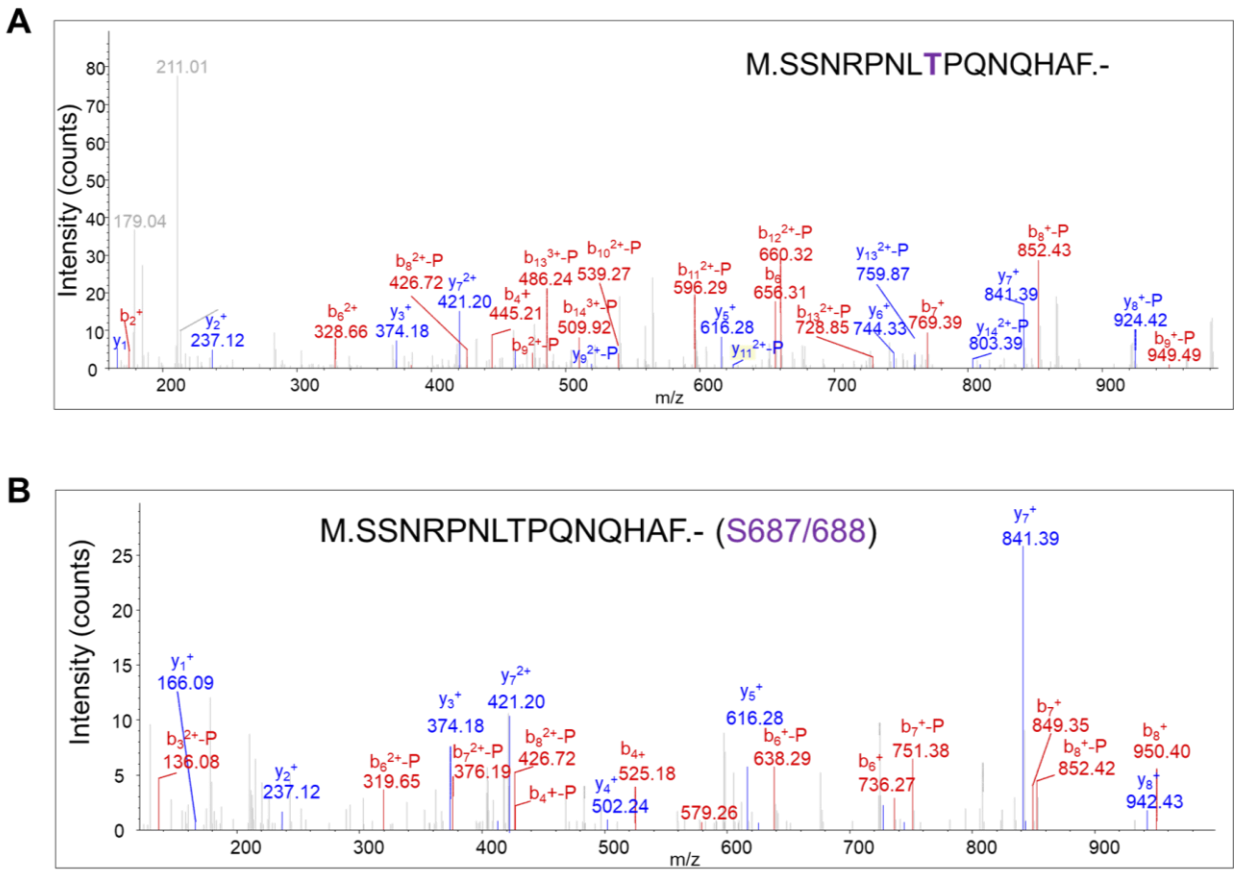

Supplementary Figure S2: MS/MS spectra of the phosphopeptides SSNRPNLTPQNQHAF phosphorylated at (A) T694 or (B) S687/688. Peptides were generated by in-gel CNBr-digestion of meprin β in Colo320 cells after stimulation with PMA.

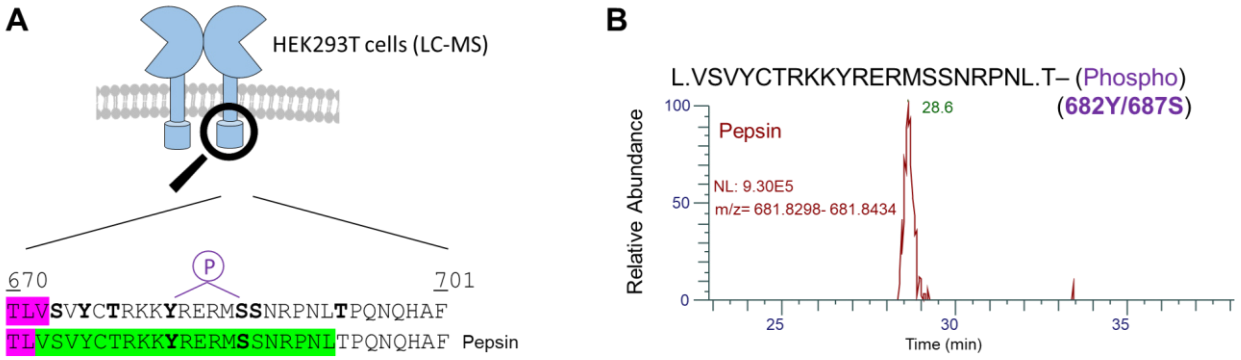

C

Annotated Sequence	Variable modifications	PSMs
[L].VSVYCTRKKYRERMsSNRPNL.[T]	S15(Phospho)	22
[L].VSVYCTRKKyRERMSSNRPNL.[T]	Y10(Phospho)	5

Supplementary Figure S3: MS analyzes of meprin β phosphorylation in transfected HEK ADAM10/17$^{-/-}$ cells after stimulation with PMA. (A) The scheme highlights the sequence coverage of the C-terminus of meprin β with identified phosphopeptide shown in green. TMD is highlighted in pink. Potential phosphorylation sites are highlighted in purple. (B) Extracted ion chromatograph of the in-gel pepsin digestion of meprin β from COLO320 cells showing a singly phosphorylated peptide. (C) Peptide-spectrum match (PSM) values of the peptide, phosphorylated either at Y682 or S687.

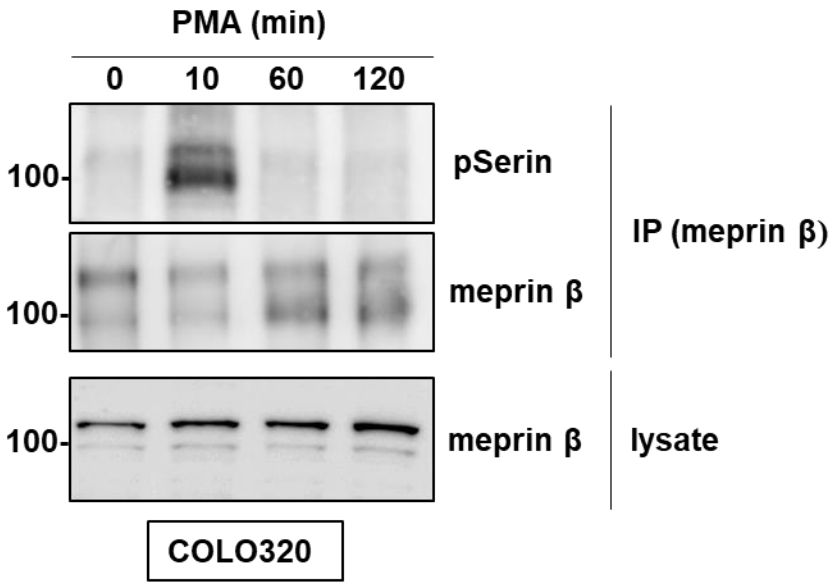

Supplementary Figure S4: Time-dependent phosphorylation of meprin β in PMA-treated COLO320 cells. COLO320 cells were treated with 5 µg/ml trypsin for 30 min to activate endogenous meprin β and afterwards stimulated with 100 ng/ml PMA for 0, 10, 60, and 120 min, respectively. After cell lysis, meprin β was immunoprecipitated and analyzed by SDS-PAGE and Western Blot using antibodies against meprin β and pSer.

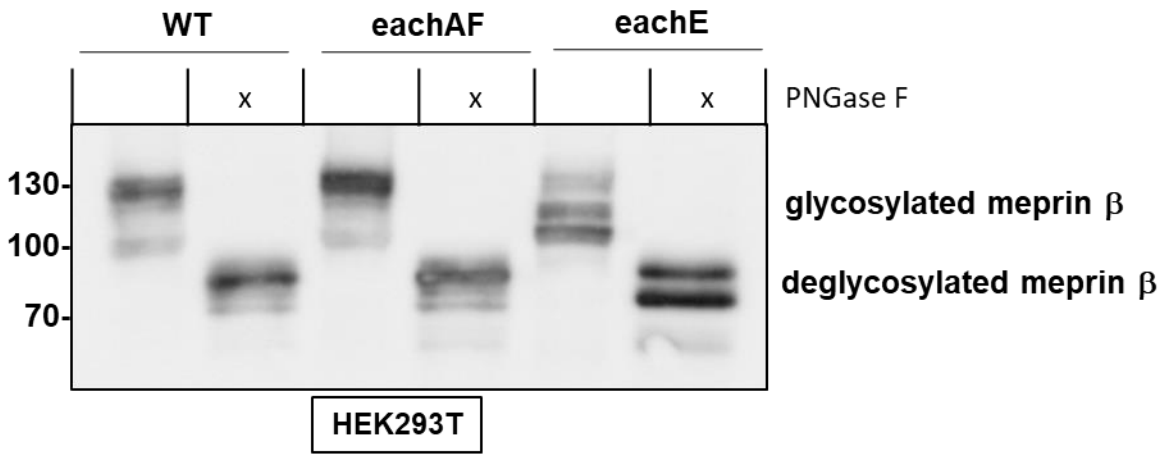

Supplementary Figure S5: PNGase F digestion of meprin β variants with mutated phosphorylation sites. HEK cells were transfected with meprin β WT or the variants eachAF and eachE. After cell lysis, the samples were treated with PNGase F and analyzed by Western Blot.

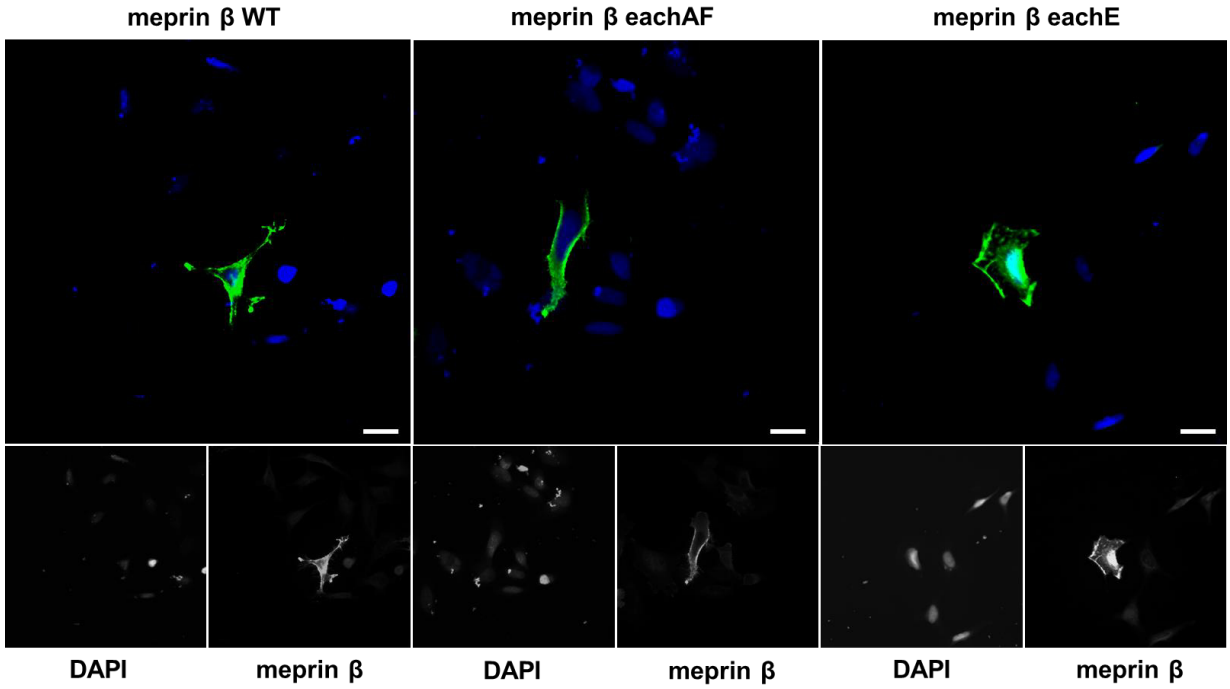

Supplementary Figure S6: Immunofluorescence microscopy images of the meprin β variants with mutated phosphorylation sites. HeLa cells were transfected with meprin β WT or the variants eachAF and eachE and immunofluorescence microscopy images were captured (scale bars, 20 µm). DAPI is displayed in blue, meprin β in green.

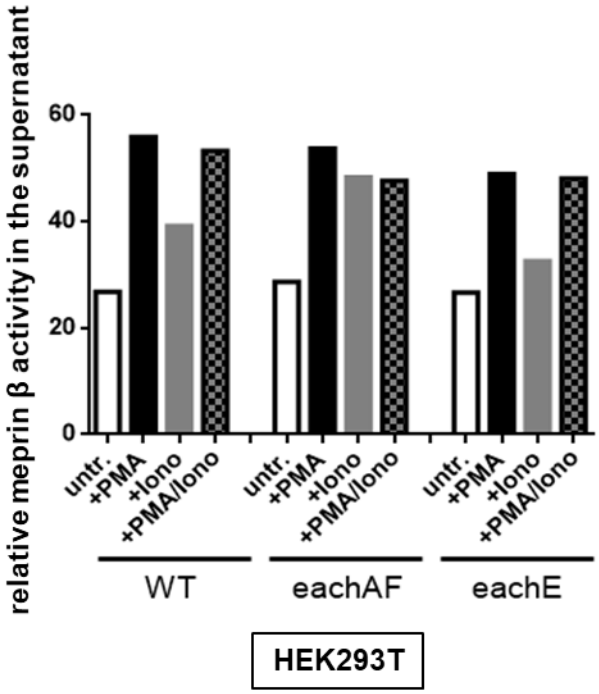

Supplementary Figure S7: Proteolytic activity of shed meprin β variants with mutated phosphorylation sites. HEK cells were transfected with meprin β WT and the variants eachAF or eachE and stimulated with PMA (100 ng/ml) and/or ionomycin (1 µM) for 2 h. After cell lysis, supernatants were measured employing the fluorogenic peptide based activity assay.

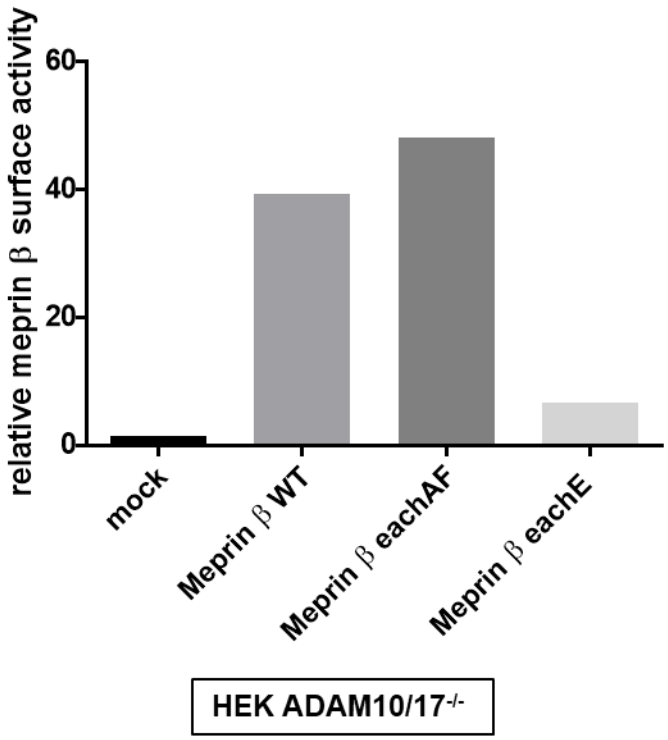

Supplementary Figure S8: Surface activity of meprin β variants with mutated phosphorylation sites in HEK ADAM10/17$^{-/-}$. HEK ADAM10/17$^{-/-}$ cells were transfected with meprin β WT and the variants eachAF or eachE. The meprin β activity at the cell surface was measured employing the fluorogenic peptide based activity assay.

Meprin β knockout reduces brain Aβ levels and rescues learning and memory impairments in the APP/lon mouse model for Alzheimer's disease

L. Marengo[1], F. Armbrust[2], C. Schoenherr[1], S. E. Storck[1], U. Schmitt[3], S. Zampar[4], O. Wirths[4], H. Altmeppen[5], M. Glatzel[5], S. Weggen[6], C. Becker-Pauly[2], C. U. Pietrzik[1*]

[1]Institute for Pathobiochemistry, University Medical Center of the Johannes Gutenberg University Mainz, Mainz, Germany.
[2]Institute of Biochemistry, Unit for Degradomics of the Protease Web, Christian-Albrechts-University Kiel, Kiel, Germany.
[3]Leibniz-Institute for Resilience Research, Mainz, Germany.
[4]Department of Psychiatry and Psychotherapy, University Medical Center Göttingen (UMG), Göttingen, Germany.
[5]Institute of Neuropathology, University Medical Center HH-Eppendorf, Hamburg, Germany.
[6]Department of Neuropathology, Heinrich Heine University, Düsseldorf, Germany.

* Correspondence should be addressed to:
Claus U. Pietrzik, Molecular Neurodegeneration, Institute for Pathobiochemistry, University Medical Center of the Johannes Gutenberg University of Mainz, Duesbergweg 6, Mainz 55099, Germany. Telephone number: +49 6131 39 25390. E-mail: pietrzik@uni-mainz.de

Abstract

β-Site amyloid precursor protein (APP) cleaving enzyme-1 (BACE1) is the major described β-secretase to generate Aβ peptides in Alzheimer's disease (AD). However, all therapeutic attempts to block BACE1 activity and to improve AD symptoms have so far failed. A potential candidate for alternative Aβ peptides generation is the metalloproteinase meprin β, which cleaves APP predominantly at alanine in p2. This process generates Aβ peptides independent of BACE1, and it is commonly found in AD brains. Here, we report the generation of the transgenic APP/lon mouse model of AD lacking the functional *Mep1b* gene (APP/lon x Mep1b$^{-/-}$), to analyze whether meprin β plays an important role in the pathogenesis of AD. Aβ levels are reduced in APP/lon mice when meprin β is absent, demonstrated by western blot analysis and ELISA. Immunohistochemical stainings of mouse brain sections revealed that N-terminally truncated Aβ2-x peptide deposition is decreased in APP/lon x Mep1b$^{-/-}$ mice. In addition, GFAP immunoreactivity in APP/lon mice show reduced levels of GFAP-positive astrocytes when meprin β was knocked-out. Importantly, loss of meprin β improved cognitive abilities and rescued learning behavior impairments in APP/lon mice. These observations indicate an important role of meprin β within the amyloidogenic pathway and Aβ production *in vivo*.

Introduction

The β-site APP cleaving enzyme 1 (BACE1) has been identified as a membrane bound aspartyl protease and it is considered the main β-secretase to generate Amyloid β peptides (Aβ) in neurons. This became particularly evident when BACE1 knockout (BACE1-/-) mice showed a dramatic decrease in Aβ production once crossed to APP-overexpressing transgenic mouse lines such as Tg2576 (1) or to 5xFAD mice (2). This

decrease was accompanied by improvements in Alzheimer's disease (AD)-related cognitive deficits, such as memory and learning impairment (3). Based on this observation, several BACE1 inhibitors were developed, reaching clinical trials as potential new treatments for AD (4). Strikingly, many of those therapeutic strategies have been suspended due to their failure to improve AD symptoms (5). Furthermore, recent evidence indicated that complete blockage of BACE1 can lead to considerable side-effects, e.g. interfering with neural progenitor cell proliferation, resulting in a decreased number of neurons (6) and synaptic plasticity impairment (7). These effects can be explained by observations from analysis of BACE1-/- mice, such as elevated pain sensitivity, reduced grip strength (8) and epileptic seizures (9). BACE1 depletion leads to accumulation of unprocessed type 3 neuregulin 1 (NRG1) and to hypomyelination in the hippocampus and peripheral nerves (10). Moreover, BACE1 inhibition increases neuronal cell surface levels of seizure protein 6 (Sez6), which controls synaptic connectivity and motor coordination in mice (11).

Aβ peptides are generated through the proteolytic processing of the Amyloid Precursor Protein (APP) by the sequential action of β- and γ-secretase. Apart from the bona fide 'full-length' Aβ (1-40, 1-42), multiple Aβ species bearing different N and C-termini have been described (12–14). The exact physiological role of the N-terminally truncated forms of Aβ (Aβx-40/ x-42) is still debated, but they are detected as major components in extracellular amyloid deposits in human brain. In fact, N-terminal truncations accounted for more than 70% of total Aβ species detected in human brain tissues from patients diagnosed with severe AD (15, 16), thus emphasizing their important role in the pathology of the disease (reviewed in (17)). Since BACE1 can only generate Aβ peptides starting at position 1 or 11 (Aβ1-x/11-x), Aβ species starting at other N-terminal positions, e.g. 4 (Aβ4–x) or 2 (Aβ2-x), cannot be assigned to BACE1 activity (16, 18). BACE1 knockout neurons do not secrete Aβ1-40/42 and Aβ11-40/42 (1) while N-terminally truncated Aβ peptides can still be detected under these conditions (19). The existence of different Aβ species in the absence of BACE1 indicates an independent pathway of APP processing by alternative β-secretases. Over the last few years other secretases, such as ADAMTS4 (20), Aminopeptidase A (21) and cathepsin B (22) have been described to be involved in BACE1-independent N-terminal truncated Aβ generation.

Another potential candidate for alternative Aβ production is the metalloproteinase meprin β. Fittingly, meprin β was recently identified as a potential risk gene associated with AD through exome-wide association analysis in a cohort of patients clinically diagnosed with AD (23). Meprin β is predominantly membrane-bound and co-localizes with APP in the late secretory pathway or at the cell membrane (24). Of note, it was demonstrated that meprin β cleaves APP and it is capable of liberating not only Aβ1-x , but also N-truncated Aβ peptides starting mainly at position 2 and 3 (25, 26), indicating a possible role of meprin β within the amyloidogenic pathway in addition to BACE1. Moreover, we have shown that meprin β even has a higher affinity to wild-type APP compared to BACE1 (25) and that the various familiar APP mutations differently affect meprin β cleavage specificity. The protective A673T APP mutant, which reduces BACE1 cleavage, also induced a 70% decrease in the Aβ2-40 generated by meprin β in vitro (24). Importantly, the change in amino acid composition around the β-site in the 'Swedish' APP mutation (K670N/M671L) almost fully abolished generation of N-terminally truncated Aβ2-40/42 variants (24). However, this Swedish mutation (APPswe) is commonly introduced into mouse models of AD because it strongly enhances overall Aβ production by BACE1, thus facilitating studies focusing on the role of Aβ in AD. As a consequence, though

these transgenic mouse models have substantially broadened our knowledge on the alterations underlying AD pathology, they might have also supported to oversight certain other potentially relevant pathophysiological mechanisms. In this respect, the strong affinity of BACE1 for APPswe might have concealed effects from other important enzymes such as meprin β that could be mechanistically involved in AD pathogenesis. Based on increasing evidence for alternative β-secretases, we aimed at analysing meprin β–dependent Aβ generation in vivo using an animal model for AD that does not harbor the Swedish mutation on the APP transgene. We now demonstrate that soluble Aβ levels are decreased in the AD-mouse model APP/lon, when meprin β is absent. More specifically, we found a decrease in the deposition of the N-terminally truncated Aβ2-x in the cortex of these animals knockout for meprin β. Furthermore, we show that loss of meprin β improved cognitive impairments such as memory and learning.

Results

Meprin β protein levels are increased in sporadic AD brain

We previously identified the metalloprotease meprin β as an APP-cleaving enzyme with β-secretase activity. Therefore, we wanted to investigate, whether meprin β brain protein levels differ between healthy control and AD patients. Herein, we performed immunohistochemical staining of human brain sections using anti-6E10, Bielschowsky and anti-tau to confirm the diagnosis of AD patients showing amyloid plaques and neurofibrillary tangles (Fig. 1A). Upon immunohistochemical assessment, a subpopulation of neurons in cortical layers III to VI showed prominent DAB signal of soma and neurites in all samples and was thus defined as meprin β positive. Generation and specificity of meprin β antibodies are described in the supplementary information (Fig S1). Immunohistological analyses of sections of frontal cortex show an increase in the number of meprin β-positive cortical neurons in AD (n=21) compared to control brains of non-demented patients (n=17) (Fig. 1A-B) of nearly 50% (see Supplementary Fig. S2, for all cases). In summary, the morphometric analysis revealed a significant up-regulation of meprin β specifically in AD compared to controls, thus confirming previous observations by Schlenzig and colleagues (26).

Aβ levels are reduced in APP/lon mice with a knockout for meprin β

Given that meprin β can generate N-terminally-truncated Aβ peptides in vitro (25), we hypothesized that Aβ levels would also be altered by meprin β knockout in vivo. To test this assumption, Mep1b-/- mice were crossed to an APP-overexpressing mouse model. Of note, we have shown previously that meprin β generates predominantly N-terminal truncated Aβ2-x peptides, which are fully blocked when APP carries the Swedish familial mutation close to the β-secretase cleavage site (24). Since most commonly used AD mouse models harbor the Swedish mutation in the APP sequence, these mice are not a useful model to investigate the generation of N-terminally truncated Aβ2-x peptides by meprin β. Hence, we used mice expressing APP only with a 'London' mutation (V717I) close to the γ-secretase cleavage site. This mutation also increases the amount of Aβx-42 but leaves the N-terminal region of the Aβ sequence unaltered. This model reflects more appropriately the situation for sporadic AD in terms of the accessibility and involvement of enzymes close to the N-terminus of Aβ. Brains from 15-month-old APP/lon and APP/lon x Mep1b-/- mice were dissected and processed to isolate soluble (PBS) Aβ fractions. To analyse the meprin β-dependent generation of Aβ peptides we applied two different detection methods. First, we performed an immunoprecipitation assay followed by Urea-SDS-PAGE (Fig. 2A, B). For the purpose of detecting different Aβ species we used here the IC16 antibody. A significant decrease in levels

of Aβ was detected in soluble fractions of APP/lon mice lacking Mep1b (n=10), compared to APP/lon mice (n=10) (Fig 2A-B). In a second approach, we used sandwich enzyme-linked immunosorbent assays (sELISA) for the specific detection of Aβ1-40 and Aβ1-42 (Fig. 2C-D), followed by another ELISA to detect total Aβx-40 and Aβx-42 levels (Fig. 2E). We detected a remarkable reduction in levels of soluble Aβ1-40 and Aβ1-42 in the brains of APP/lon x Mep1b-/- compared to APP/lon mice alone (n=8 animals/group). However, the Aβ1-40 and Aβ1-42 concentrations observed in the insoluble fractions were not significantly altered amongst the different genotypes (Fig. 2D). We have previously shown that meprin β generated Aβ2-x peptides exhibit a higher aggregation rate than Aβ1-x (24). Hence, we would expect a reduction of Aβ2-x peptides in insoluble fractions of APP/lon x Mep1b-/- mice. However, the antibody 82E1 used in this setup specifically detects the very N-terminus of Aβ peptides (1-x) generated by BACE1 cleavage (27). Recognition of Aβ1-40 and Aβ1-42, but not Aβ2-40, was further confirmed by immunoblot of 82E1 against synthetic peptides (Fig. S3). Reprobing of the same membrane with the IC16 antibody revealed the Aβ2-40 detection.

The amounts of Aβx-40 and Aβx-42 were even more strongly decreased when meprin β was lacking compared to APP/lon mice alone (Fig. 2E). In general, we observed that the absolute levels of x-40 and x-42 detected were almost 2-fold higher than the corresponding Aβ1-40 and Aβ1-42 (Fig. 2C and 2E for comparison). Therefore, we conclude that the remaining portion of x-40 and x-42 might correspond to all species of N-terminally truncated Aβ peptides, which have been documented previously (16, 25).

General APP processing and secretase activities are not altered in APP/lon mice lacking meprin β

Previously, we have shown that meprin β participates in the processing of APP in vitro, generating soluble N-APP fragments and Aβ peptides (25, 28). To evaluate the impact of meprin β on general APP processing in vivo, we analyzed both soluble and insoluble brain fractions of 15-month-old APP/lon and APP/lon x Mep1b-/- mice. In soluble fractions, analysis by SDS-PAGE and subsequent western blotting revealed no obvious differences in total sAPP (Fig. 3A). Similar, in insoluble fractions, full length unprocessed APP or CTFs levels were unaltered between the two groups (Fig 3B, C). This result is in part consistent with BACE1 knockout data, where also no measurable effect on full-length APP expression was detected (29, 30).

As γ-secretase is considered a key target for Aβ generation and previous work showed meprin β influence on α-secretase (31), we wanted to investigate whether the knockout of meprin β may lead to decreased secretases activities. Notch1 is a type I transmembrane protein involved in numerous pathways such as cell fate and morphogenesis in both embryonic and adult brain (32). Upon ligand binding, Notch1 is processed initially by ADAM10, by cleavage at its extracellular juxtamembrane domain. This is followed by intramembrane cleavage through γ-secretase, which generates the cytoplasmic domain of Notch (NICD). We analysed the production of these two fragments in the insoluble fraction by western blot. Loss of meprin β did not change the processing or levels of Notch1 (Fig. 3D), indicating that the metalloproteinase has no significant effect on α- or γ-secretase activity in this model. γ-Secretase is a multiprotein complex consisting of Presenilin (PSEN), Nicastrin, Aph-1, and Pen-2 and all four proteins are necessary for full intramembrane proteolytic activity (33). Exemplary we evaluated γ-secretase expression through PSEN1 and Nicastrin levels, which showed no significant difference between APP/lon (n=5) and APP/lon x Mep1b-/- (n=5) mice (Fig 3E). In sum, the meprin β

knockout has no significant effect on the activities of APP cleaving secretases.

Having ruled out alterations in α- and γ-secretase activities with regard to APP processing, we wanted to investigate whether the knockout of meprin β may lead to decreased BACE1 activity. As the majority of Aβ generation has been attributed to BACE1, lower Aβ levels observed in APP/lon x Mep1b-/- mice could be due to decreased BACE1 activity. To investigate this, we analyzed the well-described BACE1 substrate Sez6, which is involved in maintenance of dendritic arborisation and enhancing synaptic connectivity (34). The full-length Sez6 is cleaved by BACE1 and it generates a secreted soluble ectodomain and a C-terminal transmembrane fragment, which is further cleaved by γ-secretase (11). To evaluate whether meprin β affects BACE1 activity, we analyzed the meprin β knockout effect on processing of Sez6. Therefore, we used total brain lysates from Mep1b-/- mice, double knockout mice for BACE1 and meprin β compared to wild-type (WT) mice. As expected, increased levels of Sez6 were detected in the double knockout mice lacking BACE1. In contrast, levels of endogenous Sez6 from meprin β knockout brains remained the same as in WT animals (Fig. 3F), suggesting that BACE1 activity is not altered in the absence of meprin β.

N-terminally truncated Aβ2-x peptide deposition is decreased in APP/lon mice lacking meprin β

Meprin β is capable of generating Aβ2-x peptides in vitro (24, 25). Subsequently we wanted to determine whether the Mep1b knockout had any effect on Aβ2-x deposition in vivo. Thus, we evaluated plaque pathology in brains of APP/lon mice using antibodies specifically detecting Aβ peptides starting at position p1 or p2. Amyloid plaques arise in APP/lon mice at the age of 10-12 months (35). To analyze plaque deposition, sagittal brain sections of 15-month-old APP/lon and APP/lon x Mep1b-/- mice were stained using pAb77, specifically detecting Aβ2-x and mAb 80C2, which binds to Aβ1-x. The selectivity of the Aβ2-x (Aβ2-x pAb77) and Aβ1-x (80C2) antibodies have been confirmed previously (36, 37). In general, both antibodies detected mainly diffuse plaques of different sizes in cortex and hippocampus. While we observed amyloid plaques spread throughout all cortical layers, plaques in the hippocampal formation seemed to be restricted to CA1 and subiculum. Similarly to AD patients, the subiculum is the first brain region to present amyloid deposits in APP/lon mice (38). A significant decrease in Aβ2-x plaque load of about 40% was detected in the cortex of APP/lon mice lacking Mep1b compared to APP/lon mice alone (Fig. 4A, 4C). However, no significant difference between the two groups was evident for Aβ1-x staining (Fig. 4A-B). This result correlates well with the observed effect on insoluble Aβ1-40 and Aβ1-42 levels documented by ELISA (Fig. 2). Taken together, these results indicate that meprin β is involved in the generation of soluble Aβ peptides in vivo and that it has an impact on plaque deposition through the generation of Aβ2-x peptides.

Reactive astrocytes are decreased in the cortex of APP/lon x Mep1b-/- mice

Severity of AD pathology strongly correlates with the density of activated astrocytes (39). Numerous AD mouse models have demonstrated a correlation of astrocytic gliosis with plaque pathology (40, 41). Such gliosis can be identified by staining of glial fibrillary acidic protein (GFAP) in reactive astrocytes surrounding amyloid plaques (42). Since we have demonstrated decreased levels of soluble Aβ peptides and reduced Aβ2-x-derived extracellular plaques, we sought to determine whether gliosis in the brains of APP/lon x Mep1b-/- was also reduced. We analyzed cortical sections immunohistochemically stained for GFAP in 15-month-old APP/lon and APP/lon x Mep1b-/- mice. Images revealed extensive gliosis throughout the cortex of

APP/lon mice (Fig. 5A) thus confirming previous work (40). However, APP/lon x Mep1b-/- mice showed a significant decrease in the area of GFAP-positive immunostaining (Fig. 5B). This result further strengthens our observation that decreased meprin β expression reduces Aβ-peptide generation and subsequently improves brain pathology.

Meprin β knockout rescues learning behavior impairments in APP/lon mice

As we have demonstrated that absence of meprin β has no detectable influence on other APP processing enzymes, but significantly alters amounts of soluble Aβ peptides, which are strongly associated with a decline in cognitive ability, we tested whether meprin β knockout had any influence on learning behavior of APP/lon mice. As control groups, we included age-matched WT and Mep1b-/- mice. In APP/lon mice, behavior alterations start at the age of 6 months (35). To assess hippocampus-dependent learning we chose the Morris water maze hidden platform task (43). All genotypes showed the same basal motor activity indicated by unaltered swimming speed ($F(3;29)=2.489$, $p= 0.0801$) (Fig. 6A) and had no specific deficits of finding a visible platform ($F(3;29)=0.3073$ $p=0.8199$) in the pool (Fig. 6B), allowing for evaluation of cognitive performance.

APP/lon mice showed a significant learning deficit compared to wild-type (WT) mice (Fig. 6C) ($p<0.05$ on day 4 and on probe trial (PT)). Escape latency to find the visible platform from day 4 shows also a significant difference when comparing APP/lon to Mep1b-/- mice (day 4 $p<0.05$) Most interestingly, on PT day this effect is also seen when comparing APP/lon to APP/lon x Mep1b-/-($p<0.0001$). WT mice showed no different escape latency when compared to either APP/lon x Mep1b-/- or Mep1b-/-. Memory abilities were characterized on the probe trial by the number each mouse crossed the former platform location and the latency to reach the location. In line with the observations on learning, APP/lon mice showed the fewest crossings of the former platform location (Fig. 6D) ($F(3;29)=6.587$ $p=0.0016$), showing significant differences to all other genotypes ($p<0.05$). In addition, APP/lon mice showed the highest average latency ($F(3;29)=15.32$ $p<0.0001$) to find the platform location and with significant difference to all other three genotypes (Fig. 6E). Taken together, these findings indicate that the absence of meprin β in APP/lon mice ameliorates the cognitive impairments since there were no differences observed in learning behavior when compared to WT animals. APP/lon mice deficient for meprin β were able to learn the location of the hidden platform, and to find the platform location when it was removed. Hence, the present data suggest that meprin β contributes to the development of cognitive impairments in APP/lon mice.

Discussion

Generation of Aβ peptides is a hallmark of AD pathology. BACE1 was identified as the major β-secretase, however, so far, all therapeutic attempts to block BACE1 activity to hold AD progression or cure the symptoms in AD patients have not been successful. There are many possible explanations, one of which is the existence of alternative proteases acting complementary to BACE1. Here we demonstrate that loss of the alternative β-secretase meprin β is capable of rescuing the learning deficits in the APP/lon AD mouse model. Importantly, most AD mouse models carry the APPswe mutation, which is a variant that is highly prone to BACE1 activity but strongly impairs meprin β cleavage (24). We hypothesize that the wide use of APPswe models in the Alzheimer field opened just a very small window to investigate alternative amyloidogenic APP processing. Of note, the potential relevance for meprin β in AD was recently supported by a genetic study where a Mep1b variant was identified as one of the AD-associated genes in a British dementia cohort (23).

Previously, we and others have identified APP as a substrate for meprin β in vitro (26, 28). Moreover, mass spectrometry analysis of peptides incubated with meprin β revealed cleavage sites not only at the aspartate p1, but also in alanine p2 and the peptide bond in p3, resulting in an N-terminal glutamate residue (25). Together, these observations identify meprin β as a protease candidate for the generation of not only the canonical full-length Aβ peptides, but also N-terminally truncated Aβ2-x and Aβ3-x species commonly found in AD brain. Of particular interest, Aβ3-x generated by meprin β serve as a substrate for glutaminyl cyclase (QC) which converts the N-terminus into pyroglutamic acid to produce pyroglutamate Aβ peptides (pGlu-3Aβ) (26). This particular peptide is found in amyloid plaques in abundance, comprising 15-45% of total Aβ in AD brains (44). Preclinical immunotherapy aiming at the reduction of pGlu-3Aβ have shown remarkable results in cognitive improvement of AD-like mouse models (45, 46). Recently Eli Lilly & Company announced that the Phase 2 TRAILBLAZER-ALZ study using "Donanemab", a monoclonal antibody that recognizes pyroglutamated Aβ, slowed cognitive decline in people with early AD. To provide further evidence for the relevance of meprin β in vivo, we generated mouse lines to analyze whether meprin β plays an important role in the pathogenesis of AD. The present work describes the in vivo effect of meprin β gene knockout on APP processing, Aβ generation and behavioral phenotype in APP/lon mice.

The APP/lon animal model is characterized by an age-dependent, progressive increase of soluble Aβ levels (35). Interestingly, homozygous knockout of meprin β led to a decrease in soluble Aβ in this mouse model. In APP/lon mice, the absolute levels of Aβx-40 and x-42 detected by ELISA were around 2-fold higher than the corresponding specific levels of Aβ1-40 and Aβ1-42. Hence, the remaining amount of x-40 and x-42 likely corresponds to all species of N-terminally truncated Aβ peptides. (27). N-terminal truncations make up the majority of Aβ species in AD (14, 47) but, of note, are much less abundant in the transgenic mouse models that overexpress APPswe, which might explain the differences in amyloid deposition mechanisms between human and rodents (48). There are several known mutations within the APP sequence, but the majority of AD research is based on mouse models harboring the APPswe (K670N/ M671L) mutation. However, cells overexpressing meprin β and APPswe showed a lack of Aβ2-x variants (24). This result indicates that meprin β is responsible for generating N-terminally truncated Aβ2-x almost exclusively from the APPwt sequences. Essentially, wild-type APP is considered as a relatively poor substrate for BACE1, which cleaves preferentially APPswe (49). In terms of the relative abundance of specific variants of Aβ peptides, such as Aβ1–42, and N-terminally truncated Aβ2/3–42, clear differences between AD brain and APP23 mice were observed (47, 50), with Aβ1-40 being the most abundant species detected in brain lysates of the latter model.

Previously, we and others detected increased levels of meprin β mRNA in brains of demented versus non-demented control patients (25, 26). In this study, we could further strengthen this observation by providing evidence for increased meprin β protein expression levels in AD brains. We found significantly elevated amounts of strongly meprin β-positive cells in brains of sporadic AD patients, compared to brains of age-matched non-demented control patients. While cause and relevance of this clearly deserves further studies, increased meprin β-positive cell count (in combination with previously published elevated mRNA levels found in AD) supports our hypothesis of a potential role of meprin β in AD pathology. We already showed a different APP cleavage pattern in brains of meprin β knockout compared to WT mice, suggesting that meprin β is involved in N-

terminal processing of endogenous APP in vivo (24).

It has been shown that there is a difference in the Aβ pattern composition between brain samples from non-demented and demented individuals. Regarding the species composition, soluble Aβ aggregates that accumulate in AD differ from those generated during normal ageing. The higher neurotoxicity (more prone to aggregate) correlates with the predominance of N-terminally truncated species over the full-length forms (51). Overall, brain tissue of AD patients had more N-terminally truncated and pyroglutamate-modified Aβ accumulation than healthy elderly patients, suggesting that they might play a critical role in plaque formation (52). In AD temporal lobe samples, Aβ1-42 was the predominant form and the second most abundant species comigrated with synthetic Aβ2-42 (47). The concentration of soluble Aβ peptides (probably in the form of neurotoxic oligomeric assemblies) is strongly associated with cognitive decline and pathological synaptic changes in neurons (53). Because the loss of charged amino acids in the Aβ truncated forms contribute to their enhanced insolubility and resistance to enzymatic degradation, they are considered highly neurotoxic and induce faster aggregation. Thus, N-terminally truncated species might be associated with more severe neurodegeneration (51). For example, N-terminally truncated Aβ4–x peptides seem to be restricted mainly to amyloid plaque cores and cerebral amyloid angiopathy in AD patients and in AD mouse models (54). Transgenic mice expressing Aβ4-42 (Tg4-42 transgenic line) developed a massive CA1 pyramidal neuron loss in the hippocampus (55). Aβ4-42 was also identified as the major N-truncated species in postmortem brain samples from aged controls, patients with vascular dementia, and AD patients (56, 57).

AD is characterized by accumulation of different forms of Aβ peptides and their deposition into extracellular amyloid plaques. Plaque deposition in APP/lon mice arise at the age of 10-12 months and it shows patterns that are reminiscent of AD brain. Using an antibody specific to Aβ2-x peptides we were able to detect plaque load by immunohistochemistry in aged APP/lon mice in the presence or absence of meprin β. Peptides starting at p2 in the form of small round and diffuse plaques were detected in cortex and hippocampus. More interestingly, a 40% decrease in Aβ2-x plaque load was detected in the cortex of APP/lon mice lacking meprin β. These results further support the idea that in addition to BACE1, meprin β influences the generation of Aβ peptides to some extent. As a diagnostic tool, assessment of Aβ peptides in CSF has been used to support the diagnosis of AD and to identify patients who might be at risk of developing AD. Along with other truncated species, Aβ2-42, for example, is decreased in CSF (58) and enriched in AD brains (16). Moreover, deficits in learning and memory, as assessed by Morris water maze tasks, were detected at 7 months of age in APP/lon in accordance with a previous report (59). We now demonstrate that APP/lon mice lacking meprin β showed cognitive abilities similar to wild-type mice. Further accumulation of brain plaques is usually associated with increased brain inflammation that eventually lead to cognitive impairment (60). Amyloid β increased generation and accumulation lead to an extensive proliferation of reactive astrocytes that can secrete an excess of proinflammatory cytokines (61). Previous work analyzing astroglial activation demonstrated that GFAP-positive cells were mostly localized surrounding amyloid plaques in aged APP/lon (40). We have shown here decreased levels of GFAP signal in the absence of meprin β in vivo. This result supports the in vivo effect of meprin β gene knockout on amyloid pathology. Since APP/lon x Mep1b-/- mice present decreased levels of soluble AβX-40 and AβX-42 and particularly reduced Aβ2-x plaque load, the astroglial response is lower compared to APP/lon alone.

Additionally, supporting the relevance in murine AD models, the group of Dennis Selkoe (62) detected meprin β in microsomal fractions from mouse brain lysates that are responsible for the majority of Aβ production. Although a portion of BACE1 co-fractionated with ADAM10 in this higher molecular weight fractions, the majority of BACE1 protein was found in low molecular weight pools that did not contribute to Aβ generation. Instead, meprin β showed a much stronger co-fractionation in the high molecular weight fractions, which may indicate its importance for Aβ generation.

While we cannot exclude that some N-truncated amyloid peptides might arise secondarily by exopeptidase activity towards Aβ1-40/42 originally produced by BACE1, many findings point to an important role of meprin β within initial Aβ production. We here report the generation of the mouse line APP/lon x Mep1b-/- which presented improved cognitive abilities and an important decrease of total Aβ levels. We believe that our findings offer several new paths to be explored that may improve our understanding of the AD pathogenesis and, in particular, roles of previously underestimated molecules and mechanisms therein.

Experimental procedures

Human brain tissue

Post mortem brain samples of frontal isocortex from neuropathologically confirmed AD patients (n=21, 10 females, 11 males; mean age ± SD: 77.9±10.1 years) and non-demented control patients (n=17, 8 females, 9 males; 75.8 ± 11.6 years) (source: University Medical Center HH-Eppendorf (UKE)). AD cases were diagnosed as CERAD B-C, Braak stages III-VI. None of the controls suffered from dementia or any other neurodegenerative disease. Usage of anonymized human post mortem brain tissues is in accordance with regulations at the University Medical Center Hamburg-Eppendorf and approved by the Ethical Committee at the University Medical Center Hamburg-Eppendorf. The collection and its use is in agreement with ethical regulations of the 1964 Helsinki declaration, its later amendments or comparable ethical standards.

Histological and immunohistochemical analysis of formalin-fixed paraffin embedded (FFPE) human brains

Sections of FFPE frontal isocortex from healthy control and AD were stained with a Bielschowsky staining kit according to standard laboratory procedures. Immunostainings of Aβ (using monoclonal antibody 6E10; 1:100, #39320, Biolegend, CA, USA), meprin β (using rabbit polyclonal anti-meprin β antibody; 1:500) and phosphorylated Tau protein (using monoclonal antibody AT8 (MN1020); 1:5000; Thermo Scientific) were performed with a Ventana Benchmark XT system according to common protocols. Meprin β-positive neurons were counted in three representative microscopic fields of approximately 1.87 mm2 (taken along cortical layers III to VI) per patient. The mean value of meprin β-positive cells derived from these three pictures per patient (corresponding to n=1) was used for quantifications of experimental groups and statistical analysis.

Animals

hAPP[V717I] (APP/lon) (35), BACE1-/- (63), meprin β knockout (Mep1b-/-)(64) and wild-type (WT) mouse strains were maintained on a 12 h light/dark cycle with food and water ad libitum. APP/lon mice lacking Mep1b were generated by crossing Mep1b-/- mice into hAPP[V717I] mice, which we will refer to as APP/lon x Mep1b-/-. All animal studies were conducted in compliance with European and German guidelines for the care and use of laboratory animals and were approved by the Central Animal Facility of the University of Mainz and the ethical committee on animal care and use of Rhineland-Palatinate, Germany.

Mouse brain lysates

Animals were sacrificed by cervical dislocation and brains were removed. Snap frozen hemispheres were mechanically homogenized in 0.01 M PBS supplemented with protease (cOmplete, Roche) and phosphatase inhibitor cocktails (PhosSTOP, Roche) on a 1:6 ratio (weight:volume) and subsequently ultracentrifuged at 55.000 rpm for 30 min. The PBS-extracted supernatant (soluble fraction) was collected and the pellet was re-suspended in 800 µL of 0.01M PBS containing 2% SDS. Homogenates were ultracentrifuged at 55.000 rpm for 30 min and the SDS-extracted supernatant (insoluble fraction) was kept for further analysis. PBS and SDS protein extracts were stored at -80°C until use.

Immunoprecipitation of Amyloid β

Soluble fractions from mouse protein extracts were used for immunoprecipitation (IP). Magnetic Dynabeads (M-280 Sheep Anti-Mouse IgG, 11201D, Novex) containing sheep anti-mouse IgG attached to their surface were activated with the monoclonal antibody (mAb) IC16 according to the protocol of the manufacturer (direct IP method) and added to the samples. IC16 recognizes residues 1-16 of the human Aβ sequence and it was used to a final 1:100 concentration (65). Briefly, total Aβ was immunoprecipitated from soluble brain lysates by mixing 5-fold concentrated detergent buffer (50 mM HEPES [pH 7.4], 150mM NaCl, 0.5% [v/v] Nonidet P-40, 0.05% [w/v] SDS and protease inhibitor cocktail [Roche Applied Science]) with each sample. After overnight incubation at 4°C, samples were washed 3 times in 1x PBS, 0.1% (w/v) BSA, and once in 10mM Tris-HCl, pH 7.5. After heating the samples to 95°C in 15 µl sample buffer (0.36M Bis-Tris, 0.16M bicine, 1% [w/v] SDS, 15% [w/v] sucrose, and 0.0075% [w/v] bromophenol blue) the supernatants were loaded in Urea-SDS-PAGE.

UREA-SDS-PAGE

Immunoprecipitated Aβ peptides from soluble fractions were separated in a 0.75 mm 10% polyacrylamide 8 M urea SDS-gels as described (24, 66). For separation of Aβx–40 from Aβx–42, a final concentration of 0.3M H2SO4 was used in resolving gels. Peptides were transferred to an Immobilon-P PVDF membrane via semi-dry western blotting (Bio-Rad) at 47 mA for 30 minutes. Membranes were boiled for 3 minutes in PBS and then blocked in 5% powder milk in TBST (20mM Tris, 137mM NaCl, 0.1% [v/v] Tween-20) for 30 minutes afterwards. IC16 antibody was used for overnight immunostaining. After washings in TBS-T, membranes were incubated with appropriate secondary anti-mouse antibody (1:5000, Sigma). Immunoreactive bands were visualized using an ECL enhanced chemiluminescence system (Millipore, MA, USA).

SDS-PAGE

Both soluble and insoluble fractions were prepared in SDS loading buffer (4X Roti-Load, Carl Roth, Germany) and boiled at 95°C. Protein extracts were separated by SDS-PAGE, transferred onto nitrocellulose membranes (Amersham Hybond ECL), and then blocked in 5% (w/v) milk powder in TBST. Soluble fractions were used to detect total soluble N-APP (sAPP), using an anti-N-terminal APP antibody (22C11, MAB348, Millipore). Moreover, the following antibodies were used for detection in insoluble fractions: anti-CT15 1:10,000 (APP and CTFs) (67), anti-PSEN1 (7H8, C-terminal), anti-Nicastrin (Sigma N1660), anti-Notch1 (ab27526, Abcam), anti-Notch intracellular domain (NICD, New England Bioscence #2421S).

Sandwich enzyme-linked immunosorbent assay (ELISA)

Human Aβ1-40 and Aβ1-42 concentrations were measured using commercially available ELISA kits (IBL International, Hamburg, Germany) according to the manufacturer's protocol. Briefly, soluble or insoluble fractions were diluted 1:50 or 1:200, respectively, then added to wells coated either with anti-human Aβx-42 (44A3) or Aβx-40 (1A10) and incubated overnight at 4°C. Wells were washed and incubated with HRP-conjugated anti-human Aβ1-x (82E1) for 1 h. After final washing steps, TMB solution was added as a substrate. The reaction was stopped with 1N H2SO4. Optical density (OD) values were measured at 450 nm on a microplate reader (Anthos 2010). For total Aβx-40/42 levels including N-terminally truncated peptides, samples were diluted 1:10 and the ELISA was performed according to the manufacturer's instructions of LEGEND MAX™ β-Amyloid x-40 ELISA Kit (Biolegend, Cat. no.: 842301) and LEGEND MAX™ β-Amyloid x-42 ELISA Kit (Biolegend, Cat. no.: 842401).

Immunohistochemistry on FFPE mouse brain sections

15-month-old mice were sacrificed by cervical dislocation; right hemispheres were washed in 0.01 M PBS and immerged in 4% PFA 0.01M PBS for fixation for 48 h. Tissue was dehydrated and embedded in paraffin. Immunohistochemistry was performed on 4 µm sagittal paraffin sections as previously described (68). In brief, sections were deparaffinized in xylene and rehydrated in a descending series of ethanol. To block endogenous peroxidases, we treated the sections with 0.3% H_2O_2 in PBS and antigen retrieval was achieved by boiling sections in 0.01 M citrate buffer pH 6.0, followed by 3 min incubation in 88% formic acid. Non-specific binding sites were blocked by treatment with 4% skim milk and 10% fetal calf serum in PBS for 1 hour prior to the addition of the primary antibodies. We used the following antibodies: rabbit anti-polyclonal antibody 77 (pAb77, 1:500) (36), raised against residues 2-14 of the Aβ peptide, detecting N-truncated Aβ peptides (Aβ2-x); mouse anti-mAb80C2 (1:1000, # 218 231 Synaptic Systems) detecting Aβ1-x peptides (37), and mouse anti-GFAP (1:500, #173 004 Synaptic Systems). Primary antibodies were incubated overnight in a humid chamber at room temperature followed by incubation with corresponding biotinylated secondary antibodies (1:200, Dianova). Staining was visualized using the ABC method using a Vectastain kit (Vector Laboratories, Burlingame, USA) and 3,3'-diaminobenzidine (DAB) as chromogen providing a reddish-brown color. Counterstaining was carried out with hematoxylin. In case of Aβ load analysis, the counterstaining was omitted. Serial images were captured with an Olympus BX-51 microscope equipped with a Moticam pro 282 camera (Motic, Wetzlar, Germany) on three sections per animal, which were at least 50 µm afar from each other.

Morris Water Maze

For behavior analysis, 7-month-old female mice of were tested (n = 5-10 animals/group). Spatial learning and memory were assessed by the Morris water maze hidden platform task performed as previously described (43) with minor modifications. Briefly, water maze (120 cm) was filled with clear water (23ºC). Prominent symbols around the maze provided abundant extra-maze cues. The platform stayed in the same quadrant from day one to four and the animals were released from four different positions at the pool perimeter. Mice performed four trials per day on four consecutive days with a maximum length of 90 s and an inter-trial interval of 90 s. If mice did not find the platform within the given time, they were guided to the platform. Mice were allowed to stay on the platform for 10 s. On the

fifth water maze day, a probe trial (60 s) without platform was performed. Basal motor activity was evaluated by swim speed. Learning was assessed by measuring the escape latency to find the platform. Memory capabilities were characterized by the number each mouse crossed the former platform location at probe trial and the latency to reach the location. For vision abilities, a visible platform task was done after the learning assessment at day 6. It consisted of 3 trials in a row starting the mice opposite to the platform which was indicated by a table tennis ball 15 cm above the platform.

Monitoring of behavior

A computerized video recording system registered moving-path and duration in water maze tests automatically. The hardware consisted of an IBM-type AT computer combined with a video digitizer and a CCD video camera. The software used for data acquisition and analysis was EthoVision XT® release 8.0 (Noldus Information Technology, Utrecht, Netherlands).

Quantification and statistical analysis

All graphs and statistical analyses were prepared using GraphPad Prism 6 software (La Jolla, CA). Western blots were quantified by densitometry using ImageJ v.1.52 (NIH, USA) and data were analyzed by t test. For human and mouse brain immunohistochemical analysis, all statistical comparisons were made using two-tailed unpaired Student's t test. Using ImageJ, Aβ load and GFAP staining pictures were binarized to 8-bit images and a fixed intensity threshold was applied defining the DAB staining. Measurements were performed for a percentage area covered by DAB staining. Behavioral data were analyzed by two-way analysis of variance (ANOVA) with genotype factor one and time factor two by repeated measures. Other parameters without repeated measures were analyzed by one-way ANOVA followed by Tukey's post hoc test. For the analysis, p values less than or equal to 0.05 were considered as statistically significant.

Acknowledgments: The authors thank Dr. Stefan Lichtenthaler for providing us the SEZ6 antibody, Dr. Jens Wiltfang for providing the Aβ2-x antibody and Johanna Wesselowski for excellent technical assistance. We also thank the UKE Mouse Pathology Core Facility (Kristin Hartmann) for IHC of human samples. We thank KUL and reMYND for sharing the APP(V717I) mouse model. **Funding:** This work was supported by Deutsche Forschungsgemeinschaft (DFG) Grant SFB877, "Proteolysis as a Regulatory Event in Pathophysiology" (A9 [CBP], A12 [MG], A15[CUP]) and the Alzheimer Forschung Initiative e.V. to CBP, HA and CUP. **Author contributions:** L.M. performed experiments, analyzed data and wrote the manuscript with S.W., CUP and CBP. CUP and CBP conceived and designed the study. F.A performed ELISA x-40/x-42 and analyzed data. S.Z and O.W. provided 2-x antibody and performed 2-x immunohistochemistry. H.A. and M.G. provided access to human brain tissue. C.S. and H.A. performed immunohistochemistry in human brains and analyzed data. S.E.S and U.S. performed behavioral experiments. **Competing interests:** The authors declare that they have no competing interests. **Data and materials availability:** All data needed to evaluate the conclusions in the paper are present in the paper and/or the Supplementary Materials.

References

1. Y. Luo, B. Bolon, S. Kahn, B. D. Bennett, S. Babu-Khan, P. Denis, W. Fan, H. Kha, J. Zhang, Y. Gong, L. Martin, J. C. Louis, Q. Yan, W. G. Richards, M. Citron, R. Vassar, Mice deficient in BACE1, the Alzheimer's β-secretase, have normal phenotype and abolished β-amyloid generation. *Nat. Neurosci.* **4**, 231–232 (2001).
2. M. Ohno, S. L. Cole, M. Yasvoina, J. Zhao, M. Citron, R. Berry, J. F. Disterhoft, R. Vassar, BACE1 gene deletion prevents neuron loss and memory deficits in 5XFAD APP/PS1 transgenic mice. *Neurobiol. Dis.* **26**, 134–145 (2007).
3. M. Ohno, E. A. Sametsky, L. H. Younkin, H. Oakley, S. G. Younkin, M. Citron, R. Vassar, J. F. Disterhoft, BACE1 Deficiency Rescues Memory Deficits and Cholinergic Dysfunction in a Mouse Model of Alzheimer's Disease. *Neuron*. **41**, 27–33 (2004).
4. C. C. Hsiao, F. Rombouts, H. J. M. Gijsen, New evolutions in the BACE1 inhibitor field from 2014 to 2018. *Bioorganic Med. Chem. Lett.* **29** (2019), pp. 761–777.
5. N. M. Moussa-Pacha, S. M. Abdin, H. A. Omar, H. Alniss, T. H. Al-Tel, BACE1 inhibitors: Current status and future directions in treating Alzheimer's disease. *Med. Res. Rev.* **40** (2020), pp. 339–384.
6. Z. K. Chatila, E. Kim, C. Berlé, E. Bylykbashi, A. Rompala, M. K. Oram, D. Gupta, S. S. Kwak, Y. H. Kim, D. Y. Kim, S. H. Choi, R. E. Tanzi, BACE1 regulates proliferation and neuronal differentiation of newborn cells in the adult hippocampus in mice. *eNeuro*. **5** (2018), doi:10.1523/ENEURO.0067-18.2018.
7. S. Lombardo, M. Chiacchiaretta, A. Tarr, W. H. Kim, T. Cao, G. Sigal, T. W. Rosahl, W. Xia, P. G. Haydon, M. E. Kennedy, G. Tesco, BACE1 partial deletion induces synaptic plasticity deficit in adult mice. *Sci. Rep.* **9**, 1–14 (2019).
8. X. Hu, C. W. Hicks, W. He, P. Wong, W. B. MacKlin, B. D. Trapp, R. Yan, Bace1 modulates myelination in the central and peripheral nervous system. *Nat. Neurosci.* **9**, 1520–1525 (2006).
9. S. Barão, D. Moechars, S. F. Lichtenthaler, B. De Strooper, BACE1 Physiological Functions May Limit Its Use as Therapeutic Target for Alzheimer's Disease. *Trends Neurosci.* **39** (2016), pp. 158–169.
10. M. Willem, A. N. Garratt, B. Novak, M. Citron, S. Kaufmann, A. Rittger, B. DeStrooper, P. Saftig, C. Birchmeier, C. Haass, Control of peripheral nerve myelination by the β-secretase BACE1. *Science (80-.).* **314**, 664–666 (2006).
11. M. Pigoni, J. Wanngren, P. H. Kuhn, K. M. Munro, J. M. Gunnersen, H. Takeshima, R. Feederle, I. Voytyuk, B. De Strooper, M. D. Levasseur, B. J. Hrupka, S. A. Müller, S. F. Lichtenthaler, Seizure protein 6 and its homolog seizure 6-like protein are physiological substrates of BACE1 in neurons. *Mol. Neurodegener.* **11**, 1–18 (2016).
12. C. L. Masters, G. Simms, N. A. Weinman, G. Multhaup, B. L. McDonald, K. Beyreuther, Amyloid plaque core protein in Alzheimer disease and Down syndrome. *Proc. Natl. Acad. Sci. U. S. A.* **82**, 4245–4249 (1985).
13. D. L. Miller, I. A. Papayannopoulos, J. Styles, S. A. Bobin, Y. Y. Lin, K. Biemann, K. Iqbal, Peptide Compositions of the Cerebrovascular and Senile Plaque Core Amyloid Deposits of Alzheimer's Disease. *Arch. Biochem. Biophys.* **301**, 41–52 (1993).
14. N. Sergeant, S. Bombois, A. Ghestem, H. Drobecq, V. Kostanjevecki, C. Missiaen, A. Wattez, J. P. David, E. Vanmechelen, C. Sergheraert, A. Delacourte, Truncated beta-

amyloid peptide species in pre-clinical Alzheimer's disease as new targets for the vaccination approach. *J. Neurochem.* **85**, 1581–1591 (2003).

15. N. C. Wildburger, T. J. Esparza, R. D. Leduc, R. T. Fellers, P. M. Thomas, N. J. Cairns, N. L. Kelleher, R. J. Bateman, D. L. Brody, Diversity of Amyloid-beta Proteoforms in the Alzheimer's Disease Brain. *Sci. Rep.* **7** (2017), doi:10.1038/s41598-017-10422-x.
16. J. Wiltfang, H. Esselmann, P. Cupers, M. Neumann, H. Kretzschmar, M. Beyermann, D. Schleuder, H. Jahn, E. Rüther, J. Kornhuber, W. Annaert, B. De Strooper, P. Saftig, Elevation of β-Amyloid Peptide 2-42 in Sporadic and Familial Alzheimer's Disease and Its Generation in PS1 Knockout Cells. *J. Biol. Chem.* **276**, 42645–42657 (2001).
17. O. Wirths, S. Zampar, Emerging roles of N- and C-terminally truncated Aβ species in Alzheimer's disease. *Expert Opin. Ther. Targets*. **23** (2019), pp. 991–1004.
18. R. Vassar, D. M. Kovacs, R. Yan, P. C. Wong, in *Journal of Neuroscience* (Society for Neuroscience, 2009; /pmc/articles/PMC2879048/?report=abstract), vol. 29, pp. 12787–12794.
19. K. Nishitomi, G. Sakaguchi, Y. Horikoshi, A. J. Gray, M. Maeda, C. Hirata-Fukae, A. G. Becker, M. Hosono, I. Sakaguchi, S. S. Minami, Y. Nakajima, H. F. Li, C. Takeyama, T. Kihara, A. Ota, P. C. Wong, P. S. Aisen, A. Kato, N. Kinoshita, Y. Matsuoka, BACE1 inhibition reduces endogenous Abeta and alters APP processing in wild-type mice2. *J. Neurochem.* **99**, 1555–1563 (2006).
20. S. Walter, T. Jumpertz, M. Hüttenrauch, I. Ogorek, H. Gerber, S. E. Storck, S. Zampar, M. Dimitrov, S. Lehmann, K. Lepka, C. Berndt, J. Wiltfang, C. Becker-Pauly, D. Beher, C. U. Pietrzik, P. C. Fraering, O. Wirths, S. Weggen, The metalloprotease ADAMTS4 generates N-truncated Aβ4–x species and marks oligodendrocytes as a source of amyloidogenic peptides in Alzheimer's disease. *Acta Neuropathol.* **137**, 239–257 (2019).
21. J. Sevalle, A. Amoyel, P. Robert, M. C. Fournié-Zaluski, B. Roques, F. Checler, Aminopeptidase A contributes to the N-terminal truncation of amyloid β-peptide. *J. Neurochem.* **109**, 248–256 (2009).
22. V. Hook, T. Toneff, M. Bogyo, D. Greenbaum, K. F. Medzihradszky, J. Neveu, W. Lane, G. Hook, T. Reisine, Inhibition of cathepsin B reduces β-amyloid production in regulated secretory vesicles of neuronal chromaffin cells: Evidence for cathepsin B as a candidate β-secretase of Alzheimer's disease. *Biol. Chem.* **386**, 931–940 (2005).
23. T. Patel, K. J. Brookes, J. Turton, S. Chaudhury, T. Guetta-Baranes, R. Guerreiro, J. Bras, D. Hernandez, A. Singleton, P. T. Francis, J. Hardy, K. Morgan, Whole-exome sequencing of the BDR cohort: evidence to support the role of the PILRA gene in Alzheimer's disease. *Neuropathol. Appl. Neurobiol.* **44**, 506–521 (2018).
24. C. Schönherr, J. Bien, S. Isbert, R. Wichert, J. Prox, H. Altmeppen, S. Kumar, J. Walter, S. F. Lichtenthaler, S. Weggen, M. Glatzel, C. Becker-Pauly, C. U. Pietrzik, Generation of aggregation prone N-terminally truncated amyloid β peptides by meprin β depends on the sequence specificity at the cleavage site. *Mol. Neurodegener.* **11** (2016), , doi:10.1186/s13024-016-0084-5.
25. J. Bien, T. Jefferson, M. Čaušević, T. Jumpertz, L. Munter, G. Multhaup, S. Weggen, C. Becker-Pauly, C. U. Pietrzik, The metalloprotease meprin β generates amino terminal-truncated amyloid β peptide species. *J. Biol. Chem.* **287**, 33304–33313 (2012).
26. D. Schlenzig, H. Cynis, M. Hartlage-Rübsamen, U. Zeitschel, K. Menge, A. Fothe, D.

Ramsbeck, C. Spahn, M. Wermann, S. Roßner, M. Buchholz, S. Schilling, H. U. Demuth, Dipeptidyl-Peptidase Activity of Meprin β Links N-truncation of Aβ with Glutaminyl Cyclase-Catalyzed pGlu-Aβ Formation. *J. Alzheimers. Dis.* **66**, 359–375 (2018).

27. Y. Horikoshi, G. Sakaguchi, A. G. Becker, A. J. Gray, K. Duff, P. S. Aisen, H. Yamaguchi, M. Maeda, N. Kinoshita, Y. Matsuoka, Development of Aβ terminal end-specific antibodies and sensitive ELISA for Aβ variant. *Biochem. Biophys. Res. Commun.* **319**, 733–737 (2004).
28. T. Jefferson, M. Čaušević, U. Auf Dem Keller, O. Schilling, S. Isbert, R. Geyer, W. Maier, S. Tschickardt, T. Jumpertz, S. Weggen, J. S. Bond, C. M. Overall, C. U. Pietrzik, C. Becker-Pauly, Metalloprotease meprin β generates nontoxic N-terminal amyloid precursor protein fragments in vivo. *J. Biol. Chem.* **286**, 27741–27750 (2011).
29. D. Dominguez, J. Tournoy, D. Hartmann, T. Huth, K. Cryns, S. Deforce, L. Serneels, I. E. Camacho, E. Marjaux, K. Craessaerts, A. J. M. Roebroek, M. Schwake, R. D'Hooge, P. Bach, U. Kalinke, D. Moechars, C. Alzheimer, K. Reiss, P. Saftig, B. De Strooper, Phenotypic and biochemical analyses of BACE1- and BACE2-deficient mice. *J. Biol. Chem.* **280**, 30797–30806 (2005).
30. L. Devi, M. Ohno, Effects of BACE1 haploinsufficiency on APP processing and Aβ concentrations in male and female 5XFAD Alzheimer mice at different disease stages. *Neuroscience*. **307**, 128–137 (2015).
31. R. Wichert, F. Scharfenberg, C. Colmorgen, T. Koudelka, J. Schwarz, S. Wetzel, B. Potempa, J. Potempa, J. W. Bartsch, I. Sagi, A. Tholey, P. Saftig, S. Rose-John, C. Becker-Pauly, Meprin β induces activities of A disintegrin and metalloproteinases 9, 10, and 17 by specific prodomain cleavage. *FASEB J.* **33**, 11925–11940 (2019).
32. S. Weber, M. T. Niessen, J. Prox, R. Lüllmann-Rauch, A. Schmitz, R. Schwanbeck, C. P. Blobel, E. Jorissen, B. De Strooper, C. M. Niessen, P. Saftig, The disintegrin/metalloproteinase Adam10 is essential for epidermal integrity and Notch-mediated signaling. *Development*. **138**, 495–505 (2011).
33. B. De Strooper, Aph-1, Pen-2, and Nicastrin with Presenilin generate an active γ-Secretase complex. *Neuron*. **38** (2003), pp. 9–12.
34. J. M. Gunnersen, M. H. Kim, S. J. Fuller, M. De Silva, J. M. Britto, V. E. Hammond, P. J. Davies, S. Petrou, E. S. L. Faber, P. Sah, S. S. Tan, Sez-6 Proteins Affect Dendritic Arborization Patterns and Excitability of Cortical Pyramidal Neurons. *Neuron*. **56**, 621–639 (2007).
35. A. Tanghe, A. Termont, P. Merchiers, S. Schilling, H. U. Demuth, L. Scrocchi, F. Van Leuven, G. Griffioen, T. Van Dooren, Pathological hallmarks, clinical parallels, and value for drug testing in Alzheimer's disease of the APP[V717I] London transgenic mouse model. *Int. J. Alzheimers. Dis.* **2010** (2010), doi:10.4061/2010/417314.
36. A. Savastano, H. Klafki, U. Haußmann, T. J. Oberstein, P. Muller, O. Wirths, J. Wiltfang, T. A. Bayer, N-Truncated Aβ2-X Starting with Position Two in Sporadic Alzheimer's Disease Cases and Two Alzheimer Mouse Models. *J. Alzheimer's Dis.* **49**, 101–110 (2015).
37. S. Zampar, H. W. Klafki, K. Sritharen, T. A. Bayer, J. Wiltfang, A. Rostagno, J. Ghiso, L. A. Miles, O. Wirths, N-terminal heterogeneity of parenchymal and vascular amyloid-β deposits in Alzheimer's disease. *Neuropathol. Appl. Neurobiol.* **46**, 673–685 (2020).

38. J. V. Dorpe, L. Smeijers, I. Dewachter, D. Nuyens, K. Spittaels, C. Van den Haute, M. Mercken, D. Moechars, I. Laenen, C. Kuiperi, K. Bruynseels, I. Tesseur, R. Loos, H. Vanderstichele, F. Checler, R. Sciot, F. Van Leuven, Prominent cerebral amyloid angiopathy in transgenic mice overexpressing the London mutant of human APP in neurons. *Am. J. Pathol.* **157**, 1283–1298 (2000).
39. C. Acosta, H. D. Anderson, C. M. Anderson, Astrocyte dysfunction in Alzheimer disease. *J. Neurosci. Res.* **95**, 2430–2447 (2017).
40. M. T. Heneka, M. Sastre, L. Dumitrescu-Ozimek, I. Dewachter, J. Walter, T. Klockgether, F. Van Leuven, Focal glial activation coincides with increased BACE1 activation and precedes amyloid plaque deposition in APP[V717I] transgenic mice. *J. Neuroinflammation*. **2**, 22 (2005).
41. B. G. Perez-Nievas, A. Serrano-Pozo, Deciphering the astrocyte reaction in Alzheimer's disease. *Front. Aging Neurosci.* **10**, 114 (2018).
42. J. E. Burda, M. V Sofroniew, Reactive gliosis and the multicellular response to CNS damage and disease (2014), doi:10.1016/j.neuron.2013.12.034.
43. U. Schmitt, C. Hiemke, F. Fahrenholz, A. Schroeder, Over-expression of two different forms of the α-secretase ADAM10 affects learning and memory in mice. *Behav. Brain Res.* **175**, 278–284 (2006).
44. A. Piechotta, C. Parthier, M. Kleinschmidt, K. Gnoth, T. Pillot, I. Lues, H. U. Demuth, S. Schilling, J. U. Rahfeld, M. T. Stubbs, Structural and functional analyses of pyroglutamate-amyloid-β-specific antibodies as a basis for Alzheimer immunotherapy. *J. Biol. Chem.* **292**, 12713–12724 (2017).
45. G. Antonios, H. Borgers, B. C. Richard, A. Brauß, J. Meißner, S. Weggen, V. Pena, T. Pillot, S. L. Davies, P. Bakrania, D. Matthews, J. Brownlees, Y. Bouter, T. A. Bayer, Alzheimer therapy with an antibody against N-terminal Abeta 4-X and pyroglutamate Abeta 3-X. *Sci. Rep.* **5**, 17338 (2015).
46. H. Crehan, B. Liu, M. Kleinschmidt, J.-U. Rahfeld, K. X. Le, B. J. Caldarone, J. L. Frost, T. Hettmann, B. Hutter-Paier, B. O'Nuallain, M.-A. Park, M. F. DiCarli, I. Lues, S. Schilling, C. A. Lemere, Effector function of anti-pyroglutamate-3 Aβ antibodies affects cognitive benefit, glial activation and amyloid clearance in Alzheimer's-like mice. *Alzheimers. Res. Ther.* **12**, 12 (2020).
47. H. Schieb, H. Kratzin, O. Jahn, W. Möbius, S. Rabe, M. Staufenbiel, J. Wiltfang, H. W. Klafki, β-amyloid peptide variants in brains and cerebrospinal fluid from amyloid precursor protein (APP) transgenic mice: Comparison with human Alzheimer amyloid. *J. Biol. Chem.* **286**, 33747–33758 (2011).
48. W. Kalback, M. D. Watson, T. A. Kokjohn, Y. M. Kuo, N. Weiss, D. C. Luehrs, J. Lopez, D. Brune, S. S. Sisodia, M. Staufenbiel, M. Emmerling, A. E. Roher, APP transgenic mice Tg2576 accumulate Aβ peptides that are distinct from the chemically modified and insoluble peptides deposited in Alzheimer's disease senile plaques. *Biochemistry*. **41**, 922–928 (2002).
49. B. Dislich, S. F. Lichtenthaler, The membrane-bound aspartyl protease BACE1: Molecular and functional properties in Alzheimer's disease and beyond. *Front. Physiol.* **3 FEB** (2012), p. 8.
50. C. Sturchler-Pierrat, D. Abramowski, M. Duke, K. H. Wiederhold, C. Mistl, S. Rothacher,

B. Ledermann, K. Bürki, P. Frey, P. A. Paganetti, C. Waridel, M. E. Calhoun, M. Jucker, A. Probst, M. Staufenbiel, B. Sommer, Two amyloid precursor protein transgenic mouse models with Alzheimer disease-like pathology. *Proc. Natl. Acad. Sci. U. S. A.* **94**, 13287–13292 (1997).

51. A. Piccini, C. Russo, A. Gliozzi, A. Relini, A. Vitali, R. Borghi, L. Giliberto, A. Armirotti, C. D'Arrigo, A. Bachi, A. Cattaneo, C. Canale, S. Torrassa, T. C. Saido, W. Markesbery, P. Gambetti, M. Tabaton, β-amyloid is different in normal aging and in Alzheimer disease. *J. Biol. Chem.* **280**, 34186–34192 (2005).
52. E. Portelius, T. Lashley, A. Westerlund, R. Persson, N. C. Fox, K. Blennow, T. Revesz, H. Zetterberg, Brain amyloid-beta fragment signatures in pathological ageing and alzheimer's disease by hybrid immunoprecipitation mass spectrometry. *Neurodegener. Dis.* **15**, 50–57 (2015).
53. L. F. Lue, Y. M. Kuo, A. E. Roher, L. Brachova, Y. Shen, L. Sue, T. Beach, J. H. Kurth, R. E. Rydel, J. Rogers, Soluble amyloid β peptide concentration as a predictor of synaptic change in Alzheimer's disease. *Am. J. Pathol.* **155**, 853–862 (1999).
54. O. Wirths, S. Walter, I. Kraus, H. W. Klafki, M. Stazi, T. J. Oberstein, J. Ghiso, J. Wiltfang, T. A. Bayer, S. Weggen, N-truncated Aβ4-x peptides in sporadic Alzheimer's disease cases and transgenic Alzheimer mouse models. *Alzheimer's Res. Ther.* **9**, 80 (2017).
55. Y. Bouter, K. Dietrich, J. L. Wittnam, N. Rezaei-Ghaleh, T. Pillot, S. Papot-Couturier, T. Lefebvre, F. Sprenger, O. Wirths, M. Zweckstetter, T. A. Bayer, N-truncated amyloid β (Aβ) 4-42 forms stable aggregates and induces acute and long-lasting behavioral deficits. *Acta Neuropathol.* **126**, 189–205 (2013).
56. H. Lewis, D. Beher, N. Cookson, A. Oakley, M. Piggott, C. M. Morris, E. Jaros, R. Perry, P. Ince, R. A. Kenny, C. G. Ballard, M. S. Shearman, R. N. Kalaria, Quantification of Alzheimer pathology in ageing and dementia: Age-related accumulation of amyloid-β(42) peptide in vascular dementia. *Neuropathol. Appl. Neurobiol.* **32**, 103–118 (2006).
57. M. Shinohara, S. Koga, T. Konno, J. Nix, M. Shinohara, N. Aoki, P. Das, J. E. Parisi, R. C. Petersen, T. L. Rosenberry, D. W. Dickson, G. Bu, Distinct spatiotemporal accumulation of N-truncated and full-length amyloid-β42 in Alzheimer's disease. *Brain*. **140**, 3301–3316 (2017).
58. M. Bibl, M. Gallus, V. Welge, H. Esselmann, S. Wolf, E. Rüther, J. Wiltfang, Cerebrospinal fluid amyloid-β 2-42 is decreased in Alzheimer's, but not in frontotemporal dementia. *J. Neural Transm.* **119**, 805–813 (2012).
59. D. Moechars, I. Dewachter, K. Lorent, D. Reversé, V. Baekelandt, A. Naidu, I. Tesseur, K. Spittaels, C. Van Den Haute, F. Checler, E. Godaux, B. Cordell, F. Van Leuven, Early phenotypic changes in transgenic mice that overexpress different mutants of amyloid precursor protein in brain. *J. Biol. Chem.* **274**, 6483–6492 (1999).
60. W. S. Chung, C. A. Welsh, B. A. Barres, B. Stevens, Do glia drive synaptic and cognitive impairment in disease? *Nat. Neurosci.* **18**, 1539–1545 (2015).
61. S. Jo, O. Yarishkin, Y. J. Hwang, Y. E. Chun, M. Park, D. H. Woo, J. Y. Bae, T. Kim, J. Lee, H. Chun, H. J. Park, D. Y. Lee, J. Hong, H. Y. Kim, S. J. Oh, S. J. Park, H. Lee, B. E. Yoon, Y. Kim, Y. Jeong, I. Shim, Y. C. Bae, J. Cho, N. W. Kowall, H. Ryu, E. Hwang, D. Kim, C. J. Lee, GABA from reactive astrocytes impairs memory in mouse models of

Alzheimer's disease. *Nat. Med.* **20**, 886–896 (2014).
62. L. Liu, L. Ding, M. Rovere, M. S. Wolfe, D. J. Selkoe, A cellular complex of BACE1 and γ-secretase sequentially generates Aβ from its full-length precursor. *J. Cell Biol.* **218**, 644–663 (2019).
63. H. Cai, Y. Wang, D. McCarthy, H. Wen, D. R. Borchelt, D. L. Price, P. C. Wong, BACE1 is the major β-secretase for generation of Aβ peptides by neurons. *Nat. Neurosci.* **4**, 233–234 (2001).
64. L. P. Norman, W. Jiang, X. Han, T. L. Saunders, J. S. Bond, Targeted Disruption of the Meprin β Gene in Mice Leads to Underrepresentation of Knockout Mice and Changes in Renal Gene Expression Profiles. *Mol. Cell. Biol.* **23**, 1221–1230 (2003).
65. S. Jäger, S. Leuchtenberger, A. Martin, E. Czirr, J. Wesselowski, M. Dieckmann, E. Waldron, C. Korth, E. H. Koo, M. Heneka, S. Weggen, C. U. Pietrzik, α-secretase mediated conversion of the amyloid precursor protein derived membrane stub C99 to C83 limits Aβ generation. *J. Neurochem.* **111**, 1369–1382 (2009).
66. H. W. Klafki, J. Wiltfang, M. Staufenbiel, Electrophoretic separation of betaA4 peptides (1-40) and (1-42). *Anal. Biochem.* **237**, 24–29 (1996).
67. S. Soriano, D. C. Lu, S. Chandra, C. U. Pietrzik, E. H. Koo, The Amyloidogenic Pathway of Amyloid Precursor Protein (APP) Is Independent of Its Cleavage by Caspases. *J. Biol. Chem.* **276**, 29045–29050 (2001).
68. O. Wirths, G. Multhaup, C. Czech, N. Feldmann, V. Blanchard, G. Tremp, K. Beyreuther, L. Pradier, T. A. Bayer, Intraneuronal APP/Aβ trafficking and plaque formation in β-amyloid precursor protein and presenilin-1 transgenic mice. *Brain Pathol.* **12**, 275–286 (2002).

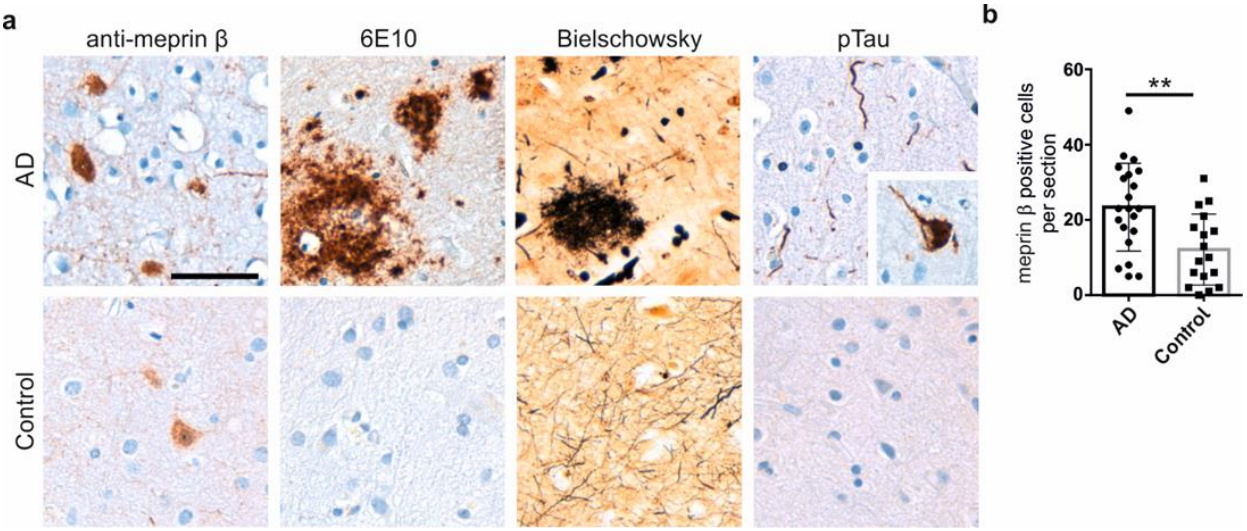

Fig.1 Meprin β expression in brains of AD patients. (A) Representative images of human brain sections from an AD patient and an age-matched, non-demented individual (control). Immunostainings were performed with anti-meprin β antibody, anti-Aβ1-16 (6E10), for the detection of Aβ aggregates, Bielschowsky silver stain, which impregnates both amyloid senile plaques and neurofibrillary tangles, and anti-phosphorylated Tau protein (AT8) antibody. Scale bars = 100 µm. Note Aβ accumulation, neuritic plaques and pTau stainings confirming AD diagnosis. **(B)** Densitometric analysis of meprin β-positive neurons in cortical sections revealed a significantly higher number of meprin β positive neurons in AD compared to control brains from non-AD individuals. Graph shows mean ± S.E.M. (n=21 AD, n=17 Control; $^{**}p<0.05$, *t*-test). Representative comparison of all cases analysed can be found in supplementary Fig. S2.

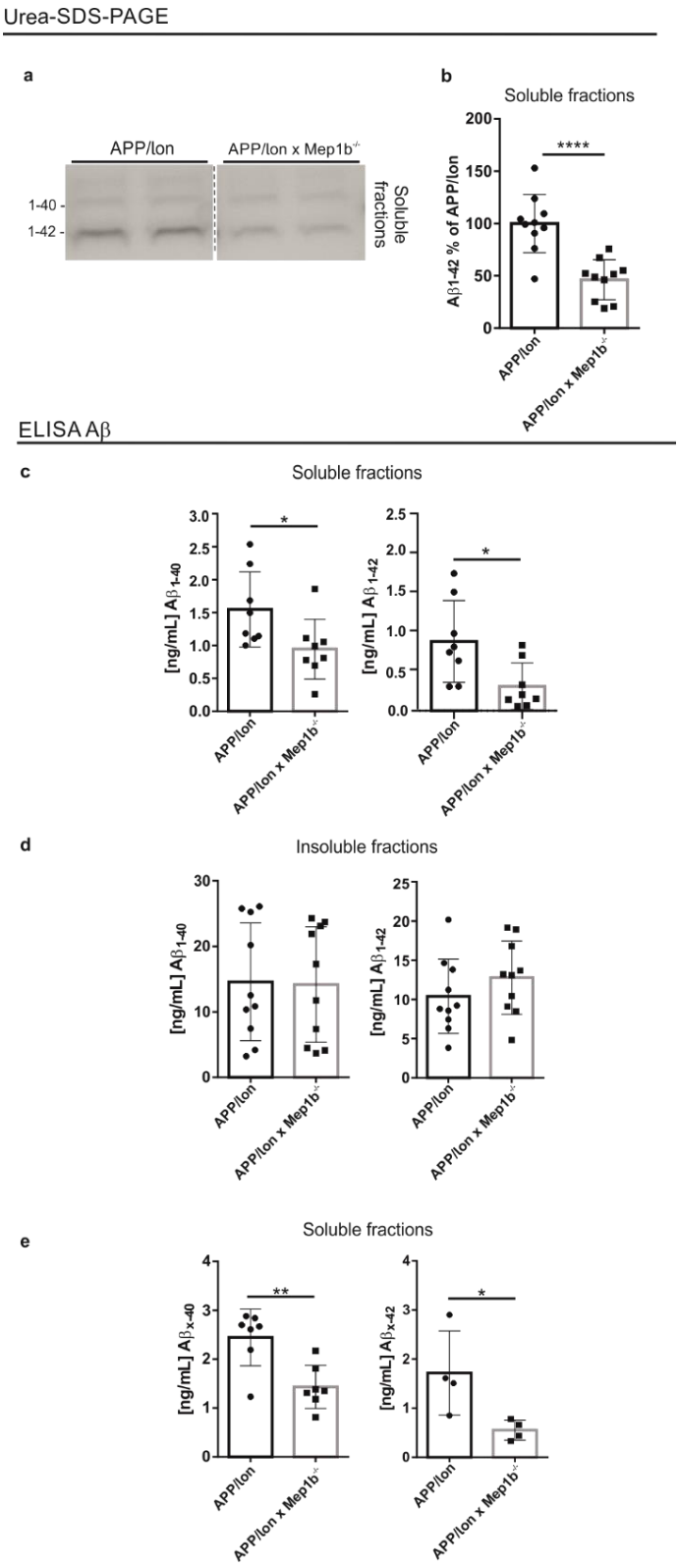

Fig.2 Aβ levels are reduced in APP/lon mice knockout for meprin β. (A) Soluble extracted brain fractions from 15-month-old APP/lon and APP/lon x Mep1b$^{-/-}$ mice were analyzed by immunoblot for Aβ peptides species. Samples were on the same gel but are rearranged for better presentation. **(B)** Densitometric analysis of $A\beta_{1\text{-}42}$ levels show a decrease in soluble fractions

(****p<0.0001, *t*-test, n= 10). **(C)** ELISA analysis showed decreased levels of 1-40 (*p<0.05, *t*-test, n= 8) and 1-42 (*p<0.05, *t*-test, n= 8) in soluble fractions of APP/lon x Mep1b$^{-/-}$ compared to APP/lon mice. **(D)** No differences were detected in insoluble brain fractions (n= 10). **(E)** A following ELISA approach revealed reduced levels of Aβ x-40 (p<0.005, *t*-test, n=7) and x-42 (p<0.05, *t*-test, n=4) in soluble brain fractions of APP/lon x Mep1b$^{-/-}$.

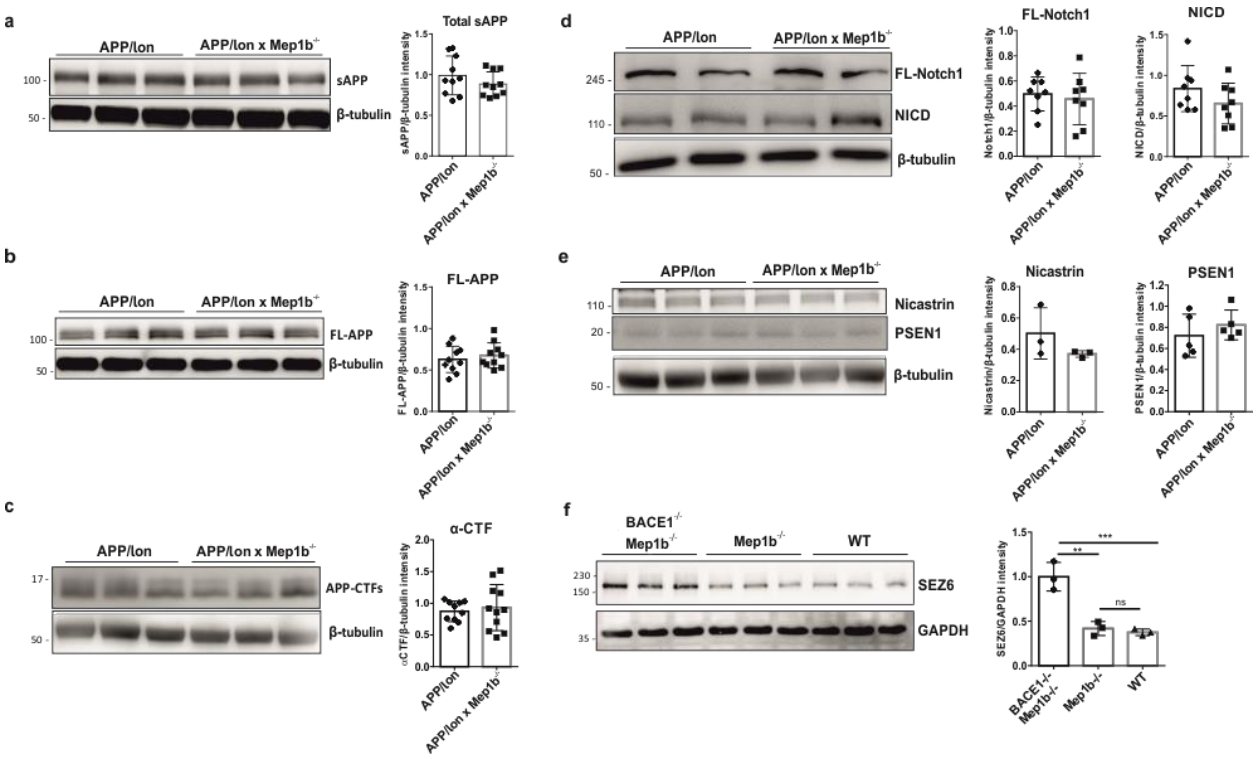

Fig.3 The meprin β knockout has no evident effect on the overall APP processing and its secretases. **(A)** Soluble brain fractions of 15-month-old APP/lon and APP/lon x Mep1b$^{-/-}$ mice (n=10/ group) were analyzed by immunoblot for sAPP forms using the monoclonal antibody 22C11. **(B)** Further immunoblot analysis of insoluble brain fractions using an antibody against the C-terminus of full-length APP and **(C)** CTFs in 15-month-old APP/lon and APP/lon x Mep1b$^{-/-}$ mice (n= 10/group). **(D)** Immunoblot analysis shows protein levels for Notch1 and NICD (n=8/ group) and **(E)** γ-secretase subunits PSEN1 and Nicastrin in insoluble fractions of APP/lon and APP/lon x Mep1b$^{-/-}$ mice (n=5/ group). **(F)** Total brain lysates from double knockout mice for BACE1 and meprin β, as well as Mep1b$^{-/-}$ and WT mice were analyzed by immunoblot for Sez6. **(A-E)** Densitometric analyses normalized to α-tubulin revealed no significant differences. **(F)** Densitometric analysis normalized to GAPDH detected an increase in levels of endogenous Sez6 in the double knockout mice lacking BACE1, but no significant differences were found in meprin β knockout compared to WT brain homogenates.

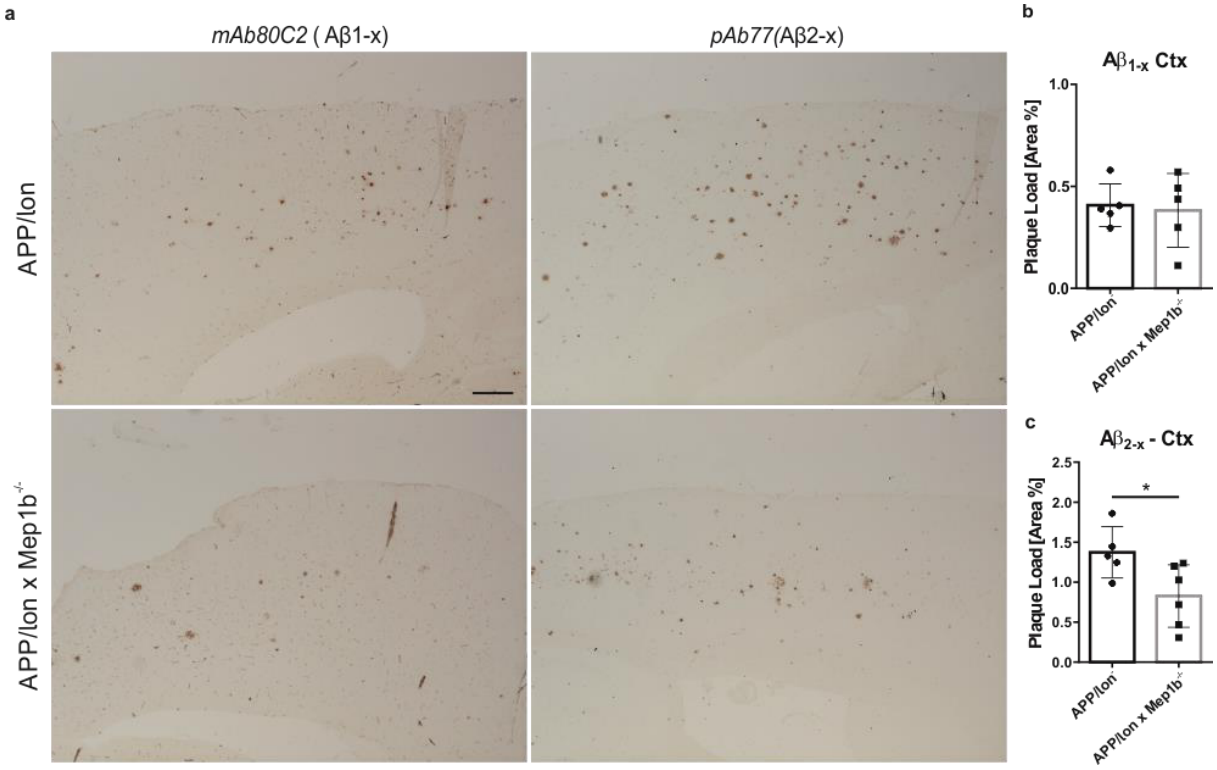

Fig.4 N-terminally truncated Aβ2-x peptide deposition is decreased in APP/lon mice lacking meprin β. (A) Representative image of cortices of sagittal brain sections from 15-month-old APP/lon and APP/lon x Mep1b$^{-/-}$ which were embedded in paraffin and stained for Aβ1-x (mAb 80C2) and Aβ2-x (pAb77) plaque load. Detection was made possible through hydrogen peroxidase and 3,3'-diaminobenzidine (DAB) reaction. **(B)** Quantitative analysis showing the percentage of stained area for Aβ1-x peptides (n=5). **(C)** Quantitative analysis showing percentage of stained area for N-terminally truncated Aβ2-x peptides (*$p<0.05$, *t*-test, n= 5-6). Scale bar = 100 µm.

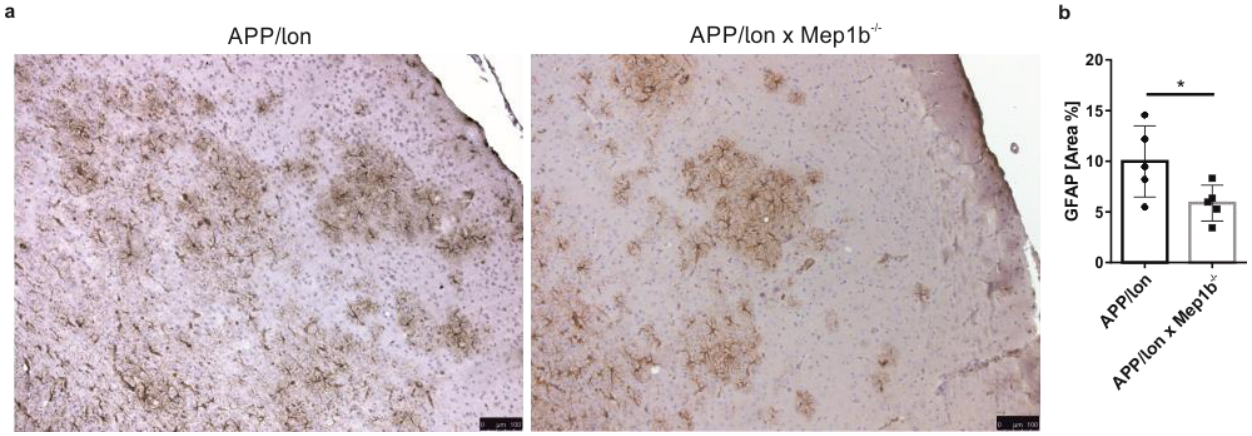

Fig.5 GFAP immunoreactivity is increased in the cortex of APPlon x Mep1b$^{-/-}$ mice. (A) Representative image of sagittal brain sections from 15-month-old APP/lon and APP/lon x Mep1b$^{-/-}$ embedded in paraffin and stained for GFAP and hematoxylin. **(B)** Quantitative analysis showing the percentage area covered by DAB staining (*$p<0.05$, *t*-test, n=5/group). Scale bar = 100 µm.

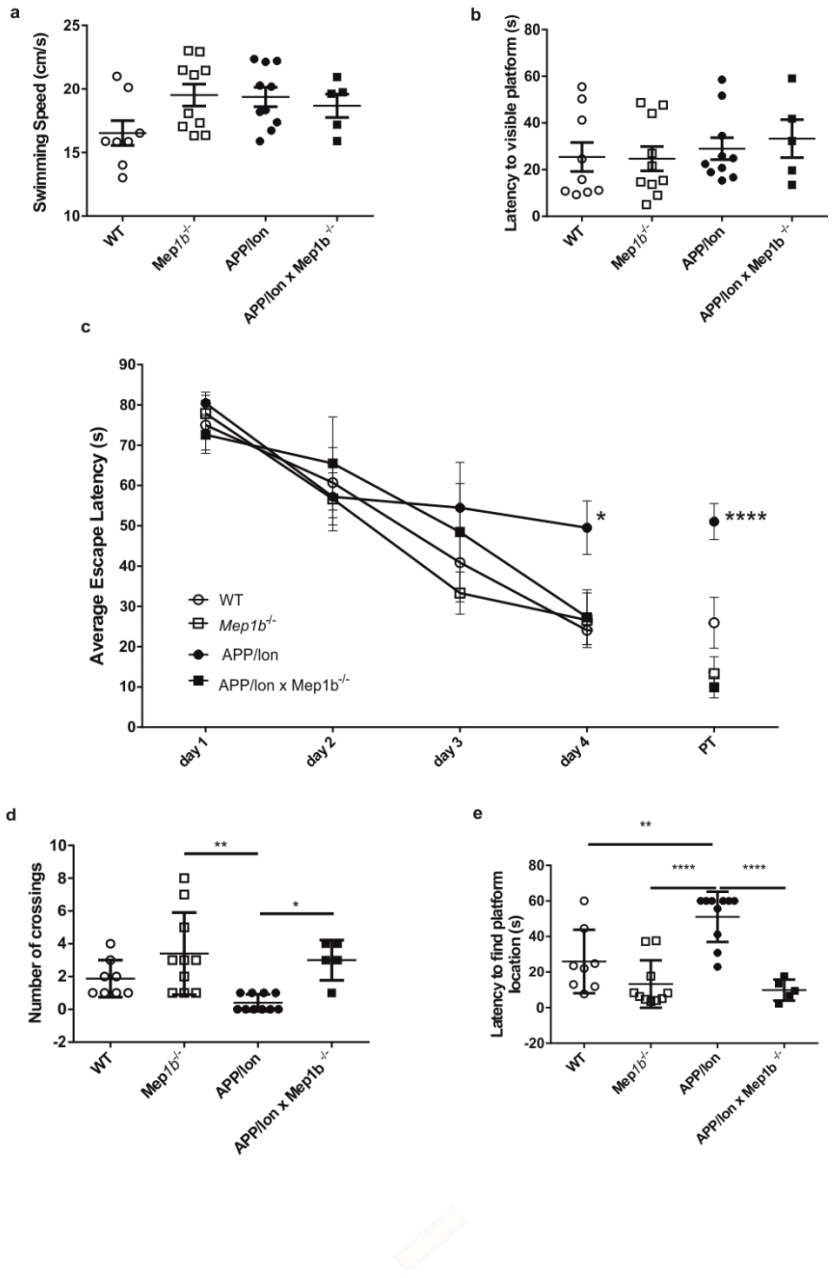

Fig.6 Meprin β knockout rescues cognitive impairments in APP/lon mice. Spatial learning and memory tests were carried out on 7-month-old APP/lon, APP/lon x Mep1b$^{-/-}$, Mep1b$^{-/-}$, and wild-type mice using the Morris water maze setting. **(A)** Swimming speed analysis showed no motor impairment in any of the groups. **(B)** Latency to find visible platform was evaluated after probe trial and no specific deficits were detected. **(C)** The average escape latency in each trial was measured for 4 days and 24 hours later all experimental groups were subjected to a probe trial (PT) in which the platform was removed. On day 4, APP/lon showed significant learning deficit compared to WT mice (*p<0.05) and to Mep1b$^{-/-}$ (*p<0.05), but not to APP/lon x Mep1b$^{-/-}$ mice. Data shown is the mean±SEM of four different trials performed on day 4. Interestingly, on PT day, cognitive deficits are prominent in APP/lon when compared to WT (*p<0.05), Mep1b-/- (****p<0.0001) and APP/lon x Mep1b$^{-/-}$ mice (***p<0.0001). Graph shows latency to find platform location in one probe trial. Data is presented as mean ±SEM. Statistical analysis

performed with one-way ANOVA followed by Tukey's post hoc test. **(D)** Memory was evaluated by measuring the numbers of crossings over the former platform location. APP/lon mice showed significant differences when compared to Mep1b$^{-/-}$ or APP/lon x Mep1b$^{-/-}$ (*$p<0.05$, **$p=0.0016$). **(E)** Latency to reach platform location in all four groups. APPlon mice took the longest time to reach platform location when compared to all other groups (**$p<0.05$, ****$p<0.0001$) Data are presented as mean± SD (n=5-10)

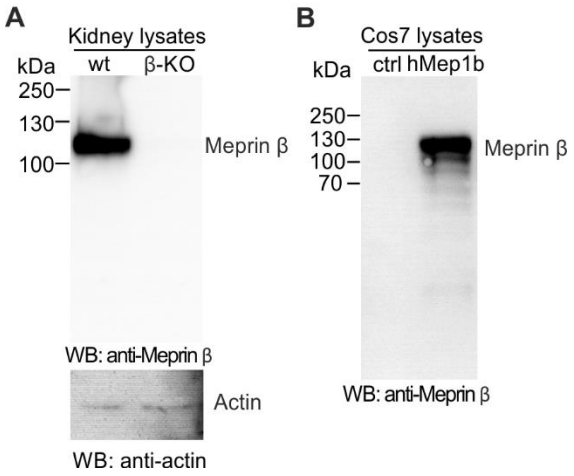

Fig. S1 Meprin β antibody specificity analysis. (A) Isolated kidneys of representative wt and Mep1b-KO mice were lysed, equal amounts of protein per sample were loaded on SDS-PAGE and meprin β expression was analyzed by immunoblot. **(B)** Cos7-cells were transfected with human wt-meprin β and immunoblot analysis was performed.

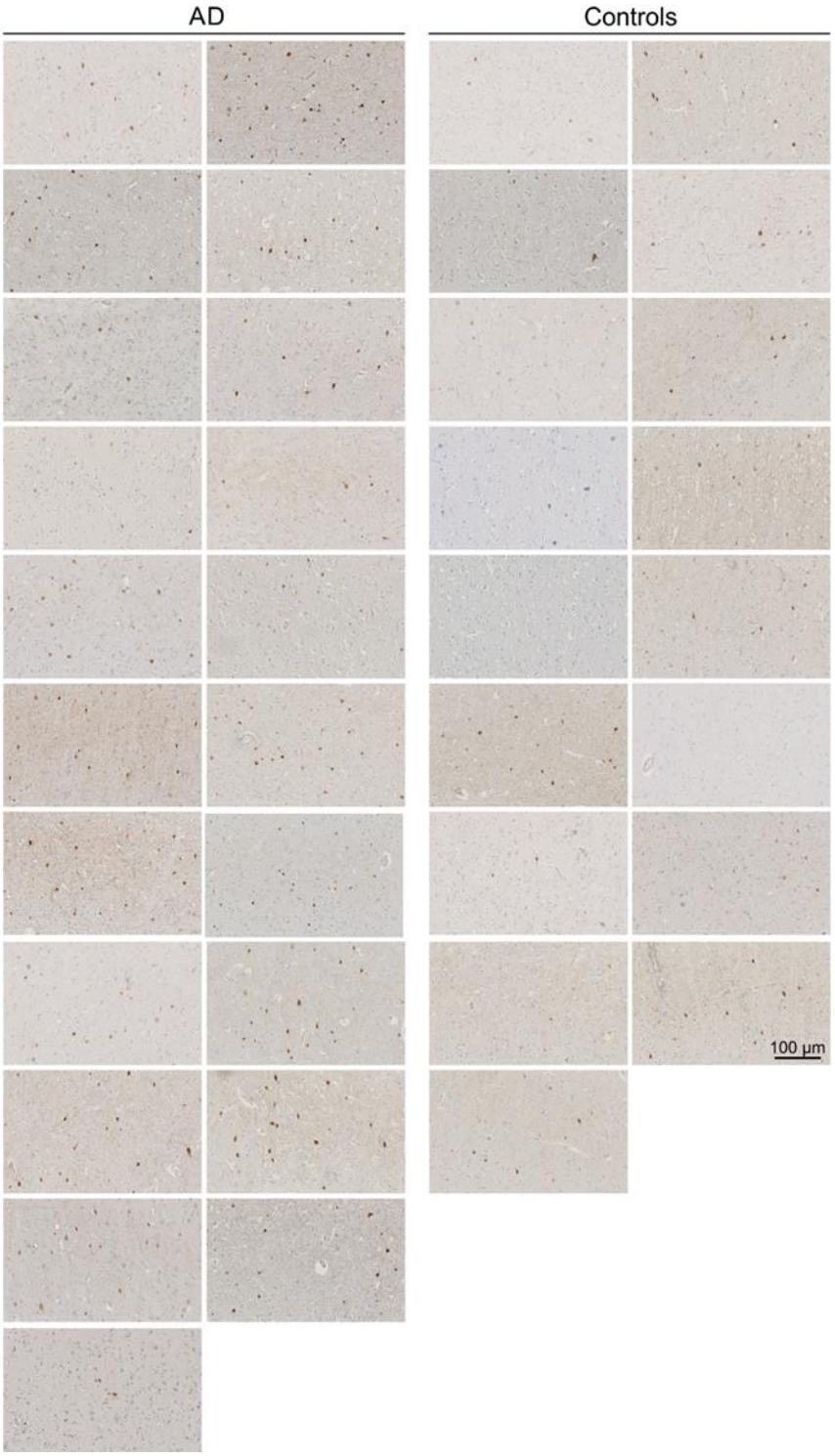

Fig. S2 Increased meprin β expression in brains of AD patients. Immunostainings of human brain slices of AD patients, non-demented and non-AD patients were performed with polyclonal anti-meprin β antibody.

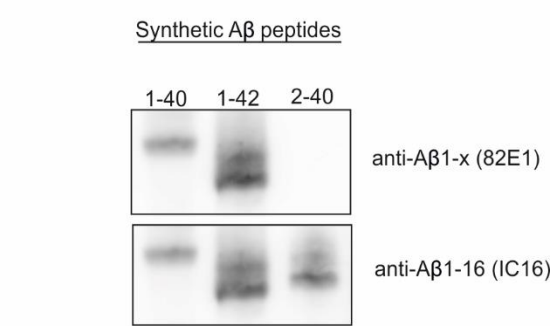

Fig. S3 Aβ1-x antibody specificity analysis. Representative image of Urea-SDS-PAGE using synthetic Aβ peptides.The 82E1 antibody detects Aβ1-40 and Aβ1-42, but not Aβ2-40. Same membrane was reprobed with the IC16 antibody and revealed the synthetic 2-40 peptide.

Received: 26 August 2019 | Revised: 3 December 2019 | Accepted: 12 March 2020

DOI: 10.1096/fj.201902183R

RESEARCH ARTICLE

THE FASEB JOURNAL

Meprin β cleaves TREM2 and controls its phagocytic activity on macrophages

Dennis Kristopher Berner[1] | Luisa Wessolowski[1] | Fred Armbrust[1] | Janna Schneppenheim[2] | Kai Schlepckow[3] | Tomas Koudelka[4] | Franka Scharfenberg[1] | Ralph Lucius[2] | Andreas Tholey[4] | Gernot Kleinberger[5,6] | Christian Haass[3,5,6] | Philipp Arnold[2] | Christoph Becker-Pauly[1]

[1]Unit for Degradomics of the Protease Web, Biochemical Institute, University of Kiel, Kiel, Germany

[2]Anatomical Institute, University of Kiel, Kiel, Germany

[3]German Center for Neurodegenerative Diseases (DZNE), Munich, Germany

[4]Systematic Proteomics & Bioanalytics, Institute for Experimental Medicine, University of Kiel, Kiel, Germany

[5]Biomedical Center, Biochemistry, Ludwig-Maximilians-Universität Munich, Munich, Germany

[6]Munich Cluster for Systems Neurology, Munich, Germany

Correspondence
Christoph Becker-Pauly, Unit for Degradomics of the Protease Web, Biochemical Institute, Christian-Albrechts-University Kiel, Otto-Hahn-Platz 9, 24118 Kiel, Germany.
Email: cbeckerpauly@biochem.uni-kiel.de

Present address
Gernot Kleinberger, ISAR Bioscience GmbH, Semmelweisstrasse 5, D-82152, Planegg, Germany

Funding information
Deutsche Forschungsgemeinschaft (DFG), Grant/Award Number: 125440785 SFB877 A9/A15, 125440785 SFB877 Z2, 125440785 SFB877 A13, BE 4086/2-2, EXC 1010 SyNergy, HA1737/16-1 and FOR2290

Abstract

The triggering receptor expressed on myeloid cells 2 (TREM2) is a multifunctional surface protein that affects survival, migration, and phagocytic capacity of myeloid cells. Soluble TREM2 levels were found to be increased in early stages of sporadic and familial Alzheimer's disease (AD) probably reflecting a defensive microglial response to some initial brain damage. The disintegrin and metalloproteases (ADAM) 10 and 17 were identified as TREM2 sheddases. We demonstrate that meprin β is a direct TREM2 cleaving enzyme using ADAM10/17 deficient HEK293 cells. LC-MS/MS analysis of recombinant TREM2 incubated with meprin β revealed predominant cleavage between Arg136 and Asp137, distant to the site identified for ADAM10/17. We further demonstrate that the metalloprotease meprin β cleaves TREM2 on macrophages concomitant with decreased levels of soluble TREM2 in the serum of *Mep1b*$^{-/-}$ mice compared to WT controls. Isolated BMDMs from *Mep1b*$^{-/-}$ mice showed significantly increased full-length TREM2 levels and enhanced phagocytosis efficiency compared to WT cells. The diminished constitutive shedding of TREM2 on meprin β deficient macrophages could be rescued by ADAM stimulation through LPS treatment. Our data provide evidence that meprin β is a TREM2 sheddase on macrophages and suggest that multiple proteases may be involved in the generation of soluble TREM2.

Abbreviations: AD, Alzheimer's disease; ADAM, a disintegrin and metalloprotease; APP, amyloid precursor protein; BMDM, bone marrow derived macrophage; CTF, C-terminal fragment; ICD, intracellular domain; TREM2, triggering receptor expressed on myeloid cells 2.

Dennis Kristopher Berner and Luisa Wessolowski contributed equally to this work.

KEYWORDS

ADAM10, Alzheimer's disease, cell surface protein, meprin β, metalloprotease, phagocytosis, protein-protein interaction, TREM2

1 | INTRODUCTION

Triggering receptor expressed on myeloid cells 2 (TREM2) is a type 1 transmembrane protein that is expressed on myeloid cells such as macrophages, dendritic cells, and microglia.[1] TREM2 is thought to be involved in different signaling pathways, thereby influencing cell differentiation, survival, proliferation, activation, and phagocytic potential.[2] Several mutations within the stalk region and the Ig-like V type domain of TREM2 were associated with an increased risk to develop Alzheimer's disease (AD).[3-6] If and how TREM2 function affects amyloid plaque metabolism is controversially discussed. It is reported that a loss of TREM2 function affects plaque morphology leading to larger and more diffuse plaques associated with more neuritic pathology and less clustered microglia (summarized in (7)). Along the same line, it was recently demonstrated that in the absence of functional TREM2 early amyloidogenesis is accelerated due to reduced phagocytic clearance of amyloid seeds despite reduced plaque-associated ApoE.[8] On the contrary, it was shown that TREM2 deficiency eliminates TREM2-positive inflammatory macrophages and ameliorates pathology in AD mouse models.[9] Although no definite endogenous ligand has been described to date a preference for anionic and lipid-like substances has been observed.[10-12] It was shown that TREM2 can bind LPS[13] and Aβ peptides,[14-16] which induces phagocytosis in cells. However, TREM2 cannot transduce the signal by itself, but requires the adaptor protein DNAX-activation protein 12 (DAP12), which can be phosphorylated, and then, stimulates a variety of intracellular pathways.[13,17] TREM2 is shed from the cell surface by the disintegrin and metalloproteases 10 and 17 (ADAM10 and ADAM17), leaving a C-terminal fragment (CTF) that is prone to proteolysis by the γ-secretase complex[18-21] (Figure 1A). Cleavage of TREM2 by ADAM10 occurs between His157 and Ser158, which is enhanced by the AD-associated variant H157Y.[20,21] Shedding of TREM2 from the cell surface may terminate signaling, and therefore, reduce the phagocytic capacity of microglia and macrophages.[18,20] The resulting soluble TREM2 (sTREM2) was shown to induce ERK and MAPK14 signaling in bone marrow derived macrophages (BMDM)[22] and NFκB signaling in microglia inducing pro-inflammatory cytokine expression and prolonged cell survival.[13,23] Additionally, sTREM2 increases early in AD and may serve as a surrogate marker for microglial activation.[18,24]

Meprin β belongs to the astacin family of metalloproteinases and exhibits striking cleavage specificity with a preference for negatively charged amino acids around the scissile bond.[25] Similar to ADAM10 and ADAM17, meprin β was found to cleave several cell surface proteins such as the amyloid precursor protein (APP) at the β-secretase site,[26] the IL-6 receptor on human granulocytes to induce IL-6 trans-signaling,[27] and CD99 on endothelial cells, thereby promoting transendothelial cell migration.[28,29]

Here, we demonstrate that meprin β sheds membrane bound TREM2 and rapidly degrades the soluble ectodomain. However, the identified major cleavage site for meprin β in TREM2 between Arg136 and Asp137 is N-terminal to the ADAM10 site, thus, generating slightly different CTFs and soluble TREM2 species. Meprin β co-expression with TREM2 significantly decreased the phagocytic potential of macrophages. Physiological relevance of this proteolytic cleavage is supported by strong accumulation of TREM2 on the surface of BMDMs isolated from meprin β knock-out mice and decreased serum levels of sTREM2 in these animals compared to wild-type controls.

2 | MATERIALS AND METHODS

2.1 | Cell culture and transient transfection

Cells were cultured in DMEM (Dulbecco's modified Eagle's medium; Gibco), supplemented with 10% (v/v) of FBS, 100 units/mL penicillin, and 100 μg/mL streptomycin. Culture conditions were under a humidified atmosphere (5% of CO_2) at 37°C. Generation of HEK293_ADAM10/17$^{-/-}$ cells was previously described.[30] For transient transfection, cells were seeded in 10 cm cell culture dishes. Plasmid cDNA for hTREM2, meprin β, ADAM10, empty vector (pcDNA3.1), or the TREM2-DAP12 fusion construct[20] was mixed with polyethylenimine (1:3) (Sigma-Aldrich) in serum-free medium and incubated at room temperature for 30 minutes. After 24 hours of transfection, medium was changed to serum-free DMEM to avoid inhibition of meprin β through FCS. For CTF analysis, 5 μM of DAPT were added to the medium at 5 and 20 hours. Cells were harvested 24 hours posttransfection. In the relevant experiments, 50 nM each of recombinant soluble meprin β (smeprin β),[31] smeprin α,[32] or of sADAM10[33] were added to the serum-free DMEM.

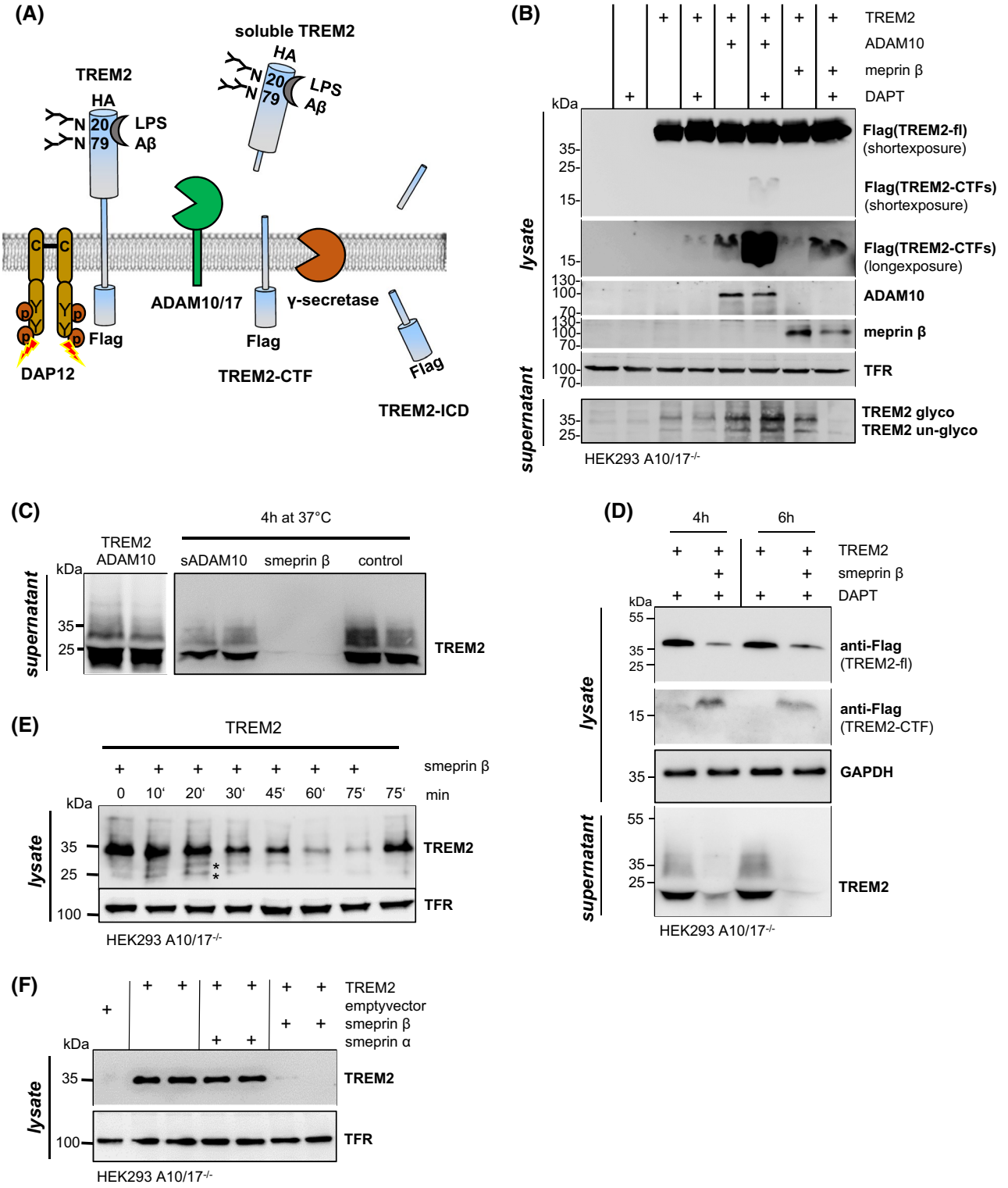

FIGURE 1 TREM2 is shed by meprin β in HEK293_ADAM10/17$^{-/-}$ cells. (A) Illustration of membrane bound TREM2 and DAP12. Upon shedding by ADAM10, the remaining C-terminal fragment (CTF) of TREM2 is cleaved within the membrane by γ-secretase, thereby releasing the intracellular domain (ICD). (B) Co-expression of TREM2 with meprin β or ADAM10 in HEK293_ADAM10/17$^{-/-}$ cells and Western blot analyses of TREM2 fragments in membrane-enriched fractions and cell supernatants. Anti-TFR antibody was used as loading control. (C) Conditioned media from TREM2 and ADAM10 transfected HEK293_ADAM10/17$^{-/-}$ cells were incubated with the recombinant ectodomains of meprin β and ADAM10 at 37°C for 4 hours. sTREM2 levels were analyzed by Western blot. (D) HEK293_ADAM10/17$^{-/-}$ cells transfected with TREM2 were incubated with recombinant meprin β and proteins from membrane-enriched fractions and cell supernatants were analyzed by Western blot. (E) Time series showing the cleavage of membrane bound TREM2 in HEK293_ADAM10/17$^{-/-}$ cells by recombinant soluble meprin β analyzed by Western blot. (F) Incubation of TREM2 overexpressing HEK293_ADAM10/17$^{-/-}$ cells with recombinant meprin α or meprin β and analysis of TREM2 by Western blot. All transient cell transfections and Western blot analyses were at least performed in biological triplicates

2.2 | Cell lysates, SDS-PAGE, and Western blot

Cell supernatants were collected and cells were harvested with a cell scraper and washed three times in ice-cold PBS. Cells were then incubated in membrane fractioning buffer (1 mM of EDTA, 1 mM of EGTA, 10 mM of TRIS, pH 7.0) for 30 minutes at 4°C and subsequently snap frozen in liquid nitrogen. After centrifugation for 30 minutes at 13 000 rpm at 4°C, pellets were suspended in EDTA-containing lysis buffer (1% (v/v) of Triton X-100 in PBS, pH 7.4) and incubated for 45 minutes. Lysates were centrifuged for 20 minutes at 15 000*g* at 4°C and protein amount was determined using the BCA protein assay kit (Thermo Fisher Scientific) following the manufacturer's instructions. Lysates were denatured in sample buffer including DTT for 10 minutes at 95°C.

Conditioned medium was collected after 24 hours, centrifuged at 1100*g* for 5 minutes and supplemented with a protease inhibitor cocktail (cOmplete EDTA-free, Roche). Supernatants were frozen at −20°C before analysis. For the analysis of soluble TREM2, 50 µL of Concanavalin A beads (C9017, Sigma) were added to 1 mL of supernatant and samples were incubated overnight. Beads were washed three times with sterile PBS before denaturation with sample buffer including DTT for 10 minutes at 95°C.

Samples were separated by SDS-PAGE (10% or 14% of gel) and blotted in a Tank Blot onto a PVDF-membrane. For immunoblot detection, the following antibodies were used: anti-human TREM2 (AF1828; R&D Systems; 1:1000), anti-murine TREM2 (clone 5F4)[34]; anti-flag (F1804; Sigma; 1:2000), anti-human meprin β (polyclonal, Pineda; 1:1000), anti-myc (9B11; Cell Signaling), anti-his (34660; Qiagen; 1:1000), anti-GAPDH (14C10; Cell Signaling; 1:2000), anti-TFR (ab84036; Abcam; 1:1000). The HRP-conjugated anti-goat (Jackson ImmunoResearch), anti-mouse (Jackson ImmunoResearch), and anti-rabbit (Jackson ImmunoResearch) were used as secondary antibodies.

2.3 | Bone marrow derived macrophages (BMDMS)

Macrophages derived from meprin β knock-out mice (*Mep1b*$^{-/-}$) were analyzed for TREM2 levels using murine-specific anti-TREM2 antibody (clone 5F4).[34] Mice were kept under specific pathogen free conditions in isolated ventilated cages, on a 12 hours light-dark cycle with food and water ad libitum. Mice were handled in accordance to the Guide for the Care and Use of Laboratory Animals of the German Animal Welfare Act on protection of animals. All animal protocols were approved by the Central Animal Facility of the University of Kiel and the relevant German authorities.

For isolation of primary macrophages, mice were killed by cervical dislocation. To get access to the BMDMs, extremities where amputated and transferred into sterile PBS. All surgical examinations took place under endotoxin-free conditions under a cell culture hood. Skin and muscles were carefully detached to isolate femur, crus, and humerus. Epiphysis were clipped off to allow access to the bone marrow in the medullary cavity of the diaphysis. By usage of sterile cannula (0.4 × 20 mm, Sterican, Braun) the medullary cavity was washed several times with DMEM. The obtained bone marrow in DMEM was then isolated with a cell strain (Falcon, A corning brand, 100 µm) and transferred into 50 mL Falcons. Collected cells where counted using a hemocytometer (C-chip, NanoEenTek, Neubauer improved, dhc-N01) and transferred into uncoated 10 cm cell culture dishes (TC-dish 100, Cell+, Sarstedt) in a density of 10^7 cells/dish and cultured in 10 mL DMEM (10% (v/v) of FCS) followed by substitution of 0.5 µg macrophage colony stimulating factor (M-CSF) per 10 mL DMEM. Cells were incubated for 5 days at 37°C. After 48 hours another 5 mL DMEM including 250 ng M-CSF were added. After 5 days, plates were washed three times with sterile PBS and macrophages were prepared for Western blotting or phagocytosis assay as described.

2.4 | Phagocytosis assay

Phagocytosis of fluorogenic *Escherichia coli* particles (pHrodo green *E coli*, Thermo Fisher Scientific) was analyzed using HEK293T ADAM10/17$^{-/-}$, PMA-induced THP-1, and U937 cells as well as primary macrophages (BMDMs) from mice. Cells were seeded in 96-well plates at a density of 8×10^4 cells per well 24 hours before phagocytosis measurements. After collection of the supernatants cells were washed two times with Live cell imaging solution (Thermo Fisher Scientific). *E coli* particles were added in a suspension of 1 µg/mL in Live cell imaging solution at a total of 50 µL/well. As a negative control, phagocytosis was inhibited with 10 µM of cytochalasin D (Life technologies), which was added 30 minutes prior to addition of pHrodo *E coli* bioparticles. Samples were incubated at 37°C for 120 minutes. Afterward, the suspension was carefully collected and cells were washed three times with MACS buffer (PBS pH 7.4, 0.5% (w/v) of BSA (Albumin Fraction V), 2 mM of EDTA). Cells were subsequently analyzed by either fluorescence-activated cell scanning (FACS) or fluorescence measurements with a microplate reader (Spark®, Tecan Group Ltd.). For Flow cytometric analysis of the phagocytosis assay, we used the FACSCanto (BD Biosciences). Data were analyzed with *FACSDiva* (BD Biosciences) and *FLOWJO Software* (Tree Star Inc).

2.5 | Deglycosylation of recombinant TREM2

Human recombinant TREM2 ectodomain (Sino Biological) was incubated with soluble recombinant meprin β in 20 mM of HEPES, pH 7.5 for 60 minutes at 37°C. For PNGaseF digestion, 4.5 µg of recombinant TREM2 were incubated with 5 nM of soluble meprin β in HEPES buffer for 2 hours. The samples were deglycosylated with PNGaseF kit (New England Biolabs) according to manufacturer's instructions and separated by SDS-PAGE. For Coomassie staining, gels were incubated in Coomassie Brilliant Blue R-250 Dye (Thermo Fisher Scientific) and subsequently destained.

2.6 | C-Terminal labeling and LC-MS/MS analysis

About 10 µg of human recombinant TREM2 (Sino Biological) were incubated with 5 nM soluble meprin β in HEPES buffer for 2 hours at 37°C. The samples were separated by SDS-PAGE and stained with Coomassie. To determine the C-terminus of the protein, a C-terminal labeling experiment was performed. Samples were excised from the gel band and further digested in heavy water ($H_2{}^{18}O$, 97% pure) with an additional protease (here LysargiNase and chymotrypsin). Newly formed C-termini, or neo-C-termini, will incorporate heavy water ($H_2{}^{18}O$), and can then be distinguished from the C-termini generated by the incubation of TREM2 with meprin β, which was performed using normal light water ($H_2{}^{16}O$).

Bands from the SDS-PAGE (Figure 2C) were excised, halved (split into two samples), cut into pieces of approximately 1 mm^3, destained, reduced with 10 mM of dithiothreitol at 56°C, alkylated with 55 mM of iodoacetamide at room temperature, washed with ammonium bicarbonate and acetonitrile (ACN), and dried in a vacuum centrifuge. Samples were subsequently digested overnight at 37°C in either 100 ng of chymotrypsin or LysargiNase (10 mM of ammonium bicarbonate, 2 mM of $CaCl_2$) in heavy water ($H_2{}^{18}O$,

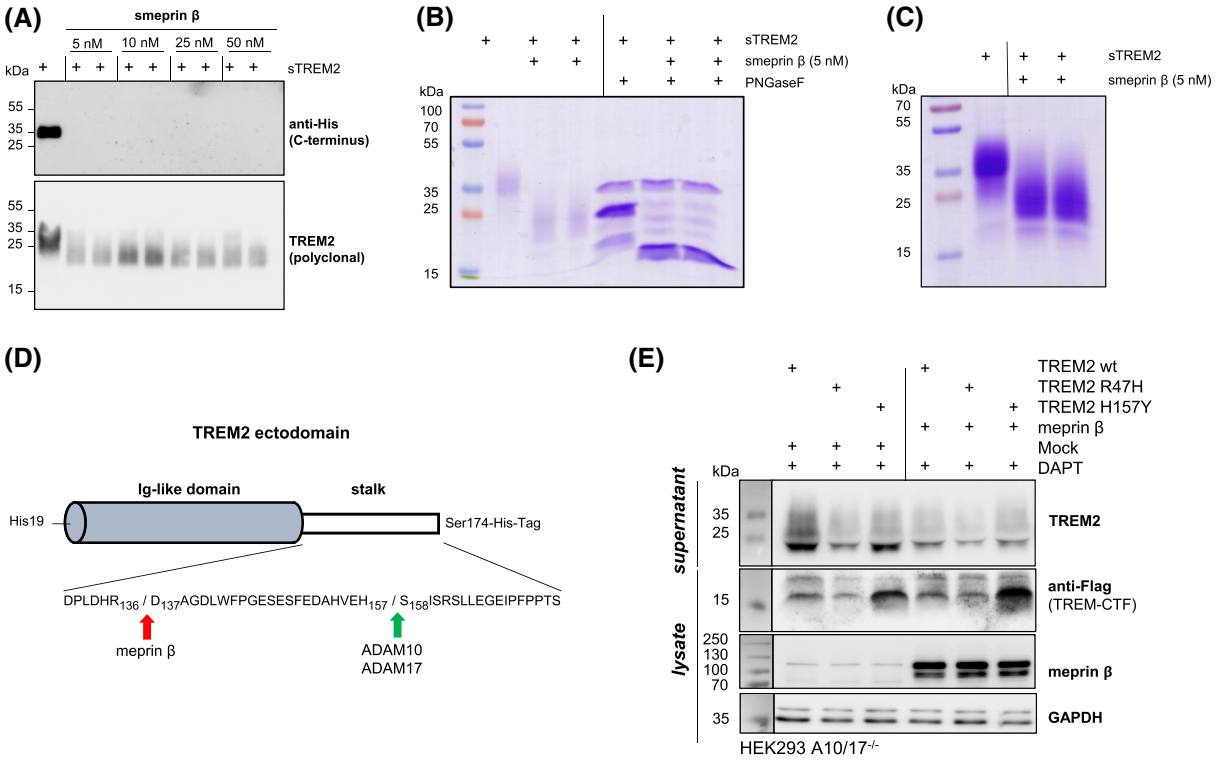

FIGURE 2 Meprin β cleaves TREM2 between arginine 136 and aspartate 137. (A) Incubation of sTREM2 with recombinant soluble meprin β (smeprin β) led to the generation of TREM2 fragments analyzed by Western blot (AF1828; R&D Systems; 1:1.000). (B) sTREM2 was incubated with smeprin β for 2 hours at 37°C and subsequently digested with PNGaseF. The meprin β generated TREM2 fragment is about 10 kDa smaller than the uncleaved TREM2 as analyzed by SDS-PAGE. (C) Coomassie stained gel of sTREM2 incubated with meprin β (2 hours at 37°C) that was used for determination of cleavage sites. Gel bands were excised, split into two samples and digested with either chymotrypsin or LysargiNase in heavy water. (E) Illustration of the TREM2 ectodomain construct used for cleavage site identification (sTREM2). While TREM2 is cleaved by ADAM10 and ADAM17 between histidine 157 and serine 158, the major meprin β cleavage site is further N-terminal between arginine 136 and aspartate 137. (F) Co-expression of TREM2 WT and AD-associated variants with meprin β in HEK293_ADAM10/17$^{-/-}$ cells and Western blot analyses of TREM2 fragments in membrane-enriched fractions and cell supernatants. Anti-GAPDH antibody was used as loading control. All transient cell transfections and Western blot analyses were at least performed in biological triplicates

97% pure). Following overnight digestion, peptides were extracted from the gel by subsequent sonication and shaking in 1% of formic acid (FA), 50% of ACN in 1% of FA, and 90% of ACN in 1% of FA, respectively. The samples were dried in a vacuum centrifuge and the peptides resuspended in 3% of ACN, 0.1% of TFA for further measurements with LC/MS.

In-gel digested samples were analyzed on a Dionex Ultimate 3000 nano-UHPLC coupled to a Q Exactive mass spectrometer (Thermo Fisher Scientific). The samples were washed on a trap column (Acclaim Pepmap 100 C18, 5 mm × 300 µm, 5 µm, 100 Å, Dionex) for 4 minutes with 3% of ACN/0.1% of TFA at a flow rate of 30 µL/min prior to peptide separation using an Acclaim PepMap 100 C18 analytical column (50 cm × 75 µm, 2 µm, 100 Å, Dionex). A flow rate of 300 nL/min using eluent A (0.05% of FA) and eluent B (80% of ACN/0.04% of FA) was used for gradient separation. Spray voltage applied on a metal-coated PicoTip emitter (10 µm tip size, New Objective, Woburn) was 1.6 kV, with a source temperature of 250°C. Full scan MS spectra were acquired between 300 and 2000 *m/z* at a resolution of 70 000 at *m/z* 400. The ten most intense precursors with charge states greater than 2+ were selected with an isolation window of 3.0 *m/z* and fragmented by HCD with normalized collision energies of 27 and at a resolution of 17 500. Lock mass (445.120025) and dynamic exclusion (15 seconds) were enabled.

The MS raw files were processed by Proteome Discover 2.2 (Thermo, version 2.2.0.388) and MS/MS spectra were searched using the Sequest HT algorithm against a database containing common contaminants (45 sequences) and the canonical human database (20 195 sequences). A semi-enzyme-specific search was performed for both chymotrypsin and LysargiNase with three and two missed cleavages allowed, respectively. An MS1 tolerance of 10 ppm and a MS2 tolerance of 0.02 Da was implemented. Oxidation (15.995 Da) of methionine residues was set as a variable modification along with C-terminal incorporation of ^{18}O (2.00425 Da). Carbamidomethyl (57.02146 Da) on cysteine residues was set as a static modification. Minimal peptide length was set to six amino acids and a peptide false discovery rate (FDR) was set to 1%.

2.7 | Generation of TBS soluble fractions

Snap-frozen brains were crunched on liquid nitrogen to generate brain powders. Several milligrams of brain powder were then thoroughly homogenized in 10 times the volume (w/v) of ice-cold TBS buffer (50 mM of Tris, 150 mM of NaCl, pH 7.4) by applying multiple strokes in protein low binding tubes (Eppendorf) using a syringe and a 26G needle. In the following, samples were incubated 30 minutes on ice with vortexing every 10 minutes. Upon centrifugation (10 minutes, 5000*g*) supernatants were subjected to ultracentrifugation (60 minutes, 130 000*g*). Supernatants were collected and frozen at −20°C until analysis.

2.8 | Murine TREM2 ELISA

For the quantification of sTREM2 levels in serum from wild-type and meprin β knock-out mice, we used the Meso Scale Discovery (MSD) platform employing the assay essentially as previously described.[35] We analyzed only male mice, as we have previously observed a gender-specific difference in TREM2 expression at a significantly lower level in female mice than in male littermates. First, an MSD Gold small spot streptavidin plate was coated with blocking buffer (3% of BSA, 0.05% of tween-20 in PBS, pH 7.4) overnight at 4C. On the next day, the plate was incubated for 90 minutes at RT with 0.125 µg/mL of biotinylated polyclonal goat anti-mouse TREM2 capture antibody (BAF1729; R&D Systems) diluted in blocking buffer. In the meantime, serum samples and TBS fractions were diluted 1:10 and 1:2, respectively, in sample dilution buffer (1% of BSA, 0.05% of tween-20 in PBS, pH 7.4) supplemented with protease inhibitor mix (Sigma). The plate was then washed two times with wash buffer (0.05% of tween-20 in PBS, pH 7.4) and serum samples were subsequently transferred onto the MSD plate for 120 minutes incubation at RT. The plate was washed two times with wash buffer and incubated in the following with 1 µg/mL rat monoclonal anti-mouse TREM2 detection antibody (clone 5F4, (34)) diluted in blocking buffer for 60 minutes at RT. The plate was again washed two times with wash buffer, and then, incubated with a SULFO-TAG-labeled goat anti-rat secondary antibody (1:1000; MSD) diluted in blocking buffer for 60 minutes at RT. Before the actual measurement, the plate was washed two times with wash buffer and another two times with PBS, pH 7.4. MSD read buffer was added to the plate and the light emission at 620 nm after electrochemical stimulation was measured using the MSD Sector Imager 2400. Concentrations of sTREM2 were finally calculated using the MSD Discovery Workbench software (v4.0.12). As a standard, we used recombinant murine TREM2 (Hölzel Diagnostika). For standard curve determination, two-fold serial dilutions were performed in sample dilution buffer supplemented with protease inhibitor mix (Sigma) on the plate spanning concentrations from 4000 to 62.5 pg/mL. sTREM2 concentrations as calculated for TBS soluble fractions were normalized to the total protein concentration as determined using the BCA assay (Interchim). In all incubation steps at RT, the plate was shaken at 300 rpm. All plate washings were performed using a plate washer (ELx405, BioTek).

2.9 | Statistics

All statistical analyses were carried out using GraphPad Prism version 6.01 for Windows (GraphPad Software, La Jolla California, USA). For multiple comparison, a One-way ANOVA followed by a Newman-Keuls multiple comparison test was performed. The comparison of two test groups was performed using an unpaired two-tailed t test. Statistical significance was assigned at the following p-values: * $P < .05$ and ** $P < .01$; **** $P < .0001$. All statistical analyses were carried out using at least three independent biological replicates and error bars are presented as standard error of the mean (SEM) or as standard deviation (SD).

3 | RESULTS

3.1 | Meprin β cleaves TREM2 at the cell surface

Several cell surface proteins were found to be similarly cleaved by ADAM10/17 and meprin β.[26,27] Therefore, we hypothesized that TREM2 may also be a shared substrate and investigated its shedding by meprin β. To avoid influence of the known TREM2 sheddases ADAM10 and ADAM17 (Figure 1A) in our experiments, we employed Crispr/Cas generated HEK293_ADAM10/17$^{-/-}$ cells.[30] We co-expressed TREM2 together with meprin β and, as a positive control, together with ADAM10. As described previously[18] ADAM10 generated a TREM2-CTF that could be enriched in membrane fractions by the addition of the γ-secretase inhibitor DAPT (Figure 1B). Indeed, co-expression with meprin β also resulted in the generation of TREM2-CTF (15 kDa), which was prone to γ-secretase cleavage as observed for the ADAM10 mediated CTF (Figure 1B). As ADAM10 cleaves TREM2 at a defined position within the stalk region[18,20] increased levels of sTREM2 could be precipitated from the cell supernatant after co-expression (Figure 1B). Surprisingly, in the presence of meprin β only faint signals were detected for sTREM2 after precipitation, even less pronounced than in TREM2 single transfected cells (Figure 1B). Therefore, we hypothesized that meprin β might not only act as a sheddase of TREM2, but also further degrades the entire ectodomain of the receptor. As a control experiment, we generated sTREM2 through co-expression of TREM2 with ADAM10, and then, added the recombinant, active ectodomains of ADAM10 (sADAM10)[33] or meprin β (smeprin β)[31] to the conditioned medium (Figure 1C). While sADAM10 showed almost no effect on sTREM2, incubation with smeprin β resulted in complete degradation of the sTREM2 ectodomain (Figure 1C). To investigate whether membrane bound TREM2 is also a substrate of soluble meprin β, we transfected the HEK293_ADAM10/17$^{-/-}$ cells with TREM2 and incubated them with smeprin β. This resulted in a decrease of full-length TREM2 and an increase in CTFs (Figure 1D). Again, we found less sTREM2 in the supernatant of cells incubated with smeprin β compared to untreated cells. To gain further insight into the cleavage dynamics and to investigate if the complete degradation of TREM2 by meprin β can already occur on the cell surface, we performed a time course experiment. To do so, HEK293_ADAM10/17$^{-/-}$ cells were transfected with TREM2 and incubated with smeprin β for different times (Figure 1E). We observed that almost 50% of full-length TREM2 was already cleaved after 30 minutes. The polyclonal antibody raised against the ectodomain of human TREM2 revealed additional bands (Figure 1E, indicated by asterisks) at lower molecular weight after 10 and 20 minutes incubation that vanished later on, supporting the observation of TREM2 degradation at the cell surface. To further validate specificity of meprin β as a sheddase and degrading enzyme of TREM2, we additionally assessed TREM2 cleavage by meprin α, a close relative of meprin β.[36] However, meprin α showed no proteolytic activity against TREM2 (Figure 1F).

3.2 | TREM2 is cleaved by meprin β between arginine 136 and aspartate 137

To determine the meprin β cleavage site in TREM2, we used recombinant human TREM2 ectodomain comprising the whole stalk region and Ig-like domain (His19 to Ser174), fused with a His-tag at its C-terminus. In Western blot analysis, we found that incubation with 5 nM of meprin β is sufficient to cleave soluble TREM2 and generate a rather stable fragment (Figure 2A). TREM2 is highly N-glycosylated (Asn20 and Asn79) and it is difficult to determine the exact size of the cleavage fragments. Therefore, we used PNGaseF to deglycosylate TREM2. This experiment showed that the meprin β generated TREM2 fragment is about 10 kDa smaller than the uncleaved TREM2 (Figure 2B). A C-terminal ^{18}O-labeling strategy followed by LC-MS/MS analysis was employed for the identification of meprin β cleavage sites in glycosylated TREM2 (Figure 2C, Tables 1 and 2). One prominent cleavage site (in terms of the number of PSMs (Peptide Spectrum Matches)) between Arg136 and Asp137 in two separate experiments (Tables 1 and 2) could be identified. Besides this major cleavage site, we also found several minor cleavage events N- and C-terminal of acidic amino acid residues from positions 131 to 147. In summary, meprin β cleaves TREM2 within the stalk region predominantly between Arg136 and Asp137, which is distinct to the ADAM10/17 identified site between His157 and Ser158 (Figure 2D).[20,21,37] However, we additionally analyzed shedding of the AD-associated variant TREM2 H157Y by meprin β (Figure 2E). Interestingly, we observed that cleavage of TREM2 H157Y by meprin β resulted in increased TREM2-CTF levels compared to the

Annotated sequence	Position in protein	# PSMs	Theo. MH+ [Da]
[L].RKVLVEVLADPLDHRDAG.[D]	[122-139]	1	2003.10325
[L].RKVLVEVLADPLDHRDA.[G]	[122-138]	2	1946.08178
[L].RKVLVEVLADPLDHR.[D]	[122-136]	8	1760.01773
[L].RKVLVEVLADPL.[D]	[122-133]	1	1351.83076
[R].KVLVEVLADPLDHR.[D]	[123-136]	2	1603.91662

TABLE 1 C-terminal peptides that were identified for meprin β hydrolyzed TREM2 following an in-gel digestion with LysargiNase. Several cleavage sites were identified including 133L.134D, 136R.137D, 138A.139G, and 139G.140D. The most abundant meprin β cleavage site (in terms of the number of PSMs (Peptide Spectrum Matches)) was observed at 136R.137D

Annotated sequence	Position in protein	# PSMs	Theo. MH+ [Da]
[L].HGSEADTLRKVLVEVLADPL.[D]	[114-133]	1	2162.18156
[L].RKVLVEVLADPLDHRDA.[G]	[122-138]	4	1946.08178
[L].RKVLVEVLADPLDHR.[D]	[122-136]	51	1760.01773
[L].RKVLVEVLADPLDH.[R]	[122-135]	2	1603.91662
[L].RKVLVEVLADPLD.[H]	[122-134]	1	1466.85771
[L].RKVLVEVLADPL.[D]	[122-133]	3	1351.83076
[L].RKVLVEVLAD.[P]	[122-131]	2	1141.69393
[L].VEVLADPLDHRDAG.[D]	[126-139]	1	1506.7547
[L].VEVLADPLDHR.[D]	[126-136]	6	1263.66918
[L].VEVLADPLDH.[R]	[126-135]	1	1107.56807
[L].DHRDAGDLWFPGES.[E]	[134-147]	2	1601.69791
[L].DHRDAGDLWFPGE.[S]	[134-146]	1	1514.66588
[L].DHRDAGDLWFPG.[E]	[134-145]	1	1385.62329

TABLE 2 C-terminal peptides that were identified for meprin β hydrolyzed TREM2 following an in-gel digestion with chymotrypsin. Several cleavage sites were identified. The most abundant meprin β cleavage site (in terms of PSMs) was observed at 136R.137D

wild-type form, although the aa exchange at position 157 is not directly influencing the newly identified meprin β cleavage site at Asp137. Therefore, we assume that this variant is somehow more accessible to meprin β (localization, protein stability, etc) rather than triggering the cleavage site.

3.3 | Co-expression of meprin β and TREM2 decreases the phagocytic potential of cells

To assess the functional consequence of TREM2 degradation by meprin β, we performed a phagocytosis assay in different cell lines. To test the phagocytic potential in ADAM10/17 deficient HEK cells, a fusion construct of TREM2 and DAP12 was used as these cells do not naturally express DAP12[18] (Figure 3A). To test if this construct is proteolytically processed, it was co-expressed with ADAM10 or meprin β (Figure 3B). Isolated membrane fractions revealed a decreased signal for full-length TREM2 upon co-expression with both proteases, confirming cleavage of this TREM2-DAP12 construct. As expected, increased levels of sTREM2 were found in precipitated supernatants upon ADAM10 co-transfection and decreased levels upon meprin β co-expression (Figure 3B). The phagocytic potential of the cells was measured by the internalization of fluorogenic pHrodo beads.[18,20] These are *E coli* bioparticles conjugated to a dye emitting fluorescence in acidic milieu. Thus, a fluorescent signal can only be measured after endocytosis of the particles and transport to the lysosome. We observed that co-expression of TREM2 and meprin β decreases the phagocytic capacity of these cells significantly when compared to TREM2 single transfected cells (Figure 3C). A similar decrease in phagocytosis was detected after co-transfection of TREM2 and ADAM10 (Figure 3C).[18] To assess this in a more physiologically relevant cell type, we repeated this experiment using the human macrophage cell lines THP-1 and U937, which endogenously expresses DAP12. Therefore, cells were transfected with TREM2 alone or together with meprin β (which is barely detectable endogenously), and at the same time, were stimulated with PMA to induce a macrophage-like differentiation.[38] After 72 hours, pHrodo beads were added and the amount of phagocytosed beads was analyzed after 120 minutes. As seen in the HEK cell experiment, co-expression of meprin β with TREM2 reduced the phagocytic potential significantly (Figure 3D,E) in both macrophage cell lines.

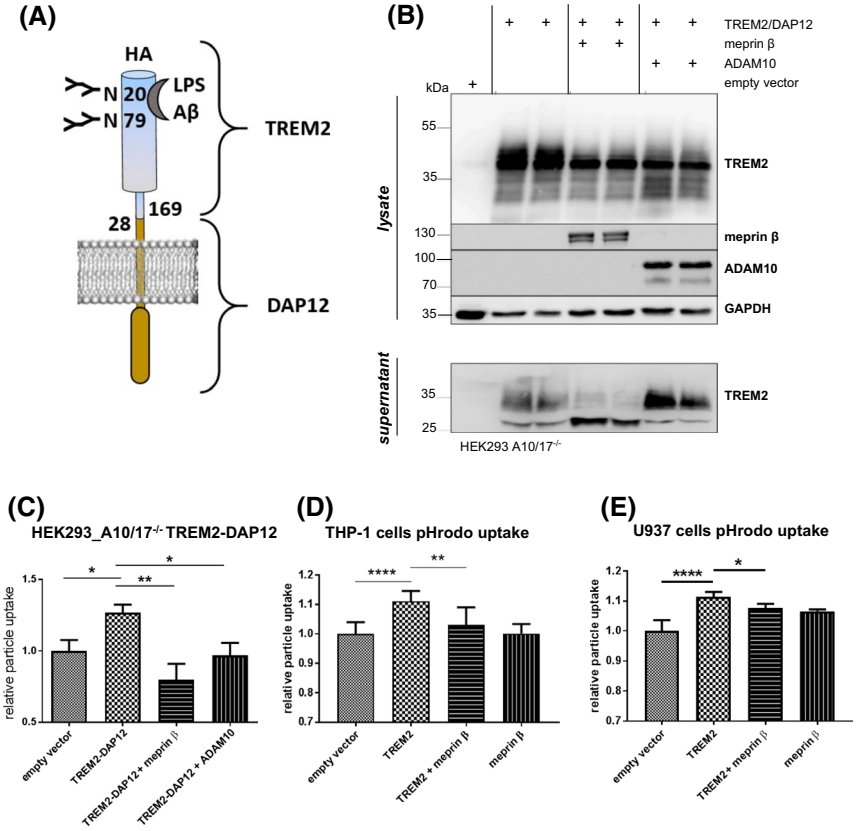

FIGURE 3 Impaired phagocytosis of fluorogenic *E coli* particles in cells co-expressing meprin β and TREM2. (A) Illustration of the TREM2/DAP12 fusion construct used in the phagocytosis assays. (B) Proteolytic cleavage of the overexpressed fusion constructs in HEK293_ADAM10/17$^{-/-}$ cells transfected with meprin β or ADAM10. Proteins from cell supernatants and membrane-enriched fractions were analyzed by Western blot. (C) Phagocytosis assay with transfected HEK293_ADAM10/17$^{-/-}$ cells. Relative particle uptake analyzed by FACS is indicated for differentially transfected cells. Data are represented as means of median fluorescence intensity ± SEM from two independent experiments and expressed relative to empty vector transfected control (n = 8 and 9, respectively). (D) Relative particle uptake of THP-1 cells transfected with wild-type TREM2 and meprin β (n = 10) was analyzed using a Tecan fluorescent reader measuring mean fluorescence intensity of a defined number of cells. (E) Relative particle uptake of U937 cells transfected with wild-type TREM2 and meprin β (n = 6) was analyzed using a Tecan fluorescent reader measuring mean fluorescence intensity of a defined number of cells. All transient cell transfections and Western blot analyses were at least performed in biological triplicates. Statistical differences were calculated by One-way ANOVA followed by a Newman-Keuls multiple comparison test. Comparison of two test groups was performed using an unpaired two-tailed *t* test (*$P < .05$; **$P < .01$; ****$P < .0001$)

3.4 | Meprin β controls TREM2 levels on primary macrophages

As we could show that membrane bound and soluble meprin β degrade TREM2, which leads to reduced phagocytosis, we were keen to evaluate if cleavage of TREM2 by meprin β is physiologically relevant. Meprin β has been reported to be expressed on macrophages important for cell migration and pro-inflammatory stimuli.[39,40] Thus, we isolated BMDMs from meprin β knock-out[41] and wild-type mice and analyzed the TREM2 levels. Mature TREM2 significantly accumulated in membrane-enriched fractions of macrophages deficient for meprin β (Figure 4A,B). After activating the BMDMs with LPS for 6 hours to induce ADAM mediated shedding, the signal intensity for mature TREM2 was similar to the one obtained for wild-type BMDMs (Figure 4A). This indicates a constitutive function for meprin β and an inducible shedding activity for ADAMs in TREM2 proteolysis. To assess a possible functional consequence, we performed the phagocytosis assay with these cells (non LPS stimulated) and found a significant increase in phagocytic potential for cells deficient for meprin β when compared to wild-type cells (Figure 4C). As a negative control, we added cytochalasin D (CytoD), an actin polymerization inhibitor that blocks phagocytosis (Figure 4C).[18] To further investigate, if meprin β is a constitutive sheddase of TREM2 in vivo, we analyzed the levels of soluble TREM2 in serum of *Mep1b*$^{-/-}$ mice. Indeed, we detected significantly reduced amounts of the soluble receptor in serum of *Mep1b*$^{-/-}$ animals compared to WT mice (Figure 4D).

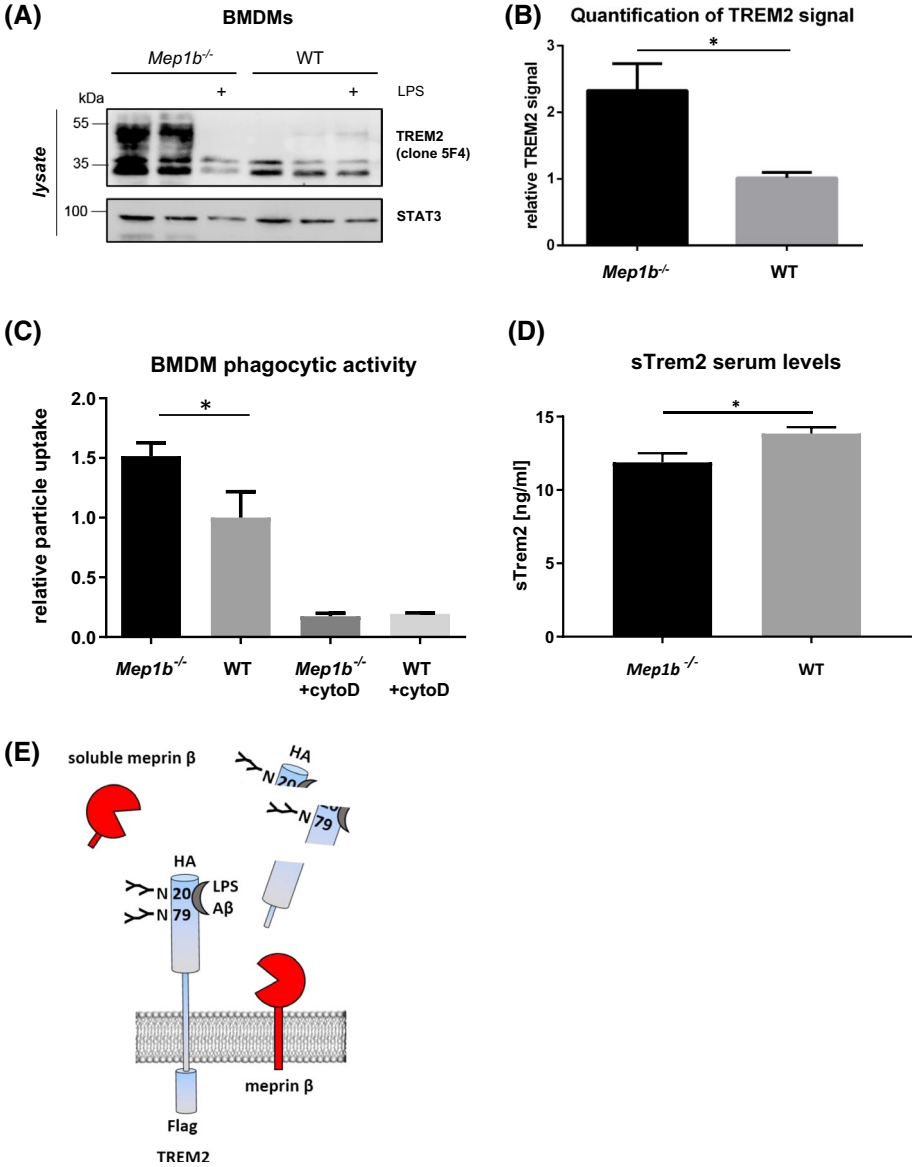

FIGURE 4 Cleavage of TREM2 on macrophages by meprin β. (A) Membrane-enriched fractions from BMDMs of *Mep1b*$^{-/-}$ mice showed higher levels of mature TREM2 than the wild-type controls visualized by Western blot. Enhanced levels of mature TREM2 at 45 kDa were detected (murine-specific anti-TREM2, clone 5F4) in samples of *Mep1b*$^{-/-}$ mice, which was decreased upon LPS stimulation. Anti-STAT3 was used as loading control. (B) Densitometric analysis of TREM2 band intensities in non LPS stimulated BMDMs from *Mep1b*$^{-/-}$ and wild-type mice as seen in (A). The comparison of two test groups (n = 5) was performed using an unpaired two-tailed *t* test. (*$P < .05$). (C) Phagocytosis assay with BMDMs from wild-type and *Mep1b*$^{-/-}$ mice. Cytochalasin D (CytoD) was used to block endocytosis. Relative particle uptake measured by FACS is indicated for different cells. Data are represented as means of median fluorescence intensity ± SD (n = 3). Statistical differences were calculated by One-way ANOVA followed by a Newman-Keuls multiple comparison test (*$P < .05$). (D) Determination of sTREM2 levels in serum reveals significantly lower levels in *Mep1b*$^{-/-}$ (n = 7, all male) than in wild-type mice (n = 5, all male). Data are represented as means ± SEM. (E) Cartoon illustrating the interaction of TREM2 with soluble and membrane bound meprin β resulting in the degradation of the TREM2 ectodomain

4 | DISCUSSION

Recently, Crowther and colleagues showed that on macrophages turnover of TREM2 is remarkably rapid, having a half-life of <1 hour. Notably, inhibition experiments revealed only minor contribution of ADAM10 in these cells.[21] The metalloprotease meprin β can cleave several cell surface proteins similar to ADAM10/17.[26,27] Hence, we investigated if TREM2 may also be a shared substrate and analyzed its shedding by meprin β. Indeed, TREM2 was cleaved by meprin β, and the soluble ectodomain of the receptor was even further degraded by the protease, which is a striking difference compared to ADAM10 cleavage. Meprin β can be physiologically shed from the cell surface by ADAM10 and

ADAM17, generating the soluble meprin β ectodomain that is still able to cleave substrates,[42-44] which was also confirmed for the cleavage of TREM2 (Figure 4E).

Besides ADAM10/17, we further validated the specificity of meprin β as a sheddase and degrading enzyme of TREM2. Therefore, we investigated TREM2 cleavage by the metalloprotease meprin α, which is closely related to meprin β.[36] Of note, meprin α displays a similar cleavage specificity with a preference for negatively charged amino acids in P1′ position of the cleavage site.[25] However, meprin α showed no proteolytic activity against TREM2. This observation is similar to APP cleavage, where meprin β but not meprin α can act as β-secretase.[45]

For meprin β the major cleavage site in TREM2 was identified between Arg136 and Asp137, which is N-terminal to the ADAM10/17 site. This cleavage site perfectly matches the meprin β preference for negatively charged amino acids at the P1′position.[25] Besides this major cleavage site, we also found several minor cleavage events N- and C-terminal of acidic amino acid residues from positions 131 to 147. Of note, for frontotemporal dementia (FTD) one missense mutation of TREM2 (D134G) is reported [46] that is in close proximity to the major meprin β cleavage site and may affect TREM2 shedding under certain conditions.

It was shown previously that the amount of functional TREM2 directly correlates with the phagocytic potential of cells.[18] This is further supported by disease-associated TREM2 variants found in AD, Nasu-Hakola disease (NHD), and FTD-like syndrome that do not reach the cell surface and dampen phagocytosis.[18,20] We were interested, if the activity of meprin β toward TREM2 alters the phagocytic potential of cells. Since meprin β has been reported to be expressed on macrophages, being important for cell migration and pro-inflammatory stimuli,[39,40] we analyzed BMDMs from *Mep1b*$^{-/-}$ mice and observed increased phagocytosis compared to wild-type cells. These findings indicate a correlation of meprin β levels and the amount of TREM2 on the cell surface of macrophages and consequently link meprin β levels to the phagocytic potential of these cells in vivo. However, we cannot fully exclude that additional meprin β substrates could influence phagocytosis or that the interaction of meprin β and TREM2 may have impact on other biological functions besides phagocytosis, such as migration. The physiological relevance of meprin β mediated TREM2 cleavage is further supported by significantly reduced levels of soluble TREM2 in the serum of *Mep1b*$^{-/-}$ mice compared to control animals. However, the role of meprin β in inflammatory diseases is still a controversial issue. Meprin β has been linked to inflammatory bowel disease[47] and it was shown to shed the IL-6R and to induce pro-inflammatory trans-signaling.[27] Meprin β promotes transendothelial migration of cells through CD99 cleavage, an important step for immune cells to reach the site of inflammation.[28] Additionally, meprin β can cleave, and thereby inactivate IL-6[48] and the important chemokine CCL2/MCP-1 leading to a reduced monocyte attraction.[49]

Taken together, we found that meprin β sheds and degrades TREM2 at the cell surface and that it controls the level of TREM2 on macrophages but not on microglial cells, at least under unchallenged conditions. We determined a major cleavage site for meprin β between Arg136 and Asp137, which is 21 aa N-terminal of the described ADAM10 cleave site. Additionally, we could show that meprin β can control the cell autonomous function of TREM2 and decreases the phagocytic potential of cells. Of note, this is not necessarily restricted to meprin β expressing cells, as we could show that the protease can act as membrane bound or soluble protease in cis and trans, respectively. In sum, soluble TREM2 generated by meprin β exhibits different properties compared to the ADAM-released ectodomain, which might interfere with already established approaches for the detection of sTREM2 in blood or CSF. This should be taken into account in TREM2 associated pathologies.

ACKNOWLEDGMENTS

We thank Inez Götting and Gaby Steinkamp for excellent help in BMDM isolation, cultivation, and differentiation. We also thank Brigitte Nuscher for technical assistance with MSD ELISA measurements.

CONFLICT OF INTEREST

C.H. collaborates with Denali Therapeutics, participated on one advisory board meeting of Biogen, and received a speaker honorarium from Novartis and Roche. C.H. is chief advisor of ISAR Bioscience.

AUTHOR CONTRIBUTIONS

DKB, LW, PA, and CBP conceived the study. DKB, LW, JS, KS, TK, FS, FA, AT, CH, PA, and CBP performed or designed experiments. KS, RL, GK, and CH provided material. DKB, LW, and CBP wrote the manuscript.

REFERENCES

1. Yeh FL, Hansen DV, Sheng M. TREM2, microglia, and neurodegenerative diseases. *Trends Mol Med*. 2017;23:512-533.
2. Colonna M, Wang Y. TREM2 variants: new keys to decipher Alzheimer disease pathogenesis. *Nat Rev Neurosci*. 2016;17:201-207.
3. Guerreiro R, Wojtas A, Bras J, et al. TREM2 variants in Alzheimer's disease. *N Engl J Med*. 2013;368:117-127.
4. Jin SC, Benitez BA, Karch CM, et al. Coding variants in TREM2 increase risk for Alzheimer's disease. *Hum Mol Genet*. 2014;23:5838-5846.
5. Jonsson T, Stefansson H, Steinberg S, et al. Variant of TREM2 associated with the risk of Alzheimer's disease. *N Engl J Med*. 2013;368:107-116.
6. Jiang T, Tan L, Chen Q, et al. A rare coding variant in TREM2 increases risk for Alzheimer's disease in Han Chinese. *Neurobiol Aging*. 2016;42:217.e211-217.e213.

7. Ulland TK, Colonna M. TREM2—a key player in microglial biology and Alzheimer disease. *Nat Rev Neurol*. 2018;14:667-675.
8. Parhizkar S, Arzberger T, Brendel M, et al. Loss of TREM2 function increases amyloid seeding but reduces plaque-associated ApoE. *Nat Neurosci*. 2019;22:191-204.
9. Jay TR, Miller CM, Cheng PJ, et al. TREM2 deficiency eliminates TREM2+ inflammatory macrophages and ameliorates pathology in Alzheimer's disease mouse models. *J Exp Med*. 2015;212:287-295.
10. Daws MR, Sullam PM, Niemi EC, Chen TT, Tchao NK, Seaman WE. Pattern recognition by TREM-2: binding of anionic ligands. *J Immunol*. 2003;171:594-599.
11. N'Diaye EN, Branda CS, Branda SS, et al. TREM-2 (triggering receptor expressed on myeloid cells 2) is a phagocytic receptor for bacteria. *J Cell Biol*. 2009;184:215-223.
12. Charles JF, Humphrey MB, Zhao X, et al. The innate immune response to *Salmonella enterica* serovar Typhimurium by macrophages is dependent on TREM2-DAP12. *Infect Immun*. 2008;76:2439-2447.
13. Zhong L, Chen XF, Zhang ZL, et al. DAP12 stabilizes the C-terminal fragment of the triggering receptor expressed on myeloid cells-2 (TREM2) and protects against LPS-induced pro-inflammatory response. *J Biol Chem*. 2015;290:15866-15877.
14. Yeh FL, Wang Y, Tom I, Gonzalez LC, Sheng M. TREM2 binds to apolipoproteins, including APOE and CLU/APOJ, and thereby facilitates uptake of amyloid-beta by microglia. *Neuron*. 2016;91:328-340.
15. Zhao Y, Jaber V, Lukiw WJ. Over-expressed pathogenic miRNAs in Alzheimer's disease (AD) and Prion disease (PrD) drive deficits in TREM2-mediated Abeta42 peptide clearance. *Front Aging Neurosci*. 2016;8:140.
16. Zhao Y, Wu X, Li X, et al. TREM2 is a receptor for beta-amyloid that mediates microglial function. *Neuron*. 2018;97:1023-1031.e1027.
17. Zhong L, Zhang ZL, Li X, et al. TREM2/DAP12 complex regulates inflammatory responses in microglia via the JNK signaling pathway. *Front Aging Neurosci*. 2017;9:204.
18. Kleinberger G, Yamanishi Y, Suarez-Calvet M, et al. TREM2 mutations implicated in neurodegeneration impair cell surface transport and phagocytosis. *Sci Transl Med*. 2014;6:243ra286.
19. Wunderlich P, Glebov K, Kemmerling N, Tien NT, Neumann H, Walter J. Sequential proteolytic processing of the triggering receptor expressed on myeloid cells-2 (TREM2) protein by ectodomain shedding and gamma-secretase-dependent intramembranous cleavage. *J Biol Chem*. 2013;288:33027-33036.
20. Schlepckow K, Kleinberger G, Fukumori A, et al. An Alzheimer-associated TREM2 variant occurs at the ADAM cleavage site and affects shedding and phagocytic function. *EMBO Mol Med*. 2017;9:1356-1365.
21. Thornton P, Sevalle J, Deery MJ, et al. TREM2 shedding by cleavage at the H157–S158 bond is accelerated for the Alzheimer's disease-associated H157Y variant. *EMBO Mol Med*. 2017;9:1366-1378.
22. Wu K, Byers DE, Jin X, et al. TREM-2 promotes macrophage survival and lung disease after respiratory viral infection. *J Exp Med*. 2015;212:681-697.
23. Zhong L, Chen XF, Wang T, et al. Soluble TREM2 induces inflammatory responses and enhances microglial survival. *J Exp Med*. 2017;214:597-607.
24. Suarez-Calvet M, Kleinberger G, Araque Caballero MA, et al. sTREM2 cerebrospinal fluid levels are a potential biomarker for microglia activity in early-stage Alzheimer's disease and associate with neuronal injury markers. *EMBO Mol Med*. 2016;8:466-476.
25. Becker-Pauly C, Barre O, Schilling O, et al. Proteomic analyses reveal an acidic prime side specificity for the astacin metalloprotease family reflected by physiological substrates. *Mol Cell Proteomics*. 2011;10:M111 009233.
26. Schonherr C, Bien J, Isbert S, et al. Generation of aggregation prone N-terminally truncated amyloid beta peptides by meprin beta depends on the sequence specificity at the cleavage site. *Mol Neurodegener*. 2016;11:19.
27. Arnold P, Boll I, Rothaug M, et al. Meprin metalloproteases generate biologically active soluble interleukin-6 receptor to induce trans-signaling. *Sci Rep*. 2017;7:44053.
28. Bedau T, Peters F, Prox J, et al. Ectodomain shedding of CD99 within highly conserved regions is mediated by the metalloprotease meprin beta and promotes transendothelial cell migration. *FASEB J*. 2017;31:1226-1237.
29. Bedau T, Schumacher N, Peters F, et al. Cancer-associated mutations in the canonical cleavage site do not influence CD99 shedding by the metalloprotease meprin beta but alter cell migration in vitro. *Oncotarget*. 2017;8:54873-54888.
30. Riethmueller S, Ehlers JC, Lokau J, et al. Cleavage site localization differentially controls interleukin-6 receptor proteolysis by ADAM10 and ADAM17. *Sci Rep*. 2016;6:25550.
31. Becker C, Kruse MN, Slotty KA, et al. Differences in the activation mechanism between the alpha and beta subunits of human meprin. *Biol Chem*. 2003;384:825-831.
32. Becker-Pauly C, Howel M, Walker T, et al. The alpha and beta subunits of the metalloprotease meprin are expressed in separate layers of human epidermis, revealing different functions in keratinocyte proliferation and differentiation. *J Invest Dermatol*. 2007;127:1115-1125.
33. Jefferson T, Auf dem Keller U, Bellac C, et al. The substrate degradome of meprin metalloproteases reveals an unexpected proteolytic link between meprin beta and ADAM10. *Cell Mol Life Sci*. 2013;70:309-333.
34. Xiang X, Werner G, Bohrmann B, et al. TREM2 deficiency reduces the efficacy of immunotherapeutic amyloid clearance. *EMBO Mol Med*. 2016;8:992-1004.
35. Kleinberger G, Brendel M, Mracsko E, et al. The FTD-like syndrome causing TREM2 T66M mutation impairs microglia function, brain perfusion, and glucose metabolism. *EMBO J*. 2017;36:1837-1853.
36. Broder C, Becker-Pauly C. The metalloproteases meprin alpha and meprin beta: unique enzymes in inflammation, neurodegeneration, cancer and fibrosis. *Biochem J*. 2013;450:253-264.
37. Feuerbach D, Schindler P, Barske C, et al. ADAM17 is the main sheddase for the generation of human triggering receptor expressed in myeloid cells (hTREM2) ectodomain and cleaves TREM2 after Histidine 157. *Neurosci Lett*. 2017;660:109-114.
38. Daigneault M, Preston JA, Marriott HM, Whyte MK, Dockrell DH. The identification of markers of macrophage differentiation in PMA-stimulated THP-1 cells and monocyte-derived macrophages. *PLoS ONE*. 2010;5:e8668.
39. Li YJ, Fan YH, Tang J, Li JB, Yu CH. Meprin-beta regulates production of pro-inflammatory factors via a disintegrin and metalloproteinase-10 (ADAM-10) dependent pathway in macrophages. *Int Immunopharmacol*. 2014;18:77-84.
40. Crisman JM, Zhang B, Norman LP, Bond JS. Deletion of the mouse meprin beta metalloprotease gene diminishes the ability of

leukocytes to disseminate through extracellular matrix. *J Immunol*. 2004;172:4510-4519.

41. Norman LP, Jiang W, Han X, Saunders TL, Bond JS. Targeted disruption of the meprin beta gene in mice leads to underrepresentation of knockout mice and changes in renal gene expression profiles. *Mol Cell Biol*. 2003;23:1221-1230.
42. Hahn D, Pischitzis A, Roesmann S, et al. Phorbol 12-myristate 13-acetate-induced ectodomain shedding and phosphorylation of the human meprinbeta metalloprotease. *J Biol Chem*. 2003;278:42829-42839.
43. Schutte A, Ermund A, Becker-Pauly C, et al. Microbial-induced meprin beta cleavage in MUC2 mucin and a functional CFTR channel are required to release anchored small intestinal mucus. *Proc Natl Acad Sci U S A*. 2014;111:12396-12401.
44. Wichert R, Ermund A, Schmidt S, et al. Mucus detachment by host metalloprotease meprin beta requires shedding of its inactive proform, which is abrogated by the pathogenic protease RgpB. *Cell Rep*. 2017;21:2090-2103.
45. Bien J, Jefferson T, Causevic M, et al. The metalloprotease meprin beta generates amino terminal-truncated amyloid beta peptide species. *J Biol Chem*. 2012;287:33304-33313.
46. Sirkis DW, Aparicio RE, Schekman R. Neurodegeneration-associated mutant TREM2 proteins abortively cycle between the ER and ER-Golgi intermediate compartment. *Mol Biol Cell*. 2017;28:2723-2733.
47. Vazeille E, Bringer MA, Gardarin A, et al. Role of meprins to protect ileal mucosa of Crohn's disease patients from colonization by adherent-invasive *E. coli*. *PLoS ONE*. 2011;6:e21199.
48. Keiffer TR, Bond JS. Meprin metalloproteases inactivate interleukin 6. *J Biol Chem*. 2014;289:7580-7588.
49. Herzog C, Haun RS, Shah SV, Kaushal GP. Proteolytic processing and inactivation of CCL2/MCP-1 by meprins. *Biochem Biophys Rep*. 2016;8:146-150.

How to cite this article: Berner DK, Wessolowski L, Armbrust F, et al. Meprin β cleaves TREM2 and controls its phagocytic activity on macrophages. *The FASEB Journal*. 2020;34:6675–6687. https://doi.org/10.1096/fj.201902183R

The Alzheimer's disease associated bacterial protease RgpB from *P. gingivalis* activates the alternative β-secretase meprin β thereby increasing Aβ generation

Fred Armbrust[1], Cynthia Colmorgen[1], Claus U. Pietrzik[2]* and Christoph Becker-Pauly[1]*

[1]Biochemical Institute, Unit for Degradomics of the Protease Web, University of Kiel, Kiel, Germany

[2]Institute for Pathobiochemistry, University Medical Center of the Johannes Gutenberg-University Mainz, Mainz, Germany

* To whom correspondence should be addressed

Claus Pietrzik email: pietrzik@uni-mainz.de
Phone: +49-6131-39-25390
Fax: +49-6131-39-26488

Christoph Becker-Pauly email: cbeckerpauly@biochem.uni-kiel.de
Phone: +49-431-880-7118
Fax: +49-431-880-2238

Fred Armbrust: farmbrust@biochem.uni-kiel.de

Cynthia Colmorgen: ccolmorgen@biochem.uni-kiel.de

Abstract

Alzheimer's disease (AD) is the most common type of dementia and characterized by tau hyperphosphorylation, oxidative stress, reactive microglia and amyloid-β (Aβ) deposits. A recent study revealed that *Porphyromonas gingivalis* infection is associated with amyloid β generation in Alzheimer's disease. Increased Aβ levels, tau degradation and neuronal toxicity were observed as a consequence of ginigipain R (RgpB) activity, a cysteine protease constitutively secreted by *P. gingivalis*. Of note, we previously identified RgpB as a potent activator of the metalloproteinase meprin β. Interestingly, meprin β is an alternative β-secretase of the amyloid precursor protein (APP), which together with the γ-secretase leads to the generation of aggregation-prone N-terminally truncated Aβ2-x peptides. Importantly, identification of a risk gene variant of meprin β (rs173032) for Alzheimer's disease using whole-exome sequencing of the BDR cohort further supports the impact of this alternative β-secretase. Thus, we wondered if increased Aβ levels as a consequence of *P. gingivalis* colonization into the brain might be due to meprin β activation by RgpB. Here, we demonstrate that i) upon incubation with RgpB the proteolytic activity of meprin β at the cell surface of transfected HEK cells or of endogenously expressed enzyme in SH-SY5Y neuroblastoma cells was significantly increased, and that ii) RgpB-mediated increase in meprin β activity leads to massive generation of Aβ-peptides. In conclusion, our findings would further explain the pathogenesis of *P. gingivalis* in AD brain.

Keywords

Alzheimer´s Disease, amyloid β, meprin β, *Porphyromonas gingivalis*, ginigipain R

Background

Porphyromonas gingivalis is the major pathogenic bacterium responsible for chronic periodontitis. Potempa and colleagues recently demonstrated that *P. gingivalis* can be found in the brains of Alzheimer's disease (AD) patients, where it releases the neurotoxic cysteine protease gingipain R (RgpB) [1]. The authors could show that this protease is associated with increased Aβ generation and aggregation, tau degradation and neuronal toxicity.

Despite the exciting results from this paper, we propose an additional molecular mechanism mediated by RgpB being relevant for the neurotoxic activity of *P. gingivalis* infection.

We have demonstrated that RgpB is a highly potent activator of the metalloprotease meprin β at the plasma membrane [2]. Interestingly, meprin β was identified as an alternative β-secretase of the amyloid precursor protein (APP), which together with the γ-secretase leads to the generation of N-terminally truncated Aβ2-x peptides [3,4]. This strongly aggregating Aβ species is particularly increased in AD [5,6], as is meprin β [4,7,8]. Intrigued by the recent study by Potempa and colleagues, demonstrating that RgpB is present in brain tissue of AD patients and associated with pathology [1], we speculated about its effect on meprin β-mediated amyloid β generation.

Main text

In order to analyze the role of meprin β in Rgpb-induced Aβ generation, we transfected HEK293 cells with APP and/or meprin β and analyzed enzyme activity and APP processing in the presence or absence of RgpB (Fig.1A). Indeed, the amount of Aβ was dramatically increased in the presence of meprin β and the bacterial protease (Fig. 1B). Additionally, meprin β specific generation of a N-terminal APP fragment was also increased upon RgpB treatment (Fig. 1C). Of note, RgpB itself showed proteolytic activity towards APP resulting in degradation of soluble APP ectodomains generated by α- and β-secretases (Fig. 1C). Increased proteolytic activity of meprin β at the cell surface upon RgpB incubation could be measured using a specific peptide cleavage assay [9], further demonstrating the specific interaction between host and pathogenic protease (Fig. 1D). To prove that the enzymatic activity of meprin β was responsible for increased Aβ generation, we applied the meprin inhibitor actinonin [10], which led to strongly decreased Aβ generation in the absence or presence of RgpB (Fig. 1E).

To analyze a more physiological situation we choose the human neuroblastoma cell line SH-SY5Y, which endogenously express meprin β and APP (Fig. 1F). Employing our peptide cleavage assay we again detected significantly increased meprin β activity at the cell surface when incubated with RgpB (Fig.1G). Of note, we observed Aβ release by RgpB-treated SH-SY5Y cells, whereas Aβ levels generated by untreated SHSY5Y cells were below the detection limit of the ELISA (Fig. 1H).

AD pathogenesis is highly influenced by pro-inflammatory stimuli and subsequent activation of microglia [11]. Several papers proposed bacterial and viral pathogens, such as *Herpes simplex* virus [12], to be involved in the onset of AD. In the recent manuscript published in Science Advances the authors detected the pathogenic bacterium *P. gingivalis*, which is predominantly responsible for periodontitis, also in the brain [1]. In a mouse model, the authors demonstrated that oral infection by *P. gingivalis* indeed leads to induced Aβ peptide formation and destabilization of tau in the murine brain, symptoms that could be diminished applying specific

inhibitors of the virulence factors. We provide evidence that *P. gingivalis* induced amyloid plaque formation in AD brain may additionally be mediated through activation of the alternative β-secretase meprin β.

Besides the detrimental role of Aβ and considering meprin β as host-protective enzyme with regard to mucus homeostasis [13,2] and antimicrobial activity [14], one can assume that brain infection by *P. gingivalis* leads to increased activation of meprin β by RgpB and an acute Aβ-generation, which in turn may serve as an antimicrobial peptide [15] (Fig. 2). Of course, there are many open questions that need to be answered and mouse work in this direction is ongoing. However, this is another small piece in the AD puzzle that contributes to our understanding of this devastating disease.

Conclusions

Potempa and colleagues observed increased Aβ levels as a consequence of RgpB secretion by *P. gingivalis* being capable of colonizing the brain [1]. Here, we demonstrate that meprin β is involved in the generation of increased Aβ levels upon activation by Rgpb. Our findings attribute meprin β a potential role in the previously reported Rgpb-dependent Aβ increase.

List of abbreviations

RgpB – ginigipain R; Aβ – amyloid β; AD – Alzheimer´s Disease; APP – amyloid precursor protein

Declarations

Ethics approval and consent to participate

Not applicable.

Consent for publication

Not applicable.

Availability of data and materials

The datasets used and/or analyzed during the current study are available from the corresponding author on reasonable request.

Competing interests

The authors declare that they have no competing interests.

Funding

This work was supported by the Deutsche Forschungsgemeinschaft (DFG) SFB 877 (Proteolysis as a Regulatory Event in Pathophysiology, Projects A9 and A15), PI379/6-2 (to C.U.P.), and BE 4086/2-2 (to C.B.-P.).

Authors' contributions

FA conducted the experiments, acquired and analyzed the data and wrote the manuscript. CC was involved in conducting experiments. CUP provided regents and revised the manuscript. CBP wrote, edited and revised the manuscript and designed the research study. All authors read and approved the final manuscript. All authors read and approved the final manuscript.

Acknowledgements

We thank Jan Potempa (University of Louisville) for providing purified RgpB protease from *P. gingivalis*.

References

1. Dominy SS, Lynch C, Ermini F, Benedyk M, Marczyk A, Konradi A, Nguyen M, Haditsch U, Raha D, Griffin C, Holsinger LJ, Arastu-Kapur S, Kaba S, Lee A, Ryder MI, Potempa B, Mydel P, Hellvard A, Adamowicz K, Hasturk H, Walker GD, Reynolds EC, Faull RLM, Curtis MA, Dragunow M, Potempa J

(2019) Porphyromonas gingivalis in Alzheimer's disease brains: Evidence for disease causation and treatment with small-molecule inhibitors. Sci Adv 5 (1):eaau3333. doi:10.1126/sciadv.aau3333
2. Wichert R, Ermund A, Schmidt S, Schweinlin M, Ksiazek M, Arnold P, Knittler K, Wilkens F, Potempa B, Rabe B, Stirnberg M, Lucius R, Bartsch JW, Nikolaus S, Falk-Paulsen M, Rosenstiel P, Metzger M, Rose-John S, Potempa J, Hansson GC, Dempsey PJ, Becker-Pauly C (2017) Mucus Detachment by Host Metalloprotease Meprin beta Requires Shedding of Its Inactive Pro-form, which Is Abrogated by the Pathogenic Protease RgpB. Cell Rep 21 (8):2090-2103. doi:10.1016/j.celrep.2017.10.087
3. Schonherr C, Bien J, Isbert S, Wichert R, Prox J, Altmeppen H, Kumar S, Walter J, Lichtenthaler SF, Weggen S, Glatzel M, Becker-Pauly C, Pietrzik CU (2016) Generation of aggregation prone N-terminally truncated amyloid beta peptides by meprin beta depends on the sequence specificity at the cleavage site. Mol Neurodegener 11:19. doi:10.1186/s13024-016-0084-5
4. Bien J, Jefferson T, Causevic M, Jumpertz T, Munter L, Multhaup G, Weggen S, Becker-Pauly C, Pietrzik CU (2012) The metalloprotease meprin beta generates amino terminal-truncated amyloid beta peptide species. J Biol Chem 287 (40):33304-33313. doi:10.1074/jbc.M112.395608
5. Bibl M, Gallus M, Welge V, Esselmann H, Wolf S, Ruther E, Wiltfang J (2012) Cerebrospinal fluid amyloid-beta 2-42 is decreased in Alzheimer's, but not in frontotemporal dementia. J Neural Transm (Vienna) 119 (7):805-813. doi:10.1007/s00702-012-0801-3
6. Wiltfang J, Esselmann H, Cupers P, Neumann M, Kretzschmar H, Beyermann M, Schleuder D, Jahn H, Ruther E, Kornhuber J, Annaert W, De Strooper B, Saftig P (2001) Elevation of beta-amyloid peptide 2-42 in sporadic and familial Alzheimer's disease and its generation in PS1 knockout cells. J Biol Chem 276 (46):42645-42657. doi:10.1074/jbc.M102790200
7. Patel T, Brookes KJ, Turton J, Chaudhury S, Guetta-Baranes T, Guerreiro R, Bras J, Hernandez D, Singleton A, Francis PT, Hardy J, Morgan K (2017) Whole-exome sequencing of the BDR cohort: evidence to support the role of the PILRA gene in Alzheimer's disease. Neuropathol Appl Neurobiol. doi:10.1111/nan.12452
8. Schlenzig D, Cynis H, Hartlage-Rubsamen M, Zeitschel U, Menge K, Fothe A, Ramsbeck D, Spahn C, Wermann M, Rossner S, Buchholz M, Schilling S, Demuth HU (2018) Dipeptidyl-Peptidase Activity of Meprin beta Links N-truncation of Abeta with Glutaminyl Cyclase-Catalyzed pGlu-Abeta Formation. J Alzheimers Dis 66 (1):359-375. doi:10.3233/JAD-171183
9. Broder C, Becker-Pauly C (2013) The metalloproteases meprin alpha and meprin beta: unique enzymes in inflammation, neurodegeneration, cancer and fibrosis. Biochem J 450 (2):253-264. doi:10.1042/BJ20121751
10. Kruse MN, Becker C, Lottaz D, Kohler D, Yiallouros I, Krell HW, Sterchi EE, Stocker W (2004) Human meprin alpha and beta homo-oligomers: cleavage of basement membrane proteins and sensitivity to metalloprotease inhibitors. Biochem J 378 (Pt 2):383-389. doi:10.1042/BJ20031163
11. Selkoe DJ, Hardy J (2016) The amyloid hypothesis of Alzheimer's disease at 25 years. EMBO Mol Med 8 (6):595-608. doi:10.15252/emmm.201606210
12. Haas JG, Lathe R (2018) Microbes and Alzheimer's Disease: New Findings Call for a Paradigm Change. Trends Neurosci 41 (9):570-573. doi:10.1016/j.tins.2018.07.001
13. Schutte A, Ermund A, Becker-Pauly C, Johansson ME, Rodriguez-Pineiro AM, Backhed F, Muller S, Lottaz D, Bond JS, Hansson GC (2014) Microbial-induced meprin beta cleavage in MUC2 mucin and a functional CFTR channel are required to release anchored small intestinal mucus. Proc Natl Acad Sci U S A 111 (34):12396-12401. doi:10.1073/pnas.1407597111
14. Vazeille E, Bringer MA, Gardarin A, Chambon C, Becker-Pauly C, Pender SL, Jakob C, Muller S, Lottaz D, Darfeuille-Michaud A (2011) Role of meprins to protect ileal mucosa of Crohn's disease patients from colonization by adherent-invasive E. coli. PLoS One 6 (6):e21199. doi:10.1371/journal.pone.0021199
15. Kumar DK, Choi SH, Washicosky KJ, Eimer WA, Tucker S, Ghofrani J, Lefkowitz A, McColl G, Goldstein LE, Tanzi RE, Moir RD (2016) Amyloid-beta peptide protects against microbial infection in mouse and worm models of Alzheimer's disease. Sci Transl Med 8 (340):340ra372. doi:10.1126/scitranslmed.aaf1059

Figures

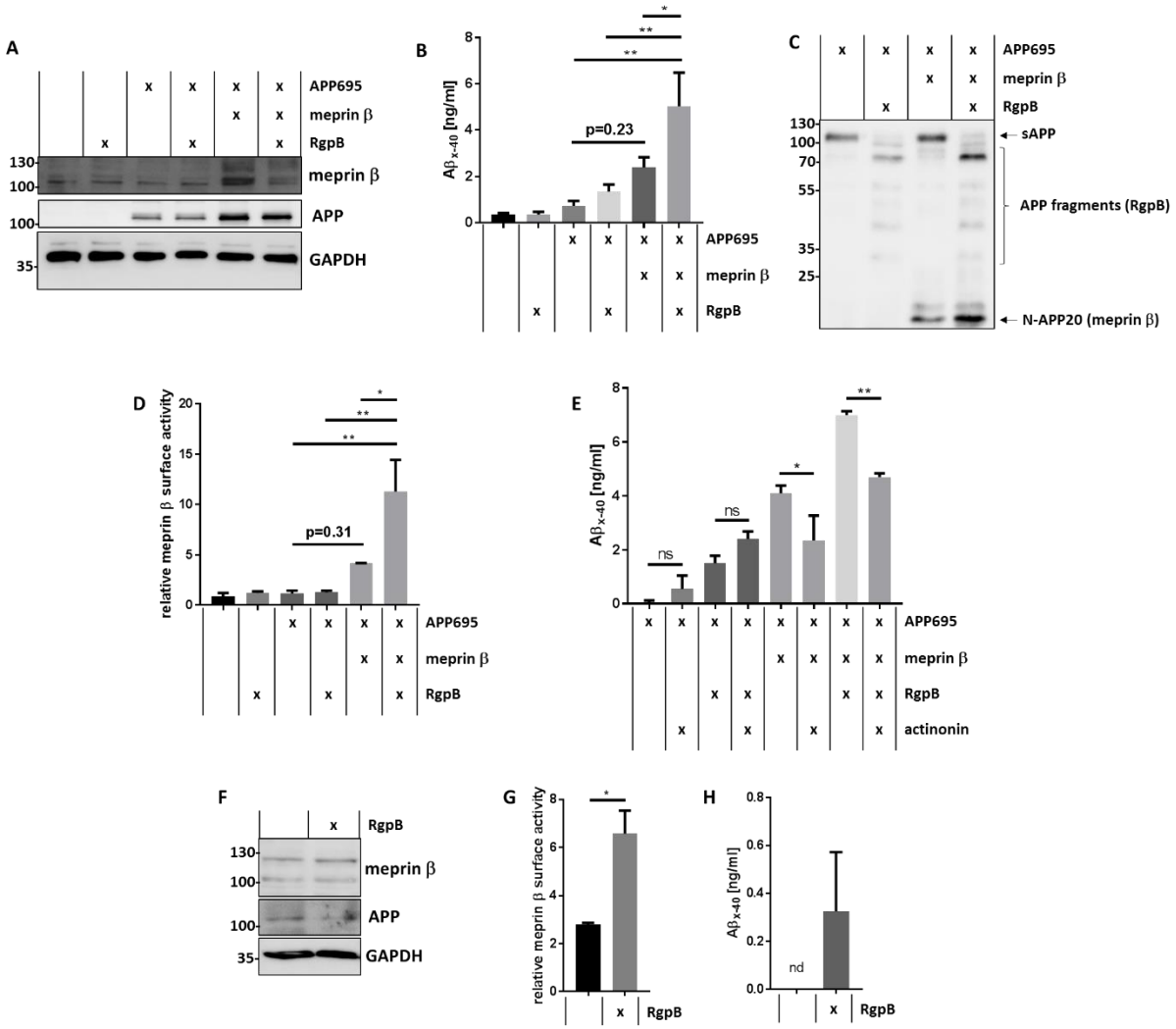

FIGURE 1 **Meprin β activation by RgpB leads to increased Aβ levels.** A) HEK cells were transfected with human APP695 and/or human meprin β. After 24 h, cells were treated with 50 nM RgpB for 30 min. Then, the medium was changed to serum-free DMEM. Cells were harvested 3 h later and lysed in an EDTA-containing Triton X-100-based lysis buffer. Proteins were analyzed by Western blot using specific antibodies against meprin β (polyclonal antibody against the ectodomain), APP (CT15, ploYclonal antibody against the last C-terminal 15 amino acids of APP) and GAPDH (14C10, Cell Signaling). B) HEK cells were treated as described in A), however, selective samples were treated with E-64 (RgpB inhibitor). Supernatants were analyzed with LEGEND MAX™ β-Amyloid x-40 ELISA Kit (Biolegend) according to manufacturer's instructions. C) HEK cells were treated as described in A) and supernatants

were analyzed by Western blot using an APP antibody (22C11, Biolegend). D) HEK cells were treated as described in A) and proteolytic activity of meprin β at the cell surface was measured using a highly specific quenched fluorogenic peptide substrate ((mca)-EDEDED-(K-e-dnp); mca: 7-methyloxycoumarin-4-yl, dnp: dinitrophenyl) [9]. E) HEK cells were treated as described in A), however, after changing medium to serum-free DMEM, 20 µM of the meprin β inhibitor actinonin was added to selected samples and β-Amyloid x-40 was measured as described in C). F) SHSY5Y cells were treated with 50 nM RgpB for 30 min and meprin β, APP and GAPDH levels were analyzed by Western blot. G) SHSY5Y cells were treated as described in F) and then analyzed for specific meprin β activity as described in D). H) SHSY5Y cells were treated as described in F) and β-Amyloid x-40 was measured as described in C). nd – below detection limit of the ELISA. All statistical analyses were performed with GraphPad Prism using a one-way ANOVA followed by a Turkey's test for B), D) and E) and a two-tailed t test for G) (*$p < 0.05$, **$p < 0.01$).

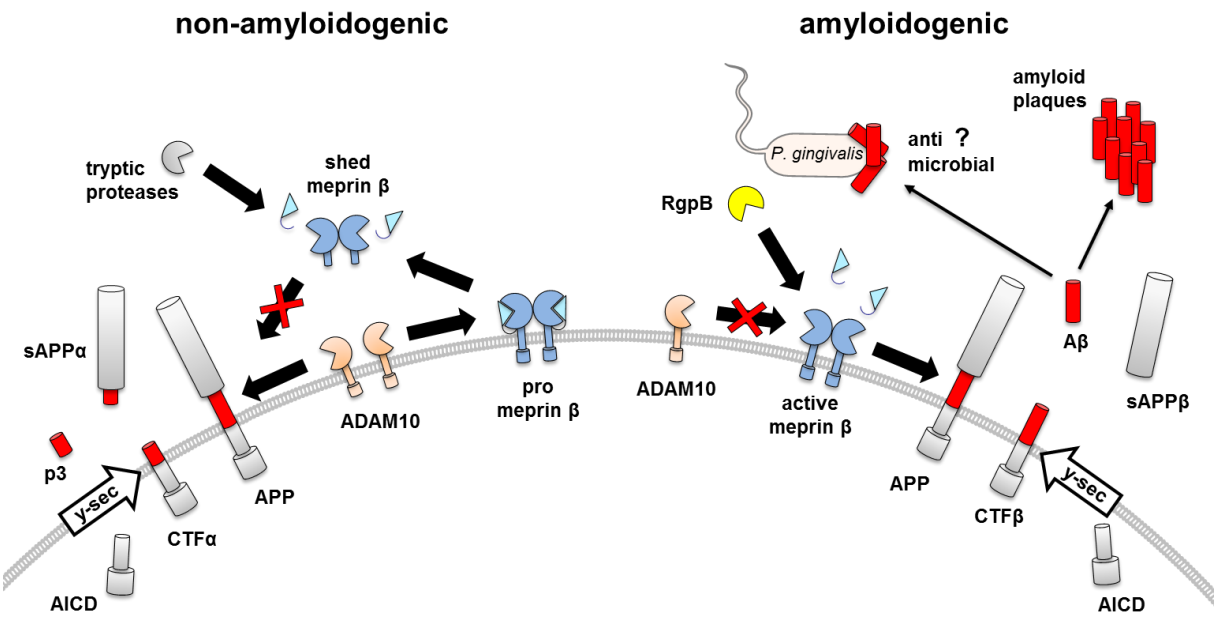

FIGURE 2. ***P. gingivalis*** **infection promotes the amyloidogenic pathway of APP processing.** The alternative β-secretase meprin β can be activated by the pathogenic protease RgpB, secreted from *P. gingivalis*. Activation of meprin β at the cell surface induces Aβ generation. Importantly, only the proform of meprin β is shed by the α-secretase ADAM10, which blocks its β-secretase activity. Hence, activation of meprin β by RgpB has a dual detrimental role, activating the β-secretase and preventing its shedding. However, it is also under debate whether Aβ-peptides might act as anti-microbial peptides in acute bacterial infection.

Cellular and Molecular Life Sciences (2019) 76:3193–3206
https://doi.org/10.1007/s00018-019-03179-1

REVIEW

Regulation of the alternative β-secretase meprin β by ADAM-mediated shedding

Franka Scharfenberg[1] · Fred Armbrust[1] · Liana Marengo[2] · Claus Pietrzik[2] · Christoph Becker-Pauly[1]

Received: 23 May 2019 / Revised: 23 May 2019 / Accepted: 29 May 2019 / Published online: 14 June 2019

Abstract

Alzheimer's Disease (AD) is the sixth-leading cause of death in industrialized countries. Neurotoxic amyloid-β (Aβ) plaques are one of the pathological hallmarks in AD patient brains. Aβ accumulates in the brain upon sequential, proteolytic processing of the amyloid precursor protein (APP) by β- and γ-secretases. However, so far disease-modifying drugs targeting β- and γ-secretase pathways seeking a decrease in the production of toxic Aβ peptides have failed in clinics. It has been demonstrated that the metalloproteinase meprin β acts as an alternative β-secretase, capable of generating truncated $A\beta_{2-x}$ peptides that have been described to be increased in AD patients. This indicates an important β-site cleaving enzyme 1 (BACE-1)-independent contribution of the metalloprotease meprin β within the amyloidogenic pathway and may lead to novel drug targeting avenues. However, meprin β itself is embedded in a complex regulatory network. Remarkably, the anti-amyloidogenic α-secretase a disintegrin and metalloproteinase domain-containing protein 10 (ADAM10) is a direct competitor for APP at the cell surface, but also a sheddase of inactive pro-meprin β. Overall, we highlight the current cellular, molecular and structural understanding of meprin β as alternative β-secretase within the complex protease web, regulating APP processing in health and disease.

Keywords Meprin β · ADAM10 · APP · β-secretase · Alzheimer's disease

Abbreviations

AD	Alzheimer's disease
APP	Amyloid precursor protein
Aβ	Amyloid-βADAM; a disintegrin and metalloproteinase domain-containing protein
BACE-1	β-Site cleaving enzyme 1
PS1/2	Presenilin 1 and 2
MT-2	Matriptase-2

✉ Claus Pietrzik
pietrzik@uni-mainz.de

✉ Christoph Becker-Pauly
cbeckerpauly@biochem.uni-kiel.de

[1] Unit for Degradomics of the Protease Web, Biochemical Institute, University of Kiel, Kiel, Germany

[2] Institute for Pathobiochemistry, University Medical Center of the Johannes Gutenberg-University Mainz, Mainz, Germany

The metalloprotease meprin β in health and disease

Meprin β is a membrane-bound multi-domain metalloenzyme (Fig. 1) and exhibits a unique cleavage specificity amongst all extracellular proteases [1]. The protease belongs to the metzincin superfamily characterized by the typical zinc-binding motif HExxHxxGxxH/D and a so-called Met-turn, the latter containing a tyrosine residue that functions as zinc-ligand [2]. Based on structural data it became obvious that all members of the metzincin superfamily, including matrix metalloproteases (MMPs), ADAMs and astacins, share a common fold of the catalytic domain, but exhibit unique features within the active site cleft [3]. Meprin β belongs to the astacin family of metalloproteases and in mammals is closely related to meprin α, bone morphogenetic protein 1 (BMP-1), mammalian tolloid (mTld), tolloid-like 1 and 2 (tll-1/2), and ovastacin [4]. Although all astacin members exhibit a cleavage preference for aspartate and glutamate in P1′, only meprin β is capable of hydrolyzing completely acidic peptides [1, 5]. Several biologically important substrates have been identified, which links meprin β activity to inflammation,

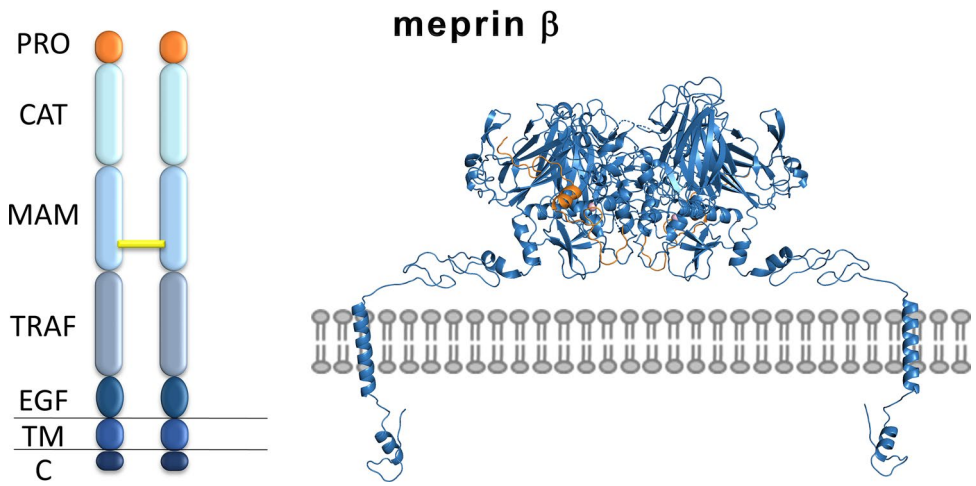

Fig. 1 Domain composition and dimeric structure of the metalloprotease meprin β. Cartoon representation of dimeric meprin β domain model (left) and a membrane-bound ribbon structure model (right) based on the crystal structure of the ectodomain of human meprin β (PDB: 4GWN) *Pro* propeptide, *CAT* catalytic domain, *MAM* meprin A5 protein tyrosine phosphatase μ domain, *TRAF* tumour-necrosis-factor-receptor-associated factor domain, *EGF* epidermal growth factor-like domain, *TM* transmembrane region, *C* C-terminal part. The disulfide bridge between the MAM domains responsible for dimerization is indicated as yellow bar

connective tissue homeostasis and neurodegeneration [6, 7].

Employing different mouse models of acute and chronic inflammation meprin β was found to be a rather pro-inflammatory enzyme [6]. The pro-inflammatory trans-signaling of interleukin 6 (IL-6) can be induced by meprin β through the shedding of the IL-6 receptor from granulocytes then acting on other cells by binding to its β-receptor gp130 and inducing signal transducer and activator of transcription 3 (STAT3) phosphorylation [8]. However, in a dextran sulfate sodium (DSS)-induced colitis model, IL-6 levels were increased in *Mep1a/b*$^{-/-}$ mice compared to wild-type animals [9]. This is further supported by a study showing that meprin β can directly cleave and inactivate IL-6 [10]. Several studies demonstrated that meprin β contributes to the onset and progression of nephritis and acute kidney failure [11, 12]. Interestingly, nanoparticle-based application of meprin β specific siRNA showed a clear benefit in a corresponding mouse model [13]. Another aspect of meprin β's pro-inflammatory activity is reflected by its capacity to promote transendothelial migration (TEM) of immune cells [14, 15]. Here, the cell adhesion molecule CD99 is a possible substrate candidate, as its cleavage by meprin β induces TEM and cell proliferation in vitro and in vivo. Meprin β was also described to promote cell migration through cleavage of extracellular matrix proteins, such as fibronectin or nidogen [16]. However, other studies highlighted a rather opposite function, because meprin β was identified as a procollagen proteinase, cleaving off the N- and C-terminal pro-domains of collagen I + III, thereby inducing collagen fibril assembly [17, 18]. This is further supported by the observations that increased meprin β expression is associated with skin and lung fibrosis [18].

In the small intestine, meprin β is essential for the detachment of the mucus by cleaving mucine 2 (MUC2) [19]. This is crucial for the functionality of the mucus barrier to impede bacterial overgrowth and infection [20]. Interestingly, the pathogenic protease gingipain R (RgpB) from *Porphyromonas gingivalis* is able to cleave meprin β thereby preventing mucus detachment [21]. Of note, cleavage by RgpB leads to activation of membrane-bound meprin β, which precludes its shedding by ADAM proteases. Solubilization of meprin β is a prerequisite for the protease to get access to the cleavage site in MUC2 [19].

Activation and shedding of meprin β are mutually exclusive events [21]. Besides RgpB, this was also demonstrated using matriptase-2 (MT-2) as a potent activator of membrane-bound meprin β [22]. The molecular mechanism why cleavage of the pro-peptide completely blocks shedding by ADAM10/17 is still ambiguous. However, it demonstrates how strict meprin β activity and localization is regulated. This is of utmost importance for the β-secretase function of meprin β in the processing of the amyloid precursor protein (APP), which is involved in the generation of Alzheimer's disease (AD) [23]. Hence, understanding the interplay of the α-secretase ADAM10 with the alternative β-secretase meprin β on molecular, cellular and disease level will help to further elucidate decisive steps in the onset and progression of AD.

β-secretases: BACE and alternatives

Neurotoxic amyloid-β (Aβ) plaques are one hallmark of AD [24, 25]. Aβ deposits in the brain are composed of peptides derived from APP and consist of up to 42 amino acids. Several publications support different molecular mechanisms for Aβ mediated synaptic dysfunction and neuronal cell death, such as membrane disruption, ion dysregulation or oxidative stress induction [26–29]. However, the Aβ biology is rather complex, mainly due to its great hydrophobic interacting potential [30]. Thus, the entire and exact role of Aβ remains elusive. Aβ peptides derive from APP by sequential cleavage at the β- and γ-secretase cleavage sites [31, 32]. Intramembranous γ-cleavage is accomplished by the aspartic peptidases presenilin 1 and 2 (PS1/2) within the γ-secretase complex at position 40 or 42 (numbering according to Aβ sequence) [32]. $Aβ_{1–40}$ is the major species, whereas $Aβ_{1–42}$ levels are low in healthy brains, however, strongly increase during the progression of AD [33]. Of note, conditional PS1/2 double knock-out mice exhibit significantly reduced Aβ levels [34]. Further, more than one hundred PS1 related mutations were identified that lead to increased Aβ levels suggesting PS1 as a susceptibility gene for AD [35]. However, β-secretase cleavage is rate limiting for the Aβ formation [36, 37]. The first identified β-secretase is the aspartic protease β-site cleaving enzyme 1 (BACE-1). It is predominantly expressed in acidic compartments and exhibits a low pH optimum. Thus, BACE-1 dependent APP cleavage occurs in endosomal/lysosomal compartments [38]. The major cleavage event by BACE-1 at the β-site of APP is at position 1 resulting in the dominant Aβ species $Aβ_{1–40/42}$ [39]. Since the Aβ formation in BACE-1 knock-out mice is strongly reduced, BACE-1 is thought to be the major β-secretase [40]. Thus, BACE-1 is one of the most promising therapeutic targets for AD treatment. However, all clinical trials using specific BACE-1 inhibitors have failed so far and have not shown any cognitive benefits for the patients (https://www.alzforum.org/news/conference-coverage/bump-road-or-disaster-bace-inhibitors-worsen-cognition; 02.11.2018). Therefore, the investigation of alternative β-secretases as potential drug targets is of great interest.

Besides the BACE-1-generated $Aβ_{1–x}$ species N-terminal truncated Aβ forms came into focus of research. Already many years ago, Konrad Beyreuther and Colin Masters described N-terminal truncated Aβ peptides in the core of amyloid plaques of AD patients [41]. Other groups have shown an increase of Aβ peptides starting at position 2 ($Aβ_{2–x}$) in the brains of AD patients compared to other dementias or non-demented subjects [42]. A number of N-terminally truncated Aβ variants starting at different other positions have been reported in the cerebrospinal fluid (CSF), blood and brain tissue of AD patients [42–44]. Since BACE-1 is incapable to generate such peptides the hunt for these enzymes was evident. For instance, cathepsin B, S and L as lysosomal proteases are discussed as alternative β-secretases generating various Aβ species [45–47]. Inhibitor studies in cells and mice indicate a direct involvement of these proteinases in Aβ generation [45]. Of note, cathepsin B is thought to be involved in $Aβ_{3–x}$ formation, which is the progenitor of highly neurotoxic pyroglutamate-modified $Aβ_{3–x}$ [46]. However, cathepsin D is involved in the clearance of Aβ [48]. The detailed role of cathepsins in this context is not revealed so far, however, their low cleavage specificity on APP suggests a Aβ degrading role [49, 50]. Other candidates generating N-terminally truncated Aβ peptides are the Aminopeptidases A and N (APA/APN). APA generates $Aβ_{2–x}$ from $Aβ_{1–x}$, whereas APN is thought to convert $Aβ_{2–x}$ to $Aβ_{3–x}$ [51, 52]. A promising alternative β-secretase that directly cleaves at p2 within full-length APP is the metalloprotease meprin β [23]. We and others could show that mRNA and protein levels of meprin β are significantly increased in AD brain [23, 53], which is in line with increased $Aβ_{2–42}$ [42]. Of note, $Aβ_{2–40}$ peptides not only exhibit a greater aggregation potential than $Aβ_{1–40}$ but additionally induce $Aβ_{1–40}$ aggregation [54]. Mass spectrometry-based degradomics identified APP as a substrate for meprin β at three different sites in the N-terminal region between Ser124/Asp125, Glu380/Thr381, and Gly383/Asp384 [55]. After incubation with all APP isoforms and meprin β, two fragments of 20 and 11 kDa were identified either in vitro or in cell culture-based assays (Fig. 2). Interestingly, these fragments derived from APP processing were found in human and wild-type mice brain lysates, but not in the brain of *Mep1b*$^{-/-}$ mice [55], proving APP as a physiological target of meprin β. The major cleavage site of meprin β in APP695 is between Asp597 and Ala598 resulting in the formation of $Aβ_{2–x}$, and to a minor extend between Met596 and Asp597 at the BACE-1 site [7, 23]. Meprin β knock-out mice brains show increased sAPPα levels which could indicate that the absence of meprin β leads to more available substrate to α-secretase. It has been shown that meprin β and APP co-localize at the cell surface and in the secretory pathway leading to APP processing by meprin β in these cellular compartments [54]. Therefore, meprin β may compete at the cell surface with ADAM10, the main α-secretase in the brain [56]. A recent publication indicates that meprin β may also act as dipeptidyl-peptidase being able to convert $Aβ_{1–x}$ to $Aβ_{3–x}$, which is the progenitor of highly neurotoxic pyroglutamate-modified $Aβ_{3–x}$ [53]. However, this observation is based on in vitro cleavage using truncated Aβ-peptides. Hence, further cell-based assays are necessary to validate these findings.

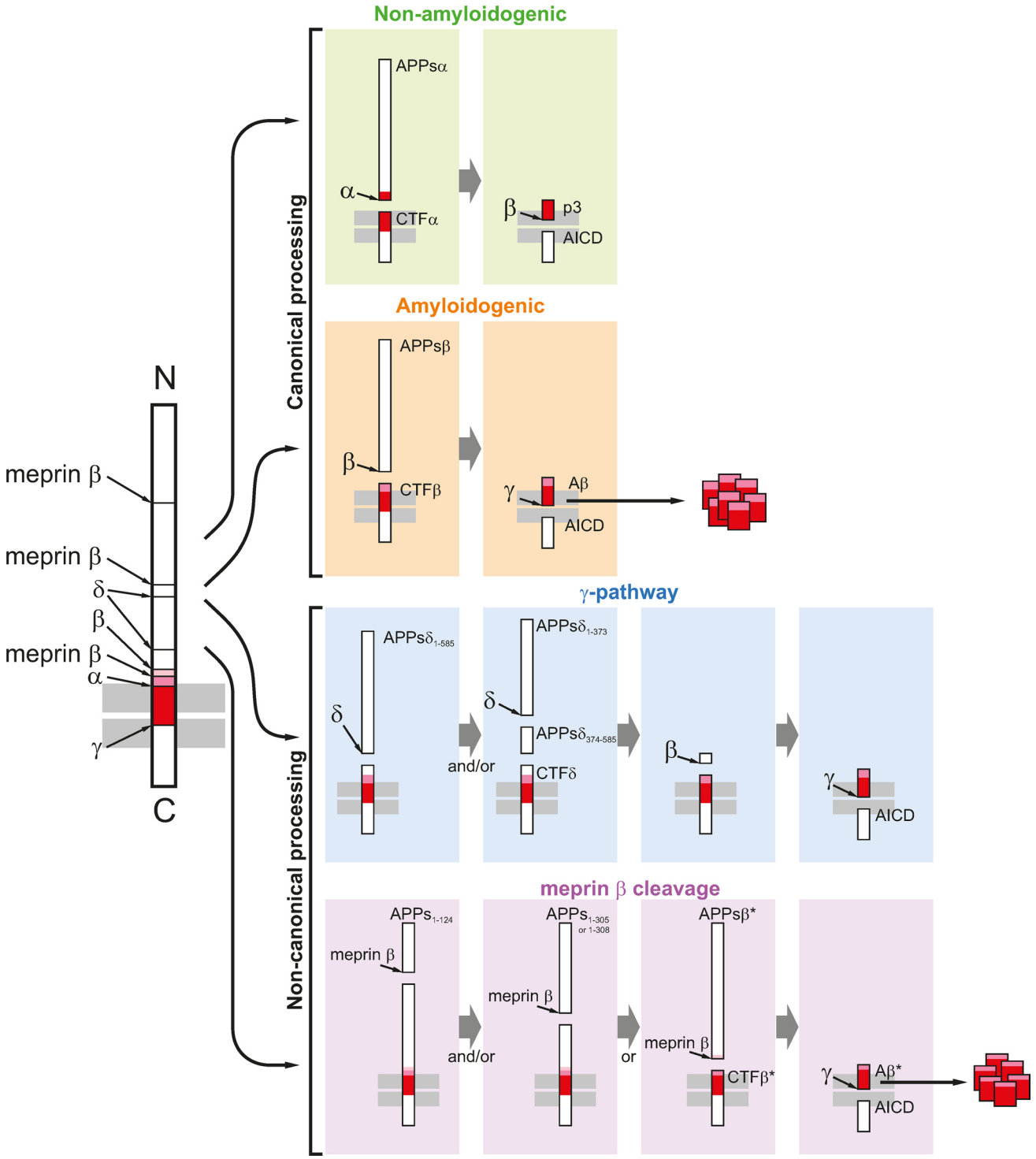

Fig. 2 APP processing by BACE-1 and meprin β in the canonical and non-canonical pathway. BACE-1 and meprin β are shown to be involved in the generation of Aβ peptides in the canonical and non-canonical pathway. The so far well-described APP processing pathways by α-, β- and δ-secretases are described in green, orange and blue. Meprin β is involved in the generation of two APP N-terminal fragments of 20 and 11 kDa as well as the cleavage of APP at the β-secretase cleavage site (purple), providing a substrate for γ-secretase releasing Aβ peptides (red)

The role of meprin β-generated $A\beta_{2-x}$ has yet not been investigated in the common AD mouse models such as 5xFAD or tg2576. These and other mouse models contain the Swedish APP (APPswe) variant bearing two point mutations (KM595/N596L) N-terminal to the β-secretase cleavage site. These mutations originate from a rare genetic APP variant identified in two Swedish families [57, 58]. APPswe mutations are connected with an early loss of memory and dramatically increased the accumulation of $A\beta_{1-x}$ generated by BACE-1 [59, 60]. Of note, BACE-1 deficiency recovers the loss of memory and $A\beta_{1-x}$ accumulation [60]. However, the β-site of APPswe is not cleaved at position 2 by meprin β, resulting in complete reduction of N-terminal truncated Aβ peptides starting at p2 in mouse models carrying the APPswe mutation [7, 54]. This leads to the assumption that alterations of the amino acid composition close to the β-secretase cleavage site may inhibit meprin β activity on the generation of N-terminal truncated Aβ peptides. This could be further validated since the "protective" A673T mutation in APP, which results in reduced Aβ levels in patients, also prevents from meprin β cleavage at position p2 [54]. The cleavage sites of BACE-1 and meprin β on APPwt and APPswe are shown in Fig. 3.

Thus, it is not possible to address the biological relevance of meprin β-generated $A\beta_{2-x}$ in APPswe based mouse models. With regard to continuously failing BACE-1 inhibitor clinical trials, AD mouse models considering truncated Aβ species in an APP wild-type background are essential to promote AD research. A potential role of meprin β expression in AD may be reflected in genetic studies. Quantitative comparison of meprin β expression revealed significantly higher mRNA levels in brain tissue from AD patients versus controls [23]. Recently, Schlenzig and colleagues also detected a fivefold increase in expression levels of meprin β in postmortem tissue samples from AD patients compared to age-matched controls [53]. In addition, a more detailed histological analysis showed a prominent meprin β immunoreactivity in tissue sections from AD cases compared to controls. Interestingly, this work detected a noticeable immunoreactivity for meprin β in glial cells, more precisely in astrocytes of AD patients [53].

Using brain tissue from the Brains for Dementia Research (BDR) cohort, which was specifically created to address the shortages of high-quality brain tissue samples from healthy individuals as well as those with dementia, Patel and colleagues performed single variant and burden analysis on coding variants to identify significant associations with late-onset AD (LOAD). Using next-generation DNA sequencing (NGS) a synonymous mutation in *MEP1B*, the gene coding for meprin β, was identified to have greater frequency in AD cases than controls [61]. Although the sample size of this cohort is rather small and needs further validation, the result may provide more evidence to imply meprin β is in close association with AD.

β-secretase cleavage of APP is not only determined by the site preferences of the different enzymes. Cellular localization of APP/protease-interaction is also an important issue. BACE-1-dependent Aβ release occurs intracellularly due to its activity in late endosomes/lysosomes, whereas meprin β-dependent Aβ generation takes place at the cell surface or even in the late secretory pathway [54]. The α-secretase ADAM10 exhibits dual anti-amyloidogenic

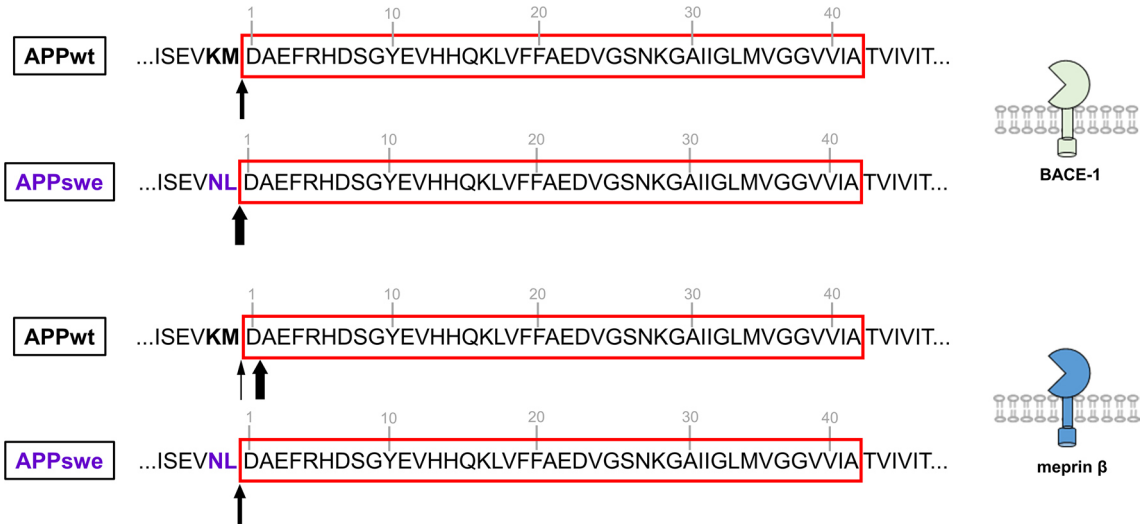

Fig. 3 Comparison of APPwt and APPswe processing by BACE-1 and meprin β. The local APP peptide sequence around the Aβ region (red boxes) is depicted. The Swedish APP mutation is highlighted by purple letters. The upper panel shows BACE-1-mediated and the lower panel meprin β-mediated APP processing at the β-site. The arrows indicate cleavage sites of BACE-1 or meprin β on APPwt in comparison to APPswe

activity by cleaving APP within the Aβ-peptide sequence and by ectodomain shedding of meprin β thereby destroying its β-secretase activity [23, 62]. Hence, in contrast to BACE-1, ADAM10 and meprin β are direct competitors for the substrate APP at the cell surface.

Shedding of meprin β

The activity of meprin β is strictly regulated within the protease web (Fig. 4) [1, 21, 22]. During the secretory pathway, meprin β gets highly glycosylated and reaches the cell surface as zymogen. For maturation, the pro-peptide of soluble meprin β can be cleaved off by tryptic serine proteases, such as trypsin or human kallikrein-related peptidases (KLKs) [1, 63]. The membrane-tethered serine protease matriptase-2 (MT-2) has been identified as a potent activator of membrane-bound meprin β [22]. ADAM10 and ADAM17 were identified as sheddases of pro-meprin β, which is then maturated by soluble tryptic proteases [21, 63–65]. Importantly, shedding of meprin β by ADAM10/17 is completely abolished upon its activation by MT-2 at the cell surface [21]. The molecular mechanism why only the pro-form of meprin β can be shed is not understood.

Interestingly, there are subtle differences between the substrate pools of membrane-bound and soluble meprin β. The adhesion molecule CD99, essential for the transendothelial migration of leukocytes, is for example cleaved by both meprin β entities [14, 15]. For the meprin β substrates collagen-1 or the cytokines IL-6 and IL-18 it is still elusive if the membrane-bound and/or soluble form is involved in cleavage and requires further investigations [10, 17, 66]. In contrast, the receptor of the pro-inflammatory cytokine IL-6 is shed by membrane-bound meprin β only, and not by the soluble form [8]. As mentioned above, a specific substrate that is only cleaved by soluble meprin β is mucin-2 [19]. This cleavage event can be abrogated by the pathogenic protease RgpB that potently converts membrane-bound pro-meprin β into its active form thereby preventing its shedding by ADAM10/17 [21].

In terms of different substrate pools of soluble and membrane-bound meprin β, APP exhibits quite unique properties. Both meprin β forms were identified to cleave APP within its N-terminal region. Certain N-terminal APP fragments (N-APP) were discussed as neurotoxic factors through binding to the neuronal death receptor DR6 and inducing caspase-mediated cell death [67, 68]. However, meprin β generated N-APP fragments do not show neurotoxic properties at all [55]. A much more valid correlation of APP and neurodegeneration is based on the amyloid hypothesis. Sequential proteolytic cleavage of APP by β- and γ-secretase leads to the generation of aggregation-prone Aβ-peptides found in neurotoxic plaques in AD brains. We identified meprin β as an alternative β-secretase predominantly generating $Aβ_{2–x}$ peptides [7, 23]. This cleavage event requires membrane-bound meprin β and is prevented

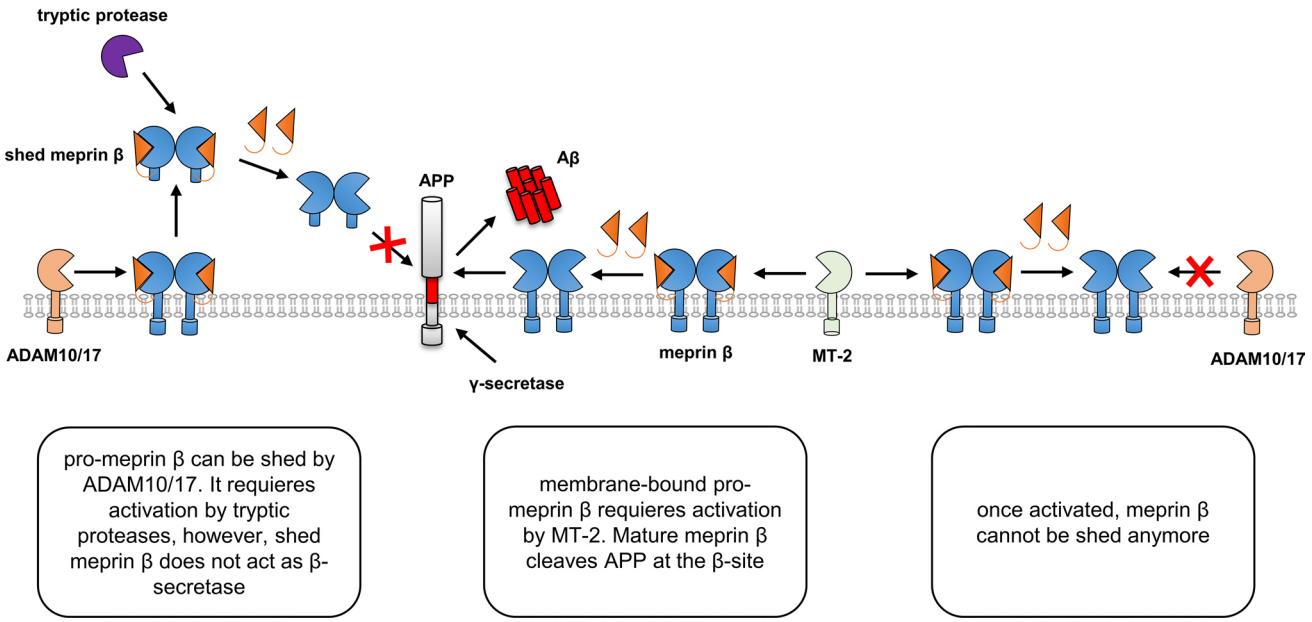

Fig. 4 Extracellular regulation of meprin β activity with respect to β-site cleavage of APP. Meprin β is expressed as zymogen at the cell surface. A disintegrin and metalloprotease 10 and 17 (ADAM10/17) act as sheddases of pro-meprin β. Shed meprin β can be activated by tryptic proteases. When activated as soluble protein, shed meprin β does not cleave at the β-site of APP. Alternatively, inactive meprin β can be maturated by the membrane-bound serine protease matriptase-2 (MT-2). Once activated at the cell surface membrane-bound meprin β cannot be shed any more and acts as β-secretase thus generating amyloid-β (Aβ)

for the soluble shed protease. Thus, the meprin β sheddases ADAM10 and 17 may exhibit a dual function in preventing from amyloidation in AD. On the one hand, ADAM10 acts as α-secretase cleaving APP within the Aβ sequence and, thus, counteract against Aβ formation [62, 69]. On the other hand, ADAM10/17 prevent from amyloidation by shedding the β-secretase meprin β from the cell surface. However, whether ADAM proteases prefer APP over meprin β as shedding substrate or vice versa is completely unknown. Of note, meprin β itself was identified as an inducer of ADAM10 activity [64]. This finding complicates the protease network around ADAM10/17-mediated prevention of Aβ generation. Thus, further research on the exact mechanism of the dual protective role of ADAM 10 and 17 is required.

Structural properties of APP, ADAM10 and meprin β

As outlined above, the processing of APP is embedded in a quite complex network of different proteolytic checkpoints. In the last years, many investigations contributed to a better biochemical and cellular understanding of these complex regulatory mechanisms. Simultaneously, the results made apparent that a comprehensive knowledge of the molecular basis of APP processing is still missing. This is likewise reflected by the failure rate in developing successful inhibitory strategies for the treatment of AD. One essential bottleneck in that context is the so far only partly available structural information on APP itself and its processing proteases.

Structural information on APP is still enigmatic

APP is a single-span type-I multi-domain membrane protein belonging to the small gene family of APP-like proteins including also the amyloid precursor-like protein (APLP) 1 and 2. Overall, these three proteins and the existing isoforms share a highly similar domain organization and proteolytic processing, while only APP contains the Aβ-peptide sequence critical in the pathogenesis of AD [70–75]. APP proteins consist of three highly conserved regions: the extracellular E1 and E2 domains separated via a single transmembrane helix from the rather small C-terminal APP intracellular domain (AICD) (Fig. 5a). The E1 is composed of an N-terminal cysteine-rich growth factor-like subdomain (GFLD) with heparin binding properties (HBD) joined by a short linker with a zinc and copper-binding subdomain (CuBD) [76–79]. A structural flexible acidic domain (AcD), constituting of nearly 50% glutamate and aspartate residues, connects the E1 domain with the E2 domain in the neuronal isoform APP695 and ALPL1. The APP751 isoform consists of an additional Kunitz-type serine protease inhibitor domain (KPI) N-terminal to the E2 domain, which is in APP770 further followed by a 19 amino acid OX-2 domain, homologues to the immunoregulatory OX-2 antigen [80, 81]. The E2 domain, also known as central APP domain (CAPPD), is the largest of the conserved domains containing several substructures with interaction sites for binding partners like a second HBD, the RERMS pentapeptide motif [82–84] and a collagen binding domain [85–87] as well as two *N*-glycosylation sites [88, 89]. The natively unstructured juxtamembrane region (JMR) harbours an additional *O*-glycosylation site as well as the α- and β-secretase cleavage sites relevant for the shedding of APP. It connects the ectodomain with the TM-Helix, containing the γ-secretase cleavage site, which is followed by the intracellular AICD domain.

Even though in the last two decades many attempts have been made to structurally characterize APP, a structure with atomic resolution of full-length APP or its entire extracellular domain is still not available. Therefore, the current understanding is based on a set of substructure information. The GFLD and CuBD subdomains of the N-terminal E1 domain were initially described as individual folding units [76–78]. Further studies showed that the overall fold of both subdomains in isolation is very similar to their structures within the entire E1 domain, both comprising αβ topologies stabilized by disulfide bridges [79, 90]. The structural rigidity of E1 domain is determined by the interface interaction between GFLD and CuBD in a pH-dependent manner. An acidic pH leads to a tight interaction resulting in a compact structural conformation of the E1 entity [79, 90, 91]. Additionally, alterations of the pH regulate the self-dimerization of the isolated E1 domain as well as one of heparin-induced E1 dimers [79, 91]. However, size exclusion and light scattering experiments demonstrated the impact of the structural flexible linker connecting the E1 and E2 on dimerization of APP in solution [91]. In particular the presence of the acidic stretch AcD interfered with self- and the heparin-induced dimerization of the E1 domain, while the binding affinity for heparin was reduced [91]. Remarkably, for the entire extracellular domain and for the isolated E2 no short-chain heparin-induced dimerization and only a low self-dimerization potential at unphysiological high protein concentrations could be observed [91]. The E2 domain itself is an almost helical structure consisting of six α-helices arranged in two distinct coiled-coil substructures, which share a long continues central helix [88, 92–94]. In case of the E2 domain, metal binding correlates with the conformational flexibility, leading to increased rigidity as well as thermostability of the domain [92]. Also an X ray structure of an antiparallel APP E2 dimer was reported [88]. In contrast to this, limited proteolysis experiments and NMR analysis suggest that only parts of this domain are rigidly folded in solution [94]. As a third

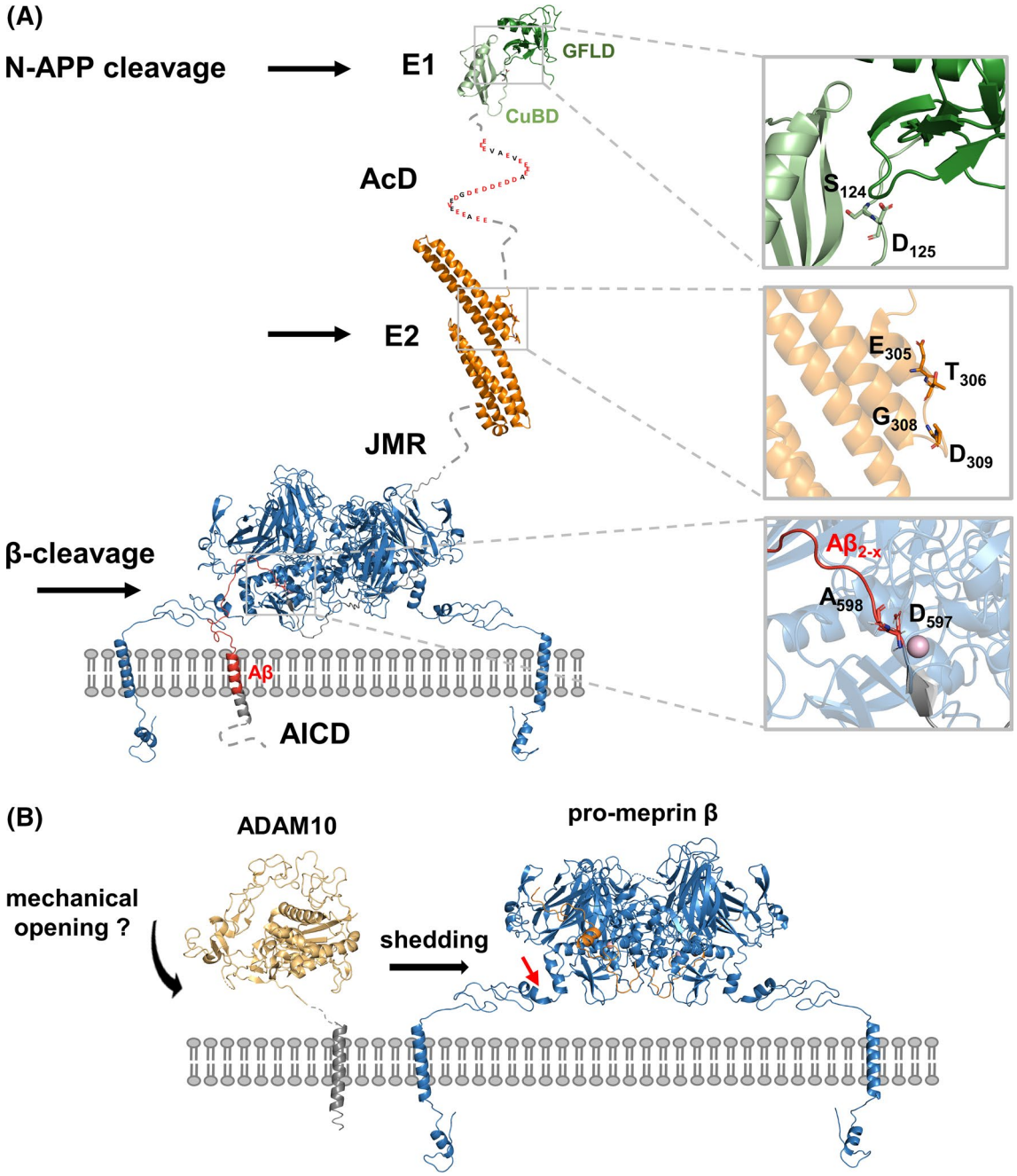

Fig. 5 Extracellular regulation of meprin β activity with respect to β-site cleavage of APP. **a** Cartoon representation of a membrane-bound meprin β model (blue) based on the crystal structure of the ectodomain (PDB: 4GWN) in complex with part of APP (grey, Aβ peptide in red). Structures of additional N-terminal domains of APP695 are also shown as cartoons: E1 (PDB: 3KTM), E2 (PDB: 3NYL). Sequence stretches of unknown structure and the AICD domain are illustrated as dashed lines. The close up views in the right panel highlight determined meprin β cleavage sites, while P1 and P1′ residues are depicted as sticks. **b** Model of a membrane-bound ADAM10 based on the ectodomain (yellow, PDB: 6BE6) and pro-meprin β (blue). The pro-peptide of meprin β is shown in orange. The red arrow indicates the shedding site within pro-meprin β. *E1/2* extracellular domains 1/2, *Acd* acidic domain, *JMR* juxtamembrane region, *AICD* APP intracellular domain

site of potential dimerization, the TM-helix was postulated. Several studies intended to understand the structure of various truncated transmembrane containing fragments under different solvent conditions [95–99]. The NMR analysis of the entire β-secretase cleavage product C99 offered for the first time a more comprehensive view on the helical nature of the transmembrane helix in presence of N- and C-terminal flanking APP regions [100]. In this structure, the β-cleavage

site itself was found to be located within the unstructured juxtamembrane region. In contrast, the α-cleavage site is in close proximity to the outer membrane leaflet at the beginning of a short extracellular so-called N-helix. Further pulsed electron paramagnetic resonance (EPR) double electron–electron resonance (DEER) experiments confirmed a flexible, highly curved nature of the transmembrane helix, which is supposed to be well suited for its interaction with the γ-secretase. Interestingly, a second C-terminal helix, structurally uncoupled from the TM-helix, was shown to be likewise surface-associated. The transmembrane segment of APP features three consecutive glycine zipper motifs known to mediate dimerization in single-pass TM proteins [101–104]. Indeed, an involvement of these motifs in the dimerization of the transmembrane region with a regulatory impact on Aβ species generation was shown [99, 105–108]. While NMR studies structurally substantiate these observations by a dimeric transmembrane segment association under micellar conditions [109, 110], a monomeric state upon cholesterol binding was suggested [111]. Following molecular dynamic simulations support a determining effect of lipid composition, membrane thickness and membrane curvature influencing the C99 overall structure and the tendency to dimerize [112–114]. Finally, the C-terminal AICD domain that is intracellularly released after γ-secretase cleavage was shown to be intrinsically disordered by nuclear magnetic resonance (NMR) and circular dichroism (CD) experiments [115, 116]. However, it has been shown that this domain can adopt different conformations depending on its interaction partner as documented by the structures in complex with Dab1 and 2 [117], X11α [118] and the phosphotyrosine-binding Fe65-PTB domains [119].

Even though major progress has been made to understand the unique APP on the structural level, it still remains enigmatic to what extent the conformation of the individual subunits and their arrangement within the whole protein influence the processing by α, β or the γ-secretase complex. Especially the different derived models of *cis*- and *trans*-dimerization of APP need further investigations to conclusively clarify, how and if all proposed and analysed dimerization regions contribute to a membrane-bound dimer. In addition, it is possible that sAPP molecules interact differently with each other once cleaved by α- or β-secretases.

Structural properties of meprin β

The structure of the ectodomain of the alternative β-secretase meprin β revealed a compact disulfide-bridged dimer [120, 121]. Interestingly, both monomers interact in a nearly symmetric fashion between the catalytic domain of one monomer and the MAM domain of the other. By that, the two catalytic domains are accessible on opposite sites of the dimer and the active site clefts locate close to the plasma membrane (Figs. 1 and 5). Maturation of meprin β requires proteolytic processing of the N-terminal pro-peptide. Comparison of the available zymogen and mature meprin β structures indicates that the zymogen is already in a preformed conformation. Solely one-seventh of the protein is rearranged to gain catalytic activity. Given by the overall rigidity of meprin β, substrate engagement most likely requires structural flexible segments able to follow a "N-like" trajectory over the dimer to enter the active site cleft of one monomer. Overall, this mechanism would be compatible with most type-I transmembrane substrates. This is also nicely in line with the flexible, unstructured juxtamembrane region of APP, which contains the β-cleavage site (Fig. 5a). Taken this into account, it is hard to envision how APP cleavage of an e.g. TM-region associated dimer should be facilitated by meprin β. So far, N-APP cleavage by meprin β was only shown for soluble meprin β [55]. N-APP cleavage sites have been identified in the E1 and E2 domain (Fig. 2) [55]. Interestingly, so far no cleavage within the AcD domain was observed, even though the sequence stretches of alternating glutamate and aspartate residues represent ideal meprin β cleavage sites [5].

The α-secretase ADAM10 is a type-I transmembrane protein

ADAM10 is also a type-I transmembrane protein with a modular domain organization (Fig. 5b). In the extracellular ectodomain, the pro-domain is followed by a metalloprotease, disintegrin and cysteine-rich domain. The recently solved X ray structure of the ectodomain of ADAM10 gives first insights in activity regulatory mechanisms of the protease [122]. The structure adopts a compact fold resembling an arrowhead with the cysteine-rich domain partially occupying the active site (Fig. 5b). This suggests that the cysteine-rich domain has an autoinhibitory function to preclude unrestricted substrate access. Therefore, the authors suggested that a transient opening of ADAM10 is permissive for substrate capture. It is possible that the disintegrin and cysteine-rich region of ADAM10 directly contacts the substrate thereby stabilizing both proteins in their open conformations to promote cleavage. Further investigations are needed to explore this hypothesis in more detail. Nevertheless, deduced from the C99 [100] and the meprin β structure [120] it is very likely that cleavage of both proteins takes place in close proximity to the plasma membrane (Fig. 5b).

Taken together, understanding the structural basis of ADAM10-mediated APP cleavage at the α-site, and its shedding activity toward meprin β as competing β-secretase, would be a breakthrough to decipher homeostasis of APP processing in health and disease.

Conclusions and future directions/perspectives

Late-onset AD, the most common neurodegenerative disorder, is a progressive and to date incurable form of dementia that develops in the elderly population. In brains of AD patients, loss of neurons and synapses occur as a result of the accumulation of Aβ peptides. The aspartyl protease BACE-1 was identified as the major APP-cleaving β-secretase. However, certain AD associated N-terminally truncated Aβ peptides could not be assigned to BACE-1 activity, indicating the presence of additional β-secretases. We demonstrated that the metalloproteinase meprin β is capable of generating N-terminal truncated $A\beta_{2-x}$ peptides that have been described in AD patients [42], which may point to an important and BACE-independent contribution of the metalloprotease meprin β within the amyloidogenic pathway.

We could demonstrate physiological relevance of meprin β mediated APP cleavage, since we observed absence of N-APP fragments and increased endogenous sAPPα levels in the brains of meprin β knock-out mice [54, 55]. Moreover, we could show an interaction of APP and meprin β by coimmunoprecipitation and direct involvement of meprin β activity on the generation of $A\beta_{2\text{-}x}$ peptides in vitro. A recent study further supports the relevance of meprin β in AD, where a potential risk gene variant of meprin β (rs173032) for AD has been identified using whole-exome sequencing of the Brains for Dementia Research (BDR) cohort. Increased meprin β mRNA and protein expression specifically in AD cases has been observed previously [23].

Recently, the laboratory of Dennis Selkoe has shown, that meprin β co-fractionates with APP and PS1 in the same high molecular weight fraction in wild type mouse brains and that this fraction is responsible for the majority of Aβ generation [123]. Interestingly, ADAM10 is also present in these high molecular weight fractions. Hence, it is important to investigate how APP cleavage within these microdomains switches between competitive non-amyloidogenic (α-secretase) and amyloidogenic (β-secretase) processing in health and disease. Furthermore, the direct interaction with ADAM10 promotes shedding of meprin β, which in its soluble form loses its β-secretase activity [23]. Identification of regulatory elements responsible for the orchestration of substrates and proteases will be decisive for a better understanding of the molecular basis for AD pathology.

Acknowledgements This work was supported by the Alzheimer Forschung Initiative e.V. (#18007) and the Deutsche Forschungsgemeinschaft (DFG) Project-number 125440785 SFB 877 (Proteolysis as a Regulatory Event in Pathophysiology, Projects A9 and A15) and BE 4086/2-2 (C.B.-P.).

References

1. Broder C, Becker-Pauly C (2013) The metalloproteases meprin alpha and meprin beta: unique enzymes in inflammation, neurodegeneration, cancer and fibrosis. Biochem J 450(2):253–264. https://doi.org/10.1042/BJ20121751
2. Bode W, Grams F, Reinemer P, Gomis-Ruth FX, Baumann U, McKay DB, Stocker W (1996) The metzincin-superfamily of zinc-peptidases. Adv Exp Med Biol 389:1–11
3. Gomis-Ruth FX (2003) Structural aspects of the metzincin clan of metalloendopeptidases. Mol Biotechnol 24(2):157–202. https://doi.org/10.1385/MB:24:2:157
4. Gomis-Ruth FX, Trillo-Muyo S, Stocker W (2012) Functional and structural insights into astacin metallopeptidases. Biol Chem 393(10):1027–1041. https://doi.org/10.1515/hsz-2012-0149
5. Becker-Pauly C, Barre O, Schilling O, Auf dem Keller U, Ohler A, Broder C, Schutte A, Kappelhoff R, Stocker W, Overall CM (2011) Proteomic analyses reveal an acidic prime side specificity for the astacin metalloprotease family reflected by physiological substrates. Mol Cell Proteomics 10(9):M111009233. https://doi.org/10.1074/mcp.m111.009233
6. Arnold P, Otte A (1864) Becker-Pauly C (2017) Meprin metalloproteases: molecular regulation and function in inflammation and fibrosis. Biochim Biophys Acta Mol Cell Res 11 Pt B:2096–2104. https://doi.org/10.1016/j.bbamcr.2017.05.011
7. Becker-Pauly C, Pietrzik CU (2016) The metalloprotease meprin beta is an alternative beta-secretase of APP. Front Mol Neurosci 9:159. https://doi.org/10.3389/fnmol.2016.00159
8. Arnold P, Boll I, Rothaug M, Schumacher N, Schmidt F, Wichert R, Schneppenheim J, Lokau J, Pickhinke U, Koudelka T, Tholey A, Rabe B, Scheller J, Lucius R, Garbers C, Rose-John S, Becker-Pauly C (2017) Meprin metalloproteases generate biologically active soluble interleukin-6 receptor to induce trans-signaling. Sci Rep 7:44053. https://doi.org/10.1038/srep44053
9. Banerjee S, Jin G, Bradley SG, Matters GL, Gailey RD, Crisman JM, Bond JS (2011) Balance of meprin A and B in mice affects the progression of experimental inflammatory bowel disease. Am J Physiol Gastrointest Liver Physiol 300(2):G273–G282. https://doi.org/10.1152/ajpgi.00504.2009
10. Keiffer TR, Bond JS (2014) Meprin metalloproteases inactivate interleukin 6. J Biol Chem 289(11):7580–7588. https://doi.org/10.1074/jbc.M113.546309
11. Oneda B, Lods N, Lottaz D, Becker-Pauly C, Stocker W, Pippin J, Huguenin M, Ambort D, Marti HP, Sterchi EE (2008) Metalloprotease meprin beta in rat kidney: glomerular localization and differential expression in glomerulonephritis. PLoS One 3(5):e2278. https://doi.org/10.1371/journal.pone.0002278
12. Bylander JE, Ahmed F, Conley SM, Mwiza JM, Ongeri EM (2017) Meprin metalloprotease deficiency associated with higher mortality rates and more severe diabetic kidney injury in mice with STZ-induced type 1 diabetes. J Diabetes Res 2017:9035038. https://doi.org/10.1155/2017/9035038
13. Alidori S, Akhavein N, Thorek DL, Behling K, Romin Y, Queen D, Beattie BJ, Manova-Todorova K, Bergkvist M, Scheinberg DA, McDevitt MR (2016) Targeted fibrillar nanocarbon RNAi treatment of acute kidney injury. Sci Transl Med 8(331):331ra339. https://doi.org/10.1126/scitranslmed.aac9647
14. Bedau T, Peters F, Prox J, Arnold P, Schmidt F, Finkernagel M, Kollmann S, Wichert R, Otte A, Ohler A, Stirnberg M, Lucius R, Koudelka T, Tholey A, Biasin V, Pietrzik CU, Kwapiszewska G, Becker-Pauly C (2017) Ectodomain shedding of CD99 within highly conserved regions is mediated by the metalloprotease meprin beta and promotes transendothelial cell migration. FASEB J 31(3):1226–1237. https://doi.org/10.1096/fj.201601113R

15. Bedau T, Schumacher N, Peters F, Prox J, Arnold P, Koudelka T, Helm O, Schmidt F, Rabe B, Jentzsch M, Rosenstiel P, Sebens S, Tholey A, Rose-John S, Becker-Pauly C (2017) Cancer-associated mutations in the canonical cleavage site do not influence CD99 shedding by the metalloprotease meprin beta but alter cell migration in vitro. Oncotarget 8(33):54873–54888. https://doi.org/10.18632/oncotarget.18966
16. Kruse MN, Becker C, Lottaz D, Kohler D, Yiallouros I, Krell HW, Sterchi EE, Stocker W (2004) Human meprin alpha and beta homo-oligomers: cleavage of basement membrane proteins and sensitivity to metalloprotease inhibitors. Biochem J 378(Pt 2):383–389. https://doi.org/10.1042/BJ20031163
17. Broder C, Arnold P, Vadon-Le Goff S, Konerding MA, Bahr K, Muller S, Overall CM, Bond JS, Koudelka T, Tholey A, Hulmes DJ, Moali C, Becker-Pauly C (2013) Metalloproteases meprin alpha and meprin beta are C- and N-procollagen proteinases important for collagen assembly and tensile strength. Proc Natl Acad Sci USA 110(35):14219–14224. https://doi.org/10.1073/pnas.1305464110
18. Kronenberg D, Bruns BC, Moali C, Vadon-Le Goff S, Sterchi EE, Traupe H, Bohm M, Hulmes DJ, Stocker W, Becker-Pauly C (2010) Processing of procollagen III by meprins: new players in extracellular matrix assembly? J Invest Dermatol 130(12):2727–2735. https://doi.org/10.1038/jid.2010.202
19. Schutte A, Ermund A, Becker-Pauly C, Johansson ME, Rodriguez-Pineiro AM, Backhed F, Muller S, Lottaz D, Bond JS, Hansson GC (2014) Microbial-induced meprin beta cleavage in MUC2 mucin and a functional CFTR channel are required to release anchored small intestinal mucus. Proc Natl Acad Sci USA 111(34):12396–12401. https://doi.org/10.1073/pnas.1407597111
20. Johansson ME, Hansson GC (2016) Immunological aspects of intestinal mucus and mucins. Nat Rev Immunol 16(10):639–649. https://doi.org/10.1038/nri.2016.88
21. Wichert R, Ermund A, Schmidt S, Schweinlin M, Ksiazek M, Arnold P, Knittler K, Wilkens F, Potempa B, Rabe B, Stirnberg M, Lucius R, Bartsch JW, Nikolaus S, Falk-Paulsen M, Rosenstiel P, Metzger M, Rose-John S, Potempa J, Hansson GC, Dempsey PJ, Becker-Pauly C (2017) Mucus detachment by host metalloprotease meprin beta requires shedding of its inactive Pro-form, which is abrogated by the pathogenic protease RgpB. Cell Rep 21(8):2090–2103. https://doi.org/10.1016/j.celrep.2017.10.087
22. Jackle F, Schmidt F, Wichert R, Arnold P, Prox J, Mangold M, Ohler A, Pietrzik CU, Koudelka T, Tholey A, Gutschow M, Stirnberg M, Becker-Pauly C (2015) Metalloprotease meprin beta is activated by transmembrane serine protease matriptase-2 at the cell surface thereby enhancing APP shedding. Biochem J 470(1):91–103. https://doi.org/10.1042/BJ20141417
23. Bien J, Jefferson T, Causevic M, Jumpertz T, Munter L, Multhaup G, Weggen S, Becker-Pauly C, Pietrzik CU (2012) The metalloprotease meprin beta generates amino terminal-truncated amyloid beta peptide species. J Biol Chem 287(40):33304–33313. https://doi.org/10.1074/jbc.M112.395608
24. Moller HJ, Graeber MB (1998) The case described by Alois Alzheimer in 1911. Historical and conceptual perspectives based on the clinical record and neurohistological sections. Eur Arch Psychiatry Clin Neurosci 248(3):111–122
25. Murphy MP, LeVine H 3rd (2010) Alzheimer's disease and the amyloid-beta peptide. J Alzheimers Dis 19(1):311–323. https://doi.org/10.3233/JAD-2010-1221
26. Sengupta U, Nilson AN, Kayed R (2016) The role of amyloid-beta oligomers in toxicity, propagation, and immunotherapy. EBioMedicine 6:42–49. https://doi.org/10.1016/j.ebiom.2016.03.035
27. Mark RJ, Lovell MA, Markesbery WR, Uchida K, Mattson MP (1997) A role for 4-hydroxynonenal, an aldehydic product of lipid peroxidation, in disruption of ion homeostasis and neuronal death induced by amyloid beta-peptide. J Neurochem 68(1):255–264
28. Abramov AY, Canevari L, Duchen MR (2004) Calcium signals induced by amyloid beta peptide and their consequences in neurons and astrocytes in culture. Biochim Biophys Acta 1742(1–3):81–87. https://doi.org/10.1016/j.bbamcr.2004.09.006
29. McLaurin J, Chakrabartty A (1996) Membrane disruption by Alzheimer beta-amyloid peptides mediated through specific binding to either phospholipids or gangliosides. Implications for neurotoxicity. J Biol Chem 271(43):26482–26489
30. Han SH, Park JC, Mook-Jung I (2016) Amyloid beta-interacting partners in Alzheimer's disease: from accomplices to possible therapeutic targets. Prog Neurobiol 137:17–38. https://doi.org/10.1016/j.pneurobio.2015.12.004
31. Venugopal C, Demos CM, Rao KS, Pappolla MA, Sambamurti K (2008) Beta-secretase: structure, function, and evolution. CNS Neurol Disord Drug Targets 7(3):278–294
32. Bohm C, Chen F, Sevalle J, Qamar S, Dodd R, Li Y, Schmitt-Ulms G, Fraser PE, St George-Hyslop PH (2015) Current and future implications of basic and translational research on amyloid-beta peptide production and removal pathways. Mol Cell Neurosci 66(Pt A):3–11. https://doi.org/10.1016/j.mcn.2015.02.016
33. Bitan G, Kirkitadze MD, Lomakin A, Vollers SS, Benedek GB, Teplow DB (2003) Amyloid beta -protein (Abeta) assembly: abeta 40 and Abeta 42 oligomerize through distinct pathways. Proc Natl Acad Sci USA 100(1):330–335. https://doi.org/10.1073/pnas.222681699
34. Beglopoulos V, Sun X, Saura CA, Lemere CA, Kim RD, Shen J (2004) Reduced beta-amyloid production and increased inflammatory responses in presenilin conditional knock-out mice. J Biol Chem 279(45):46907–46914. https://doi.org/10.1074/jbc.M409544200
35. Sun L, Zhou R, Yang G, Shi Y (2017) Analysis of 138 pathogenic mutations in presenilin-1 on the in vitro production of Abeta42 and Abeta40 peptides by gamma-secretase. Proc Natl Acad Sci USA 114(4):E476–E485. https://doi.org/10.1073/pnas.1618657114
36. Luo Y, Bolon B, Kahn S, Bennett BD, Babu-Khan S, Denis P, Fan W, Kha H, Zhang J, Gong Y, Martin L, Louis JC, Yan Q, Richards WG, Citron M, Vassar R (2001) Mice deficient in BACE1, the Alzheimer's beta-secretase, have normal phenotype and abolished beta-amyloid generation. Nat Neurosci 4(3):231–232. https://doi.org/10.1038/85059
37. Cai H, Wang Y, McCarthy D, Wen H, Borchelt DR, Price DL, Wong PC (2001) BACE1 is the major beta-secretase for generation of Abeta peptides by neurons. Nat Neurosci 4(3):233–234. https://doi.org/10.1038/85064
38. Vassar R, Bennett BD, Babu-Khan S, Kahn S, Mendiaz EA, Denis P, Teplow DB, Ross S, Amarante P, Loeloff R, Luo Y, Fisher S, Fuller J, Edenson S, Lile J, Jarosinski MA, Biere AL, Curran E, Burgess T, Louis JC, Collins F, Treanor J, Rogers G, Citron M (1999) Beta-secretase cleavage of Alzheimer's amyloid precursor protein by the transmembrane aspartic protease BACE. Science 286(5440):735–741
39. Vassar R (2002) Beta-secretase (BACE) as a drug target for Alzheimer's disease. Adv Drug Deliv Rev 54(12):1589–1602
40. Nishitomi K, Sakaguchi G, Horikoshi Y, Gray AJ, Maeda M, Hirata-Fukae C, Becker AG, Hosono M, Sakaguchi I, Minami SS, Nakajima Y, Li HF, Takeyama C, Kihara T, Ota A, Wong PC, Aisen PS, Kato A, Kinoshita N, Matsuoka Y (2006) BACE1 inhibition reduces endogenous Abeta and alters APP processing in wild-type mice. J Neurochem 99(6):1555–1563. https://doi.org/10.1111/j.1471-4159.2006.04178.x
41. Masters CL, Simms G, Weinman NA, Multhaup G, McDonald BL, Beyreuther K (1985) Amyloid plaque core protein in

Alzheimer disease and Down syndrome. Proc Natl Acad Sci USA 82(12):4245–4249
42. Wiltfang J, Esselmann H, Cupers P, Neumann M, Kretzschmar H, Beyermann M, Schleuder D, Jahn H, Ruther E, Kornhuber J, Annaert W, De Strooper B, Saftig P (2001) Elevation of beta-amyloid peptide 2-42 in sporadic and familial Alzheimer's disease and its generation in PS1 knockout cells. J Biol Chem 276(46):42645–42657. https://doi.org/10.1074/jbc.M102790200
43. Kummer MP, Heneka MT (2014) Truncated and modified amyloid-beta species. Alzheimers Res Ther 6(3):28. https://doi.org/10.1186/alzrt258
44. Bibl M, Gallus M, Welge V, Esselmann H, Wiltfang J (2012) Aminoterminally truncated and oxidized amyloid-beta peptides in the cerebrospinal fluid of Alzheimer's disease patients. J Alzheimers Dis 29(4):809–816. https://doi.org/10.3233/JAD-2012-111796
45. Schechter I, Ziv E (2011) Cathepsins S, B and L with aminopeptidases display beta-secretase activity associated with the pathogenesis of Alzheimer's disease. Biol Chem 392(6):555–569. https://doi.org/10.1515/BC.2011.054
46. Hook G, Yu J, Toneff T, Kindy M, Hook V (2014) Brain pyroglutamate amyloid-beta is produced by cathepsin B and is reduced by the cysteine protease inhibitor E64d, representing a potential Alzheimer's disease therapeutic. J Alzheimers Dis 41(1):129–149. https://doi.org/10.3233/JAD-131370
47. Munger JS, Haass C, Lemere CA, Shi GP, Wong WS, Teplow DB, Selkoe DJ, Chapman HA (1995) Lysosomal processing of amyloid precursor protein to A beta peptides: a distinct role for cathepsin S. Biochem J 311(Pt 1):299–305
48. Hamazaki H (1996) Cathepsin D is involved in the clearance of Alzheimer's beta-amyloid protein. FEBS Lett 396(2–3):139–142
49. Mueller-Steiner S, Zhou Y, Arai H, Roberson ED, Sun B, Chen J, Wang X, Yu G, Esposito L, Mucke L, Gan L (2006) Antiamyloidogenic and neuroprotective functions of cathepsin B: implications for Alzheimer's disease. Neuron 51(6):703–714. https://doi.org/10.1016/j.neuron.2006.07.027
50. Letronne F, Laumet G, Ayral AM, Chapuis J, Demiautte F, Laga M, Vandenberghe ME, Malmanche N, Leroux F, Eysert F, Sottejeau Y, Chami L, Flaig A, Bauer C, Dourlen P, Lesaffre M, Delay C, Huot L, Dumont J, Werkmeister E, Lafont F, Mendes T, Hansmannel F, Dermaut B, Deprez B, Herard AS, Dhenain M, Souedet N, Pasquier F, Tulasne D, Berr C, Hauw JJ, Lemoine Y, Amouyel P, Mann D, Deprez R, Checler F, Hot D, Delzescaux T, Gevaert K, Lambert JC (2016) ADAM30 downregulates APP-Linked defects through cathepsin D activation in Alzheimer's disease. EBioMedicine 9:278–292. https://doi.org/10.1016/j.ebiom.2016.06.002
51. Sevalle J, Amoyel A, Robert P, Fournie-Zaluski MC, Roques B, Checler F (2009) Aminopeptidase A contributes to the N-terminal truncation of amyloid beta-peptide. J Neurochem 109(1):248–256. https://doi.org/10.1111/j.1471-4159.2009.05950.x
52. Hosoda R, Saido TC, Otvos L Jr, Arai T, Mann DM, Lee VM, Trojanowski JQ, Iwatsubo T (1998) Quantification of modified amyloid beta peptides in Alzheimer disease and down syndrome brains. J Neuropathol Exp Neurol 57(11):1089–1095
53. Schlenzig D, Cynis H, Hartlage-Rubsamen M, Zeitschel U, Menge K, Fothe A, Ramsbeck D, Spahn C, Wermann M, Rossner S, Buchholz M, Schilling S, Demuth HU (2018) Dipeptidylpeptidase activity of meprin beta links N-truncation of abeta with glutaminyl cyclase-catalyzed pGlu-abeta formation. J Alzheimers Dis 66(1):359–375. https://doi.org/10.3233/JAD-171183
54. Schonherr C, Bien J, Isbert S, Wichert R, Prox J, Altmeppen H, Kumar S, Walter J, Lichtenthaler SF, Weggen S, Glatzel M, Becker-Pauly C, Pietrzik CU (2016) Generation of aggregation prone N-terminally truncated amyloid beta peptides by meprin beta depends on the sequence specificity at the cleavage site. Mol Neurodegener 11:19. https://doi.org/10.1186/s13024-016-0084-5
55. Jefferson T, Causevic M, Auf dem Keller U, Schilling O, Isbert S, Geyer R, Maier W, Tschickardt S, Jumpertz T, Weggen S, Bond JS, Overall CM, Pietrzik CU, Becker-Pauly C (2011) Metalloprotease meprin beta generates nontoxic N-terminal amyloid precursor protein fragments in vivo. J Biol Chem 286(31):27741–27750. https://doi.org/10.1074/jbc.M111.252718
56. Muller UC, Deller T, Korte M (2017) Not just amyloid: physiological functions of the amyloid precursor protein family. Nat Rev Neurosci 18(5):281–298. https://doi.org/10.1038/nrn.2017.29
57. Citron M, Oltersdorf T, Haass C, McConlogue L, Hung AY, Seubert P, Vigo-Pelfrey C, Lieberburg I, Selkoe DJ (1992) Mutation of the beta-amyloid precursor protein in familial Alzheimer's disease increases beta-protein production. Nature 360(6405):672–674. https://doi.org/10.1038/360672a0
58. Elder GA, Gama Sosa MA, De Gasperi R (2010) Transgenic mouse models of Alzheimer's disease. Mt Sinai J Med 77(1):69–81. https://doi.org/10.1002/msj.20159
59. Ohshima Y, Taguchi K, Mizuta I, Tanaka M, Tomiyama T, Kametani F, Yabe-Nishimura C, Mizuno T, Tokuda T (2018) Mutations in the beta-amyloid precursor protein in familial Alzheimer's disease increase Abeta oligomer production in cellular models. Heliyon 4(1):e00511. https://doi.org/10.1016/j.heliyon.2018.e00511
60. Ohno M, Sametsky EA, Younkin LH, Oakley H, Younkin SG, Citron M, Vassar R, Disterhoft JF (2004) BACE1 deficiency rescues memory deficits and cholinergic dysfunction in a mouse model of Alzheimer's disease. Neuron 41(1):27–33
61. Patel T, Brookes KJ, Turton J, Chaudhury S, Guetta-Baranes T, Guerreiro R, Bras J, Hernandez D, Singleton A, Francis PT, Hardy J, Morgan K (2017) Whole-exome sequencing of the BDR cohort: evidence to support the role of the PILRA gene in Alzheimer's disease. Neuropathol Appl Neurobiol 44:506–521. https://doi.org/10.1111/nan.12452
62. Kuhn PH, Wang H, Dislich B, Colombo A, Zeitschel U, Ellwart JW, Kremmer E, Rossner S, Lichtenthaler SF (2010) ADAM10 is the physiologically relevant, constitutive alpha-secretase of the amyloid precursor protein in primary neurons. EMBO J 29(17):3020–3032. https://doi.org/10.1038/emboj.2010.167
63. Ohler A, Debela M, Wagner S, Magdolen V, Becker-Pauly C (2010) Analyzing the protease web in skin: meprin metalloproteases are activated specifically by KLK4, 5 and 8 vice versa leading to processing of proKLK7 thereby triggering its activation. Biol Chem 391(4):455–460. https://doi.org/10.1515/BC.2010.023
64. Jefferson T, Auf dem Keller U, Bellac C, Metz VV, Broder C, Hedrich J, Ohler A, Maier W, Magdolen V, Sterchi E, Bond JS, Jayakumar A, Traupe H, Chalaris A, Rose-John S, Pietrzik CU, Postina R, Overall CM, Becker-Pauly C (2013) The substrate degradome of meprin metalloproteases reveals an unexpected proteolytic link between meprin beta and ADAM10. Cell Mol Life Sci 70(2):309–333. https://doi.org/10.1007/s00018-012-1106-2
65. Herzog C, Haun RS, Ludwig A, Shah SV, Kaushal GP (2014) ADAM10 is the major sheddase responsible for the release of membrane-associated meprin A. J Biol Chem 289(19):13308–13322. https://doi.org/10.1074/jbc.M114.559088
66. Banerjee S, Bond JS (2008) Prointerleukin-18 is activated by meprin beta in vitro and in vivo in intestinal inflammation. J Biol Chem 283(46):31371–31377. https://doi.org/10.1074/jbc.M802814200
67. Nikolaev A, McLaughlin T, O'Leary DD, Tessier-Lavigne M (2009) APP binds DR6 to trigger axon pruning and neuron

death via distinct caspases. Nature 457(7232):981–989. https://doi.org/10.1038/nature07767
68. Olsen O, Kallop DY, McLaughlin T, Huntwork-Rodriguez S, Wu Z, Duggan CD, Simon DJ, Lu Y, Easley-Neal C, Takeda K, Hass PE, Jaworski A, O'Leary DD, Weimer RM, Tessier-Lavigne M (2014) Genetic analysis reveals that amyloid precursor protein and death receptor 6 function in the same pathway to control axonal pruning independent of beta-secretase. J Neurosci 34(19):6438–6447. https://doi.org/10.1523/JNEUROSCI.3522-13.2014
69. Peron R, Vatanabe IP, Manzine PR, Camins A, Cominetti MR (2018) Alpha-secretase ADAM10 regulation: insights into Alzheimer's disease Treatment. Pharmaceuticals 11:1. https://doi.org/10.3390/ph11010012
70. Wasco W, Bupp K, Magendantz M, Gusella JF, Tanzi RE, Solomon F (1992) Identification of a mouse brain cDNA that encodes a protein related to the Alzheimer disease-associated amyloid beta protein precursor. Proc Natl Acad Sci USA 89(22):10758–10762
71. Pandey P, Sliker B, Peters HL, Tuli A, Herskovitz J, Smits K, Purohit A, Singh RK, Dong J, Batra SK, Coulter DW, Solheim JC (2016) Amyloid precursor protein and amyloid precursor-like protein 2 in cancer. Oncotarget 7(15):19430–19444. https://doi.org/10.18632/oncotarget.7103
72. Jacobsen KT, Iverfeldt K (2009) Amyloid precursor protein and its homologues: a family of proteolysis-dependent receptors. Cell Mol Life Sci 66(14):2299–2318. https://doi.org/10.1007/s00018-009-0020-8
73. Sprecher CA, Grant FJ, Grimm G, O'Hara PJ, Norris F, Norris K, Foster DC (1993) Molecular cloning of the cDNA for a human amyloid precursor protein homolog: evidence for a multigene family. Biochemistry 32(17):4481–4486
74. Wasco W, Gurubhagavatula S, Paradis MD, Romano DM, Sisodia SS, Hyman BT, Neve RL, Tanzi RE (1993) Isolation and characterization of APLP2 encoding a homologue of the Alzheimer's associated amyloid beta protein precursor. Nat Genet 5(1):95–100. https://doi.org/10.1038/ng0993-95
75. Coulson EJ, Paliga K, Beyreuther K, Masters CL (2000) What the evolution of the amyloid protein precursor supergene family tells us about its function. Neurochem Int 36(3):175–184
76. Rossjohn J, Cappai R, Feil SC, Henry A, McKinstry WJ, Galatis D, Hesse L, Multhaup G, Beyreuther K, Masters CL, Parker MW (1999) Crystal structure of the N-terminal, growth factor-like domain of Alzheimer amyloid precursor protein. Nat Struct Biol 6(4):327–331. https://doi.org/10.1038/7562
77. Barnham KJ, McKinstry WJ, Multhaup G, Galatis D, Morton CJ, Curtain CC, Williamson NA, White AR, Hinds MG, Norton RS, Beyreuther K, Masters CL, Parker MW, Cappai R (2003) Structure of the Alzheimer's disease amyloid precursor protein copper binding domain. A regulator of neuronal copper homeostasis. J Biol Chem 278(19):17401–17407. https://doi.org/10.1074/jbc.m300629200
78. Kong GK, Adams JJ, Harris HH, Boas JF, Curtain CC, Galatis D, Masters CL, Barnham KJ, McKinstry WJ, Cappai R, Parker MW (2007) Structural studies of the Alzheimer's amyloid precursor protein copper-binding domain reveal how it binds copper ions. J Mol Biol 367(1):148–161. https://doi.org/10.1016/j.jmb.2006.12.041
79. Dahms SO, Hoefgen S, Roeser D, Schlott B, Guhrs KH, Than ME (2010) Structure and biochemical analysis of the heparin-induced E1 dimer of the amyloid precursor protein. Proc Natl Acad Sci USA 107(12):5381–5386. https://doi.org/10.1073/pnas.0911326107
80. Kang J, Muller-Hill B (1990) Differential splicing of Alzheimer's disease amyloid A4 precursor RNA in rat tissues: pre A4(695) mRNA is predominantly produced in rat and human brain. Biochem Biophys Res Commun 166(3):1192–1200
81. Weidemann A, Konig G, Bunke D, Fischer P, Salbaum JM, Masters CL, Beyreuther K (1989) Identification, biogenesis, and localization of precursors of Alzheimer's disease A4 amyloid protein. Cell 57(1):115–126
82. Ninomiya H, Roch JM, Sundsmo MP, Otero DA, Saitoh T (1993) Amino acid sequence RERMS represents the active domain of amyloid beta/A4 protein precursor that promotes fibroblast growth. J Cell Biol 121(4):879–886
83. Ninomiya H, Roch JM, Jin LW, Saitoh T (1994) Secreted form of amyloid beta/A4 protein precursor (APP) binds to two distinct APP binding sites on rat B103 neuron-like cells through two different domains, but only one site is involved in neuritotropic activity. J Neurochem 63(2):495–500
84. Pawlik M, Otero DA, Park M, Fischer WH, Levy E, Saitoh T (2007) Proteins that bind to the RERMS region of beta amyloid precursor protein. Biochem Biophys Res Commun 355(4):907–912. https://doi.org/10.1016/j.bbrc.2007.02.047
85. Gralle M, Ferreira ST (2007) Structure and functions of the human amyloid precursor protein: the whole is more than the sum of its parts. Prog Neurobiol 82(1):11–32. https://doi.org/10.1016/j.pneurobio.2007.02.001
86. Reinhard C, Hebert SS, De Strooper B (2005) The amyloid-beta precursor protein: integrating structure with biological function. EMBO J 24(23):3996–4006. https://doi.org/10.1038/sj.emboj.7600860
87. Turner PR, O'Connor K, Tate WP, Abraham WC (2003) Roles of amyloid precursor protein and its fragments in regulating neural activity, plasticity and memory. Prog Neurobiol 70(1):1–32
88. Wang Y, Ha Y (2004) The X-ray structure of an antiparallel dimer of the human amyloid precursor protein E2 domain. Mol Cell 15(3):343–353. https://doi.org/10.1016/j.molcel.2004.06.037
89. Pahlsson P, Shakin-Eshleman SH, Spitalnik SL (1992) N-linked glycosylation of beta-amyloid precursor protein. Biochem Biophys Res Commun 189(3):1667–1673
90. Hoefgen S, Dahms SO, Oertwig K, Than ME (2015) The amyloid precursor protein shows a pH-dependent conformational switch in its E1 domain. J Mol Biol 427(2):433–442. https://doi.org/10.1016/j.jmb.2014.12.005
91. Hoefgen S, Coburger I, Roeser D, Schaub Y, Dahms SO, Than ME (2014) Heparin induced dimerization of APP is primarily mediated by E1 and regulated by its acidic domain. J Struct Biol 187(1):30–37. https://doi.org/10.1016/j.jsb.2014.05.006
92. Dahms SO, Konnig I, Roeser D, Guhrs KH, Mayer MC, Kaden D, Multhaup G, Than ME (2012) Metal binding dictates conformation and function of the amyloid precursor protein (APP) E2 domain. J Mol Biol 416(3):438–452. https://doi.org/10.1016/j.jmb.2011.12.057
93. Keil C, Huber R, Bode W, Than ME (2004) Cloning, expression, crystallization and initial crystallographic analysis of the C-terminal domain of the amyloid precursor protein APP. Acta Crystallogr D Biol Crystallogr 60(Pt 9):1614–1617. https://doi.org/10.1107/S0907444904015343
94. Dulubova I, Ho A, Huryeva I, Sudhof TC, Rizo J (2004) Three-dimensional structure of an independently folded extracellular domain of human amyloid-beta precursor protein. Biochemistry 43(30):9583–9588. https://doi.org/10.1021/bi049041o
95. Lu JX, Yau WM, Tycko R (2011) Evidence from solid-state NMR for nonhelical conformations in the transmembrane domain of the amyloid precursor protein. Biophys J 100(3):711–719. https://doi.org/10.1016/j.bpj.2010.12.3696
96. Botev A, Munter LM, Wenzel R, Richter L, Althoff V, Ismer J, Gerling U, Weise C, Koksch B, Hildebrand PW, Bittl R, Multhaup G (2011) The amyloid precursor protein C-terminal fragment C100 occurs in monomeric and dimeric stable conformations and binds

gamma-secretase modulators. Biochemistry 50(5):828–835. https://doi.org/10.1021/bi1014002
97. Nadezhdin KD, Bocharova OV, Bocharov EV, Arseniev AS (2011) Structural and dynamic study of the transmembrane domain of the amyloid precursor protein. Acta Naturae 3(1):69–76
98. Beel AJ, Mobley CK, Kim HJ, Tian F, Hadziselimovic A, Jap B, Prestegard JH, Sanders CR (2008) Structural studies of the transmembrane C-terminal domain of the amyloid precursor protein (APP): does APP function as a cholesterol sensor? Biochemistry 47(36):9428–9446. https://doi.org/10.1021/bi800993c
99. Sato T, Tang TC, Reubins G, Fei JZ, Fujimoto T, Kienlen-Campard P, Constantinescu SN, Octave JN, Aimoto S, Smith SO (2009) A helix-to-coil transition at the epsilon-cut site in the transmembrane dimer of the amyloid precursor protein is required for proteolysis. Proc Natl Acad Sci USA 106(5):1421–1426. https://doi.org/10.1073/pnas.0812261106
100. Barrett PJ, Song Y, Van Horn WD, Hustedt EJ, Schafer JM, Hadziselimovic A, Beel AJ, Sanders CR (2012) The amyloid precursor protein has a flexible transmembrane domain and binds cholesterol. Science 336(6085):1168–1171. https://doi.org/10.1126/science.1219988
101. MacKenzie KR, Prestegard JH, Engelman DM (1997) A transmembrane helix dimer: structure and implications. Science 276(5309):131–133
102. Javadpour MM, Eilers M, Groesbeek M, Smith SO (1999) Helix packing in polytopic membrane proteins: role of glycine in transmembrane helix association. Biophys J 77(3):1609–1618. https://doi.org/10.1016/S0006-3495(99)77009-8
103. Kim S, Jeon TJ, Oberai A, Yang D, Schmidt JJ, Bowie JU (2005) Transmembrane glycine zippers: physiological and pathological roles in membrane proteins. Proc Natl Acad Sci USA 102(40):14278–14283. https://doi.org/10.1073/pnas.0501234102
104. Anderson SM, Mueller BK, Lange EJ, Senes A (2017) Combination of Calpha-H Hydrogen Bonds and van der Waals Packing Modulates the Stability of GxxxG-Mediated Dimers in Membranes. J Am Chem Soc 139(44):15774–15783. https://doi.org/10.1021/jacs.7b07505
105. Munter LM, Voigt P, Harmeier A, Kaden D, Gottschalk KE, Weise C, Pipkorn R, Schaefer M, Langosch D, Multhaup G (2007) GxxxG motifs within the amyloid precursor protein transmembrane sequence are critical for the etiology of Abeta42. EMBO J 26(6):1702–1712. https://doi.org/10.1038/sj.emboj.7601616
106. Decock M, Stanga S, Octave JN, Dewachter I, Smith SO, Constantinescu SN, Kienlen-Campard P (2016) Glycines from the APP GXXXG/GXXXA transmembrane motifs promote formation of pathogenic abeta oligomers in cells. Front Aging Neurosci 8:107. https://doi.org/10.3389/fnagi.2016.00107
107. Yano Y, Kondo K, Watanabe Y, Zhang TO, Ho JJ, Oishi S, Fujii N, Zanni MT, Matsuzaki K (2017) GXXXG-Mediated Parallel and Antiparallel Dimerization of Transmembrane Helices and Its Inhibition by Cholesterol: single-Pair FRET and 2D IR Studies. Angew Chem Int Ed Engl 56(7):1756–1759. https://doi.org/10.1002/anie.201609708
108. Yan Y, Xu TH, Harikumar KG, Miller LJ, Melcher K, Xu HE (2017) Dimerization of the transmembrane domain of amyloid precursor protein is determined by residues around the gamma-secretase cleavage sites. J Biol Chem 292(38):15826–15837. https://doi.org/10.1074/jbc.M117.789669
109. Nadezhdin KD, Bocharova OV, Bocharov EV, Arseniev AS (2012) Dimeric structure of transmembrane domain of amyloid precursor protein in micellar environment. FEBS Lett 586(12):1687–1692. https://doi.org/10.1016/j.febslet.2012.04.062
110. Chen W, Gamache E, Rosenman DJ, Xie J, Lopez MM, Li YM, Wang C (2014) Familial Alzheimer's mutations within APPTM increase Abeta42 production by enhancing accessibility of epsilon-cleavage site. Nat Commun 5:3037. https://doi.org/10.1038/ncomms4037
111. Song Y, Hustedt EJ, Brandon S, Sanders CR (2013) Competition between homodimerization and cholesterol binding to the C99 domain of the amyloid precursor protein. Biochemistry 52(30):5051–5064. https://doi.org/10.1021/bi400735x
112. Dominguez L, Foster L, Straub JE, Thirumalai D (2016) Impact of membrane lipid composition on the structure and stability of the transmembrane domain of amyloid precursor protein. Proc Natl Acad Sci USA 113(36):E5281–5287. https://doi.org/10.1073/pnas.1606482113
113. Dominguez L, Foster L, Meredith SC, Straub JE, Thirumalai D (2014) Structural heterogeneity in transmembrane amyloid precursor protein homodimer is a consequence of environmental selection. J Am Chem Soc 136(27):9619–9626. https://doi.org/10.1021/ja503150x
114. Pantelopulos GA, Straub JE, Thirumalai D, Sugita Y (2018) Structure of APP-C991-99 and implications for role of extra-membrane domains in function and oligomerization. Biochim Biophys Acta Biomembr 1860:1698–1708. https://doi.org/10.1016/j.bbamem.2018.04.002
115. Ramelot TA, Gentile LN, Nicholson LK (2000) Transient structure of the amyloid precursor protein cytoplasmic tail indicates preordering of structure for binding to cytosolic factors. Biochemistry 39(10):2714–2725
116. Ando K, Iijima KI, Elliott JI, Kirino Y, Suzuki T (2001) Phosphorylation-dependent regulation of the interaction of amyloid precursor protein with Fe65 affects the production of beta-amyloid. J Biol Chem 276(43):40353–40361. https://doi.org/10.1074/jbc.M104059200
117. Yun M, Keshvara L, Park CG, Zhang YM, Dickerson JB, Zheng J, Rock CO, Curran T, Park HW (2003) Crystal structures of the Dab homology domains of mouse disabled 1 and 2. J Biol Chem 278(38):36572–36581. https://doi.org/10.1074/jbc.M304384200
118. Zhang Z, Lee CH, Mandiyan V, Borg JP, Margolis B, Schlessinger J, Kuriyan J (1997) Sequence-specific recognition of the internalization motif of the Alzheimer's amyloid precursor protein by the X11 PTB domain. EMBO J 16(20):6141–6150. https://doi.org/10.1093/emboj/16.20.6141
119. Radzimanowski J, Simon B, Sattler M, Beyreuther K, Sinning I, Wild K (2008) Structure of the intracellular domain of the amyloid precursor protein in complex with Fe65-PTB2. EMBO Rep 9(11):1134–1140. https://doi.org/10.1038/embor.2008.188
120. Arolas JL, Broder C, Jefferson T, Guevara T, Sterchi EE, Bode W, Stocker W, Becker-Pauly C, Gomis-Ruth FX (2012) Structural basis for the sheddase function of human meprin beta metalloproteinase at the plasma membrane. Proc Natl Acad Sci USA 109(40):16131–16136. https://doi.org/10.1073/pnas.1211076109
121. Peters F, Scharfenberg F, Colmorgen C, Armbrust F, Wichert R, Arnold P, Potempa B, Potempa J, Pietrzik CU, Hasler R, Rosenstiel P, Becker-Pauly C (2019) Tethering soluble meprin alpha in an enzyme complex to the cell surface affects IBD-associated genes. FASEB J 2019:fj201802391R. https://doi.org/10.1096/fj.201802391r
122. Seegar TCM, Killingsworth LB, Saha N, Meyer PA, Patra D, Zimmerman B, Janes PW, Rubinstein E, Nikolov DB, Skiniotis G, Kruse AC, Blacklow SC (2017) Structural Basis for Regulated Proteolysis by the alpha-Secretase ADAM10. Cell 171(7):1638–1648 e1637. https://doi.org/10.1016/j.cell.2017.11.014
123. Liu L, Ding L, Rovere M, Wolfe MS, Selkoe DJ (2019) A cellular complex of BACE1 and gamma-secretase sequentially generates Abeta from its full-length precursor. J Cell Biol 218(2):644–663. https://doi.org/10.1083/jcb.201806205

THE FASEB JOURNAL • RESEARCH • www.fasebj.org

Tethering soluble meprin α in an enzyme complex to the cell surface affects IBD-associated genes

Florian Peters,* Franka Scharfenberg,* Cynthia Colmorgen,* Fred Armbrust,* Rielana Wichert,* Philipp Arnold,† Barbara Potempa,‡ Jan Potempa,‡ Claus U. Pietrzik,§ Robert Häsler,¶ Philip Rosenstiel,¶ and Christoph Becker-Pauly*,[1]

*Unit for Degradomics of the Protease Web, Biochemical Institute, †Anatomical Institute, and ¶Institute of Clinical Molecular Biology, University of Kiel, Kiel, Germany; ‡Department of Microbiology, Faculty of Biochemistry, Biophysics, and Biotechnology, Jagiellonian University, Krakow, Poland; and §Institute of Pathobiochemistry, University Medical Center of Mainz, Mainz, Germany

ABSTRACT: Biologic activity of proteases is mainly characterized by the substrate specificity, tissue distribution, and cellular localization. The human metalloproteases meprin α and meprin β share 41% sequence identity and exhibit a similar cleavage specificity with a preference for negatively charged amino acids. However, shedding of meprin α by furin on the secretory pathway makes it a secreted enzyme in comparison with the membrane-bound meprin β. In this study, we identified human meprin α and meprin β as forming covalently linked membrane-tethered heterodimers in the early endoplasmic reticulum, thereby preventing furin-mediated secretion of meprin α. Within this newly formed enzyme complex, meprin α was able to be activated on the cell surface and detected by cleavage of a novel specific fluorogenic peptide substrate. However, the known meprin β substrates amyloid precursor protein and CD99 were not shed by membrane-tethered meprin α. On the other hand, being linked to meprin α, activation of or substrate cleavage by meprin β on the cell surface was not altered. Interestingly, proteolytic activity of both proteases was increased in the heteromeric complex, indicating an increased proteolytic potential at the plasma membrane. Because meprins are susceptibility genes for inflammatory bowel disease (IBD), and to investigate the physiologic impact of the enzyme complex, we performed transcriptome analyses of intestinal mucosa from meprin-knockout mice. Comparison of the transcriptional gene analysis data with gene analyses of IBD patients revealed that different gene subsets were dysregulated if meprin α was expressed alone or in the enzyme complex, demonstrating the physiologic and pathophysiological relevance of the meprin heterodimer formation.—Peters, F., Scharfenberg, F., Colmorgen, C., Armbrust, F., Wichert, R., Arnold, P., Potempa, B., Potempa, J., Pietrzik, C. U., Häsler, R., Rosenstiel, P., Becker-Pauly, C. Tethering soluble meprin α in an enzyme complex to the cell surface affects IBD-associated genes. FASEB J. 33, 7490–7504 (2019). www.fasebj.org

KEY WORDS: protease · quaternary structure · chronic intestinal inflammation · meprin β

The cellular localization of proteases is essential for protease regulation by activators and inhibitors and for their access to substrates. The astacin metalloproteases meprin α and meprin β are expressed as membrane-bound dimers in comparison with the other family members bone morphogenetic protein-1, mammalian tolloid (Tll), Tll1, and Tll2, which lack a transmembrane region and cannot form covalently connected dimers. Meprin α is shed by furin on the secretory pathway, oligomerized, and secreted into the extracellular space (1, 2). Meprin β, on the other hand, stays at the cell membrane until it is shed by a disintegrin and metalloproteases (ADAMs) to reach a different subset of substrates (3, 4). Shortly after discovery of meprins, it was shown that both proteases form heterodimers in mice and rats when coexpressed (1, 5). However, the human isoforms and their heterooligomeric connection have not been investigated in detail yet.

Meprin α and meprin β are highly expressed in epithelial cells of the intestine and kidney (6–8). Here, heterodimerization would have a huge impact on meprin α localization. The absence or mislocalization of meprins has been linked to various types of diseases like inflammatory bowel disease (IBD) and renal ischemia-reperfusion

ABBREVIATIONS: ADAM, a disintegrin and metalloprotease; APP, amyloid precursor protein; CM, $CaCl_2$ and $MgCl_2$; dnp, K-ε-2,4-dinitrophenyl; ER, endoplasmic reticulum; FCS, fetal calf serum; GAPDH, glyceraldehyde-3-phosphate dehydrogenase; IBD, inflammatory bowel disease; MAM, meprin, A-5 protein, and receptor protein-tyrosine phosphatase μ; mca, 7-methyloxycoumarin-4-yl; meprin-SF, meprin Strep/Flag-tagged; PDB, Protein Data Bank; RgpB, Arg-gingipain B; RNAseq, transcriptional gene analysis; SF, Strep/Flag; TBS, Tris-buffered saline; Tll, tolloid; WT, wild type

[1] Correspondence: Unit for Degradomics of the Protease Web, Biochemical Institute, University of Kiel, Otto-Hahn-Platz 9, Kiel, D-24098 Germany. E-mail: cbeckerpauly@biochem.uni-kiel.de

doi: 10.1096/fj.201802391R
This article includes supplemental data. Please visit *http://www.fasebj.org* to obtain this information.

0892-6638/19/0033-7490 © FASEB

(9–11). Therefore, it is important to study the complex formations of these enzymes and the functional consequences for different tissues under pathophysiological conditions. Meprins are expressed as zymogens and require activation by serine proteases (12, 13) or other enzymes exhibiting a trypsin-like specificity (14). The propeptide of membrane-bound meprin β is removed by matriptase-2 (15) or the bacterial protease Arg-gingipain B (RgpB) (4). Additionally, it was shown that activated meprin β could not be shed anymore from the plasma membrane by ADAM10 or ADAM17 (4). However, it is not known whether meprin α in a heterooligomeric complex can be activated itself at the cell surface to gain an additional substrate spectrum or impair meprin β activation or whether shedding of the enzyme complex is altered.

To elucidate the molecular and functional consequences of a meprin α/meprin β-enzyme complex, we employed cell-based assays to demonstrate that human meprin heterodimers are disulfide linked like the murine proteins and locate meprin α to the cell surface. Importantly, meprin α could be activated on the cell surface but did not cleave typical meprin β substrates. We could show that neither shedding by ADAM10 and ADAM17 nor activation of the heterodimer was impaired. However, coexpression of meprins increased proteolytic activity of the protease in the enzyme complex. Finally, gene expression in intestinal tissue of meprin-knockout mice was analyzed by employing transcriptional gene analysis (RNAseq) and compared with gene expression data of IBD patients. The absence or altered localization of meprin α affected different subsets of genes. These findings strengthen the physiologic relevance of meprin heterodimer formation.

MATERIALS AND METHODS

Chemicals

All chemicals obtained were of analytical grade from MilliporeSigma (Burlington, MA, USA), Carl Roth (Karlsruhe, Germany), Merck (Darmstadt, Germany), Roche (Basel, Switzerland), or Thermo Fisher Scientific (Waltham, MA, USA).

Animals

The generation *Mep1b*$^{-/-}$ and *Mep1a*$^{-/-}$ mice has been previously described in refs. 9 and 16. Mice were kept under specific pathogen-free conditions in isolated ventilated cages on a 12-h light/dark cycle with food and water *ad libitum*. Our investigations were carried out in accordance with the *Guide for the Care and Use of Laboratory Animals* of the German Animal Welfare Act on protection of animals. All animal protocols were approved by the relevant German authorities.

Cells, antibodies, plasmids, and transfection

HeLa cells were grown in DMEM supplemented with 10% fetal calf serum (FCS), glutamine, and 1% penicillin and streptomycin (Thermo Fisher Scientific) and cultured at 37°C at 5% CO_2 atmosphere and 95% relative humidity. Transient transfection was performed with polyethylenimine according to the manufacturer's instructions. The following plasmids were used: human (h) Meprinß in PSG5 vector, hMeprinß in pcDNA4/TO-3x-Flag vector, hMeprinα in PSG5 vector, hMeprinα in pcDNA4/TO vector, hMatriptase-2-Myc in pcDNA3.1 vector, APP695 in pCI-neo, hCD99-Myc in pCMV6, and pcDNA3.1 as empty vector control. The following antibodies were used: polyclonal anti–meprin β and polyclonal anti-meprin α (Pineda Antibody-Service, Berlin, Germany), monoclonal anti–glyceraldehyde-3-phosphate dehydrogenase (GAPDH) (2118, 14C10; Cell Signaling Technology, Danvers, MA, USA), polyclonal anti-actin (A2066; MilliporeSigma), monoclonal anti-Flag (M2, F1804; MilliporeSigma), monoclonal anti-Strep (1023944; Qiagen, Hilden Germany), polyclonal anti-transferrin receptor (ab84036; Abcam, Cambridge, United Kingdom), monoclonal anti-Myc (9B11, 2276; Cell Signaling Technology), polyclonal anti-mouse meprin β (R&D Systems, Minneapolis, MN, USA), polyclonal anti–amyloid precursor protein (APP) (Thermo Fisher Scientific), monoclonal anti–N-terminal APP (22C11; MilliporeSigma), and monoclonal anti–soluble APPα (6E10; Covance, Princeton, NJ, USA).

Inhibitor treatment of cells

Transfected HeLa cells were treated 6 h after transfection with brefeldin A (5 μg/ml; BioLegend, San Diego, CA, USA), kifunensine (2 μg/ml; Cayman Chemical, Ann Arbor, MI, USA), swainsonine (2 μg/ml; Cayman Chemical), or control overnight.

Cell lysis, SDS-PAGE, and Western blot analysis

At 24 h after transfection, cells were harvested and lysed in lysis buffer containing 1% Triton X-100 and protease inhibitor tablet with EDTA (Roche) in PBS. Protein concentration was measured using bicinchoninic acid assay (Thermo Fisher Scientific). Total protein lysate (30 μg) was separated by SDS-PAGE and transferred onto nitrocellulose membranes (GE Healthcare, Waukesha, WI, USA). Membranes were blocked with 5% milk in Tris-buffered saline (TBS) for 1 h at room temperature, incubated overnight with primary antibody in milk at 4°C, washed 3 times with TBS, and incubated with horseradish peroxidase–conjugated secondary antibodies in TBS at room temperature. After further washes, membranes were developed with SuperSignal West Femto (Thermo Fisher Scientific) in a chemiluminescence detection system (LAS-3000; Fujifilm, Tokyo, Japan).

Cloning

Human meprin α and human meprin β were cloned into pcDNA4/TO vector with C-terminal 3 times Flag-tag *via* a 2-primer strategy. An N-terminal 2 times Strep-tag was inserted between the signal peptide and propeptide. Cysteine-mutation variants were cloned *via* the 2-primer strategy and insertion of a point mutation. Primers were purchased from MilliporeSigma, and plasmid sequences were validated by DNA sequencing (Eurofins Scientific, Luxembourg).

Immunoprecipitation

Cells were grown and transiently transfected as previously described. At 24 h after transfection, cells were harvested and lysed in lysis buffer containing 1% Triton X-100 and protease inhibitor tablet with EDTA (Roche) in PBS. Protein concentration was measured using bicinchoninic acid assay (Thermo Fisher Scientific), and equal amounts of protein per sample were supplemented with anti-Flag or anti-Strep antibody and incubated

rolling overnight at 4°C. Protein G Agarose beads (Thermo Fisher Scientific) were centrifuged, washed 3 times with lysis buffer, and blocked overnight at 4°C in 3% bovine serum albumin and H_2O. Beads were washed in lysis buffer the next day and added to the samples. After an incubation of 30 min at 4°C, samples were washed 3 times in lysis buffer and denatured with 1 times laemmli buffer at 95°C for 10 min.

Cell surface protein biotinylation

HeLa cells were transiently transfected with meprin α, meprin β, or empty vector and incubated for 24 h. Cells were washed twice with ice-cold PBS–$CaCl_2$ and $MgCl_2$ (CM: 0.1 mM $CaCl_2$ and 1 mM $MgCl_2$ in PBS) and treated with 1 mg/ml biotin solution (Sulfo-NHS-SS-Biotin; Thermo Fisher Scientific) in PBS-CM for 30 min at 4°C. Biotin solution was removed, and cells were incubated with quenching buffer (50 mM Tris-HCl in PBS-CM, pH 8) for 10 min at 4°C, washed 3 times with PBS-CM, and harvested.

Immunofluorescence microscopy

Tissue from mice was dissected, fixed in 4% (w/v) paraformaldehyde in PBS overnight, paraffin embedded, and sectioned. Tissue sections were rehydrated, boiled in 10 mM citric buffer (pH 5.5), and blocked with 5% FCS and PBS. Primary antibody was diluted in 5% FCS and PBS and applied overnight at 4°C in a humid, dark chamber (rabbit anti–meprin α tier 1, 1:1000; goat anti-meprin β, 1:2000; R&D Systems). Tissue was washed 3 times with PBS and incubated with secondary antibody for 2 h at room temperature (Alexa Fluor 488 donkey anti-rabbit and Alexa Fluor 594 donkey anti-goat, 1:300; Thermo Fisher Scientific). Excessive secondary antibody was removed by 3 washes in PBS. A 5-min incubation with 1 μg/ml DAPI and PBS was used for nuclear staining following an additional 3 washes with PBS. Stained tissue was mounted with Faramount Aqueous Mounting Medium (Agilent Technologies, Santa Clara, CA, USA).

Immunofluorescence staining with cells, which were seeded on coverslips, was performed after 24 h transfection. Cells were washed with PBS and fixed with 4% (w/v) paraformaldehyde in PBS for 10 min at room temperature followed by incubation with 0.12% (w/v) glycine in PBS for 10 min at room temperature. Cells were then blocked and permeabilized with 10% FCS and 0.2% (w/v) saponin in PBS for 30 min at room temperature. For cell surface staining, saponin was excluded from the buffers. Primary antibody was diluted in the same solution and applied for 1 h at room temperature in a humid, dark chamber (mouse anti-Flag, 1:1000; MilliporeSigma; mouse anti-Strep, 1:1000; Qiagen; rabbit anti–meprin α hEcto1, 1:1000; rabbit anti-meprin β hEcto1, 1:1000), following 5 washes in 0.2% (w/v) saponin in PBS. Secondary antibody was applied for 1 h at room temperature (Alexa Fluor 488 donkey anti-rabbit and Alexa Fluor 594 donkey anti-mouse, 1:300; Thermo Fisher Scientific). Excessive antibody was removed by 5 washes in 0.2% (w/v) saponin and PBS and 2 washes in double-distilled H_2O. The coverslips were mounted onto slides with a mixture of 17% (w/v) Mowiol, 33% (v/v) glycerol, and 50 mg/ml 1,4-diazabicyclo[2.2.2]octane (MilliporeSigma) supplemented with 1 μg/ml DAPI for nuclear staining.

Images were acquired with a confocal laser scanning microscope (FV1000; Olympus, Tokyo, Japan).

Protein deglycosylation assay

Total protein lysate (50 μg) of transfected HeLa cells was deglycosylated using a protein deglycosylation mix according to the manufacturer's instructions (P6039; New England Biolabs, Ipswich, MA, USA).

Activity assays

To quantify meprin α and meprin β activity on the cell surface and in the supernatant, specific fluorogenic peptide substrates for meprin α [7-methyloxycoumarin-4-yl (mca)–HVANDPIW–K-ε-2,4-dinitrophenyl (dnp); Genosphere Biotechnologies, Paris, France] and meprin β (mca-EDEDED-dnp; Genosphere Biotechnologies) were used in final concentrations of 10 and 50 μM, respectively. These consisted of a fluorophore (mca), a specific substrate peptide for meprin α (HVANDPIW) or meprin β (EDEDED), and a quencher (dnp). Fluorescence intensity was detected at 37°C every 30 s for 120 min using a spectrophotometer (Tecan, Männedorf, Switzerland). For determination of meprin activity at the cell surface, HeLa cells were transfected and treated with the bacterial protease RgpB (50 nM for 5 h). Cells were counted, and 0.2×10^6 cells were plated onto 48-well plates in a total volume of 300 μl. Equal amounts of corresponding cell supernatants were plated onto 96-well plates, and half of them were also incubated with 10 μg/ml trypsin (420 nm) or 50 nM RgpB for 30 min at 37°C. Remaining cell supernatants and cell lysates were used for Western blot analysis. Activity assays of recombinant active meprin β (1 nM), meprin α (5 nM), RgpB (50 nM), trypsin (10 μg/ml), and intestinal lysates (50 μg) were performed in 100 μl total volume in 96-well plates.

For data analysis, slope of equal linear activity range was compared from 3 individual experiments.

Homology modeling

The model of human meprin α/β heterodimer was built based on the crystal structure of human meprin β [Protein Data Bank (PDB) code: 4gwm; *https://www.rcsb.org/*] using the Swiss-Model workspace (17). For the analysis of the interaction, the interface PDBsum (18) was used. Structure visualization and analysis was carried out using PyMOL (Schrödinger, New York, NY, USA).

RNAseq data and IBD

Transcriptome sequencing was carried out on a HiSeq 4000 (Illumina, San Diego, CA, USA) employing the TruSeq stranded totalRNA library protocol (Illumina) following the manufacturer's guidelines. A mean of 25 million 125-nt paired-end reads per sample was obtained. Subsequently, raw reads were subjected to trimming using cutadapt (19) for removal of adapter and low-quality sequences. Alignment to the mm10/Ensemble Genome Reference Consortium Mouse Build 38 patch (GRCm38) reference genome was performed using TopHat2 (20). Quantitative gene expression values were generated using HTSeq (21). Finally, differential gene expression levels were analyzed employing the Bioconductor package DESeq2 (22).

Gene ontology analysis of RNAseq data

Gene ontology analysis was conducted by retrieving ontology terms (*http://www.geneontology.org*) for differentially expressed genes and a subsequent 2-sided Fisher's exact test to assess significance of enrichment or depletion as previously described by Tavazoie *et al.* (23).

Statistical analysis

All statistical analyses were performed with Prism 5 software (GraphPad Software, La Jolla, CA, USA) for 1-way ANOVA followed by Tukey's posttest, or 2-way ANOVA followed by a Bonferroni posttest. Values are expressed as means ± SD. The null hypothesis was rejected at $P < 0.05$.

RESULTS

Coexpression and molecular interaction of human meprin α and meprin β

The coexpression of the metalloproteases meprin α and meprin β has been widely studied for the rodent isoforms. Here, meprin α and meprin β monomers are able to form heterodimers, which then oligomerize to heterotetramers at the cell surface (1, 5). However, coexpression and interaction of the human isoforms remains elusive. It is unclear if and where both proteases form a heterodimer and if it is covalently connected. Furthermore, formation of this complex may have an impact on the shedding of meprin α by furin or of meprin β by ADAM10 or ADAM17. Finally, tethering and activation of meprin α at the cell surface might widen its substrate spectrum, which could overlap with meprin β–specific substrates (**Fig. 1*A***).

We overexpressed both human proteases and observed altered band patterns in Western blot analyses of single or cotransfected HeLa cells. Meprin α single transfection resulted in a double-band pattern of 110- and 90-kDa signals in the cell lysate (Fig. 1*B*). The presence of meprin β increased the 110-kDa signal and decreased the 90-kDa signal. Interestingly, an additional band for meprin α of 100 kDa appeared in the coexpression with meprin β, which was also found in cell supernatants and, to a lower extent, in the single transfection (Fig. 1*B, C*). Meprin β signals were obtained as a double band at 120 and 100 kDa (Fig. 1*B*). The upper band shifted downwards when meprin α was coexpressed. The same shift appeared in the cell supernatants of shed meprin β, which might be an effect of cleavage or other post-translational modification.

To investigate the direct interaction of both proteases further, we utilized variants of meprin α and meprin β containing a 2 times Strep-tag N-terminal of the propeptide and a C-terminal 3 times Flag-tag and named them meprin Strep/Flag (SF) (meprin SF-tagged) (Fig. 1*C, D*). We performed coimmunoprecipitation experiments to study a direct interaction of both human isoforms. By using a Strep-tag antibody to precipitate meprin α from transfected HeLa cells, 2 meprin α bands were detected after single transfection and 3 bands after cotransfection with meprin β (Fig. 1*C*). Only 1 band at 110 kDa was detected with the Flag-tag antibody, revealing full-length meprin α with an intact C terminus. Hence, the lower migrating bands detected with a meprin α–specific antibody were products of C-terminal proteolytic processing. Interestingly, both meprin β bands appeared in the pulldown fractions when meprin α was present. In the opposite experiment, when using the tagged meprin β and the Flag-tag antibody for precipitation, both meprin β bands were observed by Western blot (Fig. 1*D*). Here, mainly the 100-kDa fragment of meprin α was coprecipitated with meprin β, and the 110-kDa fragment to a lesser extent.

Human meprin β homodimer is connected *via* an intermolecular disulfide bridge at position C305 between the meprin, A-5 protein, and receptor protein-tyrosine phosphatase μ (MAM) domains. For the rat isoform, a previous study showed that the corresponding cysteine residue could also be linked to a meprin α monomer (24). We mutated the C305 to a serine in human meprin β as well as the corresponding C308 in human meprin α and repeated the immunoprecipitation experiment. The meprin α C308S variant appeared as a double band in Western blot and was secreted into the supernatant like the wild-type (WT) form (Fig. 1*E*). However, WT meprin β was not coprecipitated in that approach. Transfection of the meprin β C305S variant led to the same observation that WT meprin α did not bind to mutated meprin β (Fig. 1*F*). Furthermore, only 2 bands appeared for meprin α in the cotransfection lysates, whereas the band shift of meprin β was present, although not bound to meprin α. Conclusively, human meprins are able to form heterodimers *via* a disulfide bond between their MAM domains.

Based on the solved crystal structure of human meprin β homodimer (PDB code: 4gwm) (25) (**Fig. 2*A***), we generated a homology model of the meprin α/meprin β enzyme complex (Fig. 2*B*). Because the disulfide bond of meprin β homodimer was not resolved, the approximate position in the heterodimer was highlighted *via* a yellow line. Interestingly, all interaction sites between 2 meprin β monomers were also found in the heterodimer, with an additional salt-bridge formed between E270 (meprin β) and R578 (meprin α) and a hydrogen bond between S257 (meprin β) and D201 (meprin α).

Interaction of meprin heterodimers occurs in the early endoplasmic reticulum

The interaction studies prompted us to further analyze assembly and localization of the human meprin heterodimer. We therefore performed cell surface biotinylation experiments of transfected HeLa cells in order to validate whether the presence of membrane-bound meprin β leads to a localization of meprin α at the cell surface. The biotin-pulldown revealed that no meprin α signal occurred in the single transfection, whereas coexpression with meprin β induced a strong signal for the 100-kDa form of meprin α (**Fig. 3*A***). For meprin β, only the band of higher molecular mass was detected in the biotinylated fraction, whereas the 100-kDa form likely corresponds to immature protein in the endoplasmic reticulum (ER) and Golgi. We confirmed these results employing immunofluorescence microscopy of HeLa cells that were transfected with the tagged meprin constructs. Meprin α and Flag-tagged meprin β showed fluorescence signals on the cell surface as well as intracellularly (Fig. 3*B*). Use of an antibody against the C-terminal Flag-tag of meprin α revealed that full-length meprin α, including its C terminus, was not located on the plasma membrane. Only meprin β could be detected on the cell surface. Therefore, we concluded that only furin-cleaved meprin α, which appeared as a 100-kDa fragment in Western blot, is located at the cell membrane *via* interaction with meprin β.

To investigate whether disulfide linkage of the heterodimer is necessary for cell surface localization, we performed immunofluorescence staining with the cysteine-mutated variants. HeLa cells were cotransfected with meprin β and meprin α WT or C308S variant. As expected, both WT proteases colocalized on the secretory pathway and on the cell surface of nonpermeabilized cells (Fig. 3*C*).

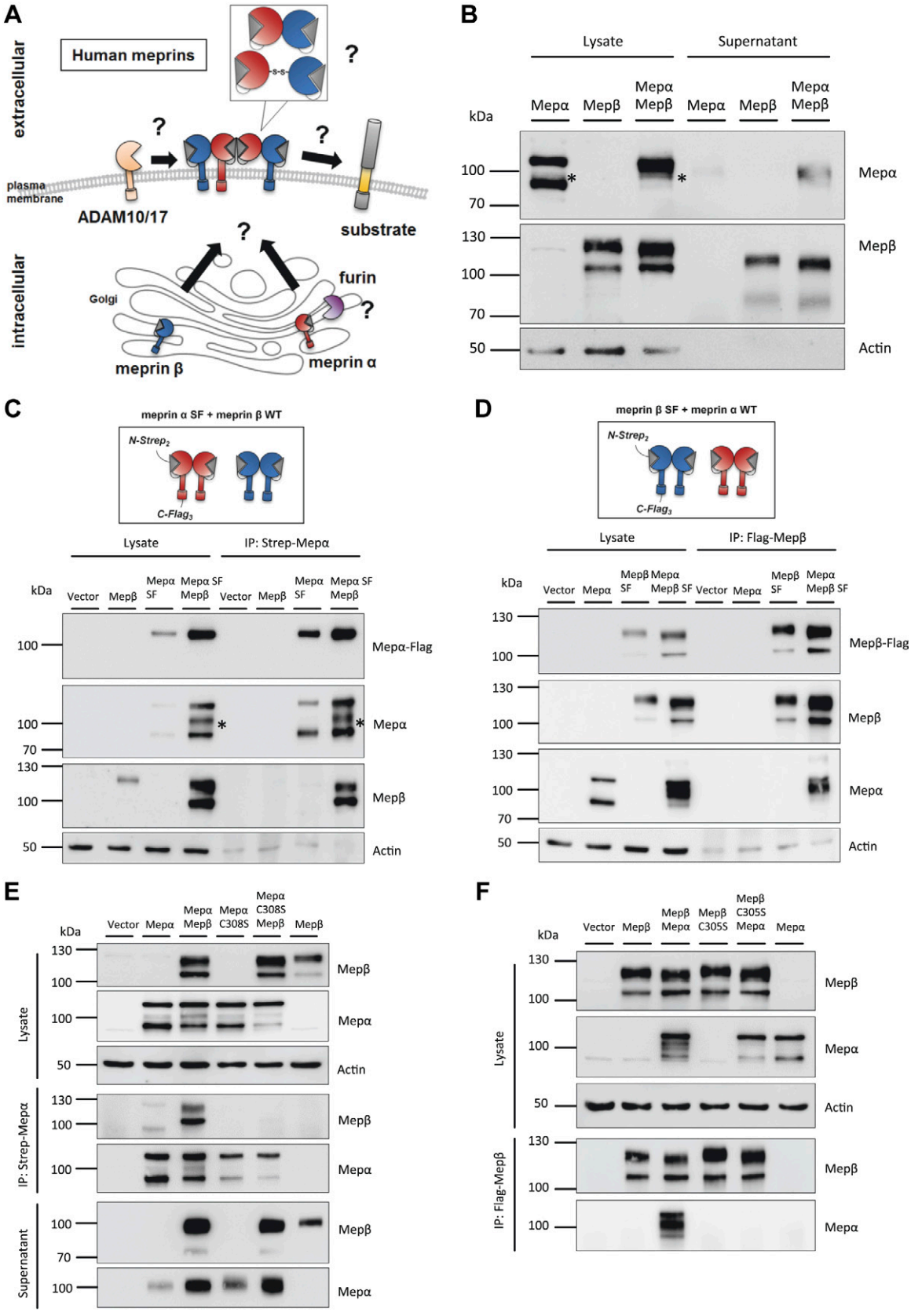

Figure 1. Molecular interaction of the human meprin α and meprin β complex. *A*) Diagram summarizing possible interaction modes of human meprin α and meprin β with unknown influence on shedding and substrate cleavage. *B*) Transfection of HeLa cells with human meprin α, human meprin β, or both. Cell lysates and supernatants were analyzed *via* immunoblotting using specific meprin α or meprin β antibodies. β-Actin served as loading control. The 100-kDa fragment of meprin α is marked with an asterisk. *C*) Transfection of HeLa cells with meprin β WT and meprin α SF construct. Diagram of double-tagged meprin α

(*continued on next page*)

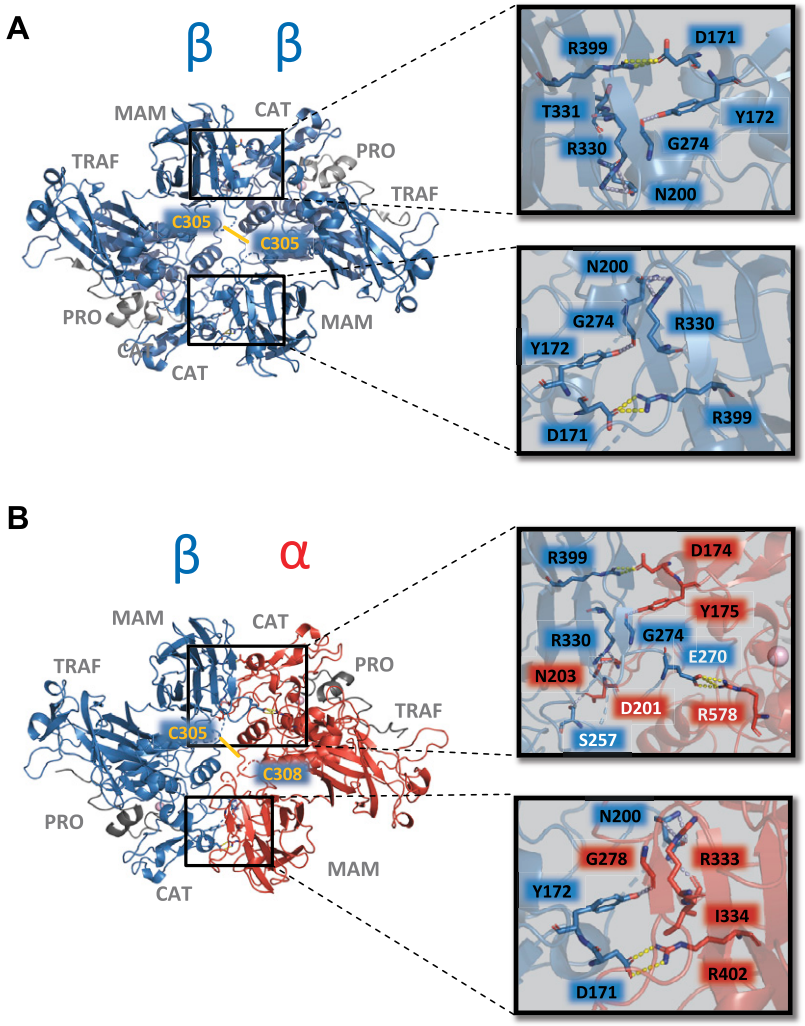

Figure 2. Structure of human meprin β homodimer and homology model of human meprin α/β heterodimer. *A*) Structure of human meprin β homodimer with interacting amino acid residues at the interface of both monomers (PDB code: 4gwm). Because the segment containing the intermolecular disulfide bond between C305 residues is disordered in the zymogen structure, disulfide bond is highlighted *via* a yellow line. *B*) Structural properties of a meprin α/β heterodimer homology model based on the ectodomain of meprin β (PDB code: 4gwm). The approximate position of the intermolecular disulfide bond between C305 and C308 of the meprin β (blue)/meprin α (red) heterodimer is highlighted *via* a yellow line. Additional stabilization of the α/β interaction is given by several hydrogen bonds (light-blue dashes) and 3 salt bridges (yellow dashes) as shown in the close-up view (right panel). Binding residues are presented as sticks and the secondary structure is shown as transparent cartoon. Except the salt-bridge formed by E270 and R578 and the hydrogen bond between S257 and D201, all identified interaction sites are conserved between the meprin β monomer and the meprin α/β heterodimer. CAT, catalytic domain; PRO, propeptide; TRAF, tumor necrosis factor receptor-associated factor.

However, the missing disulfide bond in the C308S variant led to intracellular staining of meprin α and to complete absence on the cell surface, although meprin β was coexpressed. Therefore, disulfide linkage of the heterodimers is crucial for meprin α to be located on the cell surface instead of secreted.

Disulfide bonds are mainly formed in the ER after protein translation. However, it is not known where meprin α and meprin β monomers meet at first. Therefore, we used brefeldin A to inhibit the transport of proteins from the ER to the Golgi apparatus in transfected HeLa cells. Immunofluorescence microscopy showed retention of both proteases in the ER of permeabilized cells, whereas no signals could be detected on the cell surface. Subsequent immunoprecipitation of meprin α revealed that meprin β was already connected to meprin α in the ER (Fig. 3*D*). Additionally, only 1 band was obtained for each of the proteases, confirming that the 110-kDa meprin α fragment is the unprocessed full-length form in the ER as observed before. In summary, meprin α and meprin β are covalently linked in the ER directly after translation and are further transported to the Golgi, where meprin α loses its membrane anchor by furin cleavage (Fig. 3*E*).

Complex formation of meprin α and meprin β alters post-translational modifications

In order to elucidate the different band patterns of meprins observed by Western blot and to investigate whether proteolytic processing or altered glycosylation

construct (upper panel). Coimmunoprecipitation was performed using Strep-tag antibody against the meprin α N terminus and analyzed *via* immunoblotting (lower panel). The 100-kDa fragment of meprin α is marked with an asterisk. *D*) Transfection of HeLa cells with meprin α WT and meprin β SF construct. Diagram of double-tagged meprin β construct (upper panel). Coimmunoprecipitation was performed using Flag-tag antibody against the meprin β C terminus and analyzed *via* immunoblotting (lower panel). *E*) Transfection of HeLa cells using meprin α SF, meprin α C308S SF variant, and meprin β WT. Coimmunoprecipitation was performed using Strep-tag antibody against the meprin α N terminus and analyzed *via* immunoblotting. *F*) Transfection of HeLa cells using meprin β SF, meprin β C305S SF variant, and meprin α WT. Coimmunoprecipitation was performed using Flag-tag antibody against the meprin β C terminus and analyzed *via* immunoblotting. C-, C terminus; IP, immunoprecipitation; N-, N terminus; Mep, meprin.

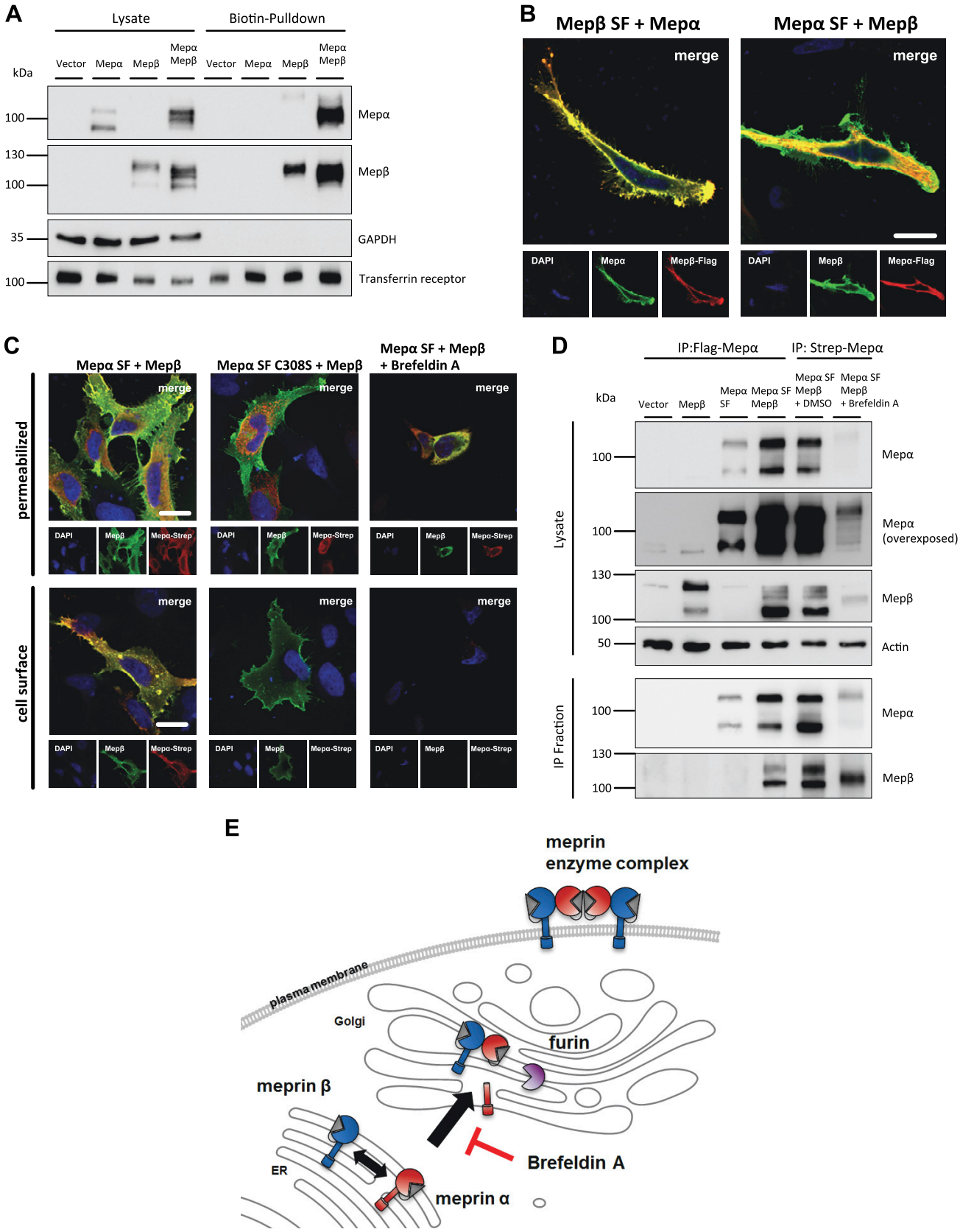

Figure 3. Meprin interaction on the cell surface and secretory pathway. *A*) Transfection of HeLa cells with meprin α WT and meprin β WT constructs. Cell surface proteins were labeled by primary amine biotinylation, pulled down with streptavidin sepharose beads, and analyzed *via* immunoblotting. GAPDH and transferrin receptor served as loading controls. *B*) Immunofluorescence staining of transfected HeLa cells with meprin β SF and meprin α WT constructs (left panel) or meprin α SF and meprin β WT constructs (right panel). Nuclear staining was visualized using DAPI. Images were taken by confocal

(*continued on next page*)

are responsible (**Fig. 4*A***), we used the N- and C-terminal–tagged meprin constructs (Fig. 1*C, D*) for the following experiments. We repeated single and cotransfection in HeLa cells and performed Western blot analyses with the lysates. In case of tagged meprin α and untagged meprin β, we again confirmed that the 110-kDa upper band was meprin α still containing its C terminus, whereas the other bands were not visualized with the Flag-tag antibody (Fig. 4*B*). Those bands reappeared after incubation with the Strep-tag– or meprin α–specific antibody as products of C-terminal proteolytic processing. When expressing the tagged meprin β and untagged meprin α, the meprin β double band was observed using a Flag-tag–, a Strep-tag–, and a meprin β–specific antibody, which excludes that the shift of the upper band is a result of proteolysis at the N or the C terminus (Fig. 4*C*). We therefore focused on differential glycosylation that could alter the molecular mass of the protein and might occur when both meprins are coexpressed. Indeed, deglycosylation of meprin β led to a similar band pattern in single and cotransfection; therefore, the observed band shift was an effect of altered glycosylation (Fig. 4*D*). Deglycosylation of meprin α still showed a double band in the single transfection, confirming that the band of lower molecular mass is a result of proteolysis. Interestingly, the 100-kDa fragment of meprin α in the cotransfection vanished after deglycosylation (Fig. 4*D*). Therefore, the 100-kDa fragment of meprin α might be a higher-glycosylated version of the 90-kDa protein, which is either secreted or held at the cell surface by meprin β. In order to investigate whether glycosylation itself has an influence on the interaction of both meprins, we used 2 compounds that inhibit maturation of sugar trees by α-mannosidases in the ER (kifunensine) or in the Golgi apparatus (swainsonine). Immunoprecipitation of cotransfected meprins showed that both proteases were indeed differentially glycosylated but still interacted after addition of each of the inhibitors (Fig. 4*E*). Mutation of known glycosylation sites in meprins did not affect protein interaction or it resulted in inappropriate folding and instability of the proteases (unpublished results) (26).

Heteromeric complex of meprin α and meprin β does not change protease activation but increases proteolytic activity

In order to investigate the physiologic consequences of meprin heterodimer formation, we performed experiments to analyze whether the functional properties of each meprin are altered within the heteromeric complex. For meprin β activity, we used an already described specific fluorogenic peptide consisting of negatively charged amino acids (**Fig. 5*A***) (27). For meprin α, we designed a new substrate based on proteomic identification of protease cleavage site specificity (28) and validated its specificity using recombinant active meprin α, meprin β, and trypsin (Fig. 5*B* and Supplemental Fig. S1*A*). Of note, only meprin α and not meprin β was able to cleave the peptide HVANDPIW. The specificity for meprin α could even be demonstrated using protein lysates from the small intestine of WT and meprin-knockout mice (Supplemental Fig. S1*B*). With specific substrates for meprin α and meprin β in hands, we measured cell surface protease activities of transfected HeLa cells with each meprin alone or in the heteromeric enzyme complex. Meprin β activities were obtained in single transfection and cotransfection with meprin α, revealing an unaffected proteolytic activity after activation with the soluble pathogenic protease RgpB (Fig. 5*C*) (4) or membrane-bound protease matriptase-2 (Supplemental Fig. S1*C, D*) (15). Remarkably, meprin α could also be activated with RgpB in the enzyme complex at the cell surface, making it a membrane-tethered protease with possible access to so far unknown membrane-bound substrates (Fig. 5*D, E*).

Due to furin cleavage within the inserted domain, meprin α is a soluble protease when expressed alone (Fig. 5*E*). Meprin β, on the other hand, requires shedding through ADAM10 or ADAM17 to get access to its soluble substrates, which is only possible in its proform (3, 4). Shedding of the meprin enzyme complex has not yet been investigated. Therefore, we performed Western blot analyses of cell lysates and supernatants used for the activity assays and observed both proteases in the supernatants (Fig. 5*F*). Of note, activation of the proteases by RgpB prevented shedding of both meprin β homodimer and the enzyme complex. Furthermore, cell supernatants were incubated with trypsin or RgpB, and meprin activities were measured. Meprin β showed significantly increased proteolytic activity in the heteromeric enzyme complex compared with the single transfection (Fig. 5*G*). Similar results were obtained using the meprin α–specific substrate (Fig. 5*H*).

Membrane-bound meprin α does not cleave meprin β–specific substrates

Meprin α and meprin β have a common preference for negatively charged amino acids around the scissile

fluorescence microscopy. Scale bar, 20 μm. *C*) Immunofluorescence staining of transfected HeLa cells using meprin α SF, meprin α C308S SF, and meprin β WT constructs. Cells were treated overnight with brefeldin A at 5 μg/ml or DMSO control. Cell surface staining was performed by excluding saponin from buffers. Nuclear staining was visualized using DAPI. Images were taken by confocal fluorescence microscopy. Scale bars, 20 μm. *D*) Transfection of HeLa cells using meprin α SF and meprin β WT constructs. Cells were treated overnight with brefeldin A at 5 μg/ml or DMSO control. Coimmunoprecipitation was performed using Flag-tag antibody against meprin α C terminus or Strep-tag antibody against meprin α N terminus as indicated. Protein fractions were analyzed by immunoblotting. *E*) Diagram of meprin α and meprin β interacting in the ER and being transported to the cell surface. Treatment of cells with brefeldin A inhibits the transport from the ER to Golgi apparatus. IP, immunoprecipitation; Mep, meprin.

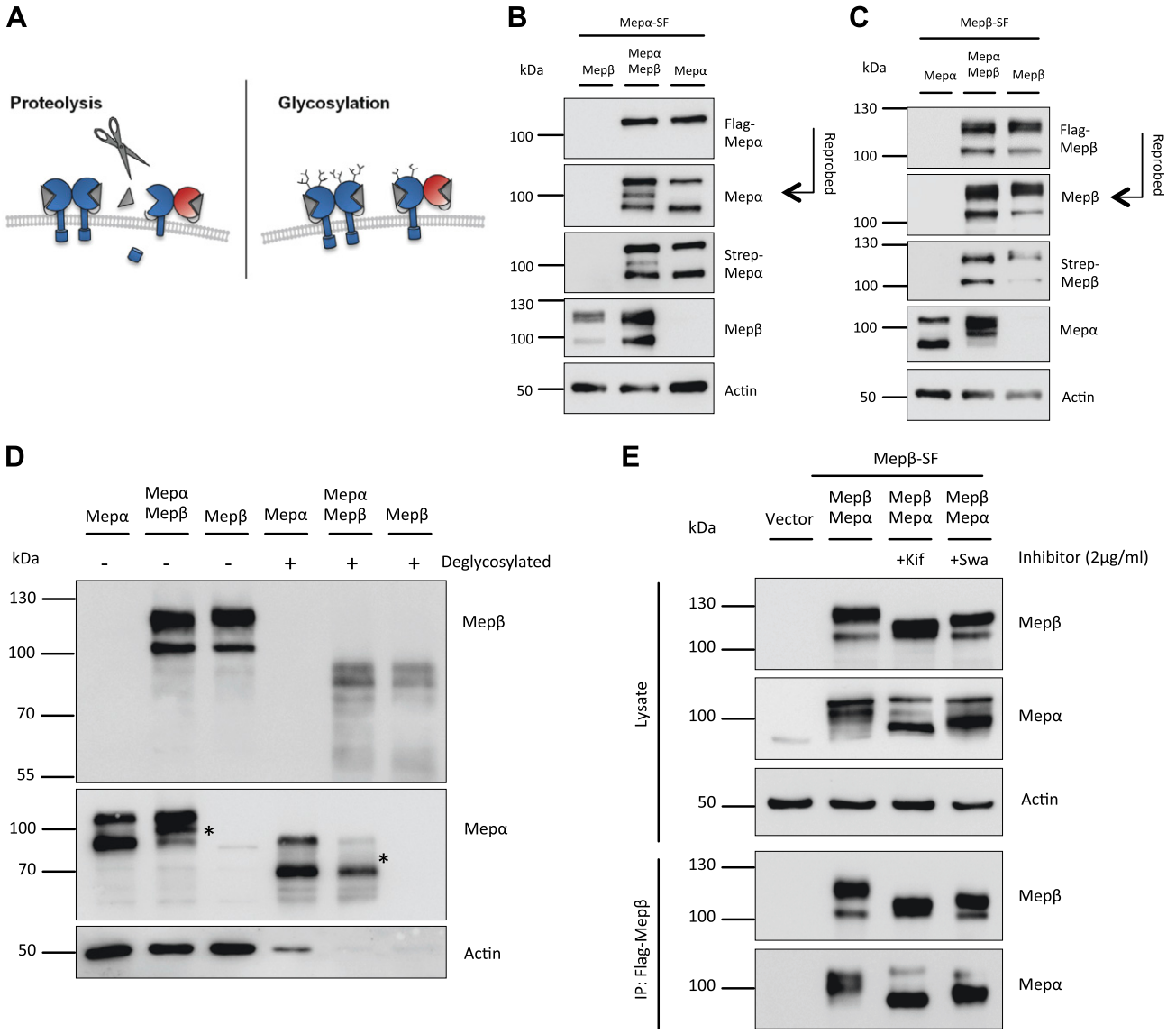

Figure 4. Post-translational modifications of meprins. *A*) Diagram of possible post-translational modifications of human meprin β in the meprin enzyme complex. Proteolysis could lead to loss of either C or N terminus (left panel), or altered maturation of sugar trees (right panel) could affect the size of the protein. *B*) Transfection of HeLa cells with meprin α SF and meprin β WT constructs. Protein fractions were visualized *via* immunoblotting using meprin-specific antibodies or Strep- and Flag-tag antibodies against N and C terminus of meprin α. *C*) Transfection of HeLa cells with meprin β SF and meprin α WT constructs. Protein fractions were visualized *via* immunoblotting using meprin-specific antibodies or Strep- and Flag-tag antibodies against N and C terminus of meprin β. *D*) Transfection of HeLa cells using meprin α WT and meprin β WT constructs. Protein lysates were treated with deglycosylation mix and compared with untreated lysates by immunoblotting. The 100-kDa fragment of meprin α is marked with an asterisk. *E*) HeLa cells were transfected with meprin β SF and meprin α WT constructs. Cells were treated overnight with kifunensine (Kif) or swainsonine (Swa) as indicated. Coimmunoprecipitation was performed using Flag-tag antibody against meprin β C terminus and analyzed *via* immunoblotting. IP, immunoprecipitation; Mep, meprin.

bond (28). However, most likely due to their different localization, substrate specificities differ between the proteases. The APP was described as substrate for membrane-bound meprin β, which cleaves the N terminus and acts as β-secretase, subsequently leading to Aβ formation by the γ-secretase (**Fig. 6*A***) (29, 30). Soluble shed meprin β as well as secreted meprin α are not able to cleave APP at the β-secretase site (unpublished results). Because membrane localization is crucial for APP cleavage by meprin β, we investigated whether APP can also be a substrate for membrane-bound meprin α. We cotransfected APP with each protease or the enzyme complex. To exclude meprin β cleavage, we also used the catalytically inactive meprin β variant E153A for the enzyme complex. APP was processed in all samples transfected with active meprin β, leading to soluble APPβ, N-terminal APP fragments, and Aβ formation (Fig. 6*B*). Interestingly, meprin α alone or expressed in the enzyme complex was not able to process APP. This indicates that although both proteases can be activated in the hetero-oligomer, their substrate pools clearly differ within the enzyme complex. Equal

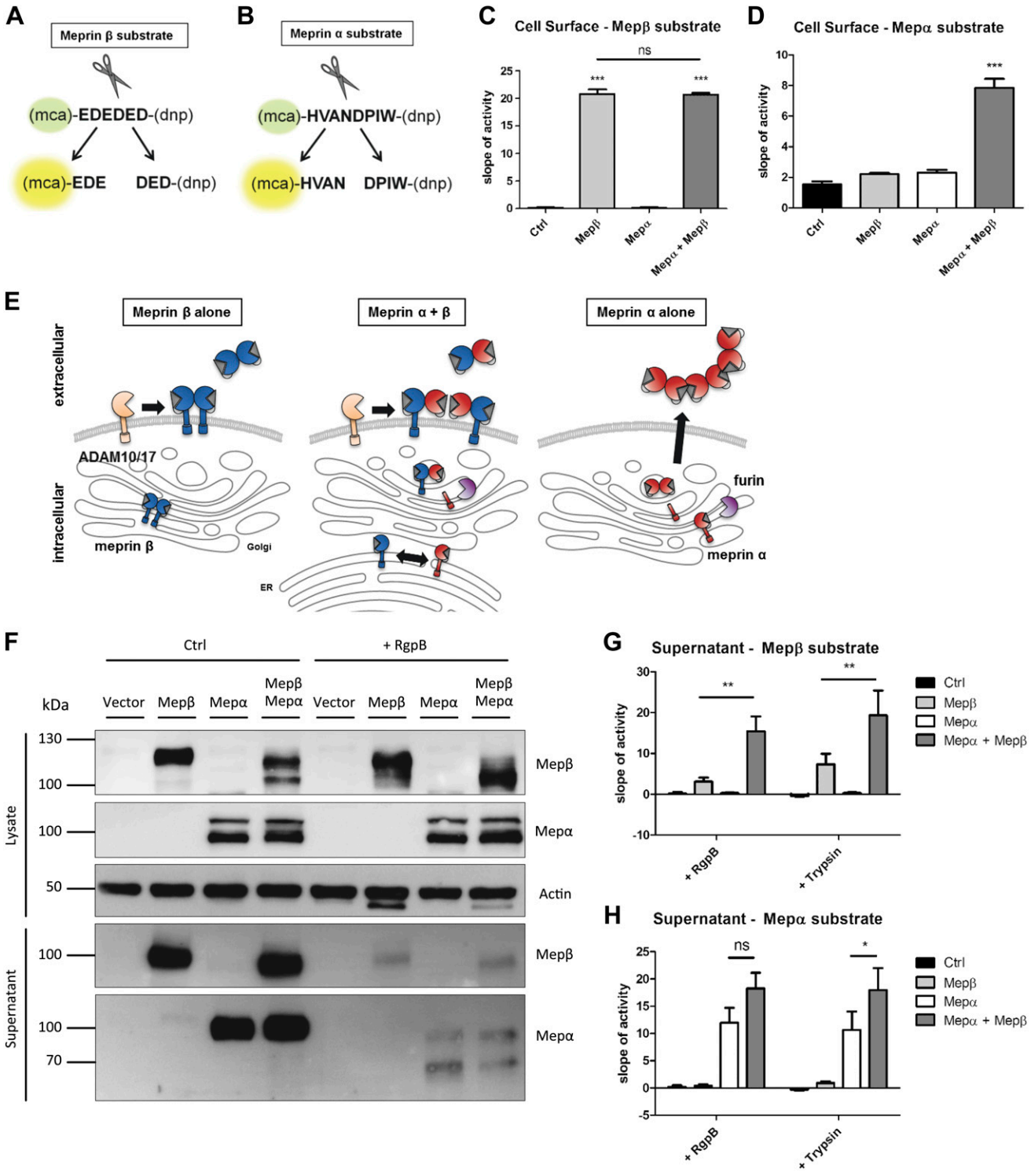

Figure 5. Proteolytic activity and shedding of the meprin heterodimer. *A*) Representation of the meprin β–specific quenched fluorogenic peptide used for activity assays. *B*) Representation of the meprin α–specific quenched fluorogenic peptide used for activity assays. *C*) Cell surface activity of meprin β on transfected HeLa cells. *D*) Cell surface activity of meprin α on transfected HeLa cells. *E*) Diagram of meprin β shedding by ADAM10 and ADAM17 as homo- or heterodimer. Meprin α is shed by furin in the Golgi apparatus and secreted into the extracellular space when expressed alone. *F*) HeLa cells were transfected with meprin α WT and meprin β WT constructs. Cells were stimulated with bacterial protease RgpB for meprin activation as indicated. Cell lysates and supernatants were analyzed *via* immunoblotting. *G*) Meprin β activity in either RgpB- or trypsin-stimulated cell supernatants of transfected HeLa cells. *H*) Meprin α activity in either RgpB or trypsin incubated cell supernatants of transfected HeLa cells. Ctrl, control; Mep, meprin; ns, not significant. Data are presented as means ± SD, and statistical analysis was assessed by 1-way ANOVA followed by Tukey's posttest (*C*, *D*), or 2-way ANOVA followed by a Bonferroni posttest (*G*, *H*) from 3 biologic replicates. $*P < 0.05$, $**P < 0.01$, $***P < 0.001$.

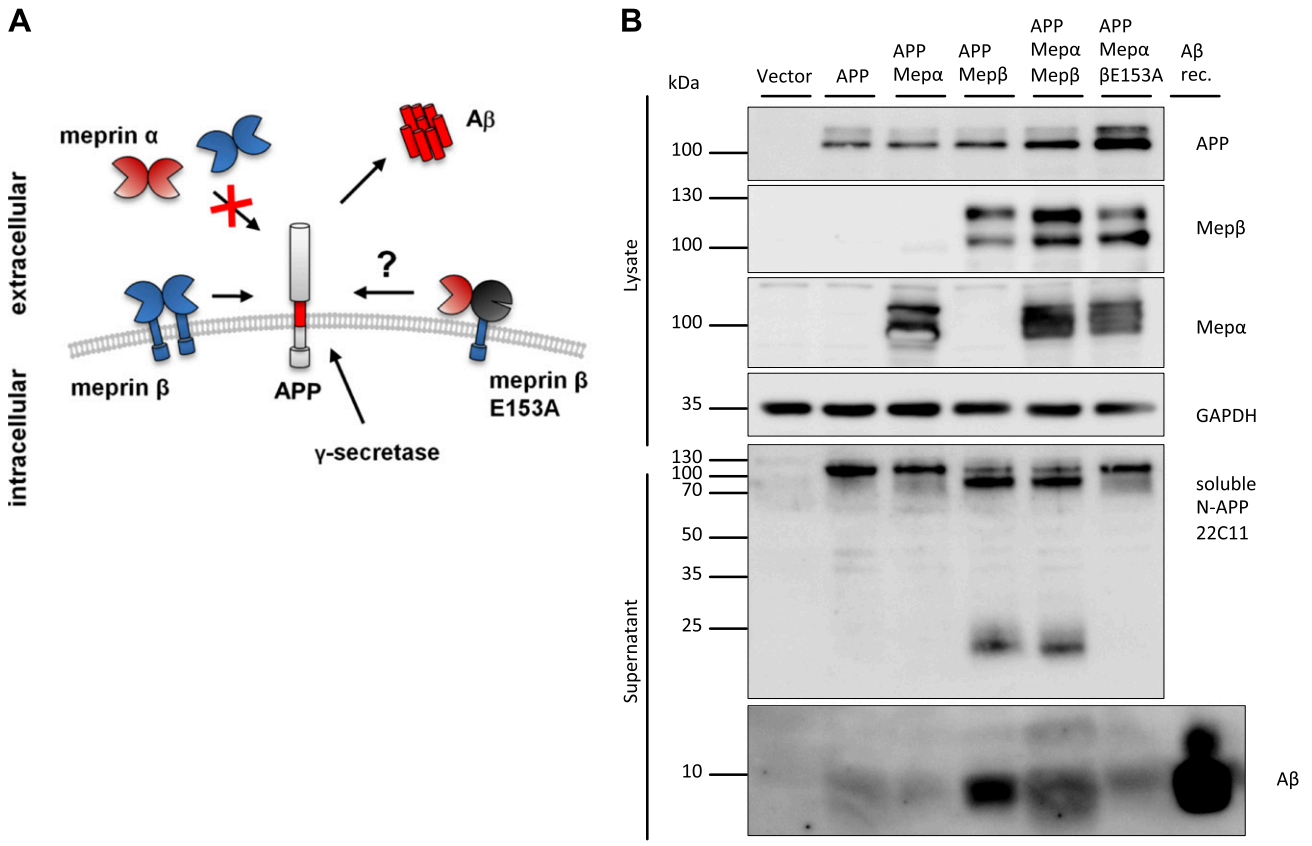

Figure 6. APP cleavage by the meprin heterodimer. *A*) Diagram of APP cleavage by cell surface–bound meprin β and impaired cleavage by soluble meprins. Cleavage of cell surface–bound meprin β and subsequent γ-secretase cleavage leads to generation of accumulating Aβ fragments in the extracellular space. Catalytically inactive meprin β E153A was used for the meprin enzyme complex to exclude meprin β cleavage. *B*) Transfection of HeLa cells with APP, meprin WT, or meprin β E153A variant. Immunoblotting of cell lysates and supernatants revealed cleavage of APP and Aβ generation by active meprin β, not by membrane-bound meprin α or inactive meprin β. Recombinant Aβ served as positive control. Mep, meprin; N-, N terminus; rec., recombinant.

observations were made with another membrane-bound meprin β substrate, the adhesion molecule CD99 (31), which was only shed by active meprin β and not by meprin α in the enzyme complex (Supplemental Fig. S2).

Localization of meprin α at the cell surface alters gene expression in murine intestinal tissue

Having investigated the molecular and cellular functions of the human meprin enzyme complex, we were further interested in its biologic relevance *in vivo*. We first validated cell surface localization of meprin α in murine WT small intestine, which was not detected in meprin β–knockout mice (**Fig. 7*A***). By Western blot analysis of small intestine lysates, we obtained similar results as observed in the *in vitro* experiments with human meprins (Fig. 7*B*). In the WT situation, meprin α appeared as a strong distinct band of 110 kDa. Expressed alone in meprin β–knockout mice, the meprin α band pattern looked more heterogeneous, consisting of shed and probably further processed meprin α. For meprin β, a slight shift in MW was observed in meprin α–knockout mice, which might also be a cause of altered glycosylation as seen in the human protein. Because we have not identified a specific membrane-bound substrate of meprin α so far, we performed RNAseq of meprin-knockout mice small intestine samples in order to see the biologic impact of meprin α expression and localization. Total absence or decreased expression of meprin α in murine and human colon and small intestine was associated with a higher risk for IBD progression (9, 32). We wondered whether loss of meprin α membrane localization might also promote and change gene expression with regard to IBD. Therefore, we compared the obtained gene expression data of meprin-knockout mice with data of a recently analyzed IBD patient cohort (32). In total, we identified 340 dysregulated genes in meprin-knockout mice that were found to be altered in the human IBD cohort (Fig. 7*C, D* and Supplemental Table S1). A total of 157 of these genes were only dysregulated in meprin β–knockout mice compared with WT mice, with 45.2% of genes being dysregulated in the same direction as in IBD patients. Interestingly, 136 genes were differentially expressed in meprin α–knockout mice compared with WT mice, with only 30.9% of genes showing the same tendency as in the IBD cohort. A total of 47 genes were found in both knockout conditions with

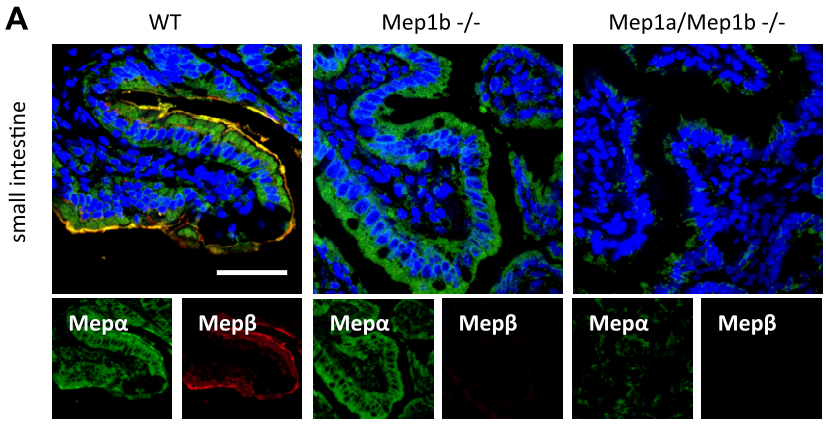

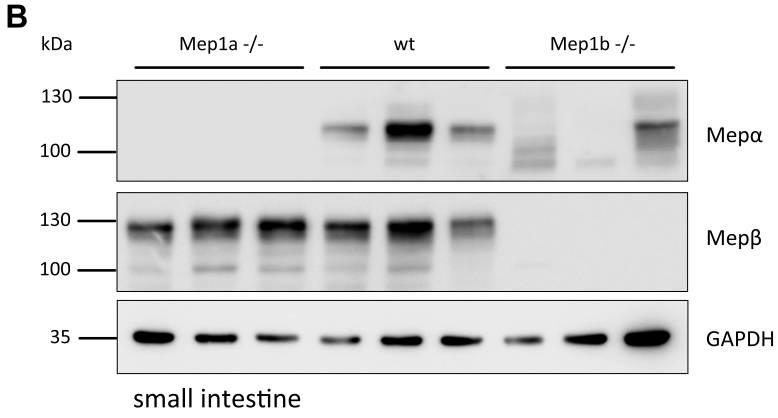

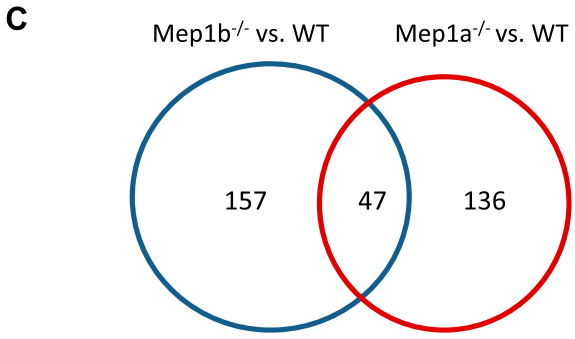

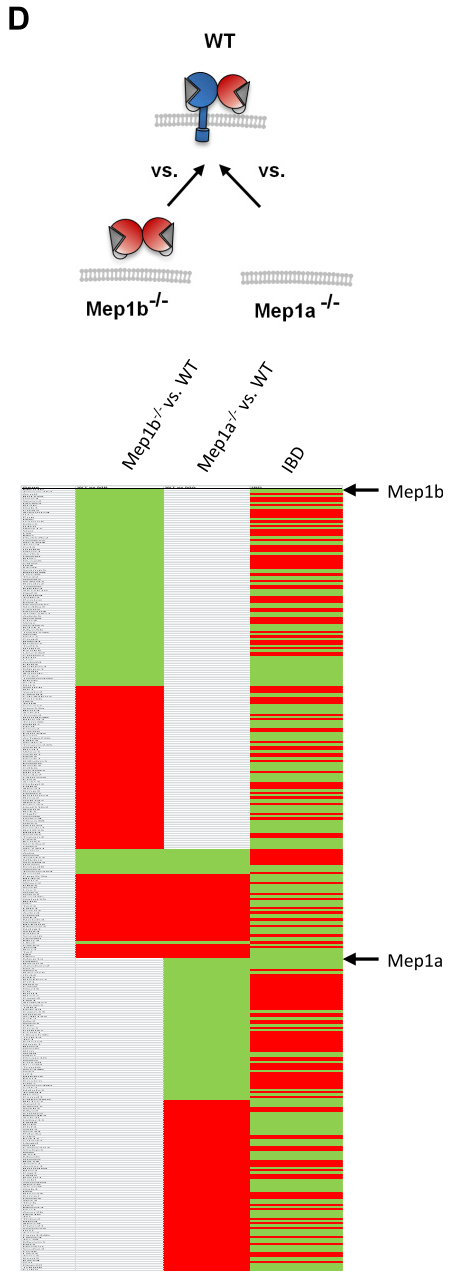

	Total genes	% as in IBD	% contrary to IBD
Only Mep1b$^{-/-}$ vs. WT	157	45,2	54,8
Only Mep1a$^{-/-}$ vs. WT	136	30,9	69,1
Mep1b$^{-/-}$ and Mep1a$^{-/-}$ vs. WT	47	25,5	74,5

Figure 7. Expression and transcriptional analysis of meprin heterodimer *in vivo*. *A*) Immunofluorescence microscopy of small intestine from WT, *Mep1b*$^{-/-}$, and *Mep1a*$^{-/-}$ mice using specific meprin antibodies. Staining revealed absence of meprin α at the cell surface in Mep1b$^{-/-}$ mice. Scale bar, 40 μm. *B*) Immunoblotting of small intestine lysates of WT, *Mep1b*$^{-/-}$, and *Mep1a*$^{-/-}$ mice using specific meprin antibodies. GAPDH served as loading control. *C*) Analysis of RNA sequencing of WT, *Mep1b*$^{-/-}$, and Mep1a$^{-/-}$ mice small intestine samples. Obtained data were compared with transcriptome analyses of IBD patients (32), and matching and overlapping genes of each condition were depicted. *D*) Representation of matching up- and down-regulated genes in WT, *Mep1b*$^{-/-}$, and *Mep1a*$^{-/-}$ mice small intestine samples and IBD patients. Green, down-regulation, red, up-regulation. Mep, meprin.

25.5% identical regulation as in IBD. Those 47 genes were equally dysregulated in both genotypes, indicating that loss of meprin α at the cell surface in meprin β–knockout mice had the same regulatory effect as the total loss of meprin α for this gene subset. To further contextualize the differentially expressed genes, a gene ontology analysis was performed, resulting in several significantly enriched and depleted biologic processes (Supplemental Fig. S3*A*, *B*). A large proportion of biologic processes identified is functionally associated with wound healing, tissue regeneration, innate immunity, and inflammatory mechanisms. In particular, the innate immune response was depleted in genes down-regulated in both *Mep1a*- and *Mep1b*-deficient scenarios.

DISCUSSION

The metalloproteases meprin α and meprin β exhibit unique molecular features among the members of the astacin family, being membrane bound and expressed as disulfide-linked dimers. Although both proteins are found in the same tissues, like small intestine and proximal tubuli of the kidney, their genes are located on different chromosomes and expressed independently from each other because of different promoter regions (33). Nevertheless, coexpression and homology of the proteases raised the question of whether meprins form also heterodimers (1, 2, 5). Indeed, meprin α and meprin β enzyme complexes were observed in rats and mice; however, the type of connection between both monomers was discussed controversially and was not yet shown for human meprins (2, 34–36). We now demonstrate that human meprin α and meprin β also form an enzyme complex that is covalently connected *via* a disulfide bridge in the MAM domain as described for murine meprins (24). The human meprins are linked between C305 in meprin β and C308 in meprin α, respectively, after translation in the early ER and before glycosylation sites are further modified. The interaction complex is transported to the cell surface, which tethers meprin α at the plasma membrane, although meprin α is shed by furin in the Golgi compartment. Interestingly, the glycosylation pattern of meprin β was altered when coexpressed with meprin α both *in vitro* for the human and *in vivo* for the murine isoform. This modification was not a cause of the disulfide-linked enzyme complex *per se* because altered glycosylation was also observed in the cysteine-mutated variants. Hence, the presence of meprin α within the secretory pathway might have a direct or indirect effect on glycosylation-maturating enzymes such as glycosyltransferases.

Both meprin α and meprin β are expressed as zymogens and require proteolytic activation by tryptic proteases on the cell surface or in the extracellular space (12–14). The meprin β homodimer was shown to be activated on the cell surface by matriptase-2 or the pathologic protease RgpB (4, 15). We observed that activation of meprin β was not impaired and was even significantly elevated for shed meprin β in the enzyme complex using a meprin β–specific fluorogenic substrate. Additionally, shedding of the enzyme complex by ADAM proteases was not impaired. However, once being activated on the cell surface, meprin α and meprin β could not be released into the extracellular space, thus behaving like the meprin β homodimer (4). This regulatory mechanism traps meprin α on the cell surface and is contrary to meprin α single expression, in which the protease is always secreted by the cells. To investigate proteolytic activity of meprin α, we designed a fluorogenic peptide based on a cleavage site specificity screen (28) and validated specificity with recombinant human proteins and knockout murine small intestine lysates. Interestingly, meprin α could also be activated in complex on the cell surface of transfected HeLa cells. Astonishingly, meprin α activity was elevated both on the cell surface and in the supernatant, although protein levels were unchanged as observed in Western blot analysis. Most likely, both proteases benefit from enzyme complex formation regarding increased stability, as predicted from the structure model, and may also promote consecutive substrate processing. Because meprin α and meprin β have a preference for acidic amino acid residues (28), we investigated whether meprin α in complex could also cleave known substrates of meprin β. Both the APP (29, 37) and CD99 (31) could not be shed by membrane-bound meprin α in cell culture, suggesting additional regulatory mechanisms of substrate cleavage besides cellular localization and amino acid sequences. However, cleavage of other substrates needs to be investigated.

The altered proteolytic activity of 2 enzymes has been shown for G-calpain, a noncovalently formed complex of calpain 8 and calpain 9 (38). An active site mutant of calpain 8 compromised proteolytic activity of the whole enzyme complex. However, a comparable covalently linked enzyme complex that increases proteolytic activity of the monomers as shown for meprins has, to our knowledge, not yet been identified.

Being localized on the cell membrane and being able to get activated, meprin α might broaden its substrate spectrum, which would no longer be restricted to soluble substrates. Another way for meprin α to get access to cell surface substrates was shown recently (39). Loss of meprin α binding to heparan sulfate in a noncovalent manner increased inflammatory cell recruitment and neutrophil transmigration in lungs of idiopathic pulmonary arterial hypertension patients. However, cell membrane localization of meprin α in the enzyme complex was not considered in the study.

Absence of meprin α in the gut is a risk for IBD, which was proven in a dextran sulfate sodium mouse model (9). In contrast, meprin β–knockout mice were protected against dextran sulfate sodium colitis because of loss of proinflammatory cytokines (10). Down-regulation of both the *MEP1A* and the *MEP1B* genes was observed in transcriptome analyses of IBD patients (32). However, the physiologic role of meprins in the gut with regard to cleavage of substrates needs to be elucidated. It is not known if loss of meprin α at the cell surface might play a role in the meprin β–knockout mouse for the protection or if it is a concomitant. For meprin β, it was also shown that cleavage of mucin 2 and its detachment is important for proper mucus barrier function (40). Additionally, shedding of meprin β by ADAM proteases is crucial for

subsequent mucus cleavage, which can be abolished through its activation by the pathogenic protease RgpB (4). Being covalently connected to meprin β in an enzyme complex, meprin α release into the extracellular space would be a regulated process and requires limited proteolysis. We performed transcriptome analysis of meprin-knockout mice in order to compare differences in gene expression between total absence of meprin α and both cellular localizations. The obtained data were matched with transcriptome analyses of IBD patients (32), and we identified different gene subsets when meprin α localization was altered. Interestingly, 47 overlapping genes were found that were equally dysregulated in membrane and total meprin α absence, probably crucial for the protective role of meprin α in IBD. In addition, only ~31% of the meprin α–knockout mice gene subset matched to observations of up- or down-regulation in IBD patients. This is further supported by our gene ontology analysis indicating that processes functionally associated with wound healing, tissue regeneration, innate immunity, and inflammatory mechanisms are dominating the picture. Although we believe that regulatory miRNA plays a key role as previously illustrated by Ágg *et al.* (41), our experimental setup does not allow us to draw conclusions on interconnections between the transcripts identified here and previously identified regulatory miRNAs. Hence, further investigations are necessary to demonstrate whether meprins are key factors in the onset and progression of intestinal inflammatory conditions, or if these proteases are only dysregulated as bystander genes.

In summary, we identified human meprin α and meprin β to form a covalently linked heterodimer, which alters post-translational modifications, localization, and proteolytic activity of both enzymes. Furthermore, solubilization of meprin α complexed at the cell surface requires regulated shedding of meprin β and changes transcription of IBD-related genes. Fj

ACKNOWLEDGMENTS

The authors thank Judith Bond (Pennsylvania State University, State College, PA, USA) for intense discussions on biochemical properties of meprin oligomerization. The authors also thank Lennard Arp (University of Kiel) for excellent technical assistance. This work was supported by the Deutsche Forschungsgemeinschaft (DFG) SFB 877 (Proteolysis as a Regulatory Event in Pathophysiology, Projects A9, A13, and A15) under Germany's Excellence Strategy, EXC 22167-390884018, and BE 4086/2-2 and BE 4086/5-1 (both to C.B.P.). J.P. is supported by the U.S. National Institutes of Health (NIH), National Institute of Dental and Craniofacial Research (NIDCR) (Grant DE 022597). The authors declare no conflicts of interest.

AUTHOR CONTRIBUTIONS

F. Peters, F. Scharfenberg, C. Colmorgen, F. Armbrust, R. Wichert, P. Arnold, and R. Häsler performed research; B. Potempa, J. Potempa, and C. U. Pietrzik provided materials; R. Häsler and P. Rosenstiel performed and analyzed RNA sequencing experiments; and F. Peters and C. Becker-Pauly conceived the experiments and wrote the manuscript.

REFERENCES

1. Marchand, P., Tang, J., Johnson, G. D., and Bond, J. S. (1995) COOH-terminal proteolytic processing of secreted and membrane forms of the alpha subunit of the metalloprotease meprin A. Requirement of the I domain for processing in the endoplasmic reticulum. *J. Biol. Chem.* **270**, 5449–5456
2. Bertenshaw, G. P., Norcum, M. T., and Bond, J. S. (2003) Structure of homo- and hetero-oligomeric meprin metalloproteases. Dimers, tetramers, and high molecular mass multimers. *J. Biol. Chem.* **278**, 2522–2532
3. Herzog, C., Haun, R. S., Ludwig, A., Shah, S. V., and Kaushal, G. P. (2014) ADAM10 is the major sheddase responsible for the release of membrane-associated meprin A. *J. Biol. Chem.* **289**, 13308–13322
4. Wichert, R., Ermund, A., Schmidt, S., Schweinlin, M., Ksiazek, M., Arnold, P., Knittler, K., Wilkens, F., Potempa, B., Rabe, B., Stirnberg, M., Lucius, R., Bartsch, J. W., Nikolaus, S., Falk-Paulsen, M., Rosenstiel, P., Metzger, M., Rose-John, S., Potempa, J., Hansson, G. C., Dempsey, P. J., and Becker-Pauly, C. (2017) Mucus detachment by host metalloprotease meprin β requires shedding of its inactive pro-form, which is abrogated by the pathogenic protease RgpB. *Cell Rep.* **21**, 2090–2103
5. Johnson, G. D., and Hersh, L. B. (1992) Cloning a rat meprin cDNA reveals the enzyme is a heterodimer. *J. Biol. Chem.* **267**, 13505–13512
6. Beynon, R. J., Shannon, J. D., and Bond, J. S. (1981) Purification and characterization of a metallo-endoproteinase from mouse kidney. *Biochem. J.* **199**, 591–598
7. Sterchi, E. E., Green, J. R., and Lentze, M. J. (1982) Non-pancreatic hydrolysis of N-benzoyl-l-tyrosyl-p-aminobenzoic acid (PABA-peptide) in the human small intestine. *Clin. Sci. (Lond.)* **62**, 557–560
8. Barnes, K., Ingram, J., and Kenny, A. J. (1989) Proteins of the kidney microvillar membrane. Structural and immunochemical properties of rat endopeptidase-2 and its immunohistochemical localization in tissues of rat and mouse. *Biochem. J.* **264**, 335–346
9. Banerjee, S., Oneda, B., Yap, L. M., Jewell, D. P., Matters, G. L., Fitzpatrick, L. R., Seibold, F., Sterchi, E. E., Ahmad, T., Lottaz, D., and Bond, J. S. (2009) MEP1A allele for meprin A metalloprotease is a susceptibility gene for inflammatory bowel disease. *Mucosal Immunol.* **2**, 220–231
10. Banerjee, S., Jin, G., Bradley, S. G., Matters, G. L., Gailey, R. D., Crisman, J. M., and Bond, J. S. (2011) Balance of meprin A and B in mice affects the progression of experimental inflammatory bowel disease. *Am. J. Physiol. Gastrointest. Liver Physiol.* **300**, G273–G282
11. Trachtman, H., Valderrama, E., Dietrich, J. M., and Bond, J. S. (1995) The role of meprin A in the pathogenesis of acute renal failure. *Biochem. Biophys. Res. Commun.* **208**, 498–505
12. Grünberg, J., Dumermuth, E., Eldering, J. A., and Sterchi, E. E. (1993) Expression of the alpha subunit of PABA peptide hydrolase (EC 3.4. 24.18) in MDCK cells. Synthesis and secretion of an enzymatically inactive homodimer. *FEBS Lett.* **335**, 376–379
13. Johnson, G. D., and Bond, J. S. (1997) Activation mechanism of meprins, members of the astacin metalloendopeptidase family. *J. Biol. Chem.* **272**, 28126–28132
14. Ohler, A., Debela, M., Wagner, S., Magdolen, V., and Becker-Pauly, C. (2010) Analyzing the protease web in skin: meprin metalloproteases are activated specifically by KLK4, 5 and 8 vice versa leading to processing of proKLK7 thereby triggering its activation. *Biol. Chem.* **391**, 455–460
15. Jäckle, F., Schmidt, F., Wichert, R., Arnold, P., Prox, J., Mangold, M., Ohler, A., Pietrzik, C. U., Koudelka, T., Tholey, A., Gütschow, M., Stirnberg, M., and Becker-Pauly, C. (2015) Metalloprotease meprin β is activated by transmembrane serine protease matriptase-2 at the cell surface thereby enhancing APP shedding. *Biochem. J.* **470**, 91–103
16. Norman, L. P., Jiang, W., Han, X., Saunders, T. L., and Bond, J. S. (2003) Targeted disruption of the meprin beta gene in mice leads to underrepresentation of knockout mice and changes in renal gene expression profiles. *Mol. Cell. Biol.* **23**, 1221–1230
17. Waterhouse, A., Bertoni, M., Bienert, S., Studer, G., Tauriello, G., Gumienny, R., Heer, F. T., de Beer, T. A. P., Rempfer, C., Bordoli, L., Lepore, R., and Schwede, T. (2018) SWISS-MODEL: homology

modelling of protein structures and complexes. *Nucleic Acids Res.* **46**, W296–W303
18. Laskowski, R. A., Jabłońska, J., Pravda, L., Vařeková, R. S., and Thornton, J. M. (2018) PDBsum: Structural summaries of PDB entries. *Protein Sci.* **27**, 129–134
19. Martin, M. (2011) Cutadapt removes adapter sequences from high-throughput sequencing reads. *EMBnet J.* **17**, 10–12
20. Trapnell, C., Roberts, A., Goff, L., Pertea, G., Kim, D., Kelley, D. R., Pimentel, H., Salzberg, S. L., Rinn, J. L., and Pachter, L. (2012) Differential gene and transcript expression analysis of RNA-seq experiments with TopHat and Cufflinks. *Nat. Protoc.* **7**, 562–578; erratum: 9, 2513
21. Anders, S., Pyl, P. T., and Huber, W. (2015) HTSeq–a Python framework to work with high-throughput sequencing data. *Bioinformatics* **31**, 166–169
22. Love, M. I., Huber, W., and Anders, S. (2014) Moderated estimation of fold change and dispersion for RNA-seq data with DESeq2. *Genome Biol.* **15**, 550
23. Tavazoie, S., Hughes, J. D., Campbell, M. J., Cho, R. J., and Church, G. M. (1999) Systematic determination of genetic network architecture. *Nat. Genet.* **22**, 281–285
24. Chevallier, S., Ahn, J., Boileau, G., and Crine, P. (1996) Identification of the cysteine residues implicated in the formation of alpha 2 and alpha/beta dimers of rat meprin. *Biochem. J.* **317**, 731–738
25. Arolas, J. L., Broder, C., Jefferson, T., Guevara, T., Sterchi, E. E., Bode, W., Stöcker, W., Becker-Pauly, C., and Gomis-Rüth, F. X. (2012) Structural basis for the sheddase function of human meprin β metalloproteinase at the plasma membrane. *Proc. Natl. Acad. Sci. USA* **109**, 16131–16136
26. Ishmael, S. S., Ishmael, F. T., Jones, A. D., and Bond, J. S. (2006) Protease domain glycans affect oligomerization, disulfide bond formation, and stability of the meprin A metalloprotease homo-oligomer. *J. Biol. Chem.* **281**, 37404–37415
27. Broder, C., and Becker-Pauly, C. (2013) The metalloproteases meprin α and meprin β: unique enzymes in inflammation, neurodegeneration, cancer and fibrosis. *Biochem. J.* **450**, 253–264
28. Becker-Pauly, C., Barré, O., Schilling, O., Auf dem Keller, U., Ohler, A., Broder, C., Schütte, A., Kappelhoff, R., Stöcker, W., and Overall, C. M. (2011) Proteomic analyses reveal an acidic prime side specificity for the astacin metalloprotease family reflected by physiological substrates. *Mol. Cell. Proteomics* **10**, M111.009233
29. Bien, J., Jefferson, T., Causević, M., Jumpertz, T., Munter, L., Multhaup, G., Weggen, S., Becker-Pauly, C., and Pietrzik, C. U. (2012) The metalloprotease meprin β generates amino terminal-truncated amyloid β peptide species. *J. Biol. Chem.* **287**, 33304–33313
30. Schönherr, C., Bien, J., Isbert, S., Wichert, R., Prox, J., Altmeppen, H., Kumar, S., Walter, J., Lichtenthaler, S. F., Weggen, S., Glatzel, M., Becker-Pauly, C., and Pietrzik, C. U. (2016) Generation of aggregation prone N-terminally truncated amyloid β peptides by meprin β depends on the sequence specificity at the cleavage site. *Mol. Neurodegener.* **11**, 19
31. Bedau, T., Peters, F., Prox, J., Arnold, P., Schmidt, F., Finkernagel, M., Köllmann, S., Wichert, R., Otte, A., Ohler, A., Stirnberg, M., Lucius, R., Koudelka, T., Tholey, A., Biasin, V., Pietrzik, C. U., Kwapiszewska, G., and Becker-Pauly, C. (2017) Ectodomain shedding of CD99 within highly conserved regions is mediated by the metalloprotease meprin β and promotes transendothelial cell migration. *FASEB J.* **31**, 1226–1237
32. Häsler, R., Sheibani-Tezerji, R., Sinha, A., Barann, M., Rehman, A., Esser, D., Aden, K., Knecht, C., Brandt, B., Nikolaus, S., Schäuble, S., Kaleta, C., Franke, A., Fretter, C., Müller, W., Hütt, M. T., Krawczak, M., Schreiber, S., and Rosenstiel, P. (2017) Uncoupling of mucosal gene regulation, mRNA splicing and adherent microbiota signatures in inflammatory bowel disease. *Gut* **66**, 2087–2097
33. Hahn, D., Illisson, R., Metspalu, A., and Sterchi, E. E. (2000) Human N-benzoyl-L-tyrosyl-p-aminobenzoic acid hydrolase (human meprin): genomic structure of the alpha and beta subunits. *Biochem. J.* **346**, 83–91
34. Johnson, G. D., and Hersh, L. B. (1994) Expression of meprin subunit precursors. Membrane anchoring through the β subunit and mechanism of zymogen activation. *J. Biol. Chem.* **269**, 7682–7688
35. Lottaz, D., Hahn, D., Müller, S., Müller, C., and Sterchi, E. E. (1999) Secretion of human meprin from intestinal epithelial cells depends on differential expression of the alpha and beta subunits. *Eur. J. Biochem.* **259**, 496–504
36. Lottaz, D., Maurer, C. A., Noël, A., Blacher, S., Huguenin, M., Nievergelt, A., Niggli, V., Kern, A., Müller, S., Seibold, F., Friess, H., Becker-Pauly, C., Stöcker, W., and Sterchi, E. E. (2011) Enhanced activity of meprin-α, a pro-migratory and pro-angiogenic protease, in colorectal cancer. *PLoS One* **6**, e26450
37. Jefferson, T., Čaušević, M., auf dem Keller, U., Schilling, O., Isbert, S., Geyer, R., Maier, W., Tschickardt, S., Jumpertz, T., Weggen, S., Bond, J. S., Overall, C. M., Pietrzik, C. U., and Becker-Pauly, C. (2011) Metalloprotease meprin β generates nontoxic N-terminal amyloid precursor protein fragments in vivo. *J. Biol. Chem.* **286**, 27741–27750
38. Hata, S., Kitamura, F., Yamaguchi, M., Shitara, H., Murakami, M., and Sorimachi, H. (2016) A gastrointestinal calpain complex, G-calpain, is a heterodimer of CAPN8 and CAPN9 calpain isoforms, which play catalytic and regulatory roles, respectively. *J. Biol. Chem.* **291**, 27313–27322
39. Biasin, V., Wygrecka, M., Bärnthaler, T., Jandl, K., Jain, P. P., Bálint, Z., Kovacs, G., Leitinger, G., Kolb-Lenz, D., Kornmueller, K., Peters, F., Sinn, K., Klepetko, W., Heinemann, A., Olschewski, A., Becker-Pauly, C., and Kwapiszewska, G. (2018) Docking of meprin α to heparan sulphate protects the endothelium from inflammatory cell extravasation. *Thromb. Haemost.* **118**, 1790–1802
40. Schütte, A., Ermund, A., Becker-Pauly, C., Johansson, M. E. V., Rodriguez-Pineiro, A. M., Bäckhed, F., Müller, S., Lottaz, D., Bond, J. S., and Hansson, G. C. (2014) Microbial-induced meprin β cleavage in MUC2 mucin and a functional CFTR channel are required to release anchored small intestinal mucus. *Proc. Natl. Acad. Sci. USA* **111**, 12396–12401
41. Ágg, B., Baranyai, T., Makkos, A., Vető, B., Faragó, N., Zvara, Á., Giricz, Z., Veres, D. V., Csermely, P., Arányi, T., Puskás, L. G., Varga, Z. V., and Ferdinandy, P. (2018) MicroRNA interactome analysis predicts post-transcriptional regulation of ADRB2 and PPP3R1 in the hypercholesterolemic myocardium. *Sci. Rep.* **8**, 10134; erratum: 9, 12159

Received for publication November 7, 2018.
Accepted for publication February 25, 2019.